



UNIVERSITÀ DEGLI STUDI DI PAVIA

**DOTTORATO IN SCIENZE CHIMICHE E
FARMACEUTICHE E INNOVAZIONE INDUSTRIALE
(XXXIII Ciclo)**

Coordinatore: Chiar.mo Prof. Piersandro Pallavicini

***SILK PROTEIN BASED PRODUCTS FOR
PHARMACEUTICAL AND BIOMEDICAL APPLICATIONS***

Tesi di Dottorato di

Giulia Orlandi

AA 2019/2020

Tutor

Chiar.ma Prof.ssa Maria Luisa Torre

Co-tutor

Dott.ssa Sara Perteghella, Dott. Silvio Faragò

Outline

Preface.....	1
Introduction.....	2
1. The silk: general aspects.....	2
1.1 The silk fibroin.....	7
1.2 The silk sericin.....	9
1.3 The silk sericin extraction and recycling	14
1.4 Circular economy measures to apply on the silk manufacturing waste	37
2. Silk protein employment as biomaterials	42
2.1 Properties and use of silk fibroin	42
2.1.1 Silk fibroin as a biomaterial with potential for drug delivery	48
2.2 Silk sericin for pharmaceutical, biomedical, and cosmetic applications	53
3. Technologies for the characterization of silk-based materials	61
3.1 Thermal Analysis	62
3.2 Chromatographic techniques.....	65
3.2.1 Hydrophilic interaction liquid, reversed phase, and size exclusion chromatography methods, and electrophoresis SDS-PAGE	66
3.3 Spectroscopic techniques	71
3.3.1 Fourier transformed infrared spectroscopy	71
3.3.2 Ultraviolet-visible spectroscopy.....	78
3.4 Particle size analysis techniques	80
3.5 Scanning electron microscopy	84
4. References.....	86
5. Silk sericin as a biomaterial in drug delivery systems.....	98
Paper 1	99
Aim.....	129
Results	130
Paper 2	131
Paper 3	162
Paper 4	201
Conclusions	234
Acknowledgements	236

Preface

Silk is a biomaterial composed of two proteins: fibroin and sericin. Fibroin is a fibrous and hydrophobic protein, represents about 70-80% of silk filament, while sericin, a globular and hydrophilic protein, ranges from 20 to 30%.

For years, fibroin has been employed as a biocompatible and biodegradable material in medicine surgery, tissue engineering, and drug delivery. Conversely, sericin, a textile waste product, only recently has been revalued for its properties of biocompatibility, controllable biodegradability and not immunogenicity, allowing its use in pharmaceutical, biomedical and cosmetic fields. In detail, sericin exhibits antioxidant, anti-tyrosinase, anti-elastase, and anti-inflammatory activities that make it a promising bioactive protein. This intrinsic biological activity and good features as an inert excipient are exploitable for the formulations of drug delivery systems. To date, the potential of sericin for the design and development of nanosystems has not been completely investigated. In fact, nanoparticles based on silk sericin “alone” can not be produced, due to its physical-chemical instability, influenced by extreme pH, high water solubility and low temperature; for these reasons, it almost always needs to be combined with other polymers for the development of drug delivery systems.

Overall, sericin can not be considered only a waste product of the textile industry, but a high-added-value ingredient to be used in a plethora of cosmetic, cosmeceutical, and pharmaceutical products.

Introduction

1. The silk: general aspects

Silk is a protein fibre of animal origin produced by spiders of the Arachnida class (*Nephila clavipes* and *Araneus diadematus*) and insects that belong to the Lepidoptera order [1].

Spider silk is used for many vital functions like protecting eggs, for dragline formation and capture nets that can withstand high impacts and trap insects [2]. However, it is not commonly employed in biomedical and pharmaceutical fields due to the smaller yield and wilder nature of spiders compared to the silkworm and the lack of commercially established supply chains, as occurs in sericulture [3].

One of the most extensively characterized and utilized silks for textile and biomedical use is from the domesticated silkworm *Bombyx mori*. It belongs to the Bombycidae family (mulberry) and together with the Saturniidae family (non-mulberry) are the only two members to produce silk with commercial importance.

The classification of silkworms in the mulberry or non-mulberry family originates mainly from the eating habits of insects. The silkworms of the mulberry family are now completely domesticated and require human care for their growth and reproduction, which does not occur naturally. On the contrary, those not from the mulberry family are species that live wild in different geographical regions, and this is why the silk extracted from them has very different characteristics from specimen to specimen [4].

Bombyx mori produces a massive amount of silk proteins during the final stage of larval development. Two kinds of silk proteins have been distinguished as major components of the silk cocoon: the fibroin and the sericin, closely linked but different in terms of structure and properties.

The production of cocoon lasts about three days and occurs from outside in, where two fibroin core fibres (5-10 μm wide) are coated by the amorphous glue-like sericin (Figure 1), to form the silk threads, whose size ranges from 900 to 1500 m. [5]

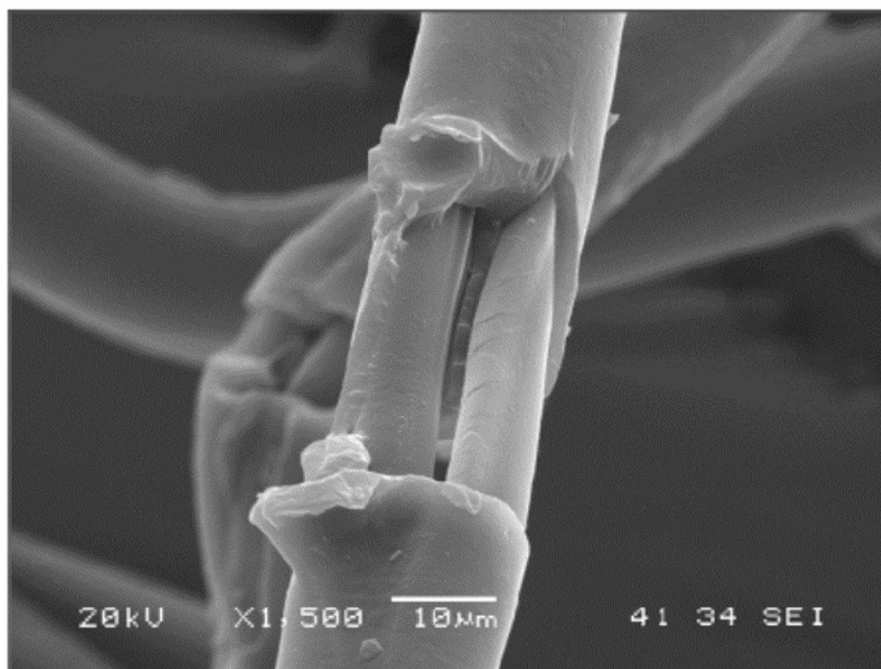


Figure 1: Scanning electron microscope (SEM) image of the silk fibre, which contains fibroin and sericin. Scale bar: 10 μm (x 1,500). Reproduced from *Soft Matter*, Crivelli, B.; Perteghella, S.; Bari, E; Sorrenti, M; Tripodo, G; Chlapanidas, T; Torre M.L., *Silk nanoparticles: from inert supports to bioactive natural carriers for drug delivery*, 4, 546-557 (2018), with permission from Royal Society of Chemistry

As a biological structural material, the cocoon has a hierarchical structure that we assume has been optimized through evolutionary pressures over millions of years to provide the optimum protection for the silkworm pupae. They are exposed to a wide range of threats such as physical attack from animals, birds or insects, or more subtle threats such as bacteria or simply harsh environmental conditions [6]. Also, a minority non-sericin like component made of fats and waxes (0.4 to 0.8%), inorganic salts (0.7%), sugars, mineral salts, pigment (0.2%) and other impurities are present in the cocoon [7] [8].

The natural silk synthesized by the silkworm and spun in the form of a silk cocoon is originally synthesized in the silk glands, a paired organ consisting of modified labial/salivary glands located at the two lateral sides under the alimentary canal. Each gland is a tube made of the glandular epithelium with two rows of cells surrounding the lumen. The cells are huge polyploid cells with an extremely ramified nucleus containing various nucleoli. Nuclear ramification develops gradually during the larva growth and reaches evident size in the fourth and fifth instars. Ramification considerably enlarges the nuclear surface and facilitates the transfer of materials related to the silk production between the nucleus and the cytoplasm. In

agreement with its morphology and function, the silk gland can be divided into a posterior, a middle, and anterior region (Figure 2).

The posterior part is long about 15 cm and is composed of about 500 secretory cells responsible for the synthesis of the silk fibroin. The middle region of the silk gland in the lumen of which silk proteins are stored until spinning is about 7 cm long and contains about 300 secretory cells producing silk sericin. It is subdivided into four areas: anterior, anterior-middle, posterior-middle, and posterior. Each area differs due to the density and morphology of the material contained in secretory vesicles, and each of them secretes three different types of sericin in the lumen. Besides, the middle region of the silk glands acts also as the reservoir

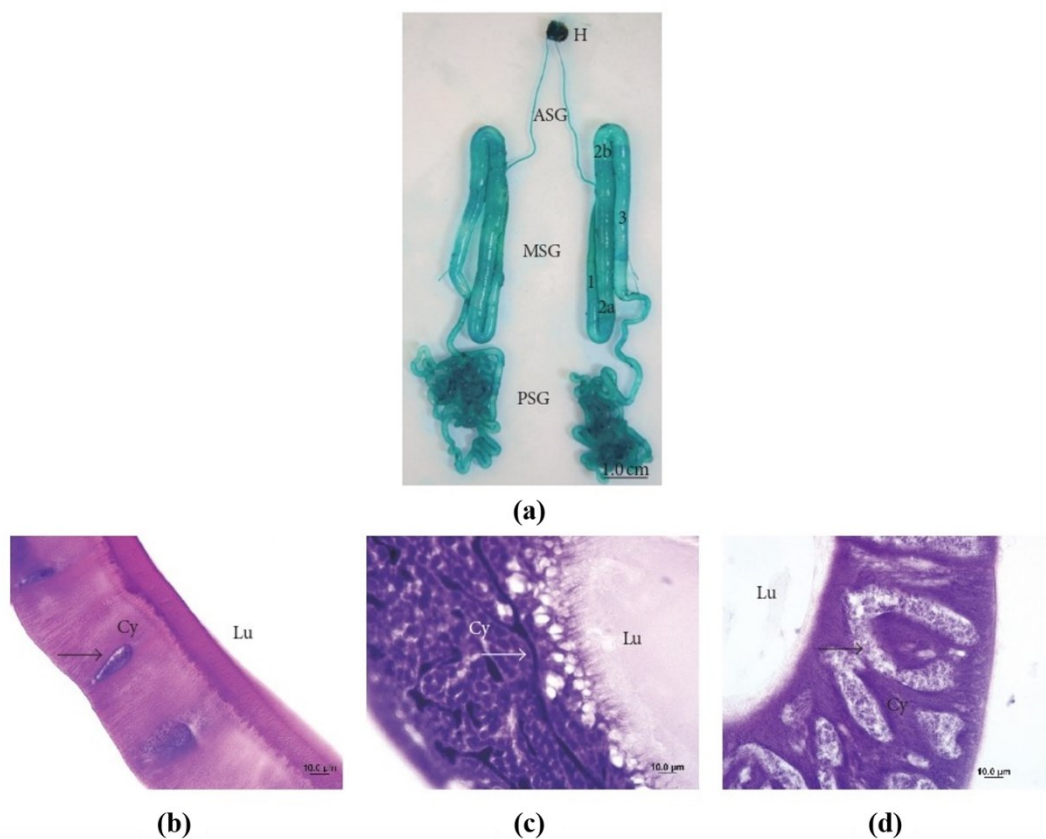


Figure 2: *Bombyx mori* silk gland (a), stained with light green 1%. Anterior (ASG), middle (MSG), and posterior silk (PSG). MSG and its areas: anterior (1), anterior-middle (2a), posterior-middle (2b), and posterior (3). Head (H). Panels (b), (c), and (d) showed the anterior, middle, and posterior regions, respectively, stained with haematoxylin and eosin. Cytoplasm (Cy), nucleus (arrows), and lumen (Lu). Reproduced from *BioMed Research International*, Kunz, R. I.; Brancalhão, R.M.C; Ribeiro, L. de F. C; Natali, M.R.M, *Silkworm Sericin: Properties and Biomedical Applications*, 19 pages (2016), Article ID 8175701 (Open Access)

for the maturation of fibroin. Finally, the anterior part is a thin duct about 2 cm long composed of about 250 cells; it is not secretory and acts as a passage to convey the silk substances to a single structure near the head called the silk-spinning organ (or the spinneret) [9].

Silk glands secrete one fibroin and three layers of sericin from each posterior and middle region as separate filaments called brins. The two brins are held together by the sericin, which hardens on exposure to air and such combined brins form a single filament called slime [10].

The life cycle of the silkworm is divided into different stages of metamorphosis (Figure 3).



Figure 3: Production cycle of *Bombyx mori* silk by the silkworm. Reproduced from *Materials and Design*, Ude, A. U.; Eshkoo, R. A.; Zulkifili, R.; Ariffin, A. K.; Dzuraidah, A. W.; Azhari, C. H., *Bombyx mori* silk fibre and its composite: A review of contemporary developments, 57, 298-305 (2014), with permission from Elsevier

The first stage of silk production is the laying of silkworm eggs. In this period the female silkworm deposits from 300 to 400 eggs at a time in a controlled environment and dies immediately afterwards. On the other hand, the male silkworm lives only a short period after that. In the second stage, the eggs are incubated for about ten days until they hatch into larvae (caterpillars). The third stage is the feeding period: the larvae are fed, for a period of four to six weeks, with mulberry leaves so that they can store enough nutrients until the caterpillar is

formed. As soon as the silkworm stops eating, it is ready to spin a silk cocoon that the caterpillar weaves wrapping the silk fibres around itself.

In just three days cocoons weighing a few grams are made of a single continuous silk strand with a length varying between 900-1500 m. After the formation of cocoons, the silkworms lose their skin for the last time and then turn into pupae (or chrysalis). Each cocoon has an ellipsoidal shape with a lesser thickness at both ends, where it comes into contact with an alkaline secretion from the silkworm, thereby allowing the insect to emerge as a moth to complete the metamorphosis [11].

Two species of silkworm exist called pure or hybrid: the first one is born from the mating of moths of the same race, while the "hybrid" insects can be traced back to the crossbreeds. Besides, *Bombyx mori* is classified according to voltinism: the races called monovoltine, bivoltine and polyvoltine complete the biological cycle respectively once, twice or several times a year. Voltinism is a hereditary character but modifiable through external factors, such as temperature, or artificial factors, such as chemical treatments; in this way, it is possible to develop more than one annual generation also in monovoltine species, hence increasing the silk production yield.

Nowadays, about 200 *Bombyx mori* strains have been identified by the CRA-Unit of Research of Apiculture and Sericulture, Padua, Italy (CRA-API), one of the most important silkworm germplasm banks in Europe. The strains differ in various characteristics such as cocoon shape, colour, volume, total weight, the amount of silk produced and some functional capabilities, which constitute a useful element for silkworm classification (Figure 4).

Most of the commercial varieties of silkworm cocoons are white and are composed of approximately 75% w/w silk fibroin fibre and 25% w/w sericin. To develop a new use for sericin, sericin-rich varieties of silkworm cocoons have been developed, producing more than 40% sericin or even spinning only sericin protein without fibroin. In the last case, the amount of sericin in the cocoon accounts for over 90% of the cocoon and the small amounts of pigment, wax, inorganic salts, carbohydrates and other impurities.



Figure 4: White and coloured *Bombyx mori* cocoons. Modified from *Materials Science and Engineering C 61*, Cao, T. T.; Zhang, Y. Q., *Processing and characterization of silk sericin from Bombyx mori and its application in biomaterials and biomedicines*, 940-952 (2016), with permission from Elsevier

Diverse chemical composition of cocoons that could often influence the biological activities of silk proteins: e.g., the colour of cocoons reflects the presence of varying proportions lutein, carotenoids and polyphenols, molecules commonly known for their biological properties (ROS-scavenging, anti-tyrosinase, anti-elastase, and anti-inflammatory). [12]

Many of these compounds derive from the silkworm larvae eating mulberry leaves. After the digestion and absorption by the silkworm, these secondary metabolites run directly into the bloodstream and finally reach the silk glands to appear in the sericin layer of the cocoon shell. Lastly, sericin layers of the cocoon contain visible and non-visible pigments, mainly including flavonoids or their glycosides, especially in the light yellow Daizo cocoon. It has been found that flavonoids with a similar structure can protect against bacteria and pests and allow the pupa to metamorphose and develop smoothly in the cocoon [8].

1.1 The silk fibroin

Bombyx mori silk fibroin is the major component of silkworm silk fibres (72-81% w/w), which consists of polypeptide chains with a molecular weight in the range of 200-350 kDa. The primary structure of fibroin is composed of repetitive glycine (Gly) and serine (Ser) sequences (–Gly–Ser–Gly–Ala–Gly–Ala–) of hydrophobic heavy chains (H-chain, 391.6 kDa) and non-repetitive hydrophilic light chains (L-chain, Mw: 27.7 kDa) with terminal C and N groups. The two chains are linked by a unique disulfide bond between the cysteine 172 of the L-chain and the cysteine C-20 (the 20th residue from the carboxy-terminal domain) of

the H-chain. Also, the glycoprotein fibrohexamerin (P25, Mw: 25.2 kDa), which is non-covalently linked to the chains mentioned above, is present in the structure of the silk fibroin and provides integrity to the entire structure. The molar ratio of H-chain, L-chain and P25 in silk is 6:6:1 [13] [4]. The hydrophilic L-chain comprises of alanine (Ala), serine (Ser), glycine (Gly) to 14%, 10%, 9%, respectively, and acetylated N-terminal Ser residues. The hydrophobic H-chain includes 45.9% Gly, 30.3% Ala, 12.1% Ser, 5.3% tyrosine (Tyr), and 1.8% valine (Val) [14]. The repetitive hydrophobic amino acid domains of H-fibroin fold and bond together via hydrogen bonds, Van der Waals forces, and hydrophobic interactions, to form an anti-parallel β -sheet crystalline structures (Figure 5).

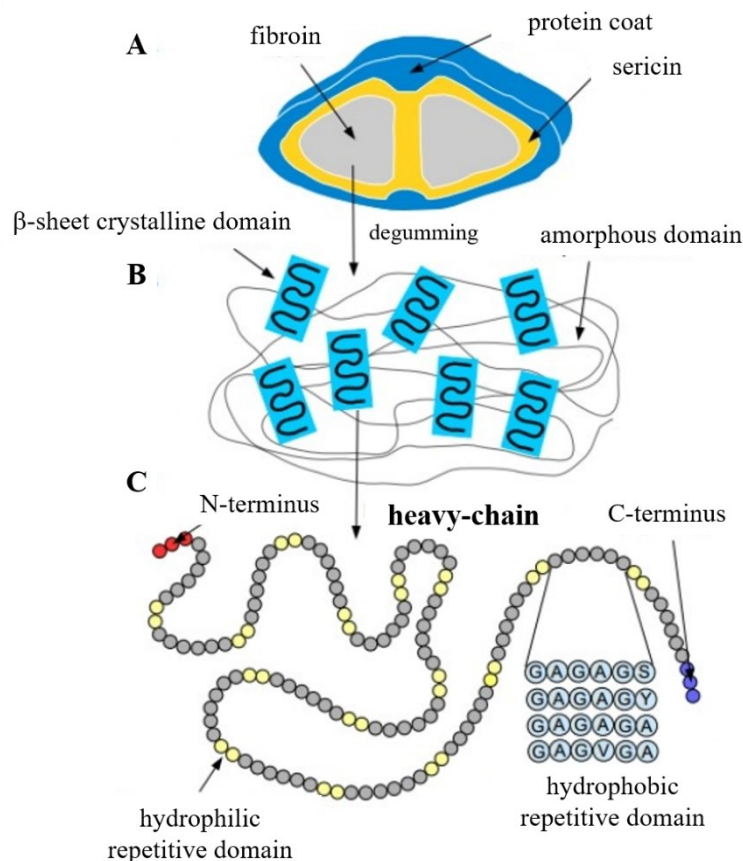


Figure 5: Schematic representation of the silk. (A) The raw silk fibre consists of two fibroin filaments coated together by sericin. After the degumming process, the sericin is removed and the fibroin fibres are dissolved in solution; (B) illustration of β -sheet crystalline and amorphous domain structure; (C) representation of the silk fibroin heavy-chain constituted of hydrophobic and hydrophilic repetitive domains. Each hydrophobic subdomain consists of different repeating units of hexapeptides ($-\text{Gly}-\text{Ser}-\text{Gly}-\text{Ala}-\text{Gly}-\text{Ala}-$). Reproduced from *J Funct Biomater.*, Jao, D.; Mou, X.; Hu, X., *Tissue Regeneration: A Silk Road.*, 7 (3), (2016) (Open Access)

These crystalline domains are highly organized at the microscopic level and act as crosslinking points in the less ordered, poorly oriented amorphous matrix, which comprises of random coils, β -turns, and/or α -helix structures and is formed of non-repetitive domains, forming a resultant molecular fishnet structure. The fishnet, the semi-crystalline structure could be considered to be the fundamental architecture of the silk. The strong β -sheet interactions, the high degree of order, and high density of β -crystallites are believed to absorb impact pressure and distribute it throughout the entire fibroin network, and so, confer excellent mechanical strength to the silk network.

The secondary structure of the silk fibroin is organized into three crystalline models called silk I, II, and III. Of these, the silk I is the solid-state structure of silk fibroin stored in the middle silk glands after drying without any external forces. It is a soluble form which remains stable and nonviscous up to high concentration without precipitating, this presumably being essential for secretion of mature silk fibres. By contrast to liquid silk, Nuclear Magnetic Resonance spectra showed that in the solid-state silk I is composed of random-coil domains together with regions with a well-defined ordered structure [5]. Contrarily, during the spinning, the fibroin structure changes from dissolved, less-ordered silk I to solidified, highly ordered and insoluble in water silk II, which features a β -sheet crystalline structure [15]. Silk fibroin possesses the intrinsic capacity to switch from one secondary structure to another and often this event is promoted by different processes: the treatment with alcohols, including ethanol and methanol, the application of physical shear, the exposure to the water annealing process, electromagnetic fields or autoclaving treatment can lead to the transition of conformation of the silk fibroin in its silk II secondary structure [3]. The possibility of controlling the internal secondary structure of silk is a method for successfully adjusting its external properties, such as mechanical strength, solubility, and biodegradability.

Lastly, silk III is a solid form of silk fibroin that features mostly trifold helical chain conformation and is found on the air/water interface [16].

1.2 The silk sericin

Bombyx mori silk sericin is a group of hydrophilic glycoproteins with a molecular weight that ranges from 20 to 400 kDa, depending on the extraction methods, temperature, pH, and processing time. Sericin comprises of 25 to 30% of the cocoon weight and similar to fibroin, it is made of 18 types of amino acids, although there are large differences in the amino acids comprising of two proteins. As mentioned above, the silk fibroin is mainly composed of non-

polar amino acids while the amino acid content of silk sericin is just the opposite; the majority is represented by polar amino acids including Ser, glutamic acid (Glu), aspartic acid (Asp), threonine (Thr), and Tyr [17]. Of course, the chemical composition of the sericin protein is slightly different depending on the silkworm variety.

Sericin is insoluble in cold water; however, it is readily hydrolyzed, and the long protein molecules break down into smaller fractions, which are easily dispersed or solubilized in hot water.

Based on histochemistry and chemical-physical evidence, silk sericin is generally considered to be composed of three layers that externally cover the fibroin filaments: an outermost layer (OL), one middle (ML), and one innermost layer (IL), which coincides with the one closest to the fibroin fibre (Figure 6). OL, ML, and IL layers represent 15%, 10.5% and 4.5% of the total silk protein, respectively. [18]

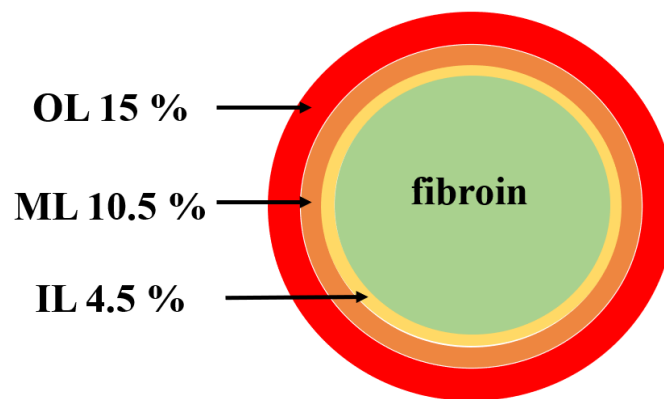


Figure 6: Schematic illustration of layered sericin in a commercial white silk cocoon

The solubility of the sericin which composes the outermost layer of the cocoon resulted in greater sizes in boiling water (at 120 °C for 2 h) than that of more internal sericin, which can be solubilized using an alkaline solution 0.2% of sodium carbonate (Na_2CO_3) after boiling for 30 min [8]. This result depends on the different amino acid composition between sericin layers [19]. As confirmation, a study conducted by Wang et collaborators has revealed that the number of hydrophobic amino acids gradually increased, while the hydrophilic amino acids gradually decreased going from the outside to the inside of sericin layers. This data suggested that the closer a sericin layer is to the silk fibroin fibres, the more similar its amino acid composition is to that of the fibroin fibre.

Moreover, the use of different degumming conditions let gets three sericin fractions that are coloured differently when exposed to the cochineal, a dye obtained from the homonymous

insect belonging to the Coccoidea family, especially from the females of the *Dactylopius*, *Dactylopius coccus* and *Kermes vermilio* species. [18]

Fibroin and sericin showed a different absorption capacity towards the dye, composed of picric and carminic acid. Fibroin can selectively absorb picric acid in an alkaline solution assuming a yellow colour. Sericin, on the other hand, thanks to its marked absorbent properties, can simultaneously absorb picric acid and carminic and since the red colour covers the yellow colour, the fibres take on a red colour. After the degumming process and treatment with the dye, the fibres appeared yellow suggesting that the sericin had been completely removed. As can be seen in Figure 7, the treatment with water at 100 °C has promoted the removal of the only outermost sericin layer, as the fibres still show a relatively intense red colour. Treatment with water at 120 °C causes the elimination of an additional layer of sericin, and thereby fibres assume one pinker colouring, while the treatment with Na₂CO₃ at 100 °C has wholly removed the sericin and fibres turn yellow.

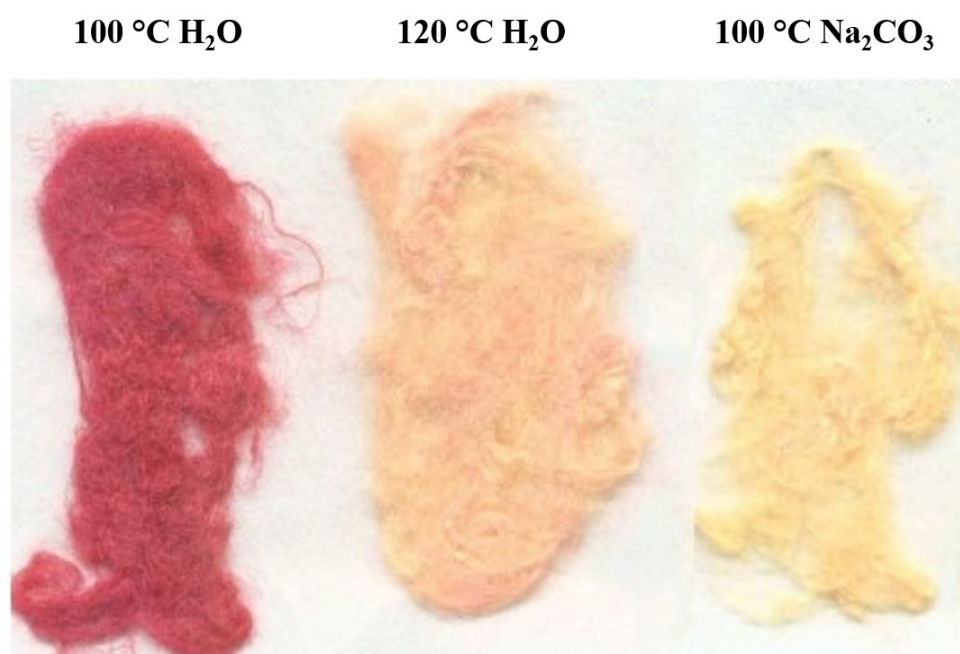


Figure 7: Silk fibres after the cochineal dyeing test. Modified from *Advanced Materials Research*, Wang, Y-J; Zhang Y-Q, *Three-layered sericins around the silk fibroin fiber from *Bombyx mori* cocoon and their amino acid composition*, Vols. 175-176, 158-163 (2011), with permission from Trans Tech Publications

Depending on the solubility, sericin can be classified into three fractions: A, B and C. [9] [3] [10] The first is in the outermost layer of the cocoon, and it is the more soluble fraction in warm water, which contains approximately 17.2% nitrogen with Ser, Thr, Gly, and Asp as more abundant amino acids. In the intermediate layer, sericin B with 16.8% of nitrogen is found, and it is composed of the same polar amino acids as sericin A but in a minor percentage. The amount of polar amino and neutral amino acids decreased (39.34, 38.62 and 23.82% mol in the outer, middle, and inner layers, respectively), with the decrease of the most prominent serine 28.00, 25.57 and 13.32% mol in the outer, middle, and inner layers, respectively, while the serine content in the silk fibroin was 7.65% mol [8]. Lastly, the fraction of sericin C is adjacent to fibroin, and it is insoluble in hot water and contains a lower content of nitrogen, 16.6%. In addition to the amino acids found in sericins A and B, fraction C also contains proline (Pro).

Considering the molecular weight, Takasu et co-workers have identified the three sericin layers as A (250 kDa), M (400 kDa), and P (150 kDa) based in place of synthesis in the anterior, middle, and posterior area of the middle silk gland of the *Bombyx mori* [20] [21]. These sericins are encoded by three different genes called Ser1, Ser2 and Ser3 [22] [23].

Ser1 was the first discovered gene, localized in chromosome 11, locus Src. It is a 24 kb single-copy gene, partially cloned and sequenced, which codes for four main mRNAs of 10.5, 9.0, 4.0 and 2.8 kb, respectively by alternative splicing. [24]

Ser1 has nine exons containing a highly conserved repeating unit of 114 bp, which codes for a peptide of 38 amino acids. The expression of sericin genes, mainly Ser1, is regulated in space and development. During the fifth stage of larval development, Ser1 is transcribed only in 150 cells of the posterior middle silk gland. Of these 150 cells, 42 are specialized in processing a pathway resulting in the production of the 2.8 kb Ser1 mRNA. [25].

The middle silk gland cells also express another sericin gene (Ser2), which is about 12 kb long and composed of 13 exons. It encodes for two proteins produced by alternative splicing with molecular weights of 230 kDa and 120 kDa [20].

Ser2 gene proved to be more complex and variable than any other known gene encoding silk proteins. Its gene organization remembered that of the Ser1 gene, especially the similar size of the first two exons encoding the signal peptides [26]. At the beginning of silkworm development, this gene is expressed in all the middle silk gland cells but, as development proceeds, expression becomes restricted to only the anterior cells. The biological effect of this topological and temporal regulation of the mode of expression of these two genes is the continuous secretion and layering of the different sericins around the silk fibroin thread.

The last gene involved in sericin synthesis, Ser3 gene, was discovered by Takasu et colleagues. It also is located in chromosome 11, locus Src-2, and with a size of about 3.5 kb contains 3 exons and encodes a simple transcript of 4.5 kb. The Ser3 gene is expressed in the anterior part of the middle silk gland after day 5 of the fifth instar [21].

The amino acid compositions of the 400 and 150 kDa sericin are similar to each other, but that of the 250 kDa component was different. This data suggests differences in the coding gene and properties of the 250 kDa sericin from the other two. In detail, sericin A is shown to be the product of Ser3, while Sericin M and sericin P are considered to be the alternatively spliced products of the Ser 1 gene.

In 2013, Dong et colleagues identified other proteins of unknown function in the *Bombyx mori* silk, among them, a large protein BGIBMGA011896 expressed by the novel sericin gene designed as Ser4. It is approximately 40 kb long and, as Ser1, Ser2, and Ser3 genes, localized on chromosome 11. Ser4 contains 34 exons and 33 introns subjected to the six alternative splicing processes to synthesize sericin four proteins with sizes 260-280 kDa localized into the inner and middle sericin layer.

Quantitative real-time PCR was performed to investigate the expression profile of the Ser4 gene in the silk gland. The Ser4 is highly transcribed in the middle and posterior area of the middle silk gland. Compared with the Ser2 gene, during different developmental stages, the Ser4 transcriptional activity gradually reduced from the third instar to the moulting fourth instar and then disappeared in the fifth instar. [27]

Also, the genes MSGS-3, MSGS-4 and MSGS-5 have been included in the sericin expression. MSGS-3, MSGS-4 and MSGS-5 codify mRNA long 3500, 2950 e 450 nucleotides, respectively, but their structures have not yet been fully clarified.

Structurally, sericin is a globular protein consisting of random-coil and β -sheet domains. Wu and collaborators discovered that the sericin is characterized by a higher percentage of random-coil regions (56.8%) compared to the β -sheet conformation (43.2%) [28], corresponding to the amorphous and crystalline regions of the protein, respectively. Changes from random-coil structure to β -sheets quickly occur in response to mechanical stretching properties, moisture absorption, and temperature, where the sol-gel transition occurs. The formation of β -sheet is favoured in the dehydrated state and can be induced by adding cross-linking agents or by treating with organic solvents [29]. In hot water, 50-60 °C or higher, protein adopts its soluble form, but at lower temperatures, the solubility is reduced, and the random-coil structure is converted into β -sheets, resulting in the formation of a gel. [9]

1.3 The silk sericin extraction and recycling

In the textile sector, silk processing from cocoons to the finished clothing articles consists of a series of steps which include: reeling, weaving, degumming, dyeing or printing, and finishing. Among these, degumming is the key process during which sericin is removed from fibroin because it is a waste product and silk fibres gain the softness, whiteness and distinctive shiny aspect highly appreciated by the consumers.

Since all-natural and acquired impurities, other than sericin, such as waxes, pigments and mineral substances, constitute only a tiny fraction and are easily removable, the degumming process can be considered mainly as a breakdown of the peptide bonds of sericin, both with hydrolytic and enzymatic methods, and its subsequent separation from fibroin by solubilization or dispersion in water.

Fibroin and sericin, as components of raw silk, differ considerably in their chemical composition and accessibility into the cocoon. While the former is water-insoluble owing to its highly oriented and crystalline fibrous structure, the latter, as a polymer present on the surface, is more easily accessible to degumming processes. Furthermore, the typical chemical composition of sericin rich in polar amino acids gives the protein a great solubility in aqueous solutions containing soap, alkali, synthetic detergents, or organic acids. [30] [31]

Despite what has been mentioned so far, recycling sericin after reeling and processing silk has long been difficult due to the complexity of recovery, high cost and low efficiency. For this reason, an extensive analysis of the extraction conditions and raw silk refining processes are important because these conditions could influence the final properties of sericin. In particular, the degumming conditions should be carefully controlled because sericin is highly susceptible to heat. [32] Various parameters, such as the types of chemicals and their concentrations, the temperature, and the treatment time will involve the degumming rate, molecular weight distribution, and even the amino acid composition of sericin. Finally, the extraction efficiency is also relevant because it will determine the economic value of the sericin extraction method. [33]

To date, there are several methods of silk degumming and raw silk refining, divided into chemical, physical, and enzymatic processes (Figure 8). [8] [34] [35]

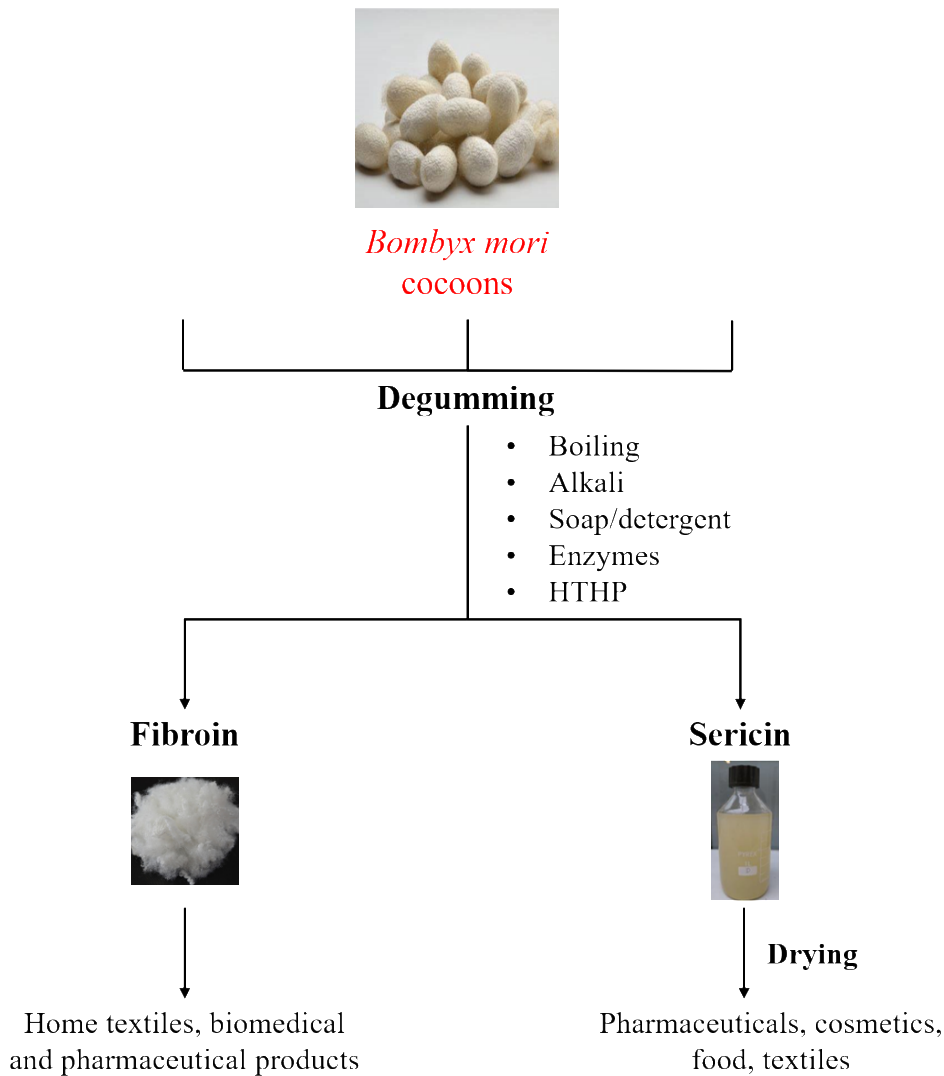


Figure 8: Silk degumming methods and recovery of the silk fibroin and sericin proteins

In the traditional process of degumming in silk manufacturing, chemical extraction with soaps and detergents is now the most widely adopted industrial technique since it causes no fibre degradation and is a relatively simple process compared to its removal by enzymes, heat or pressure. [30] One of the conventional soap-alkaline degumming processes expected the boiling of cocoons at atmospheric pressure in a Na_2CO_3 solution, resulting in the complete removal of sericin.

Yun et co-workers suggested that the optimal conditions for the *Antheraea mylitta* sericin extraction required treatment with 0.02 M Na_2CO_3 and a boiling time of 60 min. These parameters resulted in optimal conditions to extract protein from cocoons with high yields and

minimum degradation. In detail, six different extraction methods recapped in Table 1 were compared to extract sericin from *Antheraea mylitta* cocoons.

Degumming method	Temperature (°C)	Time
<i>Soap-alkaline</i> <i>Na₂CO₃ (0.02% w/v); Marseilles soap (0.03% w/v)</i>	100	1 h
<i>Hot water</i>	120	1 h
<i>Urea (8 M)</i>	80	10 min
<i>Urea (8M) / mercaptoethanol (5% v/v)</i>	80	10 min
<i>NaCl (1% w/v)</i>	25	15 h
<i>Na₂CO₃ (0.01-0.06 M)</i>	100	15-120 min

Table 1: Summary of degumming methods used in the study conducted by Yun et colleagues. Modified from *International Journal of Biological Macromolecules*, Yun, H.; Oh, H.; Kim, M. K.; Kwak, H. W.; Lee, J. Y.; Um, I. C.; Vootla, S. K.; Lee, K. H., *Extraction conditions of Antheraea mylitta sericin with high yields and minimum molecular weight degradation*, 52, 59-65 (2013), with permission from Elsevier

After the extraction, the solutions were filtered to remove the remaining cocoon pieces. Subsequently, the cocoon pieces were washed several times with warm water, dried at 50 °C for three days, and conditioned at room temperature for 12 h before being observed by the SEM micrographs (Figure 9). Finally, to quantify how much sericin could be removed from *Antheraea mylitta* cocoons by each extraction method, the cocoons were weighed before and after the extraction to determine the degumming ratio (%) as $[(W_0 - W_f) / W_0] \times 100$, where W_0 and W_f are the initial weight and the final weight of the cocoon pieces, respectively.

Before degumming, the fibroin filaments were kept together by the sericin visible in the upper layer (arrow) of the cocoon surface (Figure 9 A). After the soap-alkaline degumming, the surface of the cocoon fibre became clean, and the two brins of fibroin were separated. This result suggested the extraction of sericin from the cocoon of 100% (Figure 9 B) with the highest extraction rate ($19.5 \pm 1.90\%$, mean value \pm standard deviation). Contrary, in the SEM images of the *Antheraea mylitta* cocoon after the extraction process using the hot-water

(Figure 9 C) and urea-mercaptoethanol (Figure 9 D), the residues of sericin (indicated by arrows) were visible due to the low degumming ratio.

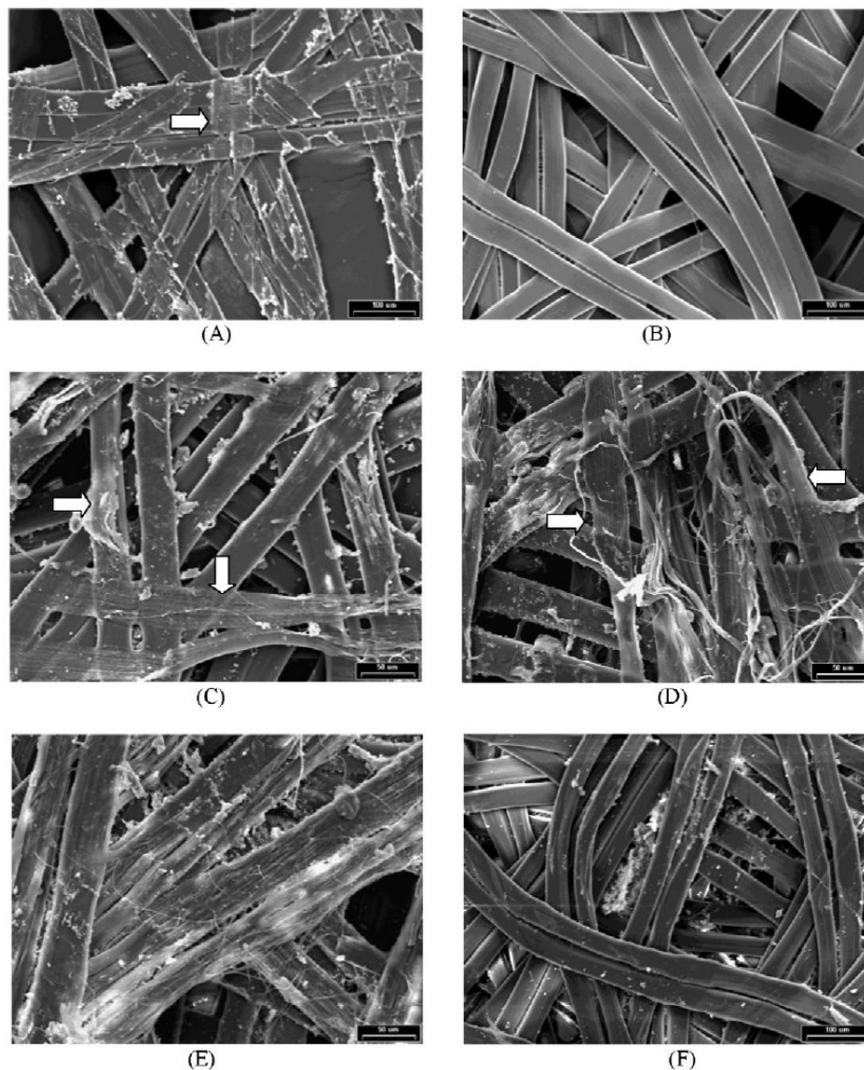


Figure 9: SEM micrographs of the *Antheraea mylitta* cocoon fibres before (A) and after different extraction methods, including soap-alkaline (B), hot-water (C), urea-mercaptoethanol (D), NaCl (E) and Na₂CO₃ (F). Scale bar: 100 μm (A, B, F); 50 μm (C, D, E). Reproduce from *International Journal of Biological Macromolecules*, Yun, H.; Oh, H.; Kim, M. K.; Kwak, H. W.; Lee, J. Y.; Um, I. C.; Vootla, S. K.; Lee, K. H., *Extraction conditions of Antheraea mylitta sericin with high yields and minimum molecular weight degradation*, 52, 59-65 (2013), with permission from Elsevier

Interestingly, the sericin that was located between the two brins of fibroin was removed although the degumming was not complete. The degumming ratios of the *Antheraea mylitta* cocoons subjected to these two methods were less than 9.0%.

The addition of sodium chloride (NaCl) can increase the ionic strength of the sericin solution facilitating its dissolution. However, this was not enough to get a suit degumming, as striations on the surface of the fibre suggested in the SEM micrograph (Figure 9 E). The degumming ratio for the cocoon was $13.5 \pm 2.0\%$ (mean value \pm standard deviation) when 0.02 M Na_2CO_3 was utilized for the extraction at 100°C for 30 min.

Figure 9 F illustrates the SEM image of the cocoon after the sodium carbonate degumming. The surface of the cocoon fibre was not as clean as the soap-alkaline method, but the two brins of fibroin could be observed, and neither a stratified surface or residues of sericin could be observed, indicating a relatively high degumming efficiency.

Because the Na_2CO_3 extraction has the best yield among the other examined extraction methods, Yun et collaborators found its optimal conditions. To do this, they decided to examine the time of sodium carbonate degumming treatment and the sodium carbonate concentration to determine their effect on the extraction ratio and amino acid composition of the sericin.

After 60 min of extraction, the degumming ratio reached a plateau ($15.5 \pm 1.0\%$, mean value \pm standard deviation) at the Na_2CO_3 concentration 0.02 M and did not significantly increase further (Figure 10, panel A). Regarding the molecular weight distribution, high performance-size exclusion chromatography (HP-SEC) analysis identified a peak at 7 mL of elution volume, which corresponds to 200 kDa, and broadband between 9 and 17 mL of elution volume, which coincides to 30-150 kDa. When the extraction time increased, the intensity related to the 200 kDa band decreased following degradation of the sericin. However, the degumming ratio did not change significantly after 60 min of extraction, indicating that there is some degradation of the *Antheraea mylitta* sericin by sodium carbonate when the extraction time is extended (Figure 10, panel B).

Also, the increase of sodium carbonate concentration caused a reduction of the sericin molecular weight. Therefore, sericin molecules that have relatively low molecular weights will be continuously degraded into more low molecular weights and finally removed from the dialysis tube.

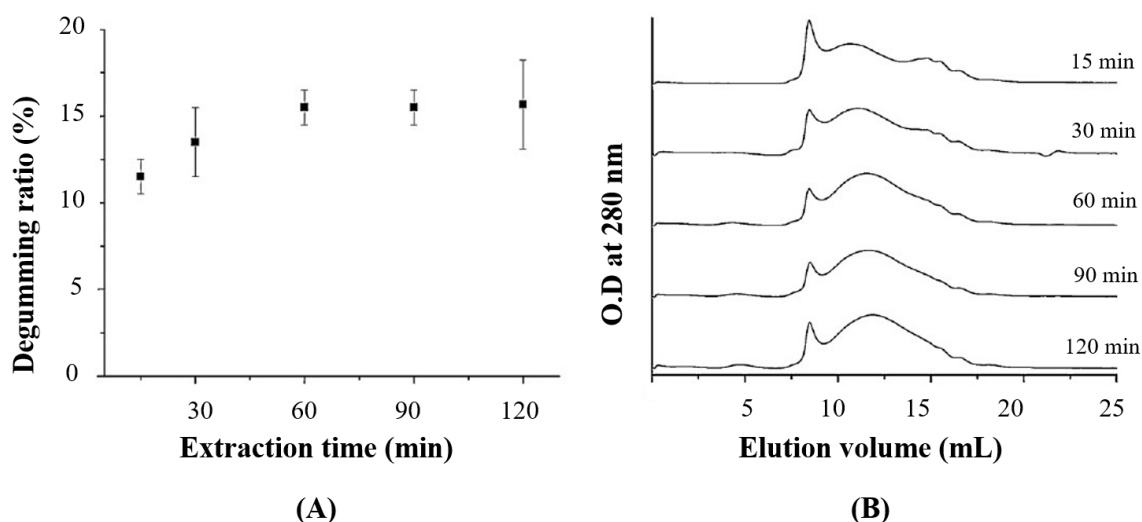


Figure 10: Effect of the Na_2CO_3 concentration on the degumming ratio of the *Antheraea mylitta* cocoon (A) and the molecular weight distribution of the extracted sericin (B). The extraction time was set at 60 min. Adapted from *International Journal of Biological Macromolecules*, Yun, H.; Oh, H.; Kim, M. K.; Kwak, H. W.; Lee, J. Y.; Um, I. C.; Vootla, S. K.; Lee, K. H., *Extraction conditions of Antheraea mylitta sericin with high yields and minimum molecular weight degradation*, 52, 59-65 (2013), with permission from Elsevier

To stay the same degumming ratio, prolonged extraction time over 60 min and the Na_2CO_3 concentration higher than 0.02 M can significantly decrease the final yield. [33]

Although the sericin degumming in a solution of Na_2CO_3 has been adopted many times, this method makes it challenging to recover high-quality silk sericin for further studies or applications, owing to the purification steps needed to remove the chemical impurities. Moreover, the degumming process causes a large amount of sericin degradation and hydrolysis, reducing its natural weight with an unavoidable loss of some functional activities. Degumming by boiling cocoons in the water at room temperature or increased pressure by autoclaving (HTHP) (120 °C for 2 h) remains the physical method of extraction mostly used in the laboratory. In both cases, impurities are not introduced, obtaining sericin aqueous solutions that can be used immediately for further applications. However, this degumming procedure is not usually applied in the silk industries because the treatment is too long, and causes significant fibroin damage without complete elimination of all the sericin layers from the silk fibres. [31]

SEM images published by Gimenes et colleagues confirmed that the hot water treatment of *Bombyx mori* cocoons preserved the primary structure and composition of the sericin enabling

its use in the development of biomaterials. However, it did not allow the removal of all protein layers from the silk fibres (Figure 11 b). [36]

The sericin C remained on the surface of the fibres because its β -sheet domains make it slightly soluble in water compared to sericin A and B and more strongly linked with the hydrophobic structure of fibroin. Sericin extracted by boiling cocoons in the water at 120 °C showed a yield of $21.99 \pm 0.96\%$ (mean value \pm standard deviation) and a range of molecular weight between 100 kDa and 200 kDa. Contrary, the chemical treatment of the cocoon with Na_2CO_3 (0.5% w/v) at 120 °C broke all protein interactions, making the water permeation inside the protein easier and complete elimination of sericin, as shown in Figure 11 a. While achieving the highest yield of $30.04 \pm 0.83\%$ (mean value \pm standard deviation), Na_2CO_3 degumming process produced the hydrolysis of sericin chain structure, losing potential properties, due to the reduction of its molecular weight below the 100 kDa.

As sericin is ordinarily present in silk industry wastewater, the recovery of sericin is also a critical environmental issue to be investigated. [37]

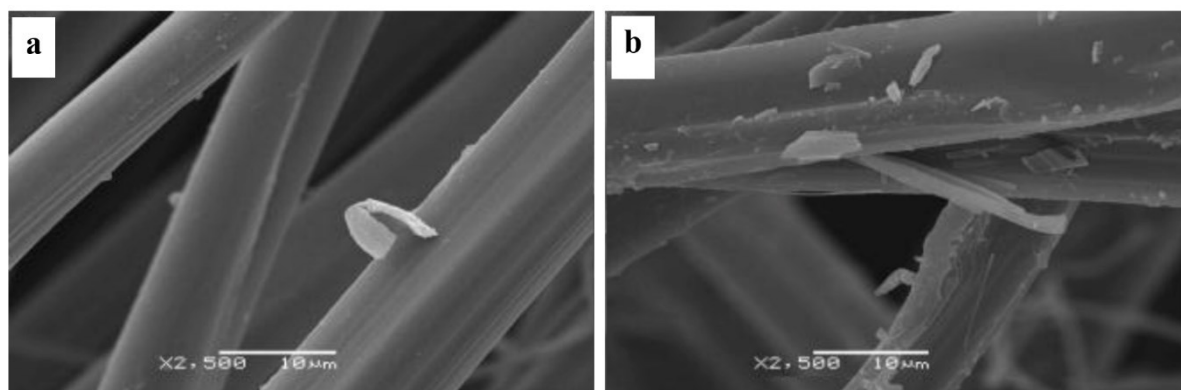


Figure 11: Surface morphology of cocoons degummed in 0.5% w/v Na_2CO_3 solution (a) or hot water (b). Scale bar: 10 μm (x 2,500). Reproduce from *International Journal of Chemical Engineering and Applications*, Gimenes, M. L.; Silva, V. R.; Vieira M. G. A.; Silva, M. G. C.; Scheer A. P., *High Molecular Sericin from Bombyx mori Cocoons: Extraction and Recovering by Ultrafiltration*, 5 (3), (2014), with permission from International Journal of Chemical Engineering and Applications

In the second part of the work conducted by Gimenes et collaborators, the ultrafiltration method resulted in an alternative degumming process useful to recovery and recycling sericin by-products. The degummed sericin in water was submitted at the ultrafiltration process to obtain retentate fractions of sericin enriched of high molecular weights (above 100 kDa) using a membrane of filtration with a cut-off of 50 kDa. [36]

Along this same research line, Wu et colleagues announced the ultrafiltration in combination with nanofiltration as the most potent example of membrane separation technology for recovery of sericin from the processing waste of silk floss (Figure 12).

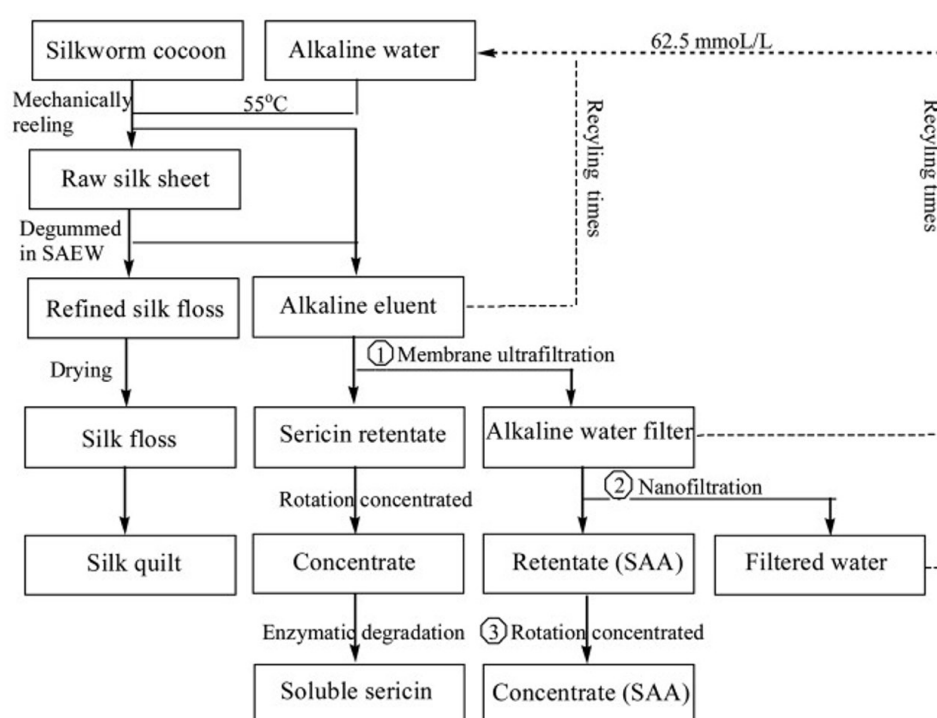


Figure 12: Schematic diagram for the recovery of the sericin by ultra- and nano-filtration from the alkaline eluent waste that generated from the processing of silk floss and the refining solution. Sericin was degummed with SAEW (pH= 11.5) to obtain the refined silk floss and the refining solution of sericin proteins. After ultrafiltration of the alkaline eluent, the sericin retentate with a range of high molecular mass sericin polypeptides was collected and concentrated by using the rotary evaporation. Contrary, the filtrate, contained lower molecular mass sericin oligopeptides and free amino acids, was directly passed through the nanofiltration membrane. The retentate contained sericin amino acids (SAA) and the filtrate (pure water) that could be re-used for preparing the alkaline eluent. Finally, the retentate was concentrated to a 20% (w/v) SAA by rotary evaporation to use for the synthesis of the sericin-based surfactant. Reproduced from *RSC Advances*, Wu, M. H.; Zhang, Y. Q., *Nanofiltration recovery of sericin from silk processing waste and synthesis of a lauroyl sericin-based surfactant and its characteristics*, 4, 4140, (2014), with permission from Royal Society of Chemistry

In the study, the sericin was degummed in the strongly alkaline electrolyzed water (SAEW, pH 11.5), defined by Cao et colleagues as an environmentally friendly and pollution-free degumming agent that allows highly efficient, low-cost recovery of silk protein, compared to the traditional neutral soap method. [38]

The work aimed to improve the processing technology used traditionally in the industrial production of silk fibres and to produce a friendly environmental silk protein-based surfactant to facilitate efficient recovery and use of sericin from wastewater. This way represented an alternative to the recycling of water and reducing the severe environmental pollution resulting from the strongly alkaline waste that contains the sericin released from the traditional procedure. [39] Despite the advantages above, this method also faces the common problem of high cost and low processing efficacy, and achieving industrial-scale recovery could require further development.

Silva et colleagues focused the attention on evaluating different extraction processes (in hot water or Na₂CO₃ solution) and the purification of silk with ultrafiltration to recovering *Bombyx mori* sericin with high molecular weight. [40]

Statistical analysis showed a significant effect of the temperature on the extraction efficiency ($p < 0.05$). In detail, the extraction with high temperature, above 120 °C and without chemical additives, provided an extraction yield between $22.5 \pm 0.4\%$ and $24.0 \pm 0.5\%$ (mean value \pm standard deviation). Among the different extraction conditions taken into consideration in the study, the degumming conducted with sodium carbonate (5.0 mg/mL) at 120 °C remained though the best with the maximum extraction yield ($30.1 \pm 0.9\%$, mean value \pm standard deviation), in accordance to what published by Gimenes et colleagues in 2014 [36].

The extraction yield is strongly correlated to the degradation grade of the sericin, as confirmed by molecular weight profiles of samples. HP-SEC showed peaks of sericin extracted with pure water at high temperature between 200 kDa and 100 kDa and sericin peptides fractions lower than 100 kDa. In comparison, the sericin solution extracted with sodium carbonate displayed molecular weights lower than 50 kDa, thereby indicating higher hydrolysis of sericin than that caused by the autoclave treatment.

The rheological profile revealed that an increase of sericin concentration in water solution is responsible for the behaviour from the Newtonian to the Pseudoplastic fluid. This behaviour is due to the increase of interactions between hydroxyl groups of the polar amino acids, allowing the gelling of the aqueous sericin solution.

The concentrations of sericin purified by the ultrafiltration system were fixed at 0.1 and 1.0 mg/mL to evaluate the effect of the sericin mass variable in the permeate flux. Polysulfone

membrane was used with cut-off 50 kDa, feed flow of 1.0 and 2.0 L/min, and transmembrane pressures were set to 0.03, 0.05, 0.07, 0.09, 0.12, and 0.12 MPa.

The feed flow rate showed a significant effect on the permeate flux for transmembrane pressure above 0.03 MPa ($p < 0.05$), while the protein concentration showed statistical significance for all ranges of transmembrane pressure considered.

For the feed flow of 1.0 L/min and 2.0 L/min, the cross-flow velocities estimated were 0.1 m/s and 0.2 m/s, respectively. However, the amount of sericin near the membrane surface for the feed flow 2.0 L/min was higher than 1.0 L/min, what could have increased the resistive effects and promoted the slight increase of the permeate flux.

The authors also investigated the dependence of the permeate flux to transmembrane pressure, for each concentration fixed at a feed flow of 1.0 L/min. The data evidenced that the highest permeate flux for sericin solution of 0.1 mg/mL was $104.6 \pm 9.7 \text{ kg m}^{-2} \text{ h}^{-1}$ and $42.0 \pm 6.1 \text{ kg m}^{-2} \text{ h}^{-1}$ (mean value \pm standard deviation) to transmembrane pressure of 0.015 MPa and 0.07, respectively.

Regarding the molecular weight distribution, the retentate flow had a large number of molecules with high molecular weight, above 200 kDa. In contrast, the permeate flow showed two main groups of molecules: one first with molecular weight 200 kDa, due to the initial process there did not appear to be resistance on the surface of the membrane, and a second sizeable molecular group of molecules lower than 50 kDa.

In recent years, various studies have dealt with the removal of sericin by using proteolytic enzymes. [30] [41] [42] Being silk degumming is a high resource-consuming process and ecologically questionable for the high environmental impact of effluents, the development of an effective extraction process based on enzymes as active agents would entail savings in terms of water, energy, chemicals, and effluent treatment. This could be made possible by the milder treatment conditions, the recycling of processing water, the recovery of valuable by-products such as sericin peptides, and the lower impact of effluents on the environment.

Several acidic, neutral, and alkaline proteases have been utilized for the manufacturing of silk protein powder in enterprises. However, some scientific studies define alkaline proteases as better than acidic and neutral ones in terms of uniform sericin removal, retention of textile properties, and improvement of surface smoothness handle, and lustre of silk.

Regarding this, Vaithanomsat et colleague demonstrated that the optimal conditions for a commercial serine protease to hydrolyze silk fibres were in the basic environment (pH: 8.0-9.0) with a temperature comprised between 55 and 60 °C, as shown by the data of response surface methodology (Figure 13). The same response surface curves showed a strong

correlation between the enzymatic concentration and the degree of hydrolysis ($p < 0.05$) (Figure 13). When the enzyme concentration raised, the hydrolysis level was consistently increased; on the contrary, the rate of reaction would seem to be slightly dependent on reaction time. The degree of hydrolysis arrived at the highest value of about 84% obtained from the most optimum hydrolysis condition, which corresponded to the enzyme concentration 1% w/w ($\text{mg}_{\text{enzyme}} / \text{mg}_{\text{substrate}}$) and reaction time for sericin hydrolysis of 60 min. [43]

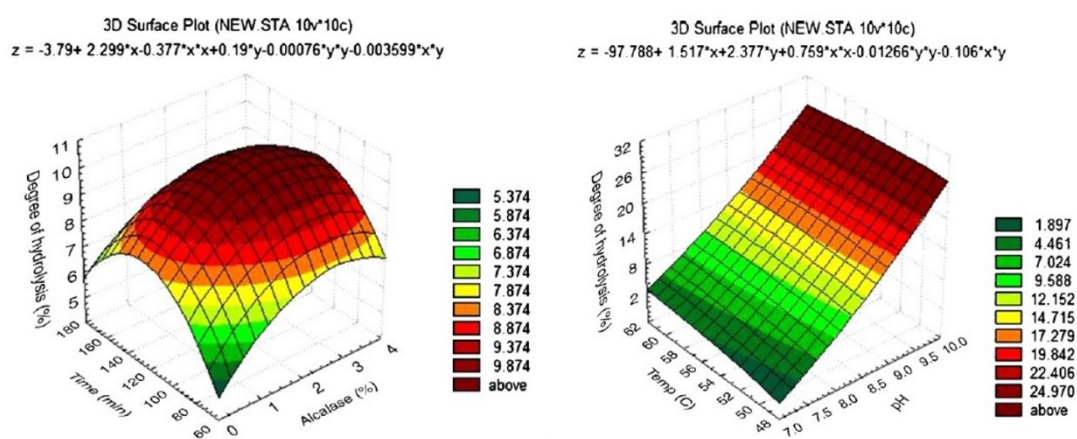


Figure 13: Response surface curves of the degree of hydrolysis (%) in correlation with the enzyme concentration (% w/w) and time (min) (left figure), pH and temperature (right figure). Reproduced from *Separation and Purification Technology*, Vaithanomsat, P.; Kitpreechavanich, V., *Sericin separation from silk degumming wastewater*, 59 (2), 129–133 (2008), with permission from Elsevier

In 2003 Freddi et co-workers studied the effectiveness of alkaline (3374-L, GC 897-H), neutral (3273-C), and acid (EC 3.4 23.18) proteases as degumming agents for the raw silk fabric (crêpe). [30]

Briefly, silk was extracted by using an alkaline solution containing Marseille soap (10 mg/mL) and Na_2CO_3 (1 mg/mL), setting the temperature at 98 °C for 1 h. After the degumming process, silk was rinsed with warm distilled water, dried at room temperature, and finally extracted with petroleum ether to remove residual fatty acids, before being immersed in a buffer solution (Tris-HCl or citric acid-Na phosphate) containing the enzyme in different dosages (0.05-2 U/g fabric). In this phase, the time of treatment was set between 5 and 240 min to study the kinetics of sericin removal.

While the soap-alkaline extraction displayed the complete removal of sericin with the degumming loss corresponded to 27% w/w, the maximal content of protein removed in 1 h

with enzymatic treatment was 17.6%, 24%, and 19% w/w for 3374-L (2 U/g fabric), GC 897-H (1 U/g fabric), and 3273-C (0.1 U/g fabric), respectively. It is worth noting that the acid protease EC 3.4.23.18 displayed a very low degumming loss (7.6% w/w, 60 U/g fabric) still after 3 h of treatment.

These results may seem disappointing because none of the proteases used in the study allowed the attainment of the complete loss of the sericin from fibroin fibres under the experimental conditions adopted. However, the crêpe fabric is one of the most difficult substrates to treat, owing to the presence of highly twisted weft yarns, and this often requires a high content of alkalis also during standard chemical degumming.

Likely, other factors besides the lack of hydrolytic power of proteases played a role in lowering the extent of degumming. This hypothesis seemed to be confirmed from the morphological characteristics of the samples, which got very close to the desired degumming loss. In detail, the morphological analysis showed that sericin was eliminated from the warp yarns of the crêpe fabric (Figure 14 a), but not from the highly twisted weft yarns, which still exhibited the presence of sericin deposits within the most internal parts of the close fibre texture (Figure 14 b–d).

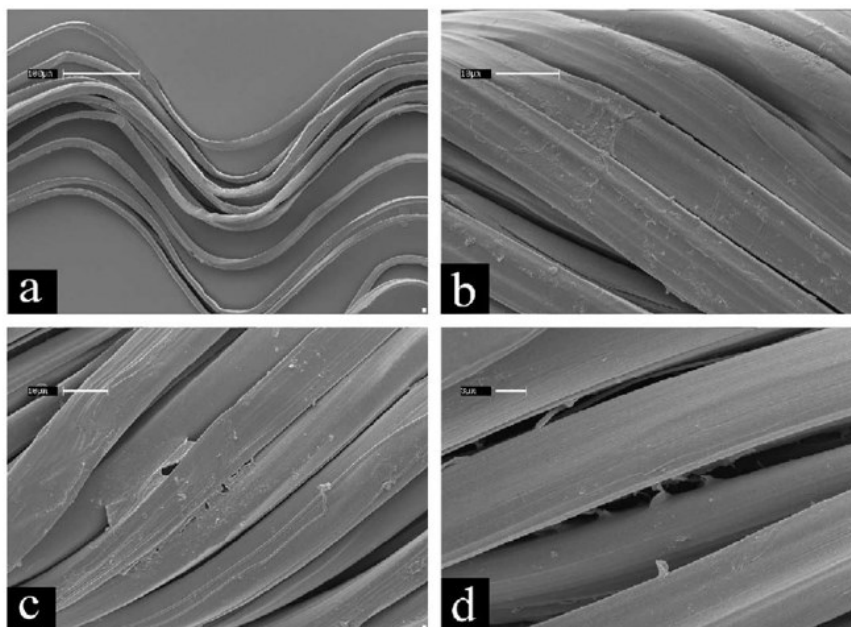


Figure 14: SEM images of warp yarns (a) and weft yarns (b–d) of the crêpe fabric after enzymatic degumming. Scale bar: 100 µm (a); 10 µm (b,c), 3 µm (d). Reproduced from *Journal of Biotechnology*, Freddi, G.; Mossotti, R.; Innocenti, R., *Degumming of silk fabric with several proteases*, 106, 101–112 (2003), with permission from Elsevier

It is interesting to note that the deposits were mainly located at the cross over points between warp and weft yarns and/or in the more internal parts of the weft yarns.

These data confirmed that proteases failed to remove sericin from the highly twisted weft yarns altogether. Since the ability of these enzymes to hydrolyze sericin is undisputed, the observed behaviour can be attributed to other factors, such as the lack of an adequate mechanical agitation in the lab-scale degumming system adopted in the study, limiting the penetration of enzymes into the close the texture of weft yarns.

Finally, the kind of enzyme used, enzyme dosage and treatment time can change the chromatographic pattern of soluble sericin peptides.

After 1 h of the alkaline and neutral proteases treatment (dosage: 2 U/g fabric), HP-SEC profiles revealed a mixture of sericin peptides ranging from 5 to 20 kDa (Figure 15) contrary to the native sericin which covers a much wider molecular weight range from 40 to 400 kDa.

The molecular weight distribution of sericin by-products is mostly dependent on the specific mechanism of action of proteases, that is, the selective cleavage of target peptide bonds along the protein chains resulting in the formation of a range of small size soluble peptides.

In particular, the sericin treated with the neutral protease 3273-C showed higher molecular weights than those hydrolyzed using the two alkaline proteases 3374-L and GC 897-H. This characteristic can be attributed to the different degree specificity of the proteases for the substrate, that is, to the chemical structure of the target cleavage site.

Despite the observations emerged in work published by Freddi et colleagues, in the silk processing, the degumming system must be optimized with the aim to scale-up the process for its implementation on industrial equipment.

Particular attention will have to be given to the investigation of the mechanical agitation effect on the degumming efficiency of proteases. This parameter is likely to enhance enzyme penetration within the closest parts of the fabric texture and to make sericin removal more effective without causing significant damage to the textile goods.

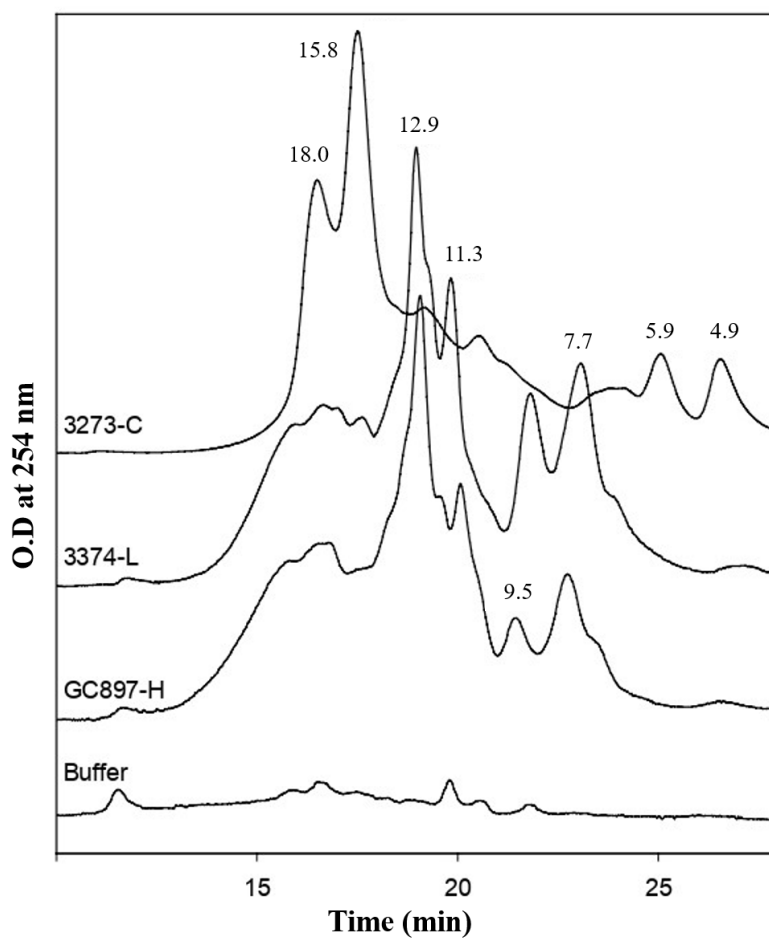


Figure 15: HP-SEC chromatograms of soluble sericin peptides obtained by enzymatic degumming using the alkaline (3374-L, GC 897-H) and the neutral (3273-C) proteases. Enzyme dosage: 2 U/g fabric, time of treatment: 1 h. Modified from *Journal of Biotechnology*, Freddi, G.; Mossotti, R.; Innocenti, R., *Degumming of silk fabric with several proteases*, 106, 101-112 (2003), with permission from Elsevier

As a consequence of complete sericin elimination, the quality of silk goods in terms of handle, appearance and tensile properties is expected to increase, due to the lower extent of chemical and physical stresses to which silk is subjected to during enzymatic processing, as compared to the traditional chemical process.

In 2020 Eom et collaborators proposed a convenient method to extract fibroin and sericin from *Bombyx mori* silk cocoons using an ultrasound system and food-grade enzymatic treatment. [42]

The work aimed to simplify the degumming process of the silk, instead of using the traditional conditions of high salt and temperature, and produce low molecular weight silk peptide evaluating their inhibitory effect on solar ultraviolet-induced skin inflammation.

In brief, *Bombyx mori* silk cocoons 1% (w/v) were dissolved in NaOH solution at 25 °C. For ultrasound system power, amplitude, and pulse were set to 750 W, 80%, and 20 s/20 s, respectively, maintaining an unchanged temperature. After ultrasonication, silk was titrated with hydrochloric acid (HCl) to the final pH of 7.0 and treated with pancreatin, protease, papain or bromelain enzymes (0.5% w/v) at 25 °C for 48 h. Finally, the inactivation of the enzyme was performed by heating at 100 °C for 10 min.

Despite the use of 8 M urea, 9 M lithium bromide or 50% w/v calcium chloride represents one of the most widely used methods for silk degumming, from an economic standpoint this practice is not suitable for mass production of silk given the low-efficiency of extraction. [8] To overcome this problem, in work published by Eom et co-workers, ultrasonic treatment was applied to the NaOH solution containing fibroin and sericin using concentrations of the salt corresponded to 0.1 N and 0.25 N.

The maximum yield of soluble silk protein was about 60% w/w and was reached after 4 h at 0.1 N NaOH and after 2 h at 0.25 N NaOH; at the same salt concentrations, the yield of extraction did not exceed 50% within 9 h without the acoustic wave employment. In fact, ultrasound-assisted extraction in the low alkaline solution can increase protein content and decrease extraction time. This is possible thanks to the ultrasonic cavitation, which improves the extraction efficiency by reducing the size of the treated material and increasing its surface area of contact with the solvent.

Electrophoresis SDS-PAGE was performed to determine the molecular weight distribution of soluble silk protein, enzymes, and hydrolyzed silk peptide after extraction using ultrasound (Figure 16).

Silk protein showed a wide range of molecular weights with more intense bands over 15 kDa, attributable to the heavy fibroin chain.

Because the signal from each enzyme was not clearly observed, the bands from enzyme-treated samples related to the well 6, 7, 8 and 9 were considered to be those of silk peptide. In particular, pancreatin and fungal protease showed a lower capacity to hydrolyze silk peptide than papain and bromelain, as suggested by the appearance of bands related to molecular weights above 25 kDa.

On the other hand, ultrasound treatment after enzyme treatment of silk peptides was not useful for the production of low molecular weight silk molecules.

After 24 h of the reaction of silk cocoons with papain, in the case of ultrasonic treatment in a neutral phase, gel permeation chromatography analysis (GPC) did not reveal significant changes in molecular weight distribution of silk peptide.

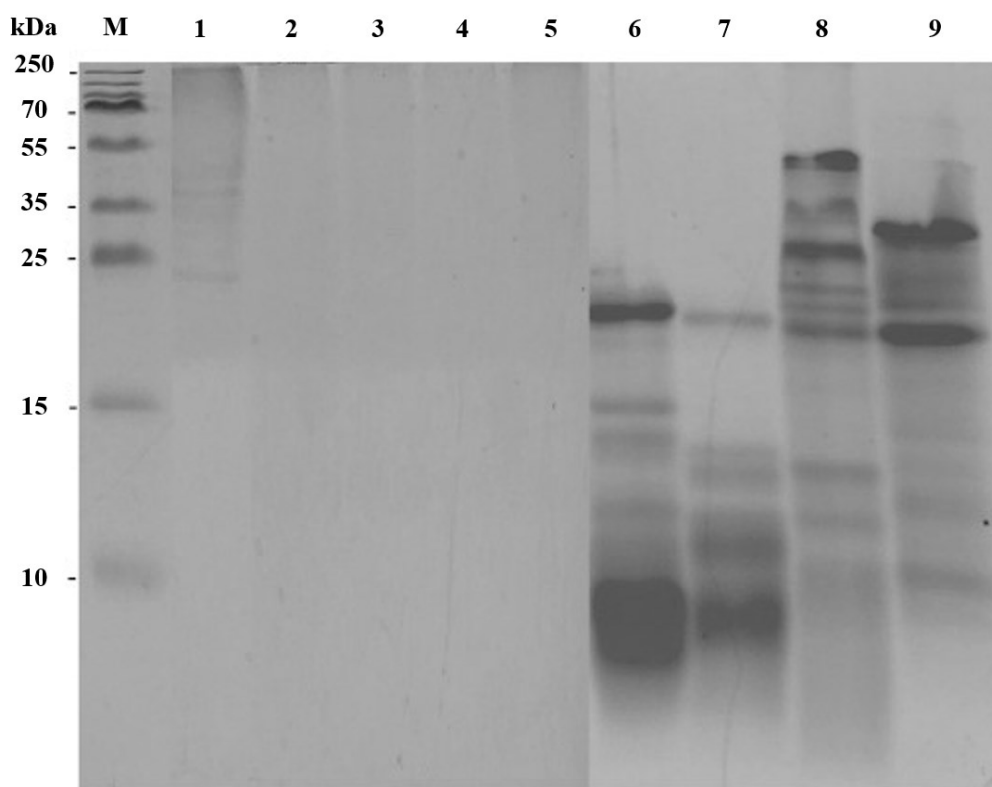


Figure 16: Electrophoresis SDS-PAGE of silk peptide treated with different enzymes (0.5% w/v). M: marker; 1: soluble silk protein extracted by ultrasonication; 2: papain; 3: bromelain; 4: pancreatin; 5: protease; 6: 1+2; 7: 1+3; 8: 1+4; 9: 1+5. Voltage was set to 80-120 V. Reproduced from *Ultrasonics – Sonochemistry*, Eom, S. J.; Lee, N. H.; Kang, M. C.; Kim, Y. H., Lim, T. G.

Song, K. M., *Silk peptide production from whole silkworm cocoon using ultrasound and enzymatic treatment and its suppression of solar ultraviolet-induced skin inflammation*, 61, 104803 (2020), with permission from Elsevier

Contrary, in 0.1 N NaOH solution, as the ultrasound treatment time became longer, the extracted silk peptide showed a wide range of molecular weight (3.4-130 kDa) and high molecular weight of silk proteins were extracted owing to ultrasonic waves.

To explore the potential anti-inflammatory activity of silk peptide on the skin, Eom et colleagues investigated their effect on inflammatory signalling pathways using sUV-induced mouse epidermal JB6 P+ cells.

Only the silk peptide produced by ultrasonication and following papain treatment showed inhibition of sUV-induced expression of COX-2 in a dose-dependent manner. Moreover, the

same silk peptide significantly reduced PGE₂ production, a product of the COX-2 enzymes, which plays a crucial role in UV-induced skin inflammation.

Years ago, Wu et co-workers developed another extraction procedure to recover sericin from wastewater by using a chilled ethanol precipitation method. The extraction yield was gradually enhanced as the ethanol concentration was increased, but the approach, although being effective and simple, did not sound economical and eco-friendly when applied to an industrial scale. [28]

In a past study, silk sericin was also successfully and wholly removed from raw silk by heating the cocoons to 110 °C in a water bath inside an infrared dyeing machine. Infrared heating is becoming popular in industries as a degumming method, thanks to the easy control of the heating temperature, its convenient application with substantial savings in terms of energy consumption as compared to the conventional high-temperature high-pressure process. [44]

The higher yield obtained with infrared heating was attributed mainly to the fact that the process consisted of radiation heating, where the energy was transferred directly to the material in the form of electromagnetic waves. The radiation caused the water to behave like an abrading agent, easing the sericin separation from the silk in addition to increasing its solubility in water via heat. This could also explain the lower degree of protein degradation observed in this method. [35]

In 2017 Lo et Chao studied a more eco-friendly and green degumming than conventional textile industry processes of extraction to remove sericin from raw silk fibres.

The goal of the research was to propose CO₂ supercritical fluid as an alternative technique of extraction which could preserve the high quality of silk fibres and to overcome the main limits of traditional degumming processes, including the high amount of wasted energy, the production of high temperatures as well as many chemicals released in the industrial effluents with consequent impact on the environment. [45]

Briefly, *Bombyx mori* raw silk was pre-treated with acetic, citric or tartaric acid solution maintaining pH below the isoelectric point of the silk proteins to charge them positively. In this way, the carboxylic group of the organic acid can replace the hydrogen bonds of the proteins helping to destabilize their amino acid structure.

After 6-8 h, silk was removed from the bath and moved to the supercritical carbon dioxide containers adding a surfactant between glycol type nonionic surfactant, lipidation glycol type nonionic surfactant, lauryl alcohol, sodium lauryl sulfate. The addition of the surfactant creates a hydrophilic site under supercritical carbon dioxide conditions and once processed,

the sericin can be removed from the fibroin quite easily in a pure water bath. In the supercritical carbon dioxide containers, the temperatures were set between 95 °C and 127 °C, CO₂ levels were kept between 150 and 400 atm and the processing time between 45 and 70 min.

Figure 17 displays the morphology of silk fibres after conventional degumming by the Na₂CO₃ solution (panel b) and by the supercritical CO₂ fluid (panel c) extraction compared to the untreated silk fibres (panel a). The latter appeared still bonded together with the sticky coating protein; contrary, sericin was eliminated with success from the surface of fibroin fibres by the supercritical CO₂ treatment.

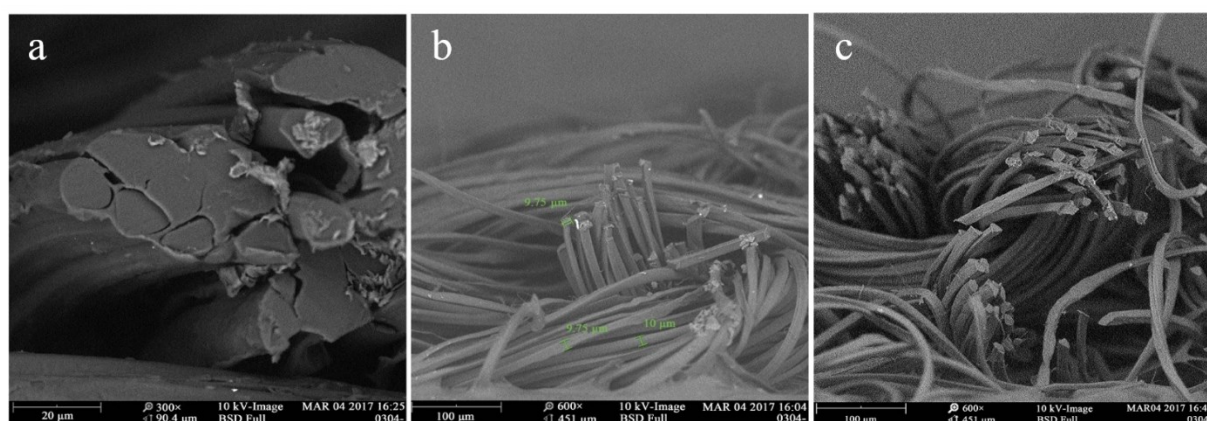


Figure 17: Commercial grade silk fibres before degumming (a) and after degumming with Na₂CO₃ (b) and supercritical CO₂ fluid (c), respectively. Scale bar: (a) 20 μm (x 300); (b,c) 100 μm (x 600). Modified from *Journal of Materials Science and Chemical Engineering*, Lo, C. H.; Chao, Y., *Degumming of Silk Fibers by CO₂ Supercritical Fluid*, 5, 1-8 (2017) (Open access)

Lastly, the colour dyeing ability testing was performed to identify the presence of sericin on untreated and degummed silk samples, respectively. Three shade acid dyes were used: red 2G-T, yellow 2RN-T and Navy blue RN-T deep, heated to 90 °C for 30-40 min. For each dyed fabric sample, reflectance (%) was measured after dyeing expressing the colour strength of dyed fabric by its colour strength (K/S) (data listed in Table 2).

Before the degumming process, the simultaneous presence of silk proteins was responsible for the evident retention of the dye by the fibres with colour strength values almost two times higher than degummed silk fabric.

The removal of sericin using either method makes it difficult for the silk fibres to retain the dye. However, the test did not show significant differences in the dyeing process of silk fibres

when comparing the sample group using the supercritical CO₂ method to the conventional scouring process. This result stays consistent with all three colours of dyes tested.

Silk fabric treatment	Type of dye		
	Red 2G-T	Yellow 2RN-T	Navy blue RN-T
<i>Untreated</i>	20.3	15.0	15.6
<i>Na₂CO₃ degumming</i>	6.6	4.4	4.0
<i>supercritical CO₂ process</i>	8.2	6.5	6.8

Table 2: Colour strength (K/S) of untreated and degummed silk fabrics as a function of the type of dye. Modified from *Journal of Materials Science and Chemical Engineering*, Lo, C. H.; Chao, Y., *Degumming of Silk Fibers by CO₂ Supercritical Fluid*, 5, 1-8 (2017) (Open access)

In 2020 Zhao and Zhang demonstrated that the type of degumming process strongly influenced the chemical/physical composition and biological activities of layered silk sericin (the outer-layer sericin, inner-layer sericin, and whole sericin). [19]

In work, three environment-friendly degumming methods were chosen, including hot water, HTHP water, and calcium hydroxide (CH) aqueous solution, and sericin layers were obtained according to the scheme of Figure 18.

Previously, Zhao et colleagues evidenced that CH aqueous solution could be used as a new type of eco-friendly degumming agent [46]. The calcium ion that existed in the degumming solution transforms into calcium salt precipitate after being neutralized with sulfuric or phosphoric acid, which not only can rapidly separate and purify sericin but also can recover calcium salt as a fertilizer to avert environmental pollution and waste of bioresources.

The authors found that after removing the outer-layer sericin in boiling water, the remaining inner-layer sericin could be easily degummed completely through HTHP water degumming.

Regarding the effect of the degumming process on the integrity of sericin layers, SDS-PAGE showed a wide range of molecular weights of sericin samples (Figure 19).

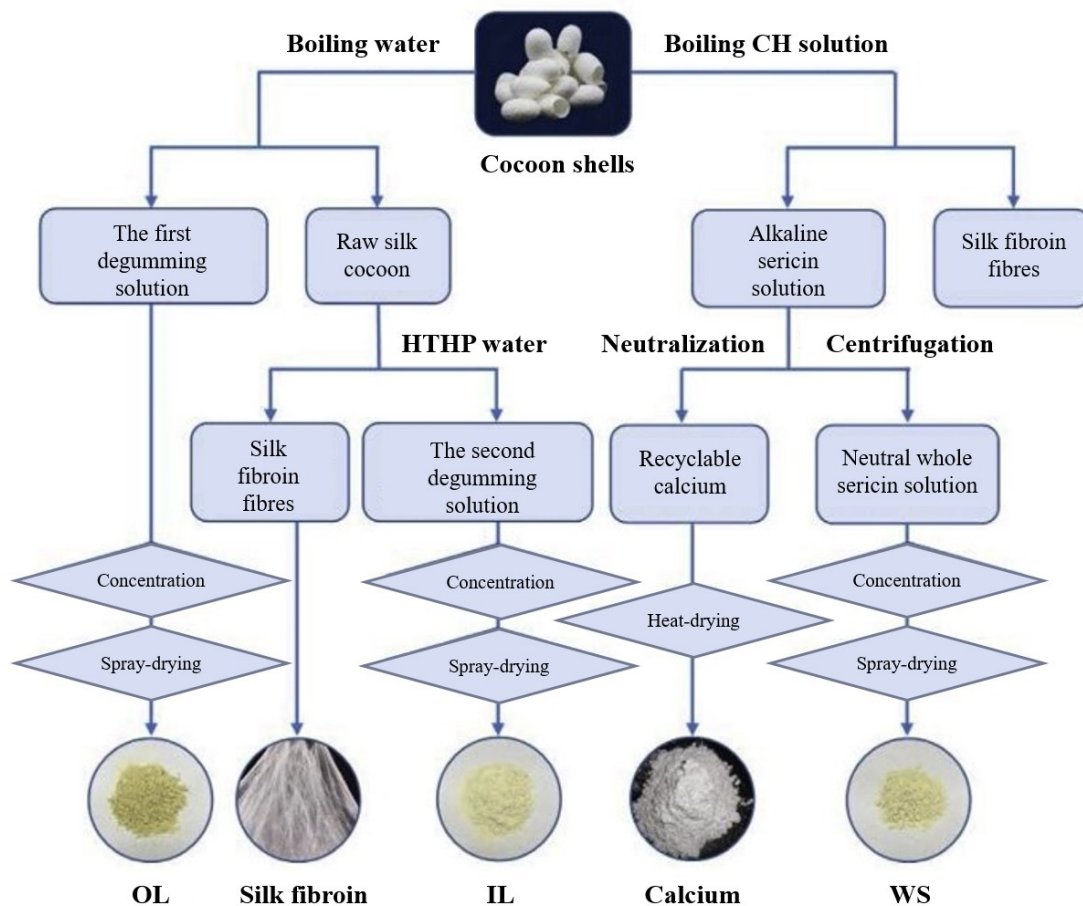


Figure 18: Flow chart of the preparation process for the outer-layer sericin (OL), inner-layer sericin (IL), and whole sericin (WS) extracted by using boiling water, HTHP water, and CH aqueous solution, respectively. After 60 min of cocoon boiling in water, the degumming sericin solution was concentrated, filtered, and spray-dried at 110 °C to obtain OL sericin powder. The inner-layered sericin was extracted by the second degumming at 120 °C HTHP water for 2 h, concentrated, and spray-dried. The whole sericin was removed after it had been boiled (20 min x 2) in a 0.025% Ca (OH)₂ solution. Once neutralized with sulfuric acid, the calcium sulphate precipitate was removed via centrifugation, and WS sericin was spray-dried. Regarding the terminology, the ‘Raw silk cocoon’ means the cocoon shell with OL removed after boiling water degumming, while the ‘Silk Fibroin fibres’ are fibres in which the sericin has been thoroughly removed. Modified from *Journal of Cleaner Production*, Zhao, Z. L.; Zhang, Y. Q., *Greener degumming production of layered sericin peptides from a silkworm cocoon and their physicochemical characteristics and bioactivities in vitro*, 261, 121080 (2020), with permission from Elsevier

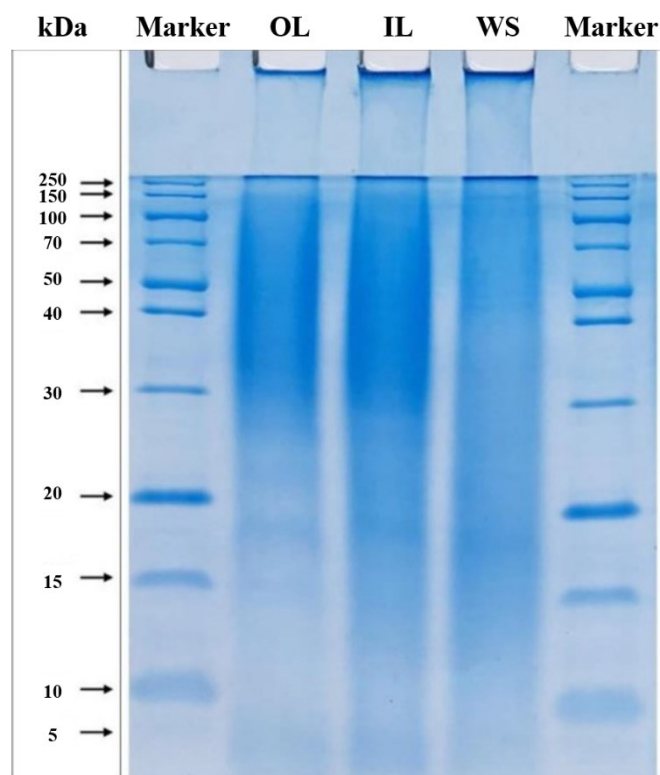


Figure 19: Electrophoresis SDS-PAGE (running gel: 15 %) of the outer-layered sericin (OL), inner-layered sericin (IL), and whole sericin (WS). Modified from *Journal of Cleaner Production*, Zhao, Z. L.; Zhang, Y. Q., *Greener degumming production of layered sericin peptides from a silkworm cocoon and their physicochemical characteristics and bioactivities in vitro*, 261, 121080 (2020), with permission from Elsevier

The OL derived from boiling water for silk exhibited a higher molecular weight (≥ 30 kDa) and a higher proportion of hydrophilic amino acids such as Glu, Ser, and Lysine (Lys) than IL extracted in the water at 120 °C. Overall, the number of hydrophilic amino acids gradually decreases while the non-polar amino acid content (Gly, Ala) gradually increases going from the outside to the inside of sericin layers (Table 3).

This result is in agreement with what published by Wang et colleagues in 2011. [18] Glu, Ser, and Lys percentage content decreased from 5.91 to 3.81% w/w, 28.36 to 27.39% w/w, 4.85 to 3.69% w/w, respectively going from OL to IL, while SF presented the highest content of hydrophobic amino acids, such as Gly (38.57% w/w) and Ala (29.41% w/w) (Table 3). A wide band of IL molecular weight from 20 kDa to over 100 kDa suggested that the polypeptide chain of the inner-layer sericin was moderately degraded. Despite above mentioned, WS exhibited the broadest molecular weight profile with bands distributed from 10 kDa to 30 kDa, which illustrates the highest degradation grade of the sericin caused by the CH solution degumming treatment.

Amino acid	OL	IL	WS	SF
<i>Asp</i>	12.26	12.35	11.74	1.35
<i>Glu</i>	5.91	3.81	4.52	1.26
<i>Cys</i>	9.18	6.81	7.02	0.62
<i>Ser</i>	28.36	27.39	29.26	8.84
<i>Gly</i>	10.55	11.56	11.32	38.57
<i>His</i>	0.34	0.35	0.28	0.02
<i>Arg</i>	4.32	4.82	5.77	0.66
<i>Thr</i>	6.70	9.22	8.08	1.73
<i>Ala</i>	3.64	4.17	3.68	29.41
<i>Pro</i>	4.03	4.36	4.15	2.28
<i>Tyr</i>	4.58	5.16	4.67	9.04
<i>Val</i>	2.53	3.22	3.09	2.42
<i>Met</i>	0.28	0.24	0.27	0.36
<i>Ile</i>	0.69	0.94	0.75	0.85
<i>Leu</i>	1.03	1.21	1.09	0.64
<i>Phe</i>	0.72	0.71	0.59	1.31
<i>Lys</i>	4.85	3.69	3.74	0.64

Table 3: The amino acid content of the outer-layer sericin (OL), inner-layer sericin (IL), whole sericin (WS) and silk fibroin (SF). Data are expressed in % w/w. Modified from *Journal of Cleaner Production*, Zhao, Z. L.; Zhang, Y. Q., *Greener degumming production of layered sericin peptides from a silkworm cocoon and their physicochemical characteristics and bioactivities in vitro*, 261, 121080 (2020), with permission from Elsevier

FTIR spectra evidenced structural differences in the three kinds of sericin powders (Figure 20). All sericins showed two characteristic peaks: the first one was attributable to the amide I and it was localized in the range of 1654, 1654, and 1650 cm^{-1} in OL, WS, and IL, respectively (C=O stretching vibrations), and the second one appeared in the range of 1600 to 1500 cm^{-1} and belonged to amide II (mainly caused by bending vibrations of the -NH bonds). The amide II signal recorded to 1538 cm^{-1} indicates that OL and WS sericin layers are composed primarily of random coil conformations. Contrary, the inner-layer sericin closed silk fibroin filament contains a higher amount of β -sheet domains than OL and WS,

responsible in the amide II peak's shift in the direction of a low wavenumber (1519 cm^{-1}). Moreover, the thermal analysis confirmed that the protection provided by the fibroin offered high thermal stability to the inner-layer sericin.

Finally, a small peak near 1245 cm^{-1} that belongs to amide III (mainly produced by C-N stretching vibrations and N-H bending vibrations) was registered, corresponded to the random coil and the β -sheet structures.

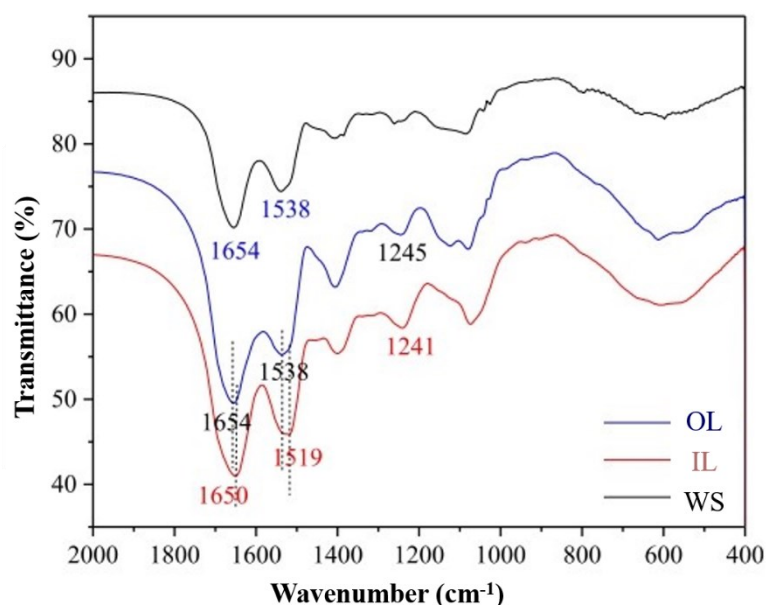


Figure 20: FTIR spectra of the outer-layered sericin (OL), inner-layered sericin (IL), and whole sericin (WS). Modified from *Journal of Cleaner Production*, Zhao, Z. L.; Zhang, Y. Q., *Greener degumming production of layered sericin peptides from a silkworm cocoon and their physicochemical characteristics and bioactivities in vitro*, 261, 121080 (2020), with permission from Elsevier

The *in vitro* antioxidant activity reached a steady-state and no longer increased already to the sericin concentration 7 mg/mL, indicating that the inhibition degree reached saturation. The boiling water degumming process resulted in best to preserve the antioxidant power of OL sample compared to that of IL and WS sericins. Furthermore, OL showed also the highest antibacterial activity against *Escherichia coli* and *Staphylococcus aureus*, which is almost twice that of IL. This result is probably due to the presence of antibacterial agents (e.g. protease inhibitors), which are concentrated in the external layer of the sericin. The alkaline conditions of CH solution during the degumming process, however, may reduce the activity

of antibacterial substances in WS. Furthermore, OL and WS samples both have a stronger anti-tyrosinase and α -glucosidase properties than the inner-layer sericin.

These results revealed that the type of degumming process strongly influences the biological activity of layered sericin and its potential for applications in different fields, such as biomaterials, cosmetics, functional health food, and biopharmaceuticals.

1.4 Circular economy measures to apply on the silk manufacturing waste

One of the most relevant trends on the international scene is the search for innovative solutions to dispose of processing waste, both for environmental and economic reasons, even going as far as to make the waste of one production the raw material of another, creating what today is called the circular economy (CE). [47]

According to the Ellen MacArthur Foundation, CE is a generic term to define an economy designed to be able to regenerate itself. In a circular economy, the flows of materials are of two types: biological ones, capable of being reintegrated into the biosphere, and technical ones, destined to be revalued without entering the biosphere. [48]

The CE is, therefore, an economic system planned to reuse materials in subsequent production cycles, minimizing waste. The linear take-make-dispose economic model is based on the accessibility of a large number of resources and energy and is increasingly less suited to the reality in which we operate. Initiatives in support of efficiency, which work to reduce resources and fossil energy consumed per unit of production, alone can delay the crisis of the economic model but are not sufficient to solve the problems given by the finite nature of the stocks.

The transition from the linear model to a circular model is, therefore, necessary, which knows how to seize every opportunity to limit the supply of matter and input energy and to minimize waste and losses, paying attention to the prevention of negative environmental externalities and the realization of new social and territorial value.

In such a vision, taking into account all the phases, from design, production, consumption, waste and end of life destination concepts need to be re-examined to preserve the value of resources, keeping them into the production and use cycle as long as possible (Figure 21). [49]

PRINCIPLES

1. Preserve and enhance natural capital by controlling finite stocks and balancing renewable resource flows - for example, replacing fossil fuels with renewable energy or using the maximum sustainable yield method to preserve fish stocks.

2. Optimise resource yields by circulating products, components and materials at the highest utility at all times in both technical and biological cycles – for example, sharing or looping products and extending product use cycles.

3. Foster system effectiveness by revealing and designing out negative externalities, such as water, air, soil, and noise pollution; climate change; toxins; congestion and negative health effects related to resource use

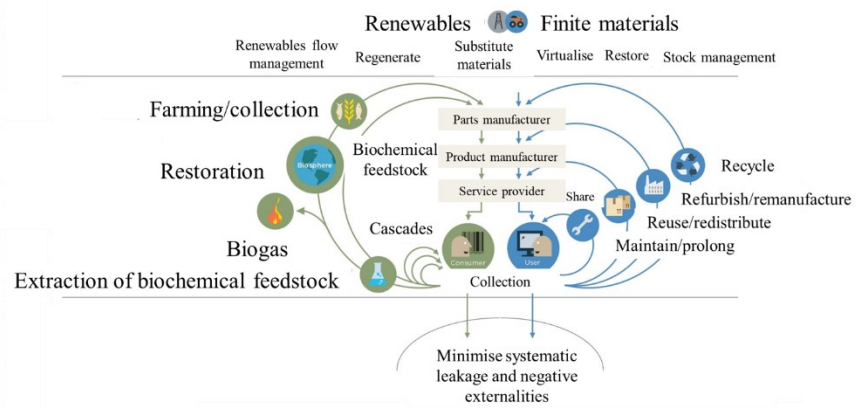


Figure 21: Principles of the circular economy system. Modified from *Ellen MacArthur Foundation, Intelligent Assets: Unlocking the Circular Economy Potential, An outline of the circular economy* 18-19 (2016), with permission from Ellen MacArthur Foundation

The textile and clothing industry is one of the most significant manufacturing sectors with a total share of over 4% in world commodity trade¹ and globally worth above \$ 400 billion in terms of nominal sales. Being one of the most important industrial sectors, it turns out to be also one of the most polluting.

Textile manufacturing causes as primary environmental burdens energy and chemicals consumption, water retirement, solid waste production and direct emissions of carbon dioxide. In the international context, silk is produced by over sixty countries in the world. Between these, Asia plays a primary role with 90% of mulberry silkworm production, while Western Europe (Italy, Germany, France, Switzerland, and the United Kingdom), Japan, China, and India represent the main destinations of raw silk yarns. Furthermore, Italy, France, Germany and Switzerland have important silk process expertise related to the development and manufacturing of highly-priced pieces, intended for Italian consumers or export to the United States or Asia.

In particular, in northern Italy, the area around Como is notorious for the agglomeration of companies with expertise involved in silk products design, in the textile manufacture, dyeing, designing and printing of high-level silk products. [50]

In 2015 a survey of the Voluntary Cosmetic Registration Program–FDA revealed that on 177 silk powder formulations on the market, more than half contains silk sericin. [51] Those silk ingredients are used at concentrations up to 1.4% in leave-on products for face powders, up to 0.1% for silk sericin hydrolysed powder, or in other cosmetic products also at higher concentrations. [50] These results in about 5 000 tons of sericin used only in the USA, and only for cosmetics every year. These volumes are usually ad-hoc manufactured in the pharmaceutical production starting from low-quality cocoons or short silk fibres restrained from the textile supply chain using high-yield performing processes which, however, can damage the quality of both fibroin and sericin.

Industrial degumming process for textile is more rapid and efficient than the one dedicated to sericin extraction for cosmetic applications. It expects the use of substances, such as soaps, alkalis, acids, surfactants challenging to dispose of remove silk sericin in a better way. [52]

By this process, large amounts of sericin are produced and discharged into wastewater as pure waste, achieving effluents with a high content of organic matter (BOD₅ equal to about 30,000-50,000 mg/L, COD over 2,000 mg/L, TSS over 1,000 mg/L) leading to the production of nitrogenous substances and odours in wastewater. [31]

Chemical/biochemical oxygen demand (COD and BOD₅, respectively), and total suspended solids (TSS) are important indexes in the control of the total content of pollution and the management of the water environment. In particular, COD measures the amount of oxygen used for the oxidation of organic and inorganic substances contained in a water sample following treatment with compounds with strong oxidizing power. A high COD value of a discharge involves a reduction of the dissolved oxygen in the receiving water body and therefore a reduction in self-purification capacity and to support aquatic life forms. [52] [53]

In 2008 Vaithanomsat and Kitpreechavanich proposed the ultrafiltration as an eco-friendly procedure to recover high-quality sericin protein from wastewater. [43]

Initially, high content of BOD₅ (4840 mg/L), COD (8870 mg/L) and nitrogen (0.11%) was found in the degumming waste solution from *Bombyx mori* silk processing obtained from the conventional Thai silk degumming process.

After the passage through the ultrafiltration system, the degummed solution showed the decrease in COD, BOD₅ and total solid of the solution from 8870 to 260 mg/L, 4840 to 158 mg/L and 1.06% to 0.01%, respectively, indicating the quality improvement of degumming product. Furthermore, the reduction in total nitrogen and protein contents, from 0.11% to 0.01% and from 0.69% to 0.06% w/w, respectively, suggested the recuperation of sericin from waste solution.

The tangential filtration method can process until 50 L/h of sericin-rich wastewater consuming half the energy consumption (16 kWh), and an 80% reduction of production cost compared with the traditional lyophilization equipment used in the pharma industry [54].

Contrary to the Direct Flow Filtration, also known as "dead-end" filtration, that applies the feed stream perpendicular to the membrane face, the Tangential Flow Filtration (or crossflow filtration) provides that the flow flows tangentially concerning the filter surface, preventing the build-up of molecules at the surface that can cause fouling and obtaining higher yields of extraction. The one portion that passes through the membrane is called permeate, while the remainder (retentate) is retained by the filter membrane and recirculates back to the feed reservoir.

In the silk district of Como, around 2,000 tons of silk are produced every year. Over 400 tons of sericin is discharged into wastewater. [55]

Sericin waste can be used to replace ad-hoc produced materials for biomedical, pharmaceutical and cosmetic applications as long as they are processed, upgraded and characterized to be compliant with those sectors manufacturing practices. The sericin extraction, recovery and reuse is possible through the correct treatment of wastewater resulting in significant environmental, economic and social benefits, according to the CE model (Figure 22). [9]



Figure 22: Manufacturing, consumption, and recycling of fibroin and sericin starting from silkworm cocoons

Industrial symbiosis is one of the circular economy proposals which aims to favour an efficient use of resources in the production chain, through the exchange among different actors and/or sectors of waste streams which can enter new production cycles as input material. This concerns benefits on the environment and economy for both the symbiotic actors, as far as the deriving economic benefit for silk textile manufacturers, as suppliers, is higher than the processing costs.

In this context, the end-user company (pharma) can use recovered sericin as input to its production processes instead of raw material (be it raw silk sericin or another excipient), benefiting from saving costs for buying the input material (recovered sericin cost is lower than the one of the raw protein, about € 200 kg) and reducing the environmental impacts due to unused equipment for sericin-extraction.

The supplier (silk textile manufacturers) company can obtain a reduction of economic and environmental impacts: on the one hand, it makes revenues by selling recovered sericin, on the other hand, it reduces the processing costs of wastewater treatment.

Surprisingly, as reported in the literature, it is estimated that about 1 million tons of cocoons produced worldwide approximately 400 000 tons of dry cocoons are generated, that have 50 000 tons of recoverable sericin. Now, assuming that only 10% of those volumes are compliant with cosmetics applications, this sericin protein should be recovered and recycled, involving relevant environmental, economic and social benefits for both manufacturers and customers. To date, there are two reasons why those volumes are not recovered for cosmetics and pharmaceutical use: firstly, the quality of the silk protein fraction could be related to the degumming method, which leads to high sericin degradation, limiting its effectiveness in cosmetics applications. In many cases, the degumming process causes the reduction of the molecular weight of sericin, thereby increasing its solubility and dissolution kinetics. In the literature, it is reported that sericin degummed by autoclave process shows many biological activities, including antioxidant, anti-ageing, whitening, antibacterial, anti-inflammatory. Moreover, it has been employed in tissue engineering and for the production of micro and nano-delivery systems. [56] [12] [9] Secondly, the discharged sericin-rich wastewater has to be treated to remove sericin from the solution. Several technologies can be used for this activity, including lyophilization, spray-drying and ultrafiltration, but all of them require additional consumption of energy and the provision of equipment. [55]

2. Silk protein employment as biomaterials

In the raw silk silkworm fibre, sericin acts as a glue protein thanks to its hydrophilic properties and allows the fibroin nucleus to be held together, lubricating and promoting the biological process of winding the thread in the formation of the cocoon.

However, fibroin and sericin cannot be employed together, both in the textile and for biomedical and pharmaceutical purposes. Indeed, in the textile industry, sericin is removed from the fibroin to guarantee the high quality of the silk fibres. In contrast, in the biomedical and pharmaceutical field, the silk applications in its native form are limited by the decreased biocompatibility due to the simultaneous presence of sericin and fibroin.

For the reasons mentioned above, the degumming process constitutes the essential starting point for procedures, on the laboratory or industrial scale, which exploit these proteins for textile or biomedical use.

2.1 Properties and use of silk fibroin

Silk is one of the most abundant naturally derived polymers. For thousands of years since the first discovery in Chinese and Indus civilizations nearly 2500 BC, silk has been known as a luxurious raw material in the textile industry. Owing to the development and spreading of sericulture, where silkworms are reared and fed with mulberry leaves to collect silk fibres from their cocoons, silk fabrics have been produced on a large scale across South Asian countries ever since. This luxurious textile material led to the establishment of the Silk Road, the great trading route that connected a part of Asia with Europe, India, and Africa. [15]

From a materials science perspective, silkworm silk possesses excellent mechanical properties, such as remarkable strength and toughness, offering unlimited opportunities for the fabrication, functionalization and processing of robust biomaterials. [1] Regarding the stiffness, silkworm silk is superior to commonly used polymeric degradable biomaterials such as collagen and polylactic acid (PLA) and the toughness of silk fibres is greater than the best synthetic materials, including Kevlar and nylon fibres (Table 4). [14]

Thanks to its dyeability, elongation, breathability, and comfort it provides in warm or cold weather, silk has been historically considered as one of the best quality natural fibres. Every year more than 120,000 tons of silks are produced globally, and the main manufacturers are found in China, India, and Japan. [15]

Materials	Stiffness (GPa)	Strength (Mpa)	Extensibility (%)	Toughness (MJ m⁻³)
<i>B. mori silk (with sericin)</i>	5-12	500	19	70
<i>B. mori silk (no sericin)</i>	15-17	610-690	4-16	70-78
<i>N. clavipes silk</i>	11-13	875-972	17-18	111-160
<i>N. clavipes silk (285 kDa recombinant)</i>	21	508	15	-
<i>Bone</i>	20	160	3	4
<i>Collagen</i>	0.0018-0.046	0.9-7.4	24-68	-
<i>Elastin</i>	0.001	2	150	2
<i>Resilin</i>	0.002	3	190	4
<i>Synthetic rubber</i>	0.001	50	850	100
<i>PLA</i>	1.2-3.0	28-50	2-6	1-3
<i>Nylon fiber</i>	5	950	18	80
<i>Kevlar 49 fiber</i>	130	3600	2.7	50

Table 4: Comparison of tensile mechanical properties between silks and other natural and synthetic materials. Adopted from *Chemical Society Reviews*, Huang, W.; Ling, S.; Li, C.; Omenetto, F. G.; Kaplan, D. L., *Silkworm silk-based materials and devices generated using bionanotechnology*, 47 (17), 6486-6504 (2018), with permission from Royal Society of Chemistry

Years ago, the Food and Drug Administration (FDA) had recognized silk fibroin as a candidate for pharmaceutical and biomedical utility due to its biocompatibility, controllable biodegradability, non-immunogenicity, and minimal inflammation in host tissue. Owing to their hierarchical structure and different range of attractive properties, silk fibroin-based materials are good candidates for more advanced applications other than their traditional use in the textile industry, including electronics and optoelectronics, optics and photonics for

implantable yet degradable medical devices along with a broader range of utility in different device applications. [14] Regarding the past and actual use of silk fibroin-based biomaterials, the routine clinical use of silk suture is noted for wound ligation, silk fabrics for the treatment of dermatological pathologies, silk surgical mesh for abdominal wall reconstruction and investigative plastic surgery applications, and also human clinical trials of silk fibroin-based film for wound healing or the tympanic membrane reconstruction [15]. For these purposes, silk fibroin is often used alone or in combination with other materials, such as chitosan, alginate, carboxymethyl cellulose, gelatin and antibacterial agents like heavy metals and antibiotics. [57] [58] [59]

Tissue engineering is a branch of the regenerative medicine that takes care of the design of scaffolds to rebuild, engineer or repair aged or damaged human organs or/and tissues without having to resort to transplantation or prosthesis. Regarding this, the cells are harvested from patients by biopsy, and they are grown in 2D-culture under aseptic conditions. Then, the cells are expanded *in vitro* and seeded onto 3D-scaffolds/matrices, which may be natural, synthetic or blends and are fabricated in various material formats, such as hydrogels, porous sponges, nanofibrous mats, micro/nanoparticles, and micro/nanopatterned surfaces. Subsequently, these cells are grown in an appropriate culture medium in the presence of bioactive factors to proliferate and differentiate into the desired tissue for implantation (Figure 23). For long-term culture, the matrices are grown in bioreactors to support and maintain the cultures in sterile conditions before being transplanted to restore the damaged tissue *in vivo*. To guarantee a favourable tissue regeneration, it is important to design appropriate scaffolds [60] that provide morphology, structural support and chemical/mechanical signals to the cells, and the interactions between cells and scaffolds have to support appropriate tissue growth. [61] [62]

To make this possible, the biocompatibility of materials is key to support cellular activities, improve tissue regeneration without local or systemic inflammation or immune responses in the host. [60] An acceptable structure and high surface area are required to promote a high number of cell interactions while supporting oxygen/nutrient transport. Also, biodegradability or absorption of the scaffold material is significant, where the degradation rate of the scaffold should match the rate of tissue regeneration to improve the transfer of functions from the artificial matrices to the native extracellular matrix (ECM) on a time-dependent basis during tissue regeneration.

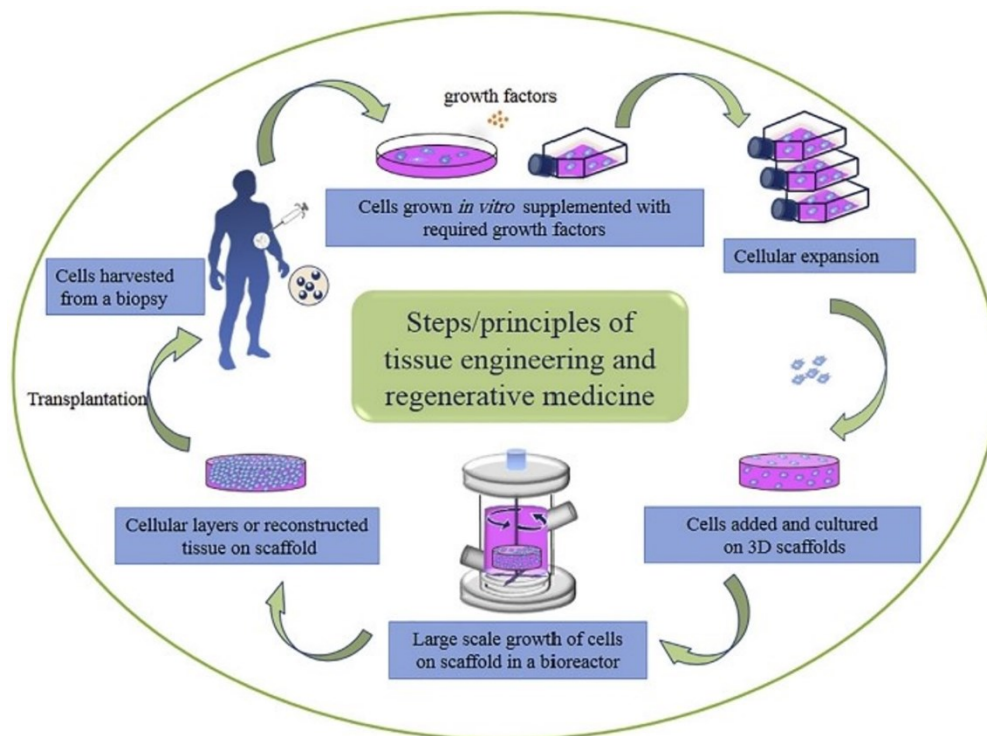


Figure 23: Principles of tissue engineering. Reproduced from *Advanced Drug Delivery Reviews*, Gholipourmalekabadi, M.; Sapru, S.; Samadikuchaksaraei, A.; Reis, R. L.; Kaplan, D. L.; Kundu, S. C., *Silk fibroin for skin injury repair: Where do things stand?*, (2019), DOI: doi.org/10.1016/j.addr.2019.09.003 with permission from Elsevier

Thereby, designing scaffolds, which mimic the structure and biological functions of native ECM and induces a suitable environment for regulating cell activities, is the main objective. To obtain such scaffolds, synthetic or natural polymer materials have been utilized to meet the above needs, each with their benefits and limitations. Although there are no universal biomaterials that meet scaffolding requirements for all types of tissues, silk fibroin as a constituent part of natural tissues is a good candidate for many applications in tissue engineering. [63] Regarding that, native fibres and regenerated silk fibroin solutions have already been processed with different approaches to obtain several systems, including films, sponges [64], microparticles [65] [66], nanoparticles [67] [68], non-woven mats [69], tubes [70], nanofibers, and hydrogels [71] (Figure 24).

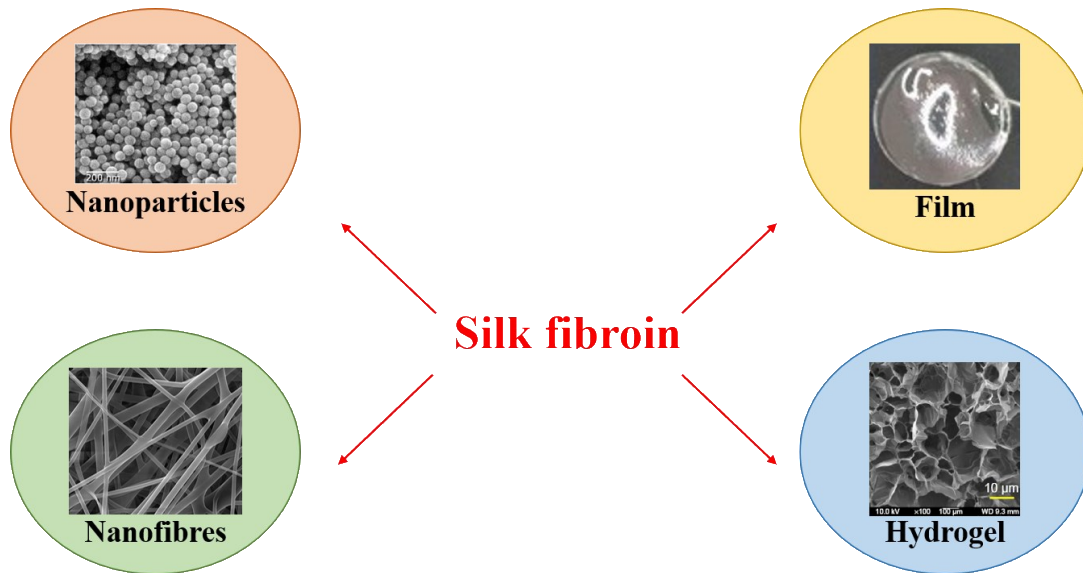


Figure 24: Examples of silk fibroin-based systems for various biomedical and pharmaceutical applications

Silk fibroin-based films seeded with osteoblasts promoted the *in vitro* bone tissue growth, as reported by Sofia et co-workers. When the films were chemically linked with the peptide arginyl glycy l aspartic acid, the interactions between cells and integrin proteins of the ECM were advanced as well as the induction of bone formation was significantly enhanced with an increase of alkaline phosphatase levels, up-regulation of bone-specific transcripts, and calcification levels over 4 weeks. Similar responses were not observed when the parathyroid hormone was immobilized and also assayed with osteoblasts. This data confirmed the utility of a silk fibroin matrix to offer many active sites for selective chemical couplings for bone tissue engineering. [72]

Silk fibroin being a mechanically robust biomaterial resulted as a good candidate for the development of a wire rope matrix for the development of autologous tissue-engineered anterior cruciate ligaments using a patient's adult stem cells. [73]

In 2011 regenerated silk fibroin-based 3D-scaffold was proposed by Chlapanidas et colleagues as a new product for advanced cartilage therapy. Silk fibroin resulted in an excellent biocompatible and biodegradable polymer for tissue engineering purposes because it promotes together with the intra-articular adipose stromal vascular fraction (SVF) the adhesion and proliferation of chondrocytes with correct scaffold colonization. [74]

Furthermore, silk fibroin non-woven mats were selected to create an adequate tridimensional microenvironment for SVF delivery in the subcutaneous tissue before diabetes induction in

mice. After the implantation of pancreatic endocrine cells encapsulated in alginate beads (alginate-PECs) on the SVF-soaked silk fibroin non-woven mats (silk-SVF), all animals were in good health with an increase of weight in time, demonstrating that silk-SVF created a microenvironment which supports vascular growth and subsequently the endocrine cell survival and engraftment. The silk-SVF system stimulated neovascularization and contributed in providing nutrients to the implanted cells allowing the systemic availability of the produced insulin. On the contrary, coadministration of SVF and pancreatic cells after diabetes induction led to poor prognosis of the treated mice. [69]

Previously, Mobini et colleagues investigated the mechanical resistance of the *Bombyx mori* silk-based composite material constituted of 3D-silk fibres embedded in a porous matrix of fibroin as reinforcement, developed for bone tissue engineering. [75]

This freeze-dried porous scaffold presented an enhanced mechanical strength to endure compressive forces. The compressive moduli and stress significantly increased thanks to the reinforcing nature of the fibres. Moreover, the porous scaffolds supported attachment, proliferation, and differentiation of human mesenchymal stem cells (hMSCs) (Figure 25).

To obtain a porous scaffold with uncompromised mechanical strength is quite challenging. Initially, to understand the effects of scaffold architecture and biomechanics, Correia et collaborators performed a study to optimize silk scaffolds in terms of architecture and stiffness. The group seeded scaffolds with human adipose tissue-derived stem cells (hASCs) to assess cell proliferation and differentiation, matrix production, and calcification. The porous silk fibroin-based scaffolds were made using the conventional freeze-drying and salt-leaching methods with the use of different solvents to obtain various pore sizes and structures (lamellar and spherical pores).

To quicken the bone formation, it was determined that the porous lamellar scaffold with size from 400 to 600 μm was the optimal bone tissue formation due to increased adipose activity, equilibrium modulus, and calcium deposition. [76]

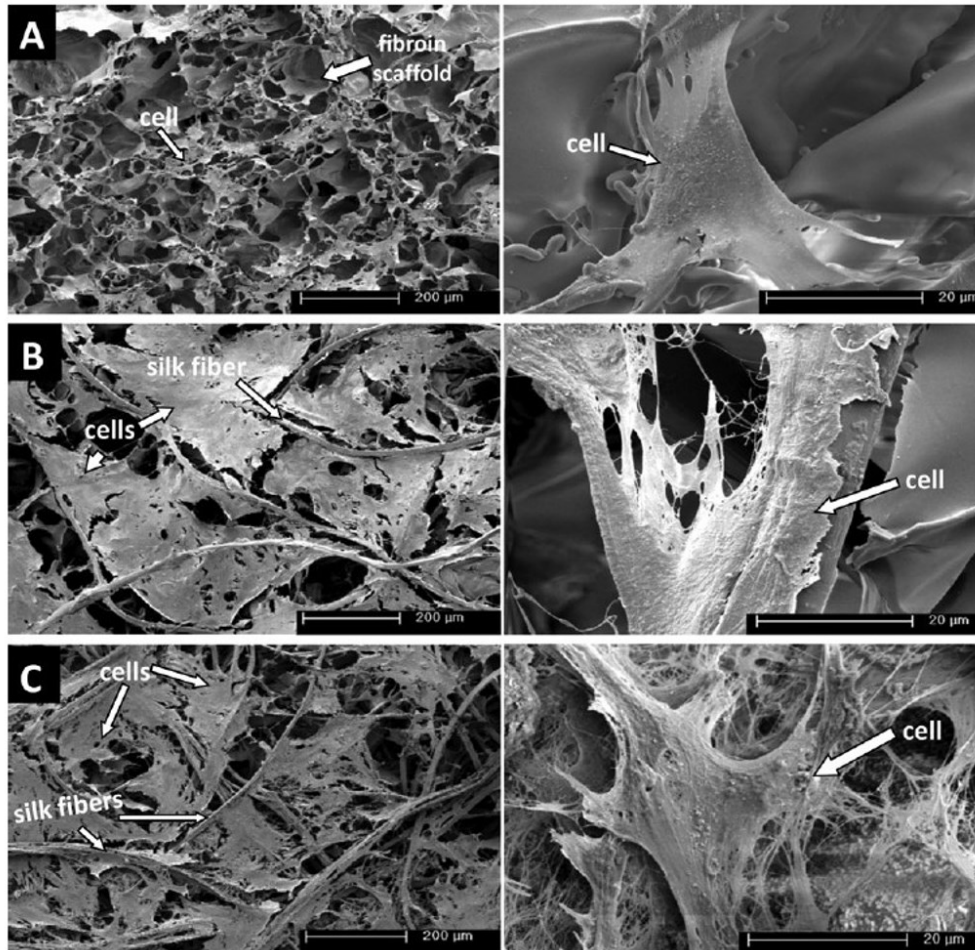


Figure 25: hMSCs attachment and morphology on fibroin scaffolds and fibre/fibroin composite scaffolds. Reproduced from *Journal of Biomedical Materials Research Part A*, Mobini, S.; Hoyer, B.; Solati-Hashjin, M.; Lode, A.; Nasim Nosoudi, N.; Samadikuchaksaraei, A; Gelinsky, M., *Fabrication and characterization of regenerated silk scaffolds reinforced with natural silk fibers for bone tissue engineering*, 101A (8), 2392-2404 (2013), with permission from Society For Biomaterials

2.1.1 Silk fibroin as a biomaterial with potential for drug delivery

Design and synthesis of efficient drug delivery systems are of vital importance for medicine and healthcare. Nanocarrier-based systems (e.g. nanoparticles with a size ranged from 1 and 100 nm) have generated great interest in drug delivery since they provide new opportunities to overcome the limitations of conventional delivery methods with regards to the drugs, such as poor aqueous solubility, low bioavailability and nonspecific distribution in the body, as well as to enhance drug efficiency.

Silk fibroin is a naturally occurring protein polymer with several unique properties that make it a suitable material for incorporation and delivery of a wide range of therapeutic agents [77] and bioactive molecules, including genes [78], small molecules, and biological drugs.

At the same time, itself acts as bioactive macromolecule having many intrinsic biological properties, such as antioxidant, anti-inflammatory, antibacterial activities, and low immunogenicity. [3]

To avoid bacterial or viral contamination, sterilization is a critical step for the production of drug delivery products. However, different standard sterilization methods are not compatible with most biodegradable synthetic polymers, such as poly (lactic-co-glycolic acid) (PLGA) or protein-based (e.g., collagen) matrices, because they have low thermal stability. For example, collagen scaffolds undergo denaturation with autoclaving, and partial denaturation and cross-linking with dry heat sterilization. Physical sterilization methods, such as γ or β irradiations could also result in instability and deterioration of PLGA, and cross-linking and/or chain scission of both PLGA and collagen-based matrices.

These limitations associated with sterilization of the polymeric matrix material can create significant obstacles for a pharmaceutical product, in addition to the increase of manufacturing costs.

Conversely, silk fibroin has good resistance to the microbial contamination, ductility and adaptability to various production processes, high compatibility with the main sterilization methods, presumably due to its high thermal stability (glass transition temperature: $T_g \cong 190\text{-}200\text{ }^\circ\text{C}$, decomposition temperature $T_d \cong 220\text{-}300\text{ }^\circ\text{C}$ for side chains, and $\geq 300\text{ }^\circ\text{C}$ for the peptide backbone) deriving from the presence of hydrogen bonds and the significant percentage of crystalline domains that need high energies to be destroyed. [16]

These characteristics have increased the interest of the scientific world towards fibroin, making it an optimal molecule in the study of controlled release systems of drugs.

For developing micro and nanostructured drug systems, the choice of an appropriate method of preparation turns to be essential to obtain a stable formulation of fibroin-based nanoparticles.

Unfortunately, it is not possible to control all the variables of the process. Regarding this, many intrinsic factors can affect the preparation of fibroin-based nanosystems, such as the high molecular weight and protein conformation, which results to be difficult to manage and control.

In the literature, the desolvation method is reported as the most commonly exploited method to obtain fibroin nanoparticles. The desolvation process consists of reducing fibroin chain

solubility, thanks to the presence of organic solvents such as ethanol, acetone, dimethyl sulfoxide and methanol, leading to phase separation. The addition of a desolvation agent induces the conformation change from silk I (soluble in water) to silk II (insoluble in water) of the fibroin, causing the aggregation of the nanoparticles by coacervation. [79]

This approach was adopted from an Italian research group to prepare fibroin nanosystems loaded with two hydrophobic drugs (celecoxib and curcumin) for the treatment of osteoarticular diseases (Figure 26). In this case, acetone was chosen as the desolvation agent, in which powders of celecoxib or curcumin were previously solubilized in different concentrations. [68] Obtained nanoparticles showed a mean diameter of about 110 nm, characterized by a defined distribution, as shown in Figure 27.

In the same year, Perteghella et collaborators used the desolvation method to load paclitaxel (PTX) as an anticancer drug into SFNs by using an exogenous approach. This method allowed the reduction of fibroin loss during the production process, obtaining a process yield higher than 80% w/w. Nanometric SFNs showed the spherical shape and smooth surface. These morphological characteristics were also maintained after nanoparticle drying, although the lyophilization contributed to the aggregation of the same. The encapsulation of PTX into fibroin nanoparticles resulted in success in reducing its toxicity while retaining the pharmacological effect, without any relevant reduction of its *in vitro* effectiveness. [67]

Previously, Chen et collaborators developed silk fibroin nanoparticles of sizes from 270 to 520 nm loaded with PTX adding a paclitaxel solution in ethanol to a regenerated fibroin solution kept under light stirring. The authors observed that the release time of the drug from the loaded nanoparticles could be up to two weeks long when the loading was approximately 3.0%. [7]

With a similar method, Wu et colleagues prepared fibroin nanoparticles loaded with the same anticancer agent, with a mean diameter of 130 nm. [80] The incorporated paclitaxel maintained its pharmacological activity. *In vivo* studies on the mouse model of carcinoma evidenced that the locoregional delivery of these nanoparticles promoted superior antitumor efficacy by delaying the growth of the tumour and reducing its weight compared with systemic administration.

Furthermore, Rahmani et colleagues identified silk fibroin nanoparticles as a high loading carrier system for the anticancer therapy based on the administration of 5-fluorouracil (5-FU). [81]

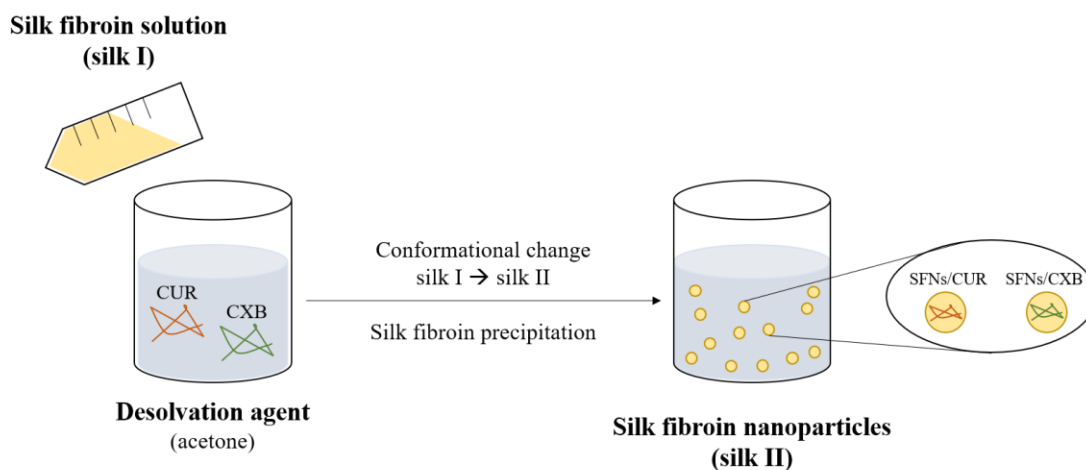


Figure 26: Preparation of silk fibroin nanoparticles (SNFs) loaded with celecoxib (SFNs/CXB) and curcumin (SFNs/CUR) by desolvation method

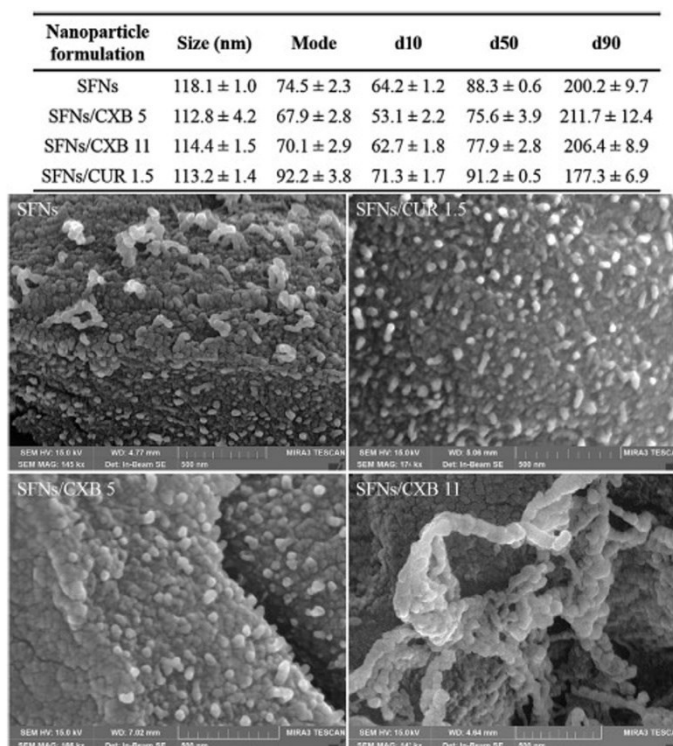


Figure 27: Morphological investigation and particle size distribution of unloaded (SFNs) and silk fibroin nanoparticles loaded with celecoxib and curcumin at different loading (SFNs/CXB-5, SFNs/CXB-11 and SFNs/CUR-1.5). Scale bar: 500 nm. NTA data are reported as the mean value ± standard deviation. Reproduced from *European Journal of Pharmaceutics and Biopharmaceutics*, Barbara Crivelli, B.; Bari, E.; Perteghella, S.; Catenacci, L.; Sorrenti, M.; Mocchi, M.; Faragò, S.; Tripodo, G.; Prina-Mello, A.; Torre, M. L., *Silk fibroin nanoparticles for celecoxib and curcumin delivery: ROS-scavenging and anti-inflammatory activities in an in vitro model of osteoarthritis*, 137, 37-45 (2019), with permission from Elsevier

5-FU is a uracil nucleotide analogue usually used for the treatment of different human cancers, including stomach, colon, rectum and breast cancers. However, a high dosage of the drug is required to satisfy an adequate treatment, causing toxicity in the gastrointestinal tract and myelotoxicity.

Regarding this, SFNs, obtained by nanoprecipitation, showed an efficient 5-FU loading capacity, promoting a sustained release profile.

FTIR spectrum confirmed three peculiar peaks of silk fibroin localized at 1654.92, 1535.34, and 1238.3 cm^{-1} , attributable to the amide I (C=O stretching), amide II (N-H bending) and amide III (C-N and N-H groups), respectively. The wavenumber location of the absorption bands of amides I indicated a predominant of random-coil domains in the silk protein. In the spectrum of 5-FU loaded SFNs, the characteristic peaks of the antitumor drug were observed, confirming its internalization into the nanoparticles, and the peak in the region of 3100-3600 cm^{-1} could confirm the hydrogen bonds between drug and fibroin. These bonds, for the formulation of the drug to polymer ratio of 1:1, were responsible for the fibroin conformational change from random-coil to β -sheets domains, thus increasing the 5-FU loading in the nanosystems.

In 2014, the research group directed by Pérez and colleagues investigated silk fibroin (RL-FNPs) as the carrier for the controlled release of resveratrol in an experimental model of inflammatory bowel disease in rats. [82]

The nanoprecipitation method was chosen to prepare nanoparticles with a median diameter of 64 nm. The absorption of the resveratrol onto the surface of the particles motivated the increase of the particle size.

Despite the resveratrol having very low solubility (0.11-0.3 mg/L) in aqueous media, RL-FNPs released the drug with a prolonged kinetics profile over 80 h. In these same nanoparticles, silk fibroin and resveratrol showed a synergistic anti-inflammatory effect on rats, in comparison with the administration of unloaded nanoparticles or resveratrol alone.

Perteghella et co-workers investigated the pharmaceutical potential of a novel carrier-in-carrier delivery system based on extracellular vehicles (EVs) produced by mesenchymal stem cells (MSCs) loaded of silk/curcumin nanoparticles. [83]

Nanosystems showed a hydrodynamic diameter of about 100 nm and a round shape not altered by the encapsulation of curcumin. Studies of cellular uptake confirmed the presence of nanoparticles in the cytosol around the nuclear membrane without cytotoxic effects on the MSCs. Moreover, the confocal analysis revealed the same localization of drug and silk fibroin into cells, suggesting the efficient internalization of curcumin into nanoparticles.

Interestingly, the confocal microscopy confirmed the co-localization of curcumin, silk fibroin and MSC-EVs, underlining the ability of MSCs to entrap silk/curcumin nanoparticles and to release EVs as the carrier-in-carrier system.

This combined biological-technological approach represents an innovative class of nanosystems, combining the favourable effects of both regenerative cell therapies and pharmaceutical nanotechnology, avoiding the use of viable replicating stem cells.

Fibroin nanoparticles have also been used for the encapsulation of protein and peptide drugs, in particular growth factors, which are often characterized by low half-life and limited tissue penetration. For example, Yan et collaborators developed fibroin nanoparticles have been covalently conjugated with insulin with cross-linking reagent glutaraldehyde. The *in vitro* half-life of the conjugates was about 2.5 times higher than that of the native insulin, demonstrating their possible development as new bioconjugate for the delivery system of enzymatic and polypeptide drugs. [84]

2.2 Silk sericin for pharmaceutical, biomedical, and cosmetic applications

Despite silk sericin has historically been considered a waste product of the textile industry, it has recently been revalued as a biocompatible and high-added-value material for biomedical, pharmaceutical and cosmetic purposes (Figure 28).

Considering that proteins can be used as biomaterials or biomedical products, the immunological response is commonly evaluated as an inflammatory reaction, with the expression or release of cytokines, especially interleukin-1 β (IL-1 β) and tumour necrosis factor α (TNF- α), both *in vitro* and *in vivo*. [9]

In 2009, Aramwit et colleagues monitored levels of these two pro-inflammatory cytokines induced by sericin in mice. A dose-dependent relationship between the release of cytokines by both mouse monocyte and alveolar macrophage cell lines and the sericin concentration in the culture medium was observed. In particular, macrophages produced a higher level of inflammatory mediators compared to monocytes, inferring that the levels of cytokines triggered by sericin constituted an acute rather than a chronic inflammatory response. The data were also confirmed *in vivo* assay using sericin-based cream applied topically on wounds on the back of rats, with a significant reduction of the expression of TNF- α and IL-1 β in the tissue so to accelerate the overall wound healing in treated animals. In this way, sericin promoted wound healing without activating the inflammatory response. [85]

Moreover, it has been reported that sericin is immunologically inert because it did not induce *in vitro* the short- and long-term expression and release of the pro-inflammatory cytokine TNF- α from RAW 264.7 murine cells. Contrary, under the same conditions, the simultaneous presence of the two silk proteins caused for synergistic effect with lipopolysaccharides the significant release of TNF- α from macrophages. Therefore, these studies have established that the two silk proteins, if used individually, do not trigger the inflammatory response but that the adverse events are only related to the combined use of fibroin and sericin. Hence, it is necessary to purify the two proteins correctly, through a careful degumming process, before using them *in vivo*. [34]



Figure 28: Possible employment of silk sericin. Silk sericin is employed as an excipient for the development of 3-D scaffold and drug delivery systems, in the cosmetics, as a moisturizing, whitening, and anti-wrinkle agent and as a pharmaceutical ingredient. Moreover, thanks to its mitogenic effect, it can be used as a supplement of the serum-free culture medium. Reproduced from *Royal Society of Chemistry-Soft Matter*, Crivelli, B; Perteghella, S; Bari, E; Sorrenti, M; Tripodo, G; Chlapanidas, T; Torre M.L, *Silk nanoparticles: from inert supports to bioactive natural carriers for drug delivery*, 4, 546-557 (2018), with permission from Royal Society of Chemistry

A study performed by Chlapanidas et collaborators revealed that sericin extracted by different strains of silkworms possessed the *in vitro* antiproliferative activity on human peripheral blood mononuclear cells (hPBMCs) stimulated with hemagglutinin (PHA). In the same work, sericin reduced the interferon-gamma (IFN- γ) levels, without having effects on the release of interleukin 10 (IL-10) and TNF- α . [12] These anti-inflammatory properties of sericin can be exploited both for dermatological and anti-tumoral purposes.

In 2014, the same Italian research group demonstrated that sericin microspheres loaded with the racemic flavanone naringenin (NRG) were more potent compared to the NRG alone in inhibiting the TNF- α release on lipopolysaccharide-stimulated hPBMCs. [86]

This study represented a starting point for the development of new topical formulations based on silk sericin for the treatment of middle-stage psoriasis. Interestingly, thanks to its occlusive effect, sericin may improve skin barrier function, thereby preventing water loss from the upper layer of the skin for improvement of the disease in a short time.

Bari et co-workers demonstrated that the silk sericin, due to its wound healing potential, in addition to being a carrier used for microcapsule fabrication, can improve the regeneration of the *Chlorella Vulgaris* (Chl) and *Arthrospira Platensis* (Art) microalgae. In work, five formulations based on algal extracts (Chl and Art) or silk sericin (Ser) or their combination (Chl, Art, Ser, Chl-Ser, Art-Ser) were prepared by using a solvent-free extraction method. [87]

All formulations resulted in cytocompatible, and the *in vitro* scratch test showed that all samples tested were effective in promoting the wound healing process. In detail, the addition of sericin to Chl formulation improved the ability of alga to close the wound, unlike Art-Ser sample.

After a skin lesion, a wound healing process, which consists of extraordinarily organized and coordinated events, including inflammation, proliferation and remodelling, is started to restore tissue integrity and functions. This healing process requires the recruitment and activity of different cell types, such as native immune response cells, endothelial progenitor cells, keratinocytes and fibroblasts (Figure 29). [88]

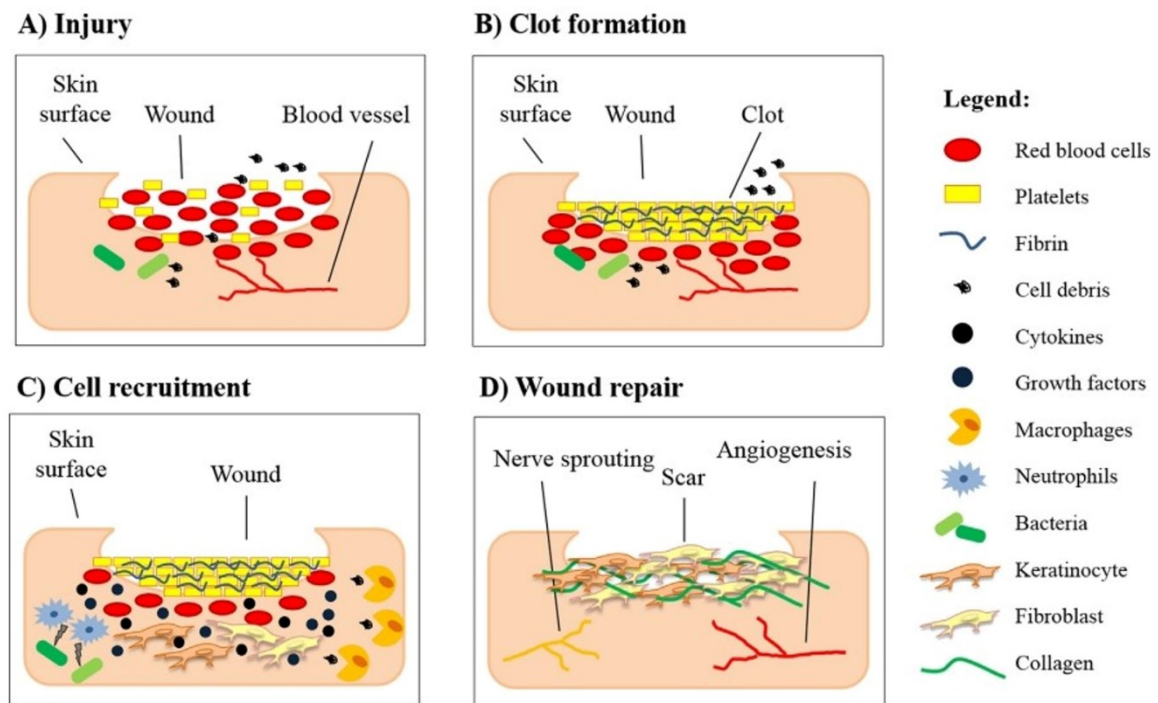


Figure 29: Schematic representation of wound healing phases. (A) After the injury, bleeding occurs as a consequence of blood vessels damage and cell debris are released. Without skin protection, bacteria penetrate the wound. (B) A clot, made of platelets and fibrin fibres is formed to stop bleeding. (C) Platelets release cytokines and growth factors to activate the immune response (D) Keratinocytes and fibroblasts start the wound repair by deposition of collagen and the angiogenesis leads to the formation of new blood vessels. Reproduce from *International Journal of Biological Macromolecules*, Bari, E.; Perteghella, S.; Faragò, S.; Torre, M. L., *Association of silk sericin and platelet lysate: Premises for the formulation of wound healing active medications*, 119, 37-47 (2018), with permission from Elsevier

In detail, re-epithelialization involves not only the proliferation of keratinocytes but also their migration after injury in a few hours, for a complete restoration of epithelial continuity.

Silk sericin was recently reported to promote this migration when used as a supplement in cell culture medium in wound healing scratch assays. This affects the trigger of cellular pathways which lead to c-Jun protein activation, which has a crucial role in wound healing and keratinocyte migration. [34]

The capacity of sericin to promote collagen formation in wounds and thereby accelerate the re-epithelialization of open wounds also represents a potential start point for the treatment of burns.

Indeed, to prevent the infection of wounds, the aim is their rapid closure, also leading to quick repair of the damaged tissue with fewer functional and aesthetical side effects [89].

For this goal, a wound treatment sericin-based cream was tested clinically for second-degree burns by Aramwit et group. Over the whole period, until complete wound healing was obtained, the presence of sericin significantly enhanced the reepithelialization process and reduced the time required for the complete healing process. The serum albumin level in the group treated with the protein was significantly higher than that in control and correlated with wound size reduction, suggesting that these factors could be related.

Other desirable features of sericin were the antibacterial activity, moisturizing action, and enhanced oxygen permeability, all of which are crucial parameters for normal and rapid wound healing [34]. Sericin also has a remarkable antioxidant activity, which is mainly due to the presence of hydroxyl functional groups in its amino acid sequence, mainly from Ser, Tyr, and Thr (Figure 30) [90]. This activity appears to be correlated with anti-elastase and anti-tyrosinase activities, which accentuate its anti-wrinkle and whitening effect, respectively. [91]

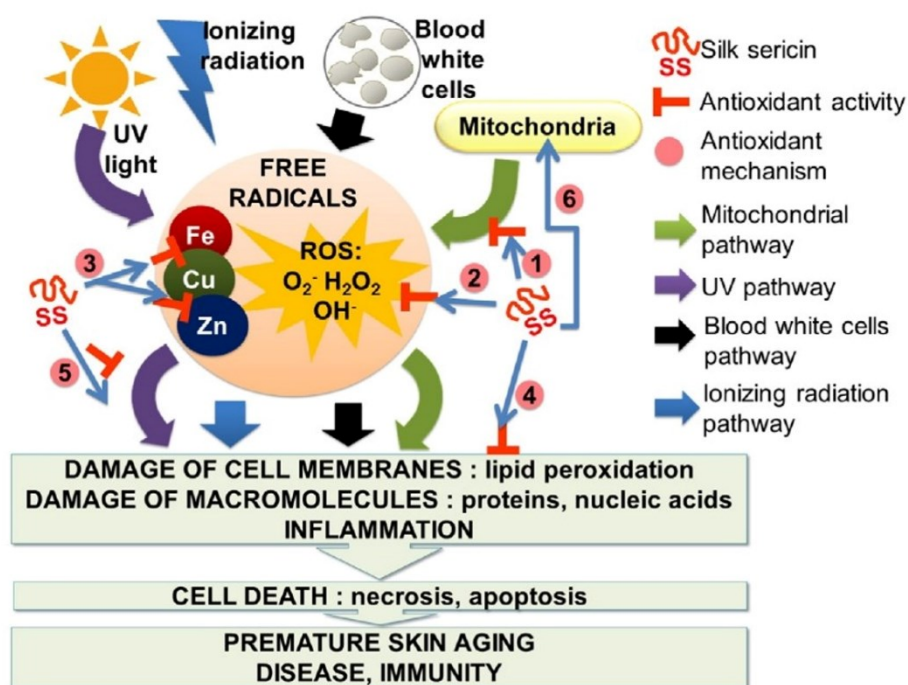


Figure 30: Mechanisms of sericin anti-oxidative activity. ROS: reactive oxygen species; 1: enhancement of antioxidant enzymes: superoxide dismutase, glutathione peroxidase; 2: ROS scavenging; 3: chelation of transition metals; 4: prevention of lipids peroxidation and inflammation; 5: inhibition of UV-induced apoptosis and sunburn effects on the skin; 6: increasing of the level of NAD⁺: improved detoxification via oxidation. Reproduce from *Biotechnology Advances*, Lamboni, L.; Gauthier, M.; Guang Yang, G.; Wang, Q., *Silk sericin: A versatile material for tissue engineering and drug delivery*, 33, 1855–1867 (2015)

Specifically, the acidic amino composition of sericin allows the elimination of free Radical Oxygen Species (ROS) and advances the activity of antioxidant enzymes, including superoxide dismutase and glutathione peroxidase. Also, Ser and Thr amino acids, with their hydroxyl groups chelate the trace elements such as iron, zinc and copper that generally catalyse oxidation reactions. Other amino acids, such as Ala and Gly, have shown a cytoprotective effect on hepatocytes or renal tubular cells against many types of damage induced by the oxidative stress. [29]

Dash et al. investigated the free radical scavenging and photoprotector potential of sericin from *Antheraea mylitta*, against ultraviolet light B (UVB) in irradiated human keratinocytes. The analysis in flow cytometry revealed that the pre-treatment with sericin inhibited apoptosis of cells exposed to UVB rays, by suppressing the expression of pro-apoptotic protein Bax, the up-regulation of bcl-2, and the activation of caspase-3. By reducing oxidative damage, silk sericin thereby protected skin keratinocytes from UVB-induced apoptosis, sunburns, and tumorigenesis.

In addition to the amino acid composition, the accumulation of natural pigments typically flavonoids and carotenoids in cocoons determine the antioxidant role of sericin. [92] [12] [93] [94]

Flavonoids are a class of polyphenolic compounds having significant human health benefits. Some of the flavonoids polymerize to form tannins, secondary metabolites synthesized by plants in hydrolysable or condensed form. The latter corresponds to that of proanthocyanidins, present in flowers, nuts, fruits, bark, and seeds of different plants, as a defence against biotic and abiotic stressors. [95] [96] Another example of flavonoids is the quercetin, which is a flavonol, primarily found in fruits and vegetables, and epigallocatechin gallate, categorized as catechin, present in tea. Various biological effects have been attributed to polyphenols, including antioxidant, anti-tyrosinase, anti-elastase, anti-inflammatory, antimicrobial and anti-cancer, and anti-diabetic property. [97] Notably, the anti-elastase activity of sericin and flavonoids may help slow down the degradation of the elastin in tissue, which is generally caused by the excess of protease activity that follows tissue damage. [98]

In a study conducted by Takechi et co-workers, the antioxidative activity was measured in white and yellow-green sericins. [99] According to the authors, the flavonoids present in the sericin layers are responsible to the higher free radical scavenging activity of yellow-green sericin than that of white sericin, as indicated by 1,1-diphenyl-2-picrylhydrazyl (DPPH), chemiluminescence, oxygen radical absorbance capacity methods. By contrast, the electron spin resonance revealed that white sericin is better probably because the antioxidant potential

of flavonoid pigments can not be involved in the elimination of hydroxyl radicals, detected by this technique. Therefore, the results confirmed that all sericins have an excellent antioxidant property against various free radicals.

Aramwit et colleagues demonstrated that the anti-tyrosinase activity of sericin was more significant when obtained from cocoons with flavonoids and carotenoids. However, the potential was also present in cocoons submitted to the pigment extraction process, showing that sericin itself has the intrinsic capacity to inhibit one of the key enzymes of skin ageing. [100]

The antioxidant properties of sericin, together with its behaviour similar to dietary fibre, could play a beneficial action for the prevention of colorectal cancer at the intestinal level, in agreement with as reported by Kaewkorn and colleagues. [101] Indeed, the authors investigated the effects of sericin on the proliferation and apoptosis of colon cancer cells and evidenced a reduction of the oxidative stress, inflammatory response and TNF- α production.

Also, a protective effect of sericin in ethanol-induced hepatic and gastric injury in mice was observed. The treated animals showed higher alcohol elimination in urine, and this lowers concentration in serum. The sericin recovered the cellular morphology and preserved the mitochondria integrity in gastric mucosa, probably based on its antioxidant potential. [102].

Previously, studies have suggested that a diet supplemented with sericin may be beneficial to human health in preventing cardiovascular and metabolic disease. In particular, the oral administration of sericin increased insulin secretion on a murine model. [103] Interestingly, the favourable effect of sericin is not only limited to the decreasing action in blood glucose levels but also the improvement of diabetes complications. Other studies have shown the antihyperlipidemic effect of sericin. Indeed, when administered orally to rats raised on a diet rich in lipids, sericin decreased the lipid blood levels, increased the glucose tolerance as well as the adiponectin blood levels, thereby regulating glucose and fatty acid catabolism. [104]

The use of silk sericin in cosmetics is widespread. Here, the free radical scavenging activity of sericin is combined with its anti-elastase (anti-wrinkle) and anti-tyrosinase (whitening) properties. [12]

In cosmetic applications, such as creams and shampoos, silk sericin is used as an excipient with remarkable moisturizing, elastic, anti-ageing, and anti-UV light effect. These properties are mainly due to its amino acids with hydrophilic side groups, which have a great capacity to absorb water.

Regarding this, the *in vivo* moisturizing effect of sericin was studied on human skin. It has been found that the protein action was to increase levels of hydroxyproline and hydration of

the epidermal cells. [105] The increase in hydration was attributed to the occlusive effect of sericin, which prevented the transepidermal water loss, responsible for skin dryness.

Furthermore, sericin is presented as a potential alternative therapy as an adjunct in the treatment of dry skin in an animal model of atopic dermatitis [106]. Interestingly, adding 1% of sericin to the diet for 10 weeks caused an enhancement in epidermal hydration, promoting the increase of total filaggrin and the reduction of molecules responsible for its degradation.

In the tissue engineering field, the amorphous structure, wide molecular weight distribution, and high water solubility make sericin a fragile material difficult to fabricate and unsuitable for many medical applications, especially when excellent mechanical properties are required.

Accordingly, diverse strategies have been applied to improve the physical properties of sericin-based materials, especially when the protein is extracted by the alkaline or autoclaving degumming method from cocoons. Fortunately, the polar side chains of sericin with hydroxyl, carboxyl, and amino groups permit the easy cross-linking, copolymerization, and blending of the protein with other polymers to yield improved biodegradable materials. [34]

An example reported in the literature regards bidimensional films and tridimensional scaffolds obtained by blending sericin with gelatin and cross-linking with glutaraldehyde. [107] Improved mechanical strength was achieved via the incorporation of gelatin, while the protein produced a homogeneous morphology and porosity in the scaffolds, which also presented high swellability. Moreover, low immunogenicity of sericin in the matrices was observed through TNF- α release, suggesting the potential of sericin as a biocompatible material for tissue engineering applications.

Interestingly, silk sericin addition to cell culture media improves cell proliferation, showing a mitogenic effect on different lines of mammalian cells [88] and cryo-protective properties. However, it is important to underline that the mechanisms by which this occurs have not yet been fully clarified.

In 2005, Terada et co-workers found that the molecular weight has a relevant role. [108] Silk sericin at the high molecular weight (Ser-A, 50-200 kDa) showed mitogenic effects lower than that having a molecular weight ranged from 5 to 100 kDa (Ser-B).

Ser-B successfully promoted the proliferation of hybridoma cells in various serum-free media, with a mitogenic effect independent from the medium. The same authors also demonstrated that Ser-B improved the established T lymphocyte cell line (CTLL-2) proliferation, under interleukine-2 starvation conditions.

Overall, even if sericin can not substitute fetal bovine serum or platelet lysate in long-term cell cultures, as it lacks the hormones and growth factors that are fundamental to support cell

proliferation, it has all the characteristics to be suitable as a cell culture supplement. Those include, other than the mitogenic features, also anti-oxidant and anti-apoptotic ones.

Finally, in the cryopreservation field, sericin has been employed in the preparation of freezing media for both mammalian and insect cells. Indeed, sericin proteins are rich in amino acids, which are well-known to be cryoprotective in anti-freeze proteins.

About that, Wu and colleagues investigated which fractions to the high or low molecular weight of protein could have a cryoprotective action. [109] The research group isolated small peptides (SM-AFP) capable of absorbing at the surface of the ice crystals, with a molecular weight of 1009,50 Da and a sequence composed of Ser, Thr, Pro, Val, Asn amino acids. Molecular models suggested that the interactions between SM-AFP and ice crystals could be partially attributed to the hydrogen bonds established between the Thr and Asp residues and the ice water atoms, to the hydrophobic interactions between the hydrophobic lateral chains of Pro and Val and to the Van der Waals and electrostatic forces.

3. Technologies for the characterization of silk-based materials

Analytical characterization ensures the identity, purity, structural and conformational integrity as well as the activity of a protein. The precise amino acid sequence, molecular weight distribution, charge variances, structural changes, and aggregation level, are among the critical components of thorough characterization of a protein molecule.

Nowadays, thanks to its biocompatibility, biodegradability, excellent mechanical properties and ease of processing, silk has been applied in many new applications in biotechnology, such as wound dressing, tissue engineering, and targeted drug delivery. [110]

It is essential to be able to determine the composition, purity grade, and stability of the protein in the considered pharmaceutical form, to guarantee the quality, therapeutic efficacy, and safety of silk-based materials.

In this framework, thermal analysis and spectrophotometric methods, supported by chromatographic, particle size analysis, and microscopic techniques, resulted in pertinent to evaluate the possible interconversion and interactions between the various conformations of the fibroin and sericin (e.g. from the most stable crystalline structures to the metastable amorphous ones), the morphology and the particle size of silk-based micro and nanosystems. About that, this chapter provides an overview of the best known applicative techniques concerning the characterization of silk proteins.

3.1 Thermal Analysis

When a transition occurs from one physical state to another, there is always absorption and emission of energy in quantity proportional to the weight of the sample. The variation causes a thermic effect, exothermic or endothermic, and always takes place at a precise temperature or characteristic temperature intervals.

To measure the thermal effects quantitatively and to record the temperature at which they occur, it is possible to characterize a material about its identity and physical structure.

To clarify the structure and identity of a substance, the most commonly used techniques of thermal analysis are differential scanning calorimetry (DSC) and thermogravimetric analysis (TGA).

The principle of the DSC consists of subjecting the sample under examination and an inert reference sample to gradual heating during a controlled temperature program. At the transition phenomenon, a finite amount of energy is supplied to the sample under examination to maintain it at the same temperature as the inert sample. Each endothermic or exothermic modification of the sample causes an imbalance in the system, which is instantly corrected to restore temperature equality. The electrical energy needed to restore balance represents the direct measurement of the thermal energy developed or absorbed for the transition.

The amount of energy transferred or absorbed during the transitions (dH / dt) is recorded as a function of temperature, where dH is the rate of heat absorbed at constant pressure and dt is the rate of temperature change. [111]

When a sample is subjected to a thermic event, the total heat capacity of the system is altered; the latent heat associated with the melting or crystallization is registered as a peak, while a change in heat capacity (e.g. a glass transition) is registered as a shift in the baseline. Conventionally, in a DSC graph, endothermic events are represented by downward oriented peaks, while crystallization exotherms by upward peaks. The area under the curve for a thermal event is proportional to the energy involved in the process; therefore, it is possible to reconstruct a qualitative and quantitative analysis of solid, semisolid, and liquid state materials by DSC instrument calibration with reference samples with well-defined melting points, heats of fusion and heat capacities.

Moreover, differential scanning calorimetry represents an analytical approach for polymorph screening. [112] A sample can exist in two polymorphic forms: amorphous and crystalline, the former less stable than the latter. Amorphous solids are characterized by a short-range

order than the long-range order typical of crystalline samples, in which molecules in a crystal reticulation are repeated along with the three crystallographic directions. By heating crystalline samples, a first-order transition occurs due to the destruction of this order at the melting, registered in DSC graphs as an endothermic event to which thermic (T_m) and enthalpic (ΔH_m) parameters are associated. Contrary, after heating an amorphous sample, this shows a second-order transition caused by a change in the physical state from glassy to rubbery, which results in correspondence to the glass transition. In the DSC graph, this effect corresponds as a deflection in the baseline that can be recognized by a temperature (T_{midpoint}) which corresponds to the midpoint of the temperature range over which glass transition takes place. The glass transition usually occurs in semicrystalline or completely amorphous solids. [113]

Unlike DSC, TGA is an analytical technique used to determine a material's thermal stability and its fraction of volatile components by monitoring the weight change that occurs as a sample is heated at a constant rate. [112] However, since many changes in physical structure induced by temperature occur without there being a change in weight (melting, glass transition), its application is limited.

For this reason, TGA is often considered as a supporting technique to investigate thermal events recorded in DSC curves. The thermogravimetric analysis is particularly advantageous for the characterization of solvated samples, where endothermic effects due to thermal desolvation in DSC graphs appear as mass losses in TGA curves. In this way, the solvent content of a sample and the solvent stoichiometry can be established, and thereby to stabilize the interaction forces between solvent and crystal packing.

Higher will be the bond forces in the crystal structure, and higher will be the energy used to rupture them, thereby reflecting in an increase of temperature of the desolvation thermal events associated.

Moreover, the evaluation of the water content through TGA measurement is useful to investigate water-protein interactions, that are important considering the function of water as a plasticiser in the structural flexibility of silk proteins. Typically, a high water amount promotes the mobility of the molecules in a material. The water content is also correlated to the glass transition temperature, that DSC graphs record at a lower temperature with the increasing of water content in the sample.

In the case of silk sericin from *Antheraea assamensis*, two principal endothermic DSC peaks were observed (Figure 31).

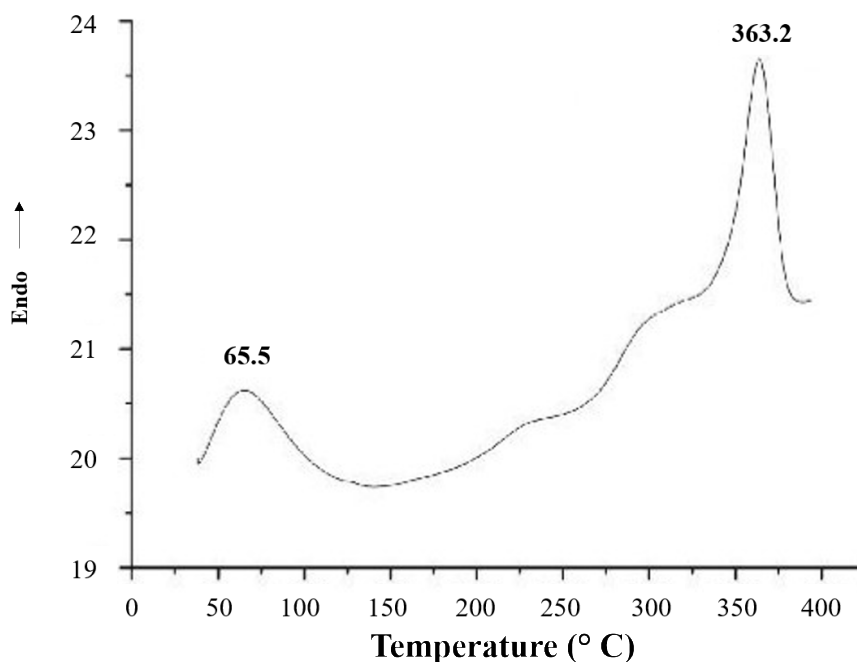


Figure 31: DSC spectrum of sericin extracted from *Antheraea assamensis* silkworms. Modified from *Global Journal of Bio-Science & Biotechnology*, Dutta, S.; Bharali, R.; Devi, R.; Devi, D., *Purification and characterization of glue like sericin protein from a wild silkworm Antheraea assamensis Helfer*, 2, 229-233 (2012), with permission from Society For Science and Nature

The first one (at 65.5 °C) was attributable to the melting point, while the second one (at 363.2 °C) appeared consequently to the decomposition of the protein.

Generally, this latter peak shifts to lower temperatures when the proteins have lower thermal stability, as observed for *Antheraea mylitta* and *Bombyx mori* sericins. [114]

Comparing DSC thermographs of *Bombyx mori* and *Eri (Philosamia ricini)* silks, Prasong et colleagues found differences. [115] Thermal properties of domesticated silk *Bombyx mori* took place in a single step. In detail, two endothermic peaks were observed at 329, and 334 °C corresponded to the silk fibre with and without sericin, respectively. Conversely, the *Philosamia ricini* silk suffered at least two thermal decomposition stages with endothermic peaks at about 240, 320, 385, and 450 °C and 240, 340, 390, and 460 °C in the presence or absence of sericin, respectively. Interestingly, the removal of sericin from fibres improved the structural stability in both silks. This illustrates that the process of sericin removing can

induce the secondary structure change of silk from random-coil to β -sheet domains with a more stable crystal formation.

In the same temperature range of the endothermic effects recorded in DSC curves, two distinct mass losses were observed. The first one was attributable to the absorbed water evaporation for the two samples at below 100 °C, and the second one over 200 °C was due to thermal decomposition of samples.

Catenacci et colleagues revealed a differential weight loss of fibroin and sericin in DTG curves, which report the maximum temperature of each mass loss step. For fibroin, the thermal decomposition peak was localized at 300 °C, while for sericin the decomposition takes place earlier at about 260 °C, due to the different way of breaking intermolecular bonds. The more stable β -sheet conformation of fibroin than to the amorphous one of sericin justifies the difference in thermal stability between the two silk proteins.

Finally, thermal analysis is a useful tool to study the thermal and structural characteristics of the treated material with respect to the native one to verify if the degumming process affects the thermal decomposition behaviour. DSC analysis performed on degummed silk fibroin by chemical method showed a less-ordered state for the fibroin resulted from the treatment. In detail, even if the thermal profile was approximately the same as the raw fibroin, the temperature of the endothermic decomposition peak was registered at a lower temperature, and a glass transition effect, due to a higher content of amorphous regions in the conformation of the protein, was observed. [113]

An exothermic effect could accompany this glass transition for the crystallization induced by the heating of amorphous portions which present the melting/decomposition at a higher temperature. [116]

3.2 Chromatographic techniques

Chromatographic methods include techniques devoted to the separation of various compounds as a step before their characterization. Their advantages are related to their high power of separation of substances, and the easy and simple manipulation, although they have as a handicap the nonspecific interactions and the difficulty in method optimization. [117]

In the following paragraph, several types of chromatographic techniques are briefly described.

3.2.1 Hydrophilic interaction liquid, reversed phase, and size exclusion chromatography methods, and electrophoresis SDS-PAGE

The chromatography is a term used for a wide variety of techniques in which a mixture of substances is fractionated by passing through some types of porous matrices.

In liquid-phase chromatography techniques, the components of the mixture can be associated with one of two alternative phases: a mobile and stationary phase. The former consists of the mobile solvent in which the protein is dissolved and the latter is the matrix through which the solvent moves. The materials that make up the stationary phase contain sites to which proteins in solution can bind. Following the interactions between proteins and the stationary phase, in the chromatographic column, the displacement of the molecules is delayed. Hence, the higher the affinity of a given molecule with the stationary phase, the slower its passage through the column. Because different proteins of the mixture have different affinities for the matrix, they are delayed differently. The proteins that have the lowest affinity for the column appear in the first emerging fractions. [118]

To separate compounds, normal or reversed-phase liquid chromatography can be used. In normal-phase liquid chromatography (NP-LC), the stationary phase is more polar compared to the mobile phase. The retention increases as the polarity of the mobile phase decreases, and thereby hydrophilic analytes are more strongly retained than non-polar ones. The opposite situation occurs in reversed-phase liquid chromatography (RP-LC). NP-LC has been widely used to separate various compounds, from nonpolar to highly polar compounds.

In the last years, the resolution of many chromatography procedures has been amplified with the development of high-performance liquid chromatography (HPLC).

Hydrophilic interaction liquid chromatography (HILIC) is an alternative HPLC mode for the separation of polar compounds. For historical reasons, it has been reported that HILIC is a variant of normal phase liquid chromatography, although the separation mechanism used in HILIC is more complicated than that in NP-LC. Like NP-LC, HILIC utilizes traditional polar stationary phases such as silica, amino or cyano, but the mobile phase used is similar to those employed in the RP-LC analysis. [119]

Since the stationary phase is hydrophilic in this technique, molecules with hydrophilic properties contained within the mobile phase will have a high affinity for the stationary phase, and therefore will adsorb to the column packing. Contrary, hydrophobic molecules experience less of an affinity for the column packing and will pass through to be eluted and detected first. Overall, the retention phenomenon in HILIC mode simultaneously depends on different types

of intermolecular interactions between the solute and the stationary phase, the solute and the mobile phase, and the stationary and mobile phases, listed in Figure 32.

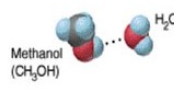

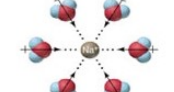
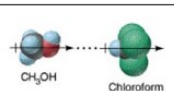
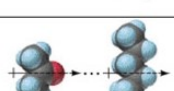
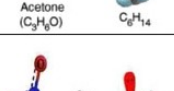

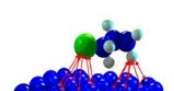
Type of interaction		Characterization	Energy [kJ·mol ⁻¹]	Example system
Chemical interactions	Hydrogen bonding	formed between hydrogen of the protodonor group and atom being hydrogen acceptor, can be formed within the same molecule, as well as between two different	- (4 - 17)	
	Donor – acceptor interactions	occurs between pairs of electron donor (Lewis base) and acceptor (Lewis acid)	- (4 - 17)	
Physical interactions	Ion – dipole	ion acts on electrically neutral molecule; leads to a multicomponents	- (4 - 17)	
	Dipole – dipole	force between two electrically neutral particles, but having determined dipole moments	- (4 - 17)	
	Dipole-induced dipole	forces between the molecule possesses clear dipole moment and non-polar molecule	- (4 - 17)	
	Temporary dipole-induced dipole	two electrically neutral particles, if they come close together, will attract on the electrostatic forces way	- (4 - 17)	
Intermolecular interactions (Van der Waals forces)		weak forces of attraction between the fragments of individual molecules, declining rapidly with increasing distance between the interacting particles, do not lead to permanent connections	- (2 - 4)	
Hydrophobic interactions		forces operating in the aquatic environment between molecules with low affinity for water	- 4	

Figure 32: Examples of interactions between the analyte, stationary phase, and mobile phase. Reproduced from *Analytical and Bioanalytical Chemistry*, Buszewski, B.; Noga, S., *Hydrophilic interaction liquid chromatography (HILIC) - a powerful separation technique*, 402, 231-247 (2012) (Open Access)

Reversed-phase chromatography (RPC) is a technique using alkyl chains covalently bonded to the stationary phase particles to create a hydrophobic stationary phase, which has a stronger affinity for hydrophobic or less polar compounds. As a result, hydrophobic molecules in the

polar mobile phase tend to adsorb to the hydrophobic stationary phase, and hydrophilic molecules in the mobile phase will pass through the column and are eluted first. Hydrophobic molecules can be eluted from the column by decreasing the polarity of the mobile phase using an organic (non-polar) solvent, which reduces hydrophobic interactions. The more hydrophobic the molecule, the more strongly it will bind to the stationary phase, and the higher the concentration of organic solvent that will be required to elute the molecule. [120] RPC can be used for the separation of a wide variety of molecules. However, NP-LC is more commonly used for separation of proteins, because the organic solvents used in RPC can quickly raise the protein denaturation.

The concept of size-based separations by chromatography was first speculated by Synge and Tiselius, based on the observation that small molecules could be excluded from the small pores of zeolites as a function of their molecular size. The term “molecular sieve,” coined by J. W. McBain to describe this property of zeolites, was subsequently used to describe the technique commonly known today as size-exclusion chromatography.

While numerous techniques have been developed to check protein aggregation, SEC has been predominantly favoured for routine and validated analyses because of both its speed and reproducibility. [121] [117]

The SEC chromatography separates proteins, peptides, and oligonucleotides based on size and molecular weight. Molecules move through a bed of porous beads, diffusing into the beads to greater or lesser degrees. Smaller molecules diffuse further into the pores of the beads and therefore move through the bed more slowly, while larger molecules enter less or not at all and thus move through the bed more quickly. Both molecular weight and three-dimensional shape contribute to the degree of retention (Figure 33).

For SEC analyses, UV continues to be the predominant mode of detection. Also, mass spectrometry (MS) is used as the method for obtaining molecular weight information. However, there are challenges to interfacing SEC with MS due to principally to the ion suppression and contamination of the mass spectrometer caused by the incompatibility of mobile phases containing high concentrations of nonvolatile salts.

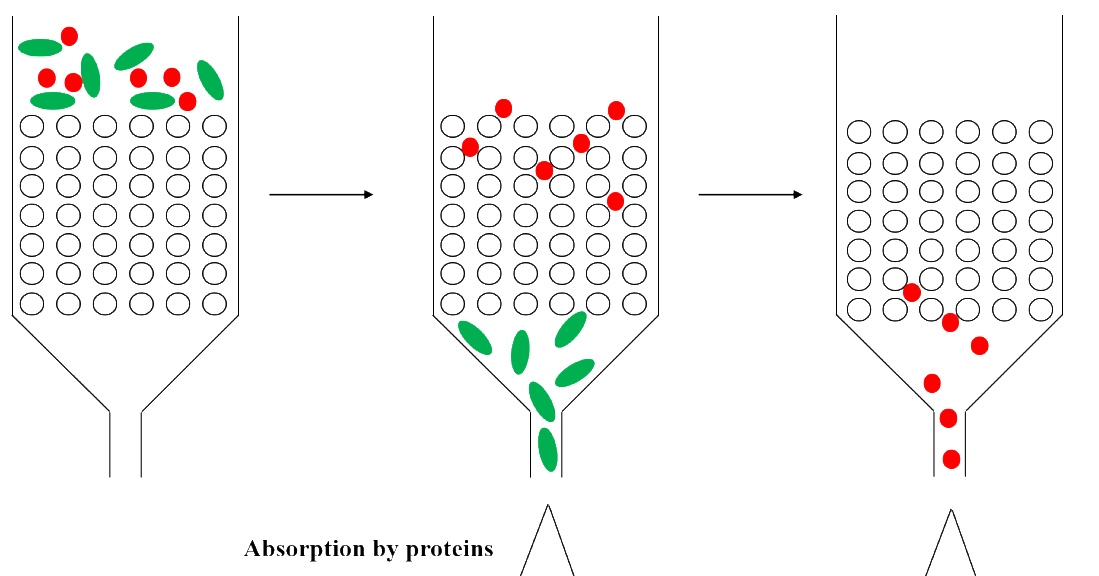


Figure 33: Schematic illustration of the protein separation by size-exclusion chromatography

To overcome this obstacle, SEC-MS techniques have been developed using denaturing mobile phases containing organic solvents and ion-pairing reagents. [121]

The most direct information regarding the condition of the historical silk textiles or silk-based modern products could be obtained from the evaluation of the molecular weight distribution of the fibroin polymer being the main component of silk fibres.

Normally, the degree of degradation of silk fabrics was measured by the loss of its mechanical resistance, colour, and crystalline structure. However, today these have been replaced by more advanced analytical methods, including the sodium dodecyl sulphate polyacrylamide gel electrophoresis (SDS-PAGE) to measure the molecular weight of silk subunits [42] [46], and the SEC [30].

Silk analysis conducted by SEC is, however, challenging. The difficulties derive mainly from the sample preparation method or more precisely the choice of the solvent, which in some cases could lead to degradation and/or aggregation of silk proteins.

Regarding this, Pawcenis et colleagues conducted a study to optimize the procedures of silk preparation and separation to achieve an accurate and reproducible analysis of the molecular weight distribution of silk fibroin, also for highly degraded samples. [110]

Two sets of artificially aged fibroin samples were prepared with and without sodium chloride in solution to explore the influence of preparation conditions. Fibroin was degummed in the LiBr solution and then dialyzed to remove the salt, which destroys stacks chromatographic

columns and prevents reproducible analyses. Contrary, rich-NaCl aqueous solutions of silk fibroin improved the quality of chromatograms.

Another effective technique widely used for the splitting up of proteins is electrophoresis. The electrophoretic separation of proteins is usually carried out with polyacrylamide gel electrophoresis (PAGE), in which the proteins migrate under the influence of an applied current through a gel composed of polymerized acrylamide as a molecular sieve. Separations are usually carried out using sodium dodecyl sulfate (SDS) as the detergent, which negatively charged proteins to migrate them towards the positively charged pole, located bottom of the gel.

The relative movement of proteins through the polyacrylamide gel depends on the charge density of the molecules. The higher is the charge density, the greater is the force with which the protein migrates through the gel, the faster its migration speed. However, in addition to charge density, size, and shape also play a crucial role in protein separation. Polyacrylamide forms a sieve: the proteins with higher molecular weight migrate more slowly compared to those with the lower weight. Typically, 5-6% polyacrylamide gel can be useful for the separation of proteins having a molecular weight between 60 and 250 kDa, while 12-15% polyacrylamide gel separates low molecular weight proteins (between 10 and 50 kDa). [118]

Unlike chromatographic techniques, electrophoresis SDS-PAGE is not a quantitative analysis, but only qualitative used to evaluate the molecular mass distribution of proteins. In particular, for silk proteins, a unique and continuous band is usually observed, revealing the wide distribution of molecular weights.

Zhang et co-workers treated degummed silk fibroin with four kinds of calcium-alcohol solutions and performed SDS-PAGE to determine the corresponding molecular weights of treated fibroins.

The regenerated silk fibroins treated with calcium nitrate in methanol and ethanol solutions showed molecular weights between 90 kDa and over 170 kDa. The calcium chloride/methanol solution fibroins ranged from about 140 to over 170 kDa, while proteins in ethanol ranged from about 100 to nearly 300 kDa. The bands to the higher molecular weight suggested that the calcium chloride dissolved in the ethanol was the best solvent that protected the integrity of the fibroin secondary structure provoking with less obvious damage compared to the other solvents. [77]

Bombyx mori silk sericin extracted by woven fabric presented a wider molecular weight distribution ranging from 6.5 to 205 kDa than standard sericin (3.5-43 kDa). This large difference of the molecular mass distribution has a significant effect on protein solubility.

While standard sericin is found to be more readily soluble in cold water, woven silk fabric can only be solubilized in hot water at the temperature of 90 °C. [122]

Interestingly, many experimental parameters, including the source of extraction, processing, degumming, and drying can lead to physicochemical stress in the silk proteins, with a relevant effect on their polymerization grade and the molecular weight distribution.

3.3 Spectroscopic techniques

Spectroscopic techniques give information on the interaction of electromagnetic radiation with a sample, thereby resulting in absorption that depends on the excitation wavelength. Therefore, a wavelength spectrum with absorption/emission peaks that depend on the material is produced. These techniques, in general, are useful to characterize materials, including also nanomaterials, since spectra are peculiar of each material. [123]

3.3.1 Fourier transformed infrared spectroscopy

Fourier transformed infrared spectroscopy (FTIR) is a spectroscopic technique based on the measurement of vibrational transitions between diverse excitation states of molecules. [124] The infrared radiation can be transferred to molecules with dipoles that oscillate with the same frequency of the incident IR light.

The relative masses of the atoms, the force constant of bonds (single, double, triple) and the geometry of the atoms, including intra and intermolecular environment, strongly affect both the vibrational frequency and the wavelength of absorption.

When an infrared photon is absorbed by the molecule, the latter passes from its fundamental vibrational state to an excited vibrational state. The vibrations can be of two types: deformation of the bond angle (bending) and stretching of the bond (stretching), with a consequent increase or decrease in the interatomic distance. As a rule, the absorption strength increases with increasing polarity of the vibrating bonds.

FTIR is a rapid and cheap technique which allows obtaining characteristic IR fingerprints of each molecule since they are a combination of the vibrational state of each atom. Among the main advantages of the FTIR, which guarantees higher performance, there is the high availability of energy which translates into a significantly better signal to noise ratio than traditional infrared spectroscopy. Moreover, the analysis times are significantly reduced. However, one of the main disadvantages of this technique is sample preparation. Dried samples are required, although some apparatus are prepared for liquid samples; in this last

case, a high concentration of the compounds to analyze is expected. Furthermore, in many cases, a technique optimization is requested to reduce the interference of the sample with water molecules, which strongly absorb and risk hiding the absorbance peaks characteristic of the material analyzed.

Concerning nanomedicines experimentation, many authors used FTIR to confirm the attachment of biomolecules onto nanomaterials surface or to verify the presence of a loaded drug into nanoparticles, since FTIR results in a band pattern as a function of the involved chemical groups. [117]

In this framework, FTIR spectroscopy can be used to study the characteristic absorption bands and molecular conformation of both fibroin and sericin. [113] Moreover, the shape, intensity and vibration frequencies of FTIR bands are often indicative of structural modifications into the protein caused by specific experimental conditions (temperature, pH, ionic force).

According to International Union of Pure and Applied Chemistry (IUPAC), in a typical infrared spectrum, we find the wavenumber (cm^{-1}) of the incident photon on the abscissa axis and on the ordinate axis the transmittance value.

In FTIR spectrum three spectral regions can be identified: the far-infrared (below 400 cm^{-1}), mid-infrared (from 400 to 4000 cm^{-1}), and the near-infrared region (from 4000 to 13000 cm^{-1}).

Among these regions, the most studied for the identification of a substance is the mid-infrared region, which in turn can be subdivided into four zones based on the absorption frequency of the principal functional groups. The main significant bands are attributable to the X-H stretching (e.g. O-H, C-H and N-H) in the region between 4000 - 2500 cm^{-1} , to the triple bond stretching whose band is localized between 2500 - 2000 cm^{-1} ($\text{C}\equiv\text{C}$ at 2300 - 2050 cm^{-1} , $\text{C}\equiv\text{N}$ at 2300 - 2200 cm^{-1}), and C=C and C=O stretching absorption in the spectral zone between 2000 and 1500 cm^{-1} .

The spectrum region between 1500 and 650 cm^{-1} is called “*fingerprint region*”, because it is characterized by a complex absorption, principally due to the presence of overlap bending vibrations. [125]

For silk proteins, the characteristic absorption bands of amides fall into the spectral zone between 650 and 4000 cm^{-1} . In detail, two absorption peaks at 3520 and 3400 cm^{-1} characterize the amides I, attributable to the symmetric and antisymmetric stretching vibrations of the N-H group.

In the case of amides II, the absorption vibrations of the same group are localized in the interval between 3500 and 3060 cm^{-1} , depending on the concentration and physical state of the sample.

The absorption of the C=O of the amides is registered at lower wavenumbers compared to the traditional carbonyl, as a result of the resonance effect.

Both for the primary and secondary amides, the absorption frequency changes if the sample is analysed in solid-state or in diluted solution depending on the presence and nature of intramolecular hydrogen bonds. For solid-state samples, the amide I bands can be slightly shifted to lower wavenumbers (3350 and 3180 cm^{-1} , respectively).

The amide I vibration peak is near 1620 cm^{-1} , increasing up to 1690 cm^{-1} in solution, whereas that of the amide II from 1640 to 1680 cm^{-1} . Contrarily, the frequency of the carbonyl of amides III, registered at 1630-1680 cm^{-1} , is independent of the physical state, because the formation of intramolecular hydrogen bonds is not possible.

Regarding the bending vibration peaks, that of the N-H amide I is localized in the spectral area between 1650 and 1580 cm^{-1} . The same band in the amide II is localized between 1570 and 1510 cm^{-1} . It is attributable to the interaction between the N-H bending and the C-N stretching in the C-N-H group. Finally, another characteristic band of this group of molecules is the stretching vibration of C-N at 1400 cm^{-1} . [113]

These absorption bands in the specific regions of amides I and II can be taken as a reference to investigate the structural conformations of both silk proteins. In fact, the position in the FTIR spectrum and intensity of the amide peaks are demonstrative of the molecular conformation and bonds in the protein chains.

Following what is reported in the literature, fibroin is in liquid water-soluble form and is regarded as silk I. On the other hand, the degummed silk fibres consist of insoluble fibroin (silk II), and thereby, requires more treatments to be transformed back to silk I. The product of this process is commonly called regenerated fibroin. A typical protocol for producing regenerated fibroin from the silkworm cocoons is summarized in Figure 34.

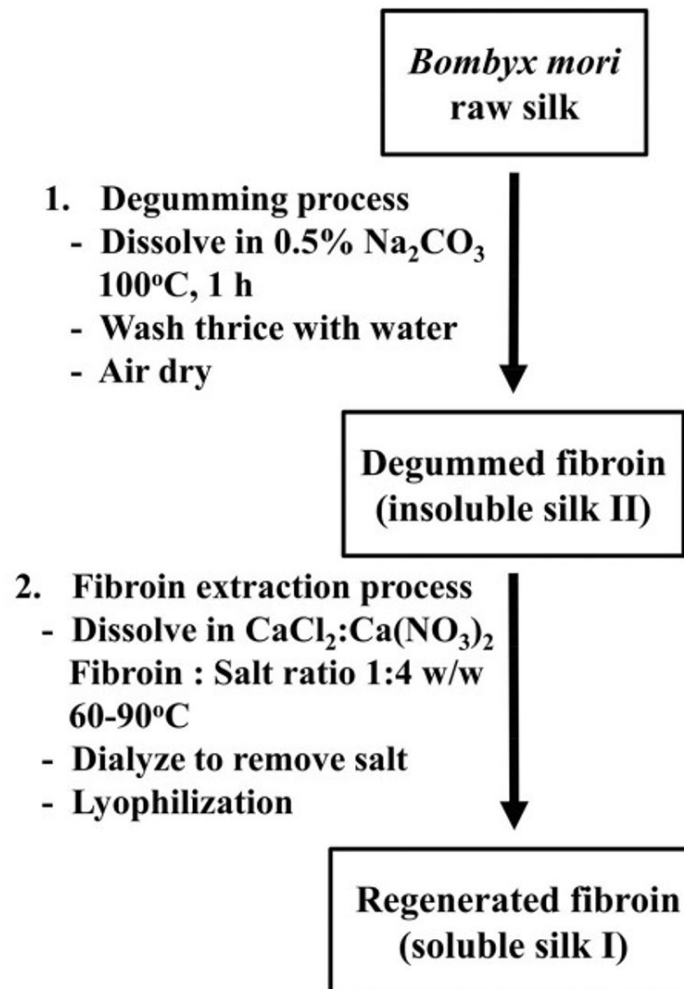


Figure 34: Schematic illustration of silk fibroin degumming and extraction processes to convert protein from silk II to silk I conformation. Reproduced from *Drug Delivery*, Duy Toan Pham, D. T.; Tiayaboonchai, W., *Fibroin nanoparticles: a promising drug delivery system*, 27 (1), 431-448 (2020) (Open Access)

The methods could be slightly different in different studies; however, the sodium carbonate is one of the most used as the degumming agent and the chaotropic salt solution (LiBr or CaCl₂) as the silk II-to-silk I transforming agent. [126]

Silk I, found mostly in the silkworm silk glands, has the lowest crystallinity with a dominant number of random coils and α -helices. These domains form a zig-zag amorphous structure belonging to the orthorhombic system, which makes silk I thermodynamically unstable and soluble in the aqueous solution. On the other hand, silk II, found mostly in the silk fibres, has the highest crystallinity with mostly antiparallel β -sheet domains and belongs to the monoclinic crystal system. [127] Noticeably, these β -sheet motifs have an asymmetrical

structure and concern silk II thermodynamically stable, water-insoluble with a high thermal and mechanical resistance.

Lastly, silk III, found in films formed naturally from the air-water interface of fibroin aqueous solution, is a unique crystalline polymorph of fibroin with a threefold helical crystal structure. It possesses a crystallinity between silk I and silk II, which makes it metastable (e.g. it is less stable than silk II but more compared to silk I). [126]

Guang et colleagues evidenced the main β -sheet structure of fibroin when it was blended with chitosan in 3D-porous composite scaffolds designed for wound dressing.

Fibroin scaffold exhibited weak peaks at 3286 cm^{-1} arising from the intra and intermolecular hydrogen bonding interaction between hydroxyl and amino groups.

The fibroin absorption peaks of amide I, II, and III were at 1625 cm^{-1} (C=O stretching), 1517 cm^{-1} (C-N stretching), and 1230 cm^{-1} (N-H bending), respectively (Figure 35). These bands, together with the absorption band at 1521 cm^{-1} demonstrated the high content of β -sheet domains in fibroin and confirmed that it is in its stable silk II conformation in the scaffold. Moreover, the infrared spectrum of the composite scaffold displayed all the characteristic peaks from chitosan and fibroin, indicating that chitosan was successfully coated to fibroin scaffold (Figure 35). [59]

The amide I band shifts to higher wavenumbers ($1644\text{-}1658\text{ cm}^{-1}$) when fibroin is in Silk I conformation; so this band can be recognized as a reference band to study the conformation transition of fibroin from silk I to silk II. [66]

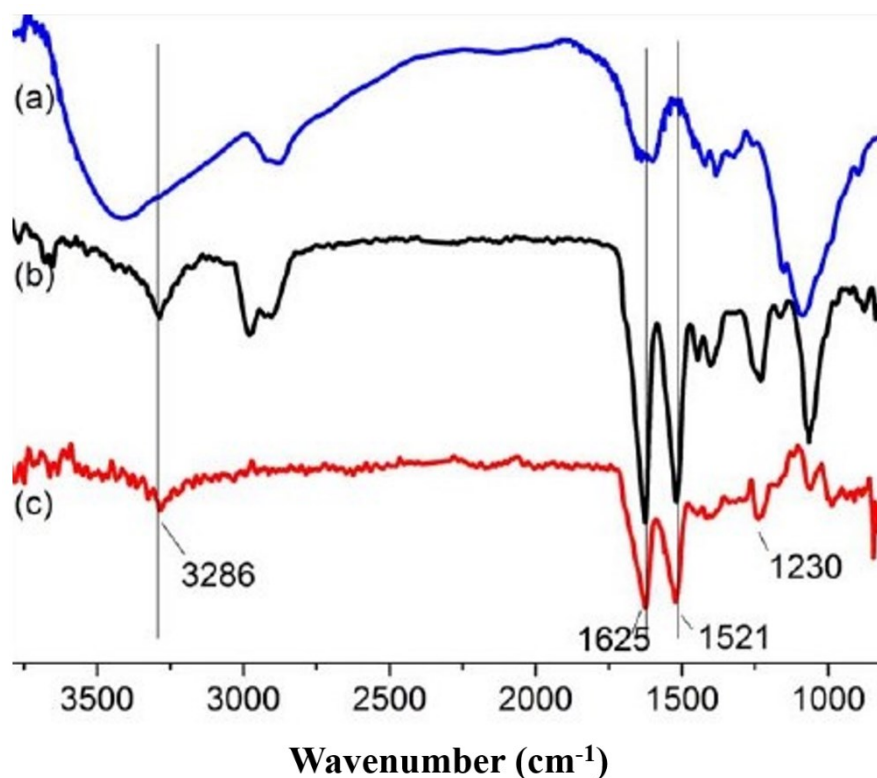


Figure 35: Comparison of FTIR spectra of (a) chitosan, (b) fibroin/chitosan composite scaffold, and (c) fibroin scaffold. Reproduced from *Journal of Applied Polymer Science*, Guang, S.; An, Y.; Ke, F.; Zhao, D.; Shen, Y.; Xu, H., *Chitosan/silk fibroin composite scaffolds for wound dressing*, 132, 42503 (2015) (Open Access)

The sericin, unlike fibroin, is mainly characterized by an amorphous conformation composed of mainly random-coil and only partially β -sheet domains.

In FTIR spectra of formulations containing sericin, alone or in association with *Chlorella vulgaris* (Chl-Ser) or *Arthrospira platensis* (Art-Ser) microalgae extracts, sericin showed typical bands at 1638 cm^{-1} , 1520 cm^{-1} , and 1241 cm^{-1} due to amide I, II, and III, respectively (Figure 36). [87]

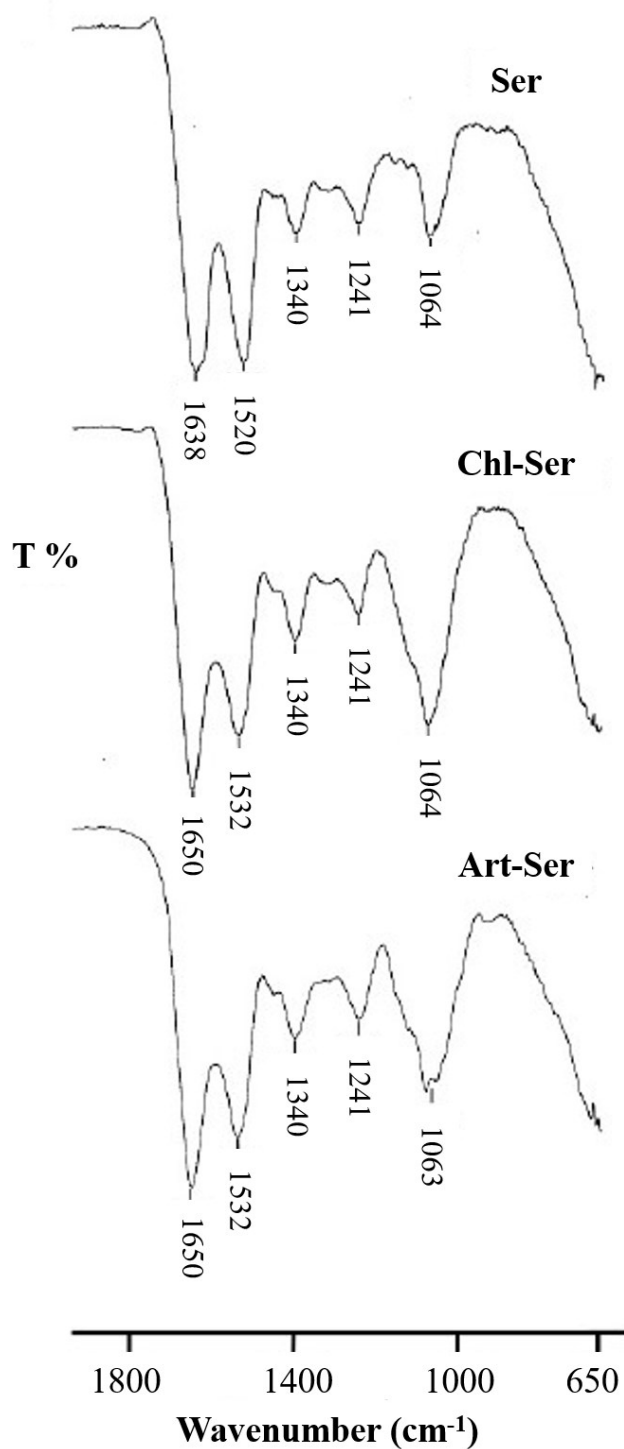


Figure 36: FTIR spectra of silk sericin (Ser), Chl-Ser, and Art-Ser samples. Modified from *Materials*, Bari, E.; Arciola, C. R.; Vigani, B.; Crivelli, B.; Moro, P.; Marrubini, G.; Sorrenti, M.; Catenacci, L.; Bruni, G.; Chlapanidas, T.; Lucarelli, E.; Perteghella, S.; Torre, M. L., *In Vitro Effectiveness of Microspheres Based on Silk Sericin and Chlorella vulgaris or Arthrospira platensis for Wound Healing Applications*, 10, 983 (2017) (Open Access)

The shift of these peaks to higher wavenumber in Chl-Ser and Art-Ser formulations suggested interactions between sericin and microalgae extracts. In particular, the C=O stretching at about 1640 cm^{-1} , the range assigned to random coil conformations, confirms the structure of sericin.

Furthermore, at wavenumbers over 1800 cm^{-1} , the stretching of the N-H bond of amides to 3330 cm^{-1} is superimposed on the O-H groups absorption of the serine and threonine amino acid residues, of which the silk protein is abundant, causing a band broadening. The weak vibration below 3000 cm^{-1} both in the fibroin and sericin spectrum can be attributed to C-H bonds from the silk protein backbone and side chains.

Finally, the absorption bands characteristic of sericin and fibroin can be taken as a reference for possible shifts due to intra and intermolecular interactions.

A combination of the spectrum of the *Bombyx mori* hybrid fibroin and sericin from against the spectra of pure proteins indicated that fibroin and sericin were not subjected to observable structural changes when they simultaneously exist in solution. In contrast, the characteristic peaks of *A. pernyi* fibroin and sericin at 1644 cm^{-1} (C=O stretching) and N-H deformation in the amide I region and 1534 cm^{-1} in amide II region shifted to 1627 cm^{-1} and 1524 cm^{-1} , respectively, suggesting an increase in the intermolecular hydrogen bonding within the silk proteins. The intensive hydrogen bonding between fibroin and sericin of *A. pernyi* silk also explained on a molecular level the strong affinity of *A. pernyi* sericin to fibroin. [128]

3.3.2 Ultraviolet-visible spectroscopy

Ultraviolet-visible (UV-Vis) spectroscopy is one of the most popular analytical techniques because it is very versatile and able to detect a high number of molecules.

When the UV-Vis light is passed through a sample, the transmittance of light is measured. [129]

From the transmittance (T), the absorbance can be calculated as $A = -\log_{10}(T)$, following the Lambert-Beer law.

A UV-vis spectrum shows the absorbance of a compound at different wavelengths. The amount of absorbance at any wavelength is due to the chemical structure of the molecule. Generally, the delocalization of electrons in aromatic systems involves the light absorption of the molecule in the near UV (150-400 nm) or the visible (400-800 nm) region. [130]

UV-Vis spectroscopy can be used qualitatively, to identify functional groups or confirm the identity of a protein by matching the absorbance spectrum. It can also be used quantitatively,

to determine the content of proteins or drugs in a sample, but also as a very popular detector for other analytical techniques, such as chromatography.

The absorption spectroscopy is suited for quantitative measurements because the absorbance of the analyte depends linearly on its concentration, accordance Beer's Law $A = \epsilon cl$, where ϵ , c , and l correspond to the molar absorption coefficient ($L \text{ mol}^{-1} \text{ cm}^{-1}$), the molar concentration and the path length in cm, respectively.

Regarding the spectrum of proteins, the peak of maximum absorbance usually appears in the region of the spectrum comprised between 275 and 280 nm. This signal is attributable to three aromatic amino acids (tryptophan, phenylalanine, and Tyr), and a small extent, by the absorbance of Cys. Interestingly, the wavelength of absorption and the strength of absorbance of the protein depend not only on its amino acid composition but also on the molecular environment in which are present of its chromophore groups. [130]

Analysing UV spectra of sericins extracted by different sources (cocoon, flats, silk waste, and woven fabric), Gupta et colleagues identified the absorption peak at 275.40 nm for all samples (Figure 37). Although this, the shape of the absorption spectra was different. [122]

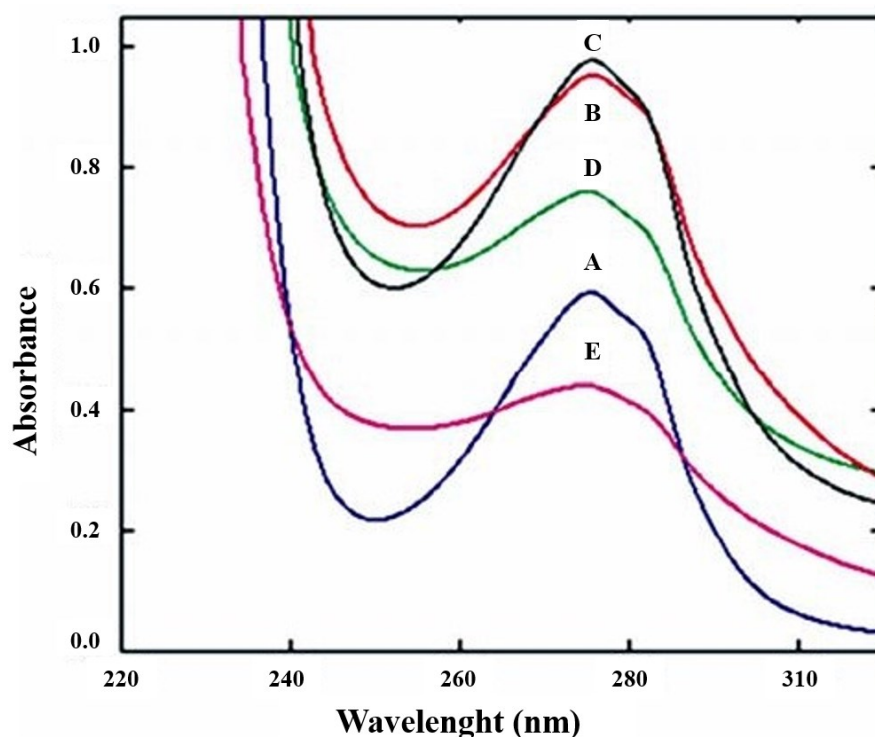


Figure 37: UV spectra of sericin extracted from different sources. Standard sericin (A), cocoons (B), silk fabric (C), silk flat (D) and silk waste (E). Modified from *Indian Journal of Fibre & Textile Research*, Gupta, D.; Agrawal, A.; Rangi, A., *Extraction and characterization of silk sericin*, 39 (4) (2014) (Open Access)

Sericin extracted from cocoons (B), silk flats (D) and waste (E) showed a more enlarged absorption peak than the *Bombyx mori* standard protein (A), suggesting that the type of source strongly can affect the quality of protein. Contrary, after the standard protein, the highest grade purity was obtained for the silk fabric (C), justifying the similarity between their spectra.

In 2011, Sionkowska et co-workers investigated the influence of UV-irradiation on regenerated silk fibroin dissolved in water. It was found that the absorption of fibroin in solution increased during UV-irradiation of the sample, most evident between 250 and 400 nm. Moreover, after UV-irradiation, a broad peak appeared between 290 and 340 nm with maximum absorption at about 305 nm. The new band suggested the formation of new photoproducts during UV-irradiation of regenerated silk protein. [131]

In this framework, the UV-vis spectroscopy has also been used to monitor the kinetics of reactions catalyzed by tyrosinase and elastase enzymes in the presence of sericin and polyphenols as inhibitors by taking repeated UV-Vis measurements over time.

Generally, the rate of the catalyzed reaction or the activity of enzymes can be determined by measuring either the decrease in substrate concentration or the increase in product concentration as a function of the reaction time. When the enzymatic substrate and the product differ in absorbance, the course of the reaction can be monitored directly by the change in absorbance (linearly related to the changes in concentration) as a function of time. [130]

3.4 Particle size analysis techniques

A common feature of all nanomaterials is their large ratio of surface area to volume, which can be orders of magnitude greater than that of macroscopic materials. However, the final dimension and structure of nanomaterials depend on many factors, including the type of the solvent used for their synthesis, the salt and surfactant used as additives during the preparation phase, the reactant concentrations, and the preservation temperature. Thereby, the understanding of physicochemical properties of nanoparticles as well as the fundamentals of the associated measuring methods is necessary before characterizing nanomaterials and achieving reproducible synthesis procedures to optimize the medical and/or pharmaceutical application of nanosystems.

Initially, microscopy and spectroscopy techniques have been proposed to characterize colloidal particles while having each diverse limits. [132]

As an example, the size of the nanocarrier obtained by TEM is not accurate, given that it should be measured in aqueous solution, i.e. the physiological environment in which the nanocarrier will perform its function. [133]

Subsequently, the attention has focalized on the dynamic light scattering (DLS), a rapid and non-invasive technique for measuring the size of particles and molecules in suspension from the dynamic changes of the scattered light intensity. [134]

When a monochromatic light beam (e.g. a laser) hits a solution containing spherical particles in Brownian motion, the wavelength of the incoming light is changed. This change in wavelength is related to the size of the particles. Unlike the larger particles, at the same temperature and viscosity, the smaller particles move quickly, creating rapid variations in the scattering intensity.

Through the complex auto-correlation function, the DLS instrument can determine the diffusion coefficient (D), inversely proportional to the size of the particles, and consequently to establish their average diameter.

To calculate the hydrodynamic radius of particles, also known as the Stokes radius, the Stoke-Einstein equation $D = (K_b T) / (6\pi\eta R_h)$ is applied, where K_b is Boltzmann's constant, T is the absolute temperature, η is the fluid viscosity, and R_h is the hydrodynamic radius of the particle. [132]

DLS-derived particle counts can be quantified averaging the size of the particle-based on intensity, volume, or z-number. Number-weighted distributions are much narrower, while volume distributions are much broader than intensity-based distribution. [133]

In the literature, the DLS technique is often mentioned provide information about the average size, size distribution, and polydispersity index (PdI) of silk protein-based micro and nanosystems. [12] [87] [68]

The DLS data evidenced a similar mean size between spray-dried silk sericin (SMs) and naringenin-loaded sericin microspheres (SNRGMs). The presence of the drug did not influence the size distribution, although the incorporation efficiency of microparticles was higher than 90%.

Notably, both microspheres showed a unimodal distribution with a mean volume-weighted diameter ($d_{4,3}$) of about 3.8 and 3.4 μm , for SMs and SNRGMs, respectively (Figure 38). [86]

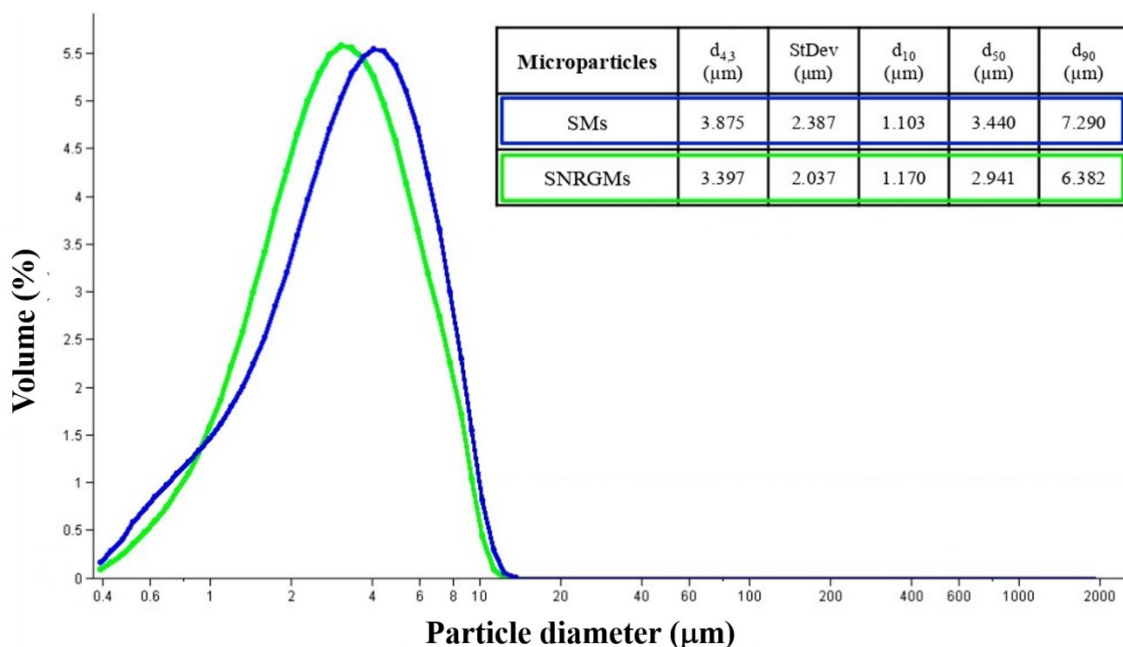


Figure 38: Particle size and particle size distribution of SMs (blue line) and SNRGMs (green line). In the inner table, the mean volume-weighted diameter ($d_{4,3}$) and standard deviation value (StDev) have been reported together with the 10th, the 50th and the 90th percentile of volume-weighted diameter (d_{10} , d_{50} and d_{90} , respectively). Modified from *International Journal of Molecular Sciences*, Chlapanidas, T.; Perteghella, S.; Leoni, F.; Faragò, S.; Marazzi, M.; Rossi, D.; Martino, E.; Gaggeri, R.; Collina, S., *TNF- α blocker effect of naringenin-loaded sericin microparticles that are potentially useful in the treatment of psoriasis*, 15, 13624-13636 (2014) (Open Access)

The same method of analysis was adopted by Faragò et colleagues to determine the surface-weighted mean $d_{3,2}$, the $d_{4,3}$, the specific surface area (SSA) and the mean/median ratio of a dried powder formulation from silk fibroin microspheres. [66]

Briefly, diverse formulations of microparticles composed of fibroin alone or fibroin and at least one of three selected excipients (alginate, poloxamer or poly-ethylene glycol), were prepared.

Overall, most microparticles presented a particle size distribution less than or equal to 3 µm, except for formulations A, E and G, composed by fibroin, fibroin + poly-ethylene glycol, fibroin + alginate + poly-ethylene glycol, respectively. Furthermore, the statistical analysis showed a higher volume-weighted mean compared to the surface-weighted mean, suggesting that not all microparticles had a spherical shape. Regarding the SSA, formulations C, D and H, containing alginate, exhibited values higher than the other samples due to their rough surface.

The mean/median ratio was considered to evaluate the normal distribution of microparticles: if values tend to 1, curves tend to normality. ANCOVA analysis showed no differences between samples. The data revealed that the presence of poloxamer and poly-ethylene glycol induced a normalization of the distribution curves, but alginate reduced this effect. Formulations B, E and F (constitute of poloxamer, PEG or both, respectively) presented values near 1, while all other formulations had a dimensional distribution negatively skewed because of the presence of small particles.

Moreover, the dynamic light scattering technique was used to determine the mean size of the self-assembled PEG-conjugated silk sericin nanoparticles. Samples showed a mean size between 200 and 400 nm when prepared by the diafiltration method. [135]

Contrary, the desolvation method allowed the preparation of sericin-based nanoparticles for controlled gene delivery with an average diameter of 100-150 nm. The PdI was 0.1 ± 0.1 , confirming the mono-dispersity of the solution and their stability in aqueous storage conditions (4 °C) [136]

Despite being the preferred technique to determine the size of nanoparticles routinely, DLS is also known to have several drawbacks, which are mainly inherent to the principles of the technique. This can be an advantage if the purpose is to detect small amounts of large particles, but it can be a major drawback for accurate size determination. Dust particles or small amounts of large aggregates can hinder the size determination if the main component has a distinctly smaller size.

In 2016, nanoparticle tracking analysis (NTA) was first commercialized as an innovative system for sizing particles from about 30 nm to 1 μm , with the lower detection limit being dependent on the refractive index of the nanoparticles.

This technique combines laser light scattering microscopy with a charge-coupled device camera, which allows the visualization and recording of nanoparticles in solution.

The NTA software is then able to identify and track individually and simultaneously nanoparticles moving under Brownian motion and by using the Stokes-Einstein equation, calculates their hydrodynamic diameters. [137]

NanoSight instruments provide high-resolution nanoparticle size, count-based concentration and aggregation measurements while a fluorescence mode provides specific results for suitably labelled particles. With real-time monitoring, subtle changes in the characteristics of particle populations are provided with all of these analyses confirmed by visual validation.

3.5 Scanning electron microscopy

The scanning electron microscope (SEM) uses a focused beam of high-energy electrons to generate a variety of signals at the surface of solid specimens. The signals that derive from electron-sample interactions reveal information about the sample, including the external morphology, chemical composition, and crystalline structure and orientation of materials making up the sample.

In most applications, data are collected over a selected area of the surface of samples, and 2-D images are generated that displays spatial variations in these properties. Areas ranging from approximately 1 cm to 5 microns in width can be imaged in a scanning mode using conventional SEM techniques (magnification ranging from x 20 to approximately x 30,000, the spatial resolution of 50 to 100 nm). The SEM is also capable of performing analyses of selected point locations on the sample; this approach is especially useful in qualitatively or semi-quantitatively determining chemical compositions using the energy dispersive x-ray spectrometry, crystalline structure, and crystal orientations by using the electron backscatter diffraction. [138]

Scanning electron microscopy (SEM) does not use photons of light like optical microscopy but an electron beam that hits the sample. Thanks to the electron wavelength much lower than that of the photons, the resolution power of a scanning electron microscope is much higher than that of an optical microscope. Furthermore, the depth of field of SEM is also much higher, allowing perfect images even for three-dimensional samples.

SEM can be used to study the morphology of proteins in raw silk. Sericin belongs to a family of proteins of the type “gluelike” which is positioned around the protein core, keeping the fibroin filaments together, as shown in Figure 39. Fibres resulted in hard and tough after sericin removal, while became soft and lustrous in its absence.

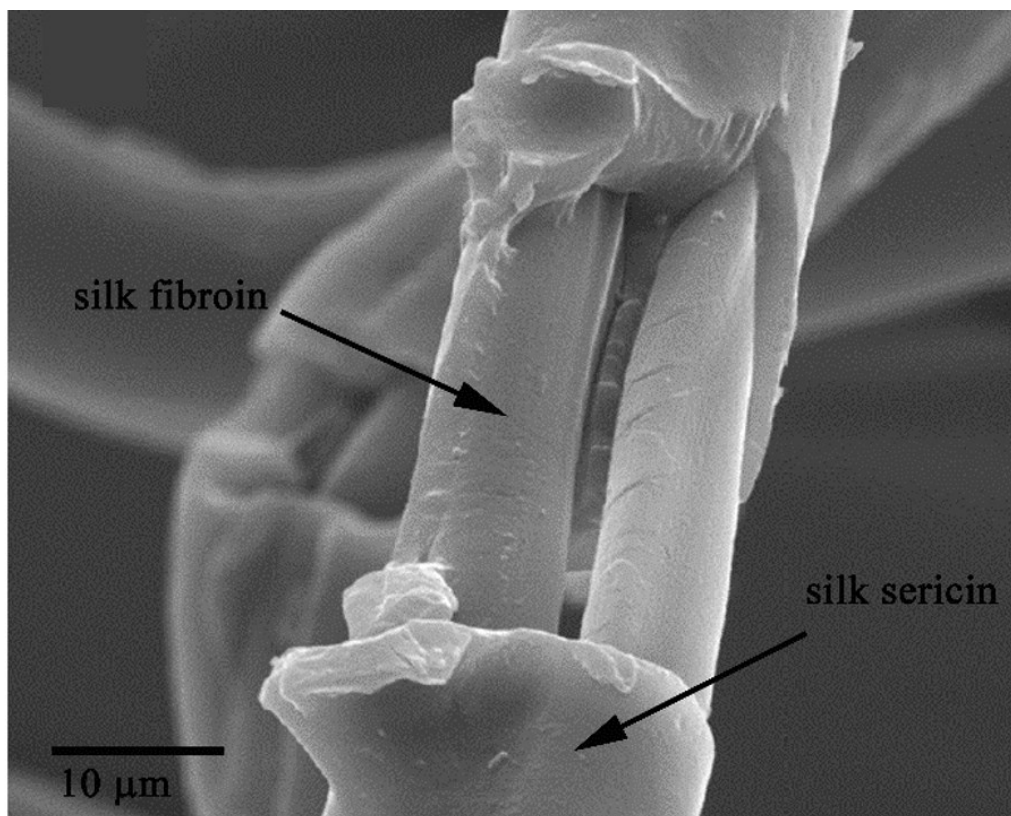


Figure 39: SEM image of partially degummed *Bombyx mori* silk fibres. Scale bar: 10 µm. Modified from Royal Society of Chemistry, Catenacci, L.; Sorrenti, M., Silk-based drug delivery systems, Chapter 7, 165-178 (2020), with permission from Royal Society of Chemistry

4. References

- [1] G.H. Altman, F. Diaz, C. Jakuba, T. Calabro, R.L. Horan, J. Chen, H. Lu, J. Richmond, D.L. Kaplan, Silk-based biomaterials, *Biomaterials* 24 (2003) 401-416.
- [2] F. Vollrath, Strength and structure of spiders' silks, *Journal of Biotechnology* 74(2) (2000) 67-83.
- [3] B. Crivelli, S. Perteghella, E. Bari, M. Sorrenti, G. Tripodo, T. Chlapanidas, M.L. Torre, Silk nanoparticles: from inert supports to bioactive natural carriers for drug delivery, *Soft Matter* 14(4) (2018) 546-557.
- [4] F. Mottaghitalab, M. Farokhi, M.A. Shokrgozar, F. Atyabi, H. Hosseinkhani, Silk fibroin nanoparticle as a novel drug delivery system, *Journal of Controlled Release* 206 (2015) 161-176.
- [5] T. Asakura, K. Okushita, M.P. Williamson, Analysis of the Structure of Bombyx mori Silk Fibroin by NMR, *Macromolecules* 48(8) (2015) 2345-2357.
- [6] M. Mondal, K. Trivedy, S.N. Kumar, The silk proteins, sericin and fibroin in silkworm, Bombyx mori Linn.- a review, *Caspian Journal environmental of Sciences* 5(2) (2007) 63-76.
- [7] M.J. Chen, Z.Z. Shao, X. Chen, Paclitaxel-loaded silk fibroin nanospheres, *Journal of Biomedical Materials Research Part A* 100A(1) (2012) 203-210.
- [8] T.T. Cao, Y.Q. Zhang, Processing and characterization of silk sericin from Bombyx mori and its application in biomaterials and biomedicines, *Materials Science & Engineering C- Materials for Biological Applications* 61 (2016) 940-952.
- [9] R.I. Kunz, R.M.C. Brancalhão, L.D.C. Ribeiro, M.R.M. Natali, Silkworm Sericin: Properties and Biomedical Applications, *Biomed Research International* (2016).
- [10] B. Joseph, S.J. Raj, Therapeutic applications and properties of silk proteins from Bombyx mori, *Frontiers in Life Science* 6(3-4) (2012) 55-60.
- [11] A.U. Ude, R.A. Eshkoo, R. Zulkifili, A.K. Ariffin, A.W. Dzuraidah, C.H. Azhari, Bombyx mori silk fibre and its composite: A review of contemporary developments, *Materials & Design* 57 (2014) 298-305.
- [12] T. Chlapanidas, S. Farago, G. Lucconi, S. Perteghella, M. Galuzzi, M. Mantelli, M.A. Avanzini, M.C. Tosca, M. Marazzi, D. Vigo, M.L. Torre, M. Faustini, Sericins exhibit ROS-scavenging, anti-tyrosinase, anti-elastase, and in vitro immunomodulatory activities, *International Journal of Biological Macromolecules* 58 (2013) 47-56.
- [13] Z. Zhao, Y. Li, M.B. Xie, Silk Fibroin-Based Nanoparticles for Drug Delivery, *International Journal of Molecular Sciences* 16(3) (2015) 4880-4903.

- [14] W.W. Huang, S.J. Ling, C.M. Li, F.G. Omenetto, D.L. Kaplan, Silkworm silk-based materials and devices generated using bio-nanotechnology, *Chemical Society Reviews* 47(17) (2018) 6486-6504.
- [15] T.P. Nguyen, Q.V. Nguyen, V.H. Nguyen, T.H. Le, V.Q.N. Huynh, D.V.N. Vo, Q.T. Trinh, S.Y. Kim, Q.V. Le, Silk Fibroin-Based Biomaterials for Biomedical Applications: A Review, *Polymers* 11(12) (2019).
- [16] T. Yucel, M.L. Lovett, D.L. Kaplan, Silk-based biomaterials for sustained drug delivery, *Journal of Controlled Release* 190 (2014) 381-397.
- [17] I.B. Khalifa, N. Ladhari, M. Touay, Application of sericin to modify textile supports, *Journal of the Textile Institute* 103(4) (2012) 370-377.
- [18] Y.J. Wang, Y.Q. Zhang, Three-layered sericins around the silk fibroin fiber from *Bombyx mori* cocoon and their amino acid composition, *Silk: Inheritance and Innovation - Modern Silk Road* 175-176 (2011) 158-+.
- [19] Z.L. Zhao, Y.Q. Zhang, Greener degumming production of layered sericin peptides from a silkworm cocoon and their physicochemical characteristics and bioactivities in vitro, *Journal of Cleaner Production* 261 (2020).
- [20] Y. Takasu, H. Yamada, K. Tsubouchi, Isolation of three main sericin components from the cocoon of the silkworm, *Bombyx mori*, *Bioscience Biotechnology and Biochemistry* 66(12) (2002) 2715-2718.
- [21] Y. Takasu, H. Yamada, T. Tamura, H. Sezutsua, K. Mita, K. Tsubouchi, Identification and characterization of a novel sericin gene expressed in the anterior middle silk gland of the silkworm *Bombyx mori*, *Insect Biochemistry and Molecular Biology* 37(11) (2007) 1234-1240.
- [22] F. Sehnal, Prospects of the practical use of silk sericins, *Entomological Research* 38 (2008) S1-S8.
- [23] R.P. Liu, D.W. Qu, J.W. Ma, Q. Luo, Y. Ou, T.T. Tan, W.H. Zeng, H.F. Xu, Insights into regulatory characteristics of the promoters of Sericin 1 and Sericin 3 in transgenic silkworms, *Biochemical and Biophysical Research Communications* 522(2) (2020) 492-498.
- [24] J.J. Michaille, P. Couble, J.C. Prudhomme, A. Garel, A single gene produces multiple sericin messenger RNAs in the silk gland of *Bombyx mori*, *Biochimie* 68 (1986) 1165-1173.
- [25] P. Couble, J.J. Michaille, A. Garel, M.L. Couble, J.C. Prudhomme, Developmental switches of sericin mRNA splicing in individual cells of *Bombyx mori* silkgland, *Developmental Biology* 124 (1987) 431-440.

- [26] B. Kludkiewicz, Y. Takasu, R. Fedic, T. Tamura, F. Sehnal, M. Zurovec, Structure and expression of the silk adhesive protein Ser2 in *Bombyx mori*, *Insect Biochemistry and Molecular Biology* 39(12) (2009) 938-946.
- [27] Z.M. Dong, K.Y. Guo, X.L. Zhang, T. Zhang, Y. Zhang, S.Y. Ma, H.P. Chang, M.Y. Tang, L.N. An, Q.Y. Xia, P. Zhao, Identification of *Bombyx mori* sericin 4 protein as a new biological adhesive, *International Journal of Biological Macromolecules* 132 (2019) 1121-1130.
- [28] J.H. Wu, Z. Wang, S.Y. Xu, Preparation and characterization of sericin powder extracted from silk industry wastewater, *Food Chemistry* 103(4) (2007) 1255-1262.
- [29] G. Locatelli, C. Ponzio, E. Bari, The Silk, in: R.S.o. Chemistry (Ed.), *Silk-based Drug Delivery Systems* 2020.
- [30] G. Freddi, R. Mossotti, R. Innocenti, Degumming of silk fabric with several proteases, *Journal of Biotechnology* 106(1) (2003) 101-112.
- [31] P. Aramwit, T. Siritientong, T. Srichana, Potential applications of silk sericin, a natural protein from textile industry by-products, *Waste Management & Research* 30(3) (2012) 217-224.
- [32] H. Teramoto, A. Kakazu, T. Asakura, Native structure and degradation pattern of silk sericin studied by C-13 NMR spectroscopy, *Macromolecules* 39(1) (2006) 6-8.
- [33] H. Yun, H. Oh, M.K. Kim, H.W. Kwak, J.Y. Lee, I.C. Um, S.K. Vootla, K.H. Lee, Extraction conditions of *Antheraea mylitta* sericin with high yields and minimum molecular weight degradation, *International Journal of Biological Macromolecules* 52 (2013) 59-65.
- [34] L. Lamboni, M. Gauthier, G. Yang, Q. Wang, Silk sericin: A versatile material for tissue engineering and drug delivery, *Biotechnology Advances* 33(8) (2015) 1855-1867.
- [35] D. Gupta, A. Agrawal, H. Chaudhary, M. Gulrajani, C. Gupta, Cleaner process for extraction of sericin using infrared, *Journal of Cleaner Production* 52 (2013) 488-494.
- [36] M.L. Gimenes, V.R. Silva, M.G.A. Vieira, S.G.C. Meuris, A.P. Scheer, High molecular sericin from *Bombyx mori* cocoons: extraction and recovering by ultrafiltration, *International Journal of Chemical Engineering and Applications*, 2014, pp. 266-271.
- [37] R. Fatahian, M. Noori, R. Khajavi, Extraction of sericin from degumming process of silk fibres and its application on nonwoven fabrics, *International Journal of Advanced Chemistry* 5(1) (2017) 25-28.
- [38] T.T. Cao, Y.J. Wang, Y.Q. Zhang, Effect of Strongly Alkaline Electrolyzed Water on Silk Degumming and the Physical Properties of the Fibroin Fiber, *Plos One* 8(6) (2013).

- [39] M.H. Wu, Y.Q. Zhang, Nanofiltration recovery of sericin from silk processing waste and synthesis of a lauroyl sericin-based surfactant and its characteristics, *Rsc Advances* 4(8) (2014) 4140-4145.
- [40] V.R. Silva, M. Ribani, M.L. Gimenes, A.P. Scheer, High molecular weight sericin obtained by high temperature and ultrafiltration process, *Chisa* 2012 42 (2012) 833-841.
- [41] M.H. Wu, J.X. Yue, Y.Q. Zhang, Ultrafiltration recovery of sericin from the alkaline waste of silk floss processing and controlled enzymatic hydrolysis, *Journal of Cleaner Production* 76 (2014) 154-160.
- [42] S.J. Eom, N.H. Lee, M.C. Kang, Y.H. Kim, T.G. Lim, K.M. Song, Silk peptide production from whole silkworm cocoon using ultrasound and enzymatic treatment and its suppression of solar ultraviolet-induced skin inflammation, *Ultrasonics Sonochemistry* 61 (2020).
- [43] P. Vaithanomsat, V. Kitpreechavanich, Sericin separation from silk degumming wastewater, *Separation and Purification Technology* 59(2) (2008) 129-133.
- [44] R. Wang, W.B. Jiang, S. Li, H.B. Yang, Y.B. Dong, Y.Q. Fu, Application research on infrared drying in silk re-reeling process, *Textile Research Journal* 82(13) (2012) 1329-1336.
- [45] C.H. Lo, Y. Chao, Degumming of silk fibers by CO₂ supercritical fluid, *Journal of Materials Science and Chemical Engineering* 5 (2017) 1-8.
- [46] Z.L. Zhao, W.W. Li, F. Wang, Y.Q. Zhang, Using of hydrated lime water as a novel degumming agent of silk and sericin recycling from wastewater, *Journal of Cleaner Production* 172 (2018) 2090-2096.
- [47] N. Ferronato, E.C. Rada, M.A.G. Portillo, L.I. Cioca, M. Ragazzi, V. Torretta, Introduction of the circular economy within developing regions: A comparative analysis of advantages and opportunities for waste valorization, *Journal of Environmental Management* 230 (2019) 366-378.
- [48] E.M. Foundation, *Intelligent Assets:Unlocking the Circular Economy Potential*, 2016.
- [49] http://ec.europa.eu/environment/circular-economy/index_en.htm.
- [50] M. Sorlini, S. Menato, From Textile To Pharmaceutical and Cosmetic Industry: Circular Economy Applied To Silk Manufacturing Wastes, in: R.S.o. Chemistry (Ed.), *Silk-based Drug Delivery Systems*.
- [51] <http://www.cir-safety.org/sites/default/files/slkprt062015rep.pdf>.
- [52] G. Capar, S.S. Aygun, M.R. Gecit, Treatment of silk production wastewaters by membrane processes for sericin recovery, *Journal of Membrane Science* 325(2) (2008) 920-931.

- [53] Q. Yang, Z. Liu, J. Yang, Simultaneous Determination of Chemical Oxygen Demand (COD) and Biological Oxygen Demand (BOD5) in Wastewater by Near-Infrared Spectrometry, *Journal of Water Resource and Protection* 4 (2009) 286-289.
- [54] W. Amaro, D. Andreani, S. Faragò, E. Oberrauch, M. Sorlini, Procedimento e apparecchiatura per la preparazione di materiali proteici derivanti da fibroina, in particolare per uso medicale e cosmetico, in: I.-S.S.p. l'Industria, S.U.P.d. svizzera (Eds.) Italy, 2013.
- [55] M. Sorlini, S. Menato, From Textile To Pharmaceutical and Cosmetic Industry: Circular Economy Applied To Silk Manufacturing Wastes R.S.o. Chemistry (Ed.), *Silk-based Drug Delivery Systems* 2020.
- [56] F. Ahsan, T.M. Ansari, S. Usmani, P. Bagga, An Insight on Silk Protein Sericin: From Processing to Biomedical Application, *Drug Research* 68(6) (2018) 317-327.
- [57] O.J. Lee, J.H. Kim, B.M. Moon, J.R. Chao, J. Yoon, H.W. Ju, J.M. Lee, H.J. Park, D.W. Kim, S.J. Kim, H.S. Park, C.H. Park, Fabrication and Characterization of Hydrocolloid Dressing with Silk Fibroin Nanoparticles for Wound Healing, *Tissue Engineering and Regenerative Medicine* 13(3) (2016) 218-226.
- [58] Y.Y. Wang, X.Y. Wang, J. Shi, R. Zhu, J.H. Zhang, Z.R. Zhang, D.W. Ma, Y.J. Hou, F. Lin, J. Yang, M. Mizuno, A Biomimetic Silk Fibroin/Sodium Alginate Composite Scaffold for Soft Tissue Engineering, *Scientific Reports* 6 (2016).
- [59] S.Y. Guang, Y. An, F.Y. Ke, D.M. Zhao, Y.H. Shen, H.Y. Xu, Chitosan/silk fibroin composite scaffolds for wound dressing, *Journal of Applied Polymer Science* 132(35) (2015).
- [60] P.X. MA Scaffolds for tissue fabrication, *Materials Today* (2004) 30-40.
- [61] Y. Tabata, Recent progress in tissue engineering, *Drug Discovery Today* 6(9) (2001) 483-487.
- [62] H. Shin, S. Jo, A.G. Mikos, Biomimetic materials for tissue engineering, *Biomaterials* 24 (2003) 4353-4364.
- [63] M. Gholipourmalekabadi, S. Sapru, A. Samadikuchaksaraei, R.L. Reis, D.L. Kaplan, S.C. Kundu, Silk fibroin for skin injury repair: Where do things stand?, *Advanced Drug Delivery Reviews* (2019).
- [64] J. Rnjak-Kovacina, L.S. Wray, K.A. Burke, T. Torregrosa, J.M. Golinski, W.W. Huang, D.L. Kaplan, Lyophilized Silk Sponges: A Versatile Biomaterial Platform for Soft Tissue Engineering, *Acs Biomaterials Science & Engineering* 1(4) (2015) 260-270.
- [65] R. Elia, J. Guo, S. Budijono, V. Normand, D. Benczedi, F. Omenetto, D.L. Kaplan, Encapsulation of volatile compounds in silk microparticles, *Journal of Coatings Technology and Research* 12(4) (2015) 793-799.

- [66] S. Farago, G. Lucconi, S. Perteghella, B. Vigani, G. Tripodo, M. Sorrenti, L. Catenacci, A. Boschi, M. Faustini, D. Vigo, T. Chlapanidas, M. Marazzi, M.L. Torre, A dry powder formulation from silk fibroin microspheres as a topical auto-gelling device, *Pharmaceutical Development and Technology* 21(4) (2016) 453-462.
- [67] S. Perteghella, C. Sottani, V. Cocce, S. Negri, L. Cavicchini, G. Alessandri, D. Cottica, M.L. Torre, E. Grignani, A. Pessina, Paclitaxel-Loaded Silk Fibroin Nanoparticles: Method Validation by UHPLC-MS/MS to Assess an Exogenous Approach to Load Cytotoxic Drugs, *Pharmaceutics* 11(6) (2019).
- [68] B. Crivelli, E. Bari, S. Perteghella, L. Catenacci, M. Sorrenti, M. Mocchi, S. Faragò, G. Tripodo, A. Prina-Mello, M.L. Torre, Silk fibroin nanoparticles for celecoxib and curcumin delivery: ROSscavenging and anti-inflammatory activities in an in vitro model of osteoarthritis, *European Journal of Pharmaceutics and Biopharmaceutics* 137 (2019) 37-45.
- [69] S. Perteghella, B. Vigani, L. Mastracci, F. Grillo, B. Antonioli, M. Galuzzi, M.C. Tosca, B. Crivelli, S. Preda, G. Tripodo, M. Marazzi, T. Chlapanidas, M.L. Torre, Stromal Vascular Fraction Loaded Silk Fibroin Mats Effectively Support the Survival of Diabetic Mice after Pancreatic Islet Transplantation, *Macromolecular Bioscience* 17(9) (2017).
- [70] M. Lovett, C. Cannizzaro, L. Daheron, B. Messmer, G. Vunjak-Novakovic, D.L. Kaplan, Silk fibroin microtubes for blood vessel engineering, *Biomaterials* 28(35) (2007) 5271-5279.
- [71] U.J. Kim, J. Park, H.J. Kim, M. Wada, D.L. Kaplan, Three-dimensional aqueous-derived biomaterial scaffolds from silk fibroin, *Biomaterials* 26(15) (2005) 2775-2785.
- [72] S. Sofia, M.B. McCarthy, G. Gronowicz, D.L. Kaplan, Functionalized silk-based biomaterials for bone formation, *Journal of Biomedical Materials Research* 54(1) (2001) 139-148.
- [73] G.H. Altman, R.L. Horan, H.H. Lu, J. Moreau, I. Martin, J.C. Richmond, D.L. Kaplan, Silk matrix for tissue engineered anterior cruciate ligaments, *Biomaterials* 23(20) (2002) 4131-4141.
- [74] T. Chlapanidas, S. Farago, F. Mingotto, F. Crovato, M.C. Tosca, B. Antonioli, M. Bucco, G. Lucconi, A. Scalise, D. Vigo, M. Faustini, M. Marazzi, M.L. Torre, Regenerated Silk Fibroin Scaffold and Infrapatellar Adipose Stromal Vascular Fraction as Feeder-Layer: A New Product for Cartilage Advanced Therapy, *Tissue Engineering Part A* 17(13-14) (2011) 1725-1733.
- [75] S. Mobini, B. Hoyer, M. Solati-Hashjin, A. Lode, N. Nosoudi, A. Samadikuchaksaraei, M. Gelinsky, Fabrication and characterization of regenerated silk scaffolds reinforced with

natural silk fibers for bone tissue engineering, *Journal of Biomedical Materials Research Part A* 101(8) (2013) 2392-2404.

[76] C. Correia, S. Bhumiratana, L.P. Yan, A.L. Oliveira, J.M. Gimble, D. Rockwood, D.L. Kaplan, R.A. Sousa, R.L. Reis, G. Vunjak-Novakovic, Development of silk-based scaffolds for tissue engineering of bone from human adipose-derived stem cells, *Acta Biomaterialia* 8(7) (2012) 2483-2492.

[77] H. Zhang, L.L. Li, F.Y. Dai, H.H. Zhang, B. Ni, W. Zhou, X. Yang, Y.Z. Wu, Preparation and characterization of silk fibroin as a biomaterial with potential for drug delivery, *Journal of Translational Medicine* 10 (2012).

[78] B. Mahendran, S.K. Ghosh, S.C. Kundu, Molecular phylogeny of silk producing insects based on internal transcribed Spacer DNA1, *Journal of Biochemistry and Molecular Biology* 39(5) (2006) 522-529.

[79] M. Mocchi, E. Bari, Silk-Fibroin based nano drug delivery systems, in: R.S.o. Chemistry (Ed.), *Silk-based Drug Delivery Systems* 2020.

[80] P.Y. Wu, Q. Liu, R.T. Li, J. Wang, X. Zhen, G.F. Yue, H.Y. Wang, F.B. Cui, F.L. Wu, M. Yang, X.P. Qian, L.X. Yu, X.Q. Jiang, B.R. Liu, Facile Preparation of Paclitaxel Loaded Silk Fibroin Nanoparticles for Enhanced Antitumor Efficacy by Locoregional Drug Delivery, *Acs Applied Materials & Interfaces* 5(23) (2013) 12638-12645.

[81] H. Rahmani, A. Fattahi, K. Sadrjavadi, S. Khaledian, Y. Shokohinia, Preparation and Characterization of Silk Fibroin Nanoparticles as a Potential Drug Delivery System for 5-Fluorouracil, *Advanced Pharmaceutical Bulletin* 9(4) (2019) 601-608.

[82] A.A. Lozano-Perez, A. Rodriguez-Nogales, V. Ortiz-Cullera, F. Algieri, J. Garrido-Mesa, P. Zorrilla, M.E. Rodriguez-Cabezas, N. Garrido-Mesa, M.P. Utrilla, L. De Matteis, J.M. de la Fuente, J.L. Cenis, J. Galvez, Silk fibroin nanoparticles constitute a vector for controlled release of resveratrol in an experimental model of inflammatory bowel disease in rats, *International Journal of Nanomedicine* 9 (2014) 4507-4520.

[83] S. Perteghella, B. Crivelli, L. Catenacci, M. Sorrenti, G. Bruni, V. Necchi, B. Vigani, M. Sorlini, M.L. Torre, T. Chlapanidas, Stem cell-extracellular vesicles as drug delivery systems: New frontiers for silk/curcumin nanoparticles, *International Journal of Pharmaceutics* 520(1-2) (2017) 86-97.

[84] H.B. Yan, Y.Q. Zhang, Y.L. Ma, L.X. Zhou, Biosynthesis of insulin-silk fibroin nanoparticles conjugates and in vitro evaluation of a drug delivery system, *Journal of Nanoparticle Research* 11(8) (2009) 1937-1946.

- [85] P. Aramwit, S. Kanokpanont, W. De-Eknamkul, T. Srichana, Monitoring of inflammatory mediators induced by silk sericin, *Journal of Bioscience and Bioengineering* 107(5) (2009) 556-561.
- [86] T. Chlapanidas, S. Perteghella, F. Leoni, S. Farago, M. Marazzi, D. Rossi, E. Martino, R. Gaggeri, S. Collina, TNF-alpha Blocker Effect of Naringenin-Loaded Sericin Microparticles that Are Potentially Useful in the Treatment of Psoriasis, *International Journal of Molecular Sciences* 15(8) (2014) 13624-13636.
- [87] E. Bari, C.R. Arciola, B. Vigani, B. Crivelli, P. Moro, G. Marrubini, M. Sorrenti, L. Catenacci, G. Bruni, T. Chlapanidas, E. Lucarelli, S. Perteghella, M.L. Torre, In Vitro Effectiveness of Microspheres Based on Silk Sericin and *Chlorella vulgaris* or *Arthrospira platensis* for Wound Healing Applications, *Materials* 10(9) (2017).
- [88] E. Bari, S. Perteghella, S. Farago, M.L. Torre, Association of silk sericin and platelet lysate: Premises for the formulation of wound healing active medications, *International Journal of Biological Macromolecules* 119 (2018) 37-47.
- [89] P. Aramwit, S. Palapinyo, T. Srichana, S. Chottanapund, P. Muangman, Silk sericin ameliorates wound healing and its clinical efficacy in burn wounds, *Archives of Dermatological Research* 305(7) (2013) 585-594.
- [90] J. Fan, L. Wu, L. Chen, X. Mao, F. Ren, Antioxidant activities of silk sericin from silkworm *Bombyx mori*, *Journal of Food Biochemistry* 33 (2009) 74-88.
- [91] K. Jena, J.P. Pandey, R. Kumari, A.K. Sinha, V.P. Gupta, G.P. Singh, Free radical scavenging potential of sericin obtained from various ecoraces of tasar cocoons and its cosmeceuticals implication, *International Journal of Biological Macromolecules* 120 (2018) 255-262.
- [92] A. Kurioka, F. Kurioka, M. Yamazaki, Characterization of sericin powder prepared from citric acid-degraded sericin polypeptides of the silkworm, *Bombyx mori*, *Bioscience Biotechnology and Biochemistry* 68(4) (2004) 774-780.
- [93] R. Devi, M. Deori, D. Devi, Evaluation of antioxidant activities of silk protein sericin secreted by silkworm *Antheraea assamensis*, *Journal of Pharmacy Research* 4(12) (2011) 4688-4691.
- [94] S. Prasong, Screening of antioxidant activity of some *Samia ricini* (Eri) silks: comparison with *Bombyx mori*, *Journal of Biological Sciences* 11(4) (2011) 336-339.
- [95] Y.S. Park, M.H. Jeon, H.J. Hwang, M.R. Park, S.H. Lee, S.G. Kim, M. Kim, Antioxidant activity and analysis of proanthocyanidins from pine (*Pinus densiflora*) needles, *Nutrition Research and Practice* 5(4) (2011) 281-287.

- [96] A. Rauf, M. Imran, T. Abu-Izneid, H. Iahfisham Ul, S. Patel, X.D. Pan, S. Naz, A.S. Silva, F. Saeed, H.A.R. Suleria, Proanthocyanidins: A comprehensive review, *Biomedicine & Pharmacotherapy* 116 (2019).
- [97] T. Hatahet, M. Morille, A. Shamseddin, A. Aubert-Pouessel, J.M. Devoisselle, S. Begu, Dermal quercetin lipid nanocapsules: Influence of the formulation on antioxidant activity and cellular protection against hydrogen peroxide, *International Journal of Pharmaceutics* 518(1-2) (2017) 167-176.
- [98] Y.H. Hong, E.Y. Jung, D.O. Noh, H.J. Suh, Physiological effects of formulation containing tannase-converted green tea extract on skin care: physical stability, collagenase, elastase, and tyrosinase activities, *Integrative Medicine Research* 3(1) (2014).
- [99] T. Takechi, R. Wada, T. Fukuda, K. Harada, H., Takamura, Antioxidant activities of two sericin proteins extracted from cocoon of silkworm (*Bombyx mori*) measured by DPPH, chemiluminescence, ORAC and ESR methods, *Biomedical Reports* 2(3) (2014) 364-369.
- [100] P. Aramwit, S. Damrongsakkul, S. Kanokpanont, T. Srichana, Properties and antityrosinase activity of sericin from various extraction methods, *Biotechnology and Applied Biochemistry* 55 (2010) 91-98.
- [101] W. Keawkorn, N. Limpeanchob, W. Tiyaboonchai, S. Pongcharoen, M. Sutheerawattananonda, The effect of dietary sericin on rats, *Scienceasia* 39(3) (2013) 252-256.
- [102] Y.G. Li, D.F. Ji, T.B. Lin, S. Zhong, G.Y. Hu, S. Chen, Protective effect of sericin peptide against alcohol-induced gastric injury in mice, *Chinese Medical Journal* 121(20) (2008) 2083-2087.
- [103] A. Ogawa, S. Terada, T. Kanayama, M. Miki, M. Morikawa, T. Kimura, A. Yamaguchi, M. Sasaki, H. Yamada, Improvement of islet culture with sericin, *Journal of Bioscience and Bioengineering* 98(3) (2004) 217-219.
- [104] Y. Okazaki, S. Kakehi, Y.H. Xu, K. Tsujimo, M. Sasaki, H. Ogawa, N. Kato, Consumption of Sericin Reduces Serum Lipids, Ameliorates Glucose Tolerance and Elevates Serum Adiponectin in Rats Fed a High-Fat Diet, *Bioscience Biotechnology and Biochemistry* 74(8) (2010) 1534-1538.
- [105] M.N. Padamwar, A.P. Pawar, A.V. Daithankar, K.R. Mahadik, Silk sericin as a moisturizer: an in vivo study, *Journal of Cosmetic Dermatology* 4(4) (2005) 250-257.
- [106] H. Kim, Y.J. Lim, J.H. Park, Y. Cho, Dietary silk protein, sericin, improves epidermal hydration with increased levels of filaggrins and free amino acids in NC/Nga mice, *British Journal of Nutrition* 108(10) (2012) 1726-1735.

- [107] B.B. Mandal, A.S. Priya, S.C. Kundu, Novel silk sericin/gelatin 3-D scaffolds and 2-D films: Fabrication and characterization for potential tissue engineering applications, *Acta Biomaterialia* 5(8) (2009) 3007-3020.
- [108] S. Terada, M. Sasaki, K. Yanagihara, H. Yamada, Preparation of silk protein sericin as mitogenic factor for better mammalian cell culture, *Journal of Bioscience and Bioengineering* 100(6) (2005) 667-671.
- [109] J.H. Wu, Y.F. Zhou, S.Y. Wang, Z.W. Wang, Y. Wu, X.Q. Guo, Laboratory-scale extraction and characterization of ice-binding sericin peptides, *European Food Research and Technology* 236(4) (2013) 637-646.
- [110] D. Pawcenis, M.A. Koperska, J.M. Milczarek, T. Lojewski, J. Lojewska, Size exclusion chromatography for analyses of fibroin in silk: optimization of sampling and separation conditions, *Applied Physics a-Materials Science & Processing* 114(2) (2014) 301-308.
- [111] K.V. Kodre, S.R. Attarde, P.R. Yendhe, R.Y. Patil, V.U. Barge, Differential scanning calorimetry: a review, *Journal of Pharmaceutical Analysis* 3(3) (2014).
- [112] S.P. Stodghill, Thermal Analysis: A Review of Techniques and Applications in the Pharmaceutical Sciences, *American Pharmaceutical Review* 13(2) (2010) 29-36.
- [113] L. Catenacci, M. Sorrenti, Physico-Chemical Characterisation of Silk-Based Materials, in: R.S.o. Chemistry (Ed.), *Silk-based Drug Delivery Systems* 2020.
- [114] S. Dutta, R. Bharali, R. Devi, D. Devi, Purification and characterization of glue like sericin protein from a wild silkworm *Antheraea assamensis* Helfer, *Global Journal of Bioscience & Biotechnology* 1(2) (2012) 229-233.
- [115] S. Prasong, S. Yaowalak, S. Wilaiwan, Characteristics of silk fiber with or without sericin component: a comparison between *Bombyx mori* and *Philosamia ricini* silks, *Pakistan Journal of Biological Sciences*, 2009, pp. 872-876.
- [116] J. Magoshi, S. Nakamura, Studies on physical properties and structure of silk. Glass transition and crystallization of silk fibroin, *Journal of Applied Polymer Science* 13(4) (1975) 1013-1015.
- [117] C. Fornaguera, C. Solans, Analytical Methods to Characterize and Purify Polymeric Nanoparticles, *International Journal of Polymer Science* (2018).
- [118] G. Karp, Isolation, purification and fractionation of proteins, in: Edises (Ed.), *Cellular and molecular biology: concepts and experiments* 2007, pp. 798-803.
- [119] B. Buszewski, S. Noga, Hydrophilic interaction liquid chromatography (HILIC)-a powerful separation technique, *Analytical and Bioanalytical Chemistry* 402(1) (2012) 231-247.

- [120] K.O. Eriksson, Reversed phase chromatography, *Biopharmaceutical processing: development, design, and implementation of manufacturing processes* 2018, pp. 433-439.
- [121] P. Hong, S. Koza, E.S.P. Bouvier, A REVIEW SIZE-EXCLUSION CHROMATOGRAPHY FOR THE ANALYSIS OF PROTEIN BIOTHERAPEUTICS AND THEIR AGGREGATES, *Journal of Liquid Chromatography & Related Technologies* 35(20) (2012) 2923-2950.
- [122] D. Gupta, A. Agrawal, A. Rangi, Extraction and characterization of silk sericin, *Indian Journal of Fibre & Textile Research* 39(4) (2014) 364-372.
- [123] K.E. Sapsford, K.M. Tyner, B.J. Dair, J.R. Deschamps, I.L. Medintz, Analyzing Nanomaterial Bioconjugates: A Review of Current and Emerging Purification and Characterization Techniques, *Analytical Chemistry* 83(12) (2011) 4453-4488.
- [124] J. Alben, F. Fiamingo, Fourier transformed infrared spectroscopy, in: D. Rousseau (Ed.), *Optical techniques in biological research* 1984, pp. 133-178.
- [125] B. Stuart, *Infrared spectroscopy*, 2015.
- [126] D.T. Pham, W. Tiyaboonchai, Fibroin nanoparticles: a promising drug delivery system, *Drug Delivery* 27(1) (2020) 431-448.
- [127] D.T. Pham, N. Saelim, W. Tiyaboonchai, Crosslinked fibroin nanoparticles using EDC or PEI for drug delivery: physicochemical properties, crystallinity and structure, *Journal of Materials Science* 53(20) (2018) 14087-14103.
- [128] S. Du, J. Zhang, W.T. Zhou, Q.X. Li, G.W. Greene, H.J. Zhu, J.L. Li, X.G. Wang, Interactions between fibroin and sericin proteins from *Antheraea pernyi* and *Bombyx mori* silk fibers, *Journal of Colloid and Interface Science* 478 (2016) 316-323.
- [129] <https://www.jove.com/science-education/10204/ultraviolet-visible-uv-vis-spectroscopy>.
- [130] F.X. Schmid, *Biological Macromolecules: UV-visible Spectrophotometry*, *Encyclopedia of Life Sciences* (2001) 1-4.
- [131] A. Sionkowska, A. Planecka, The influence of UV radiation on silk fibroin, *Polymer Degradation and Stability* 96(4) (2011) 523-528.
- [132] C.J. Chirayil, J. Abraham, R.K. Mishra, S.C. George, S. Thomas, Instrumental techniques for the characterization of nanoparticles, *Thermal and rheological measurement techniques for the characterization of nanoparticles* 2017, pp. 1-36.
- [133] A.A. Khorasani, J.L. Weaver, C. Salvador-Morales, Closing the gap: accelerating the translational process in nanomedicine by proposing standardized characterization techniques, *International Journal of Nanomedicine* 9 (2014) 5729-5751.

- [134] H.G. Merkus, Dynamic Light Scattering, in: P.t. series (Ed.), Particle Size Measurements: Fundamentals, Practice, Quality2009, pp. 299-317.
- [135] K.Y. Cho, J.Y. Moon, Y.W. Lee, K.G. Lee, J.H. Yeo, H.Y. Kweon, K.H. Kim, C.S. Cho, Preparation of self-assembled silk sericin nanoparticles, International Journal of Biological Macromolecules 32(1-2) (2003) 36-42.
- [136] S.K. Das, T. Dey, S.C. Kundu, Fabrication of sericin nanoparticles for controlled gene delivery, Rsc Advances 4(5) (2014) 2137-2142.
- [137] V. Filipe, A. Hawe, W. Jiskoot, Critical Evaluation of Nanoparticle Tracking Analysis (NTA) by NanoSight for the Measurement of Nanoparticles and Protein Aggregates, Pharmaceutical Research 27(5) (2010) 796-810.
- [138] https://serc.carleton.edu/research_education/geochemsheets/techniques/SEM.html.

5. Silk sericin as a biomaterial in drug delivery systems

Protein-based nano-systems have recently revolutionized the nanomedicine era. Thanks to their nanometric dimensions, protein nanoparticles are employed mainly as drug delivery systems to improve the cellular uptake as well as body distribution of the drug. Moreover, they are replacing many materials that are not biocompatible and harm the environment.

About that, silk sericin-based nanoparticles are advantageous in having excellent biocompatibility, controllable biodegradability, and relatively low cost.

The role of sericin can be dual in nanosystems: on the one hand, it can be used as an inert carrier, improving the bioavailability of the encapsulated drug; on the other hand, itself can be considered as an active principle, thanks to its many intrinsic biological properties.

Several problems associated with sericin nanoparticles depend on their low physicochemical stability, often responsible for agglomeration and aggregation phenomena.

Furthermore, the use of sericin alone is not possible for the development of nanoparticles, because in aqueous solution, the disassembly of nanostructures would be inevitable due to the hydrophilic character of the protein. To overcome this problem, the use of cross-linking agents or the blending with other stabilizer polymers is required.

Paper 1 that follows in this paragraph, is an overview of the principal preparation techniques of silk sericin-based nano-drug delivery systems.

Paper 1

Silk-Sericin Nano-Drug Delivery Systems

Giulia Orlandi and Elia Bari

Abstract

The excellent biocompatibility, controllable biodegradability, non-immunogenicity and intrinsic biological activity, make silk sericin an ideal candidate for the formulation of drug delivery systems. Unfortunately, nanoparticles, nanocapsules or nanofibers based on silk sericin “alone” cannot be produced due to its physicochemical instability, influenced by the high water solubility. For this reason, cross-linking, blending, or combination with other polymers/compounds is required. This chapter provides an overview of the main preparation methods of sericin-based nanoparticles and nanofibers, as reported in the literature. Their applications, both *in vitro* and *in vivo*, are also described.

6.1 Introduction

The literature reports many biomaterials to prepare nano drug delivery systems, and among them, silk derived proteins, fibroin and sericin, are gathering great attention. Indeed, silk-based nano-systems are being used to improve the cellular uptake and the body's distribution of the drug, as well as to replace materials that are not biocompatible or have a negative impact on the environment. Fibroin is officially recognized by The Food and Drug Administration as a biocompatible and biodegradable material and has been employed mainly in the formulation of drug delivery systems in the form of micro and nano-particles/fibres. Conversely, sericin has only recently appeared on the scene of the drug delivery formulations, as it has been considered, for many years, only as a textile waste product. Today, the excellent biocompatibility, biodegradability, relatively low cost and the intrinsic biological activities are considered the main critical factors for sericin exploitation in the pharmaceutical field. Nevertheless, the potential of sericin at a nanoscale level, for the design and development of nano-drug delivery systems, has not been thoroughly investigated. The main limitation for sericin-based nanosystem development is related to the high sericin water solubility, that leads to a physicochemical instability of the sericin-based nano-drug delivery systems in the biological fluids.

This chapter highlights the development of nano-drug delivery systems based on silk sericin, describing the formulation strategies proposed to increase their physicochemical stability as well as the *in vitro* and *in vivo* investigations (Table 6.1). Of note, the chapter mainly focuses on *Bombyx mori* silkworm sericin that is the most employed due to the existence of commercially established supply chains (sericulture); where present, examples of drug delivery systems based on sericin from other silkworm species will also be reported.

Drug delivery dosage form	Preparation technique	Size and morphology	Drug loaded	Intended administration route	Note	Reference
Nanoparticle	Sericin conjugation/derivatization	About 100-110 nm in size; round shape	Paclitaxel and FITC-inulin	Intravenous	Sericin from <i>Antheraea mylitta</i> was used. The type of poloxamer or solvent did not influence particle size and morphology.	[3]
		Less than 150 nm in size; round shape	Proanthocyanidins, quercetin and epigallocatechin gallate	Topical	Pluronic F-127 was used as co-excipient. A slow and controlled release of the actives in PBS was observed.	[6]
		From 200 to 400 nm in size; spherical shape	-	-	PEG was used as co-excipient to prepare sericin-PEG conjugates that subsequently self-associate to form nanoparticles through hydrophobic interaction.	[7]
		About 40 nm in size; spherical shape	Doxorubicin	Intravenous	Folate was used as co-excipient to prepare folate-conjugated sericin nanoparticles. A pH-dependent drug release was observed.	[8]
		About 180 nm in size; spherical shape	Fenofibrate	Oral	Poly-ethyl cyanoacrylate was used as co-excipient. Nanoparticles were mucoadhesive due to the presence of sericin (positively charged) which interact with the mucin (negatively charged).	[9]
	Electrospraying	Less than 80 nm in size; regular shape and spherical structure	-	-	Particle size (but no morphology) was strongly influenced by the variation of the process parameters (sericin concentration, applied voltages, nozzle-collector distance and feed rate). A reduction in sericin crystallinity was observed.	[11]

	Desolvation + cross-linking	From 150 to 200 nm in size; uniform spherical shape	Atorvastatin	Oral	Ethanol was used as a desolvating agent, and genipin was used as cross-linker. A sustained drug release was provided.	[12]
		About 200 nm in size; spherical shape	Doxorubicin	Intravenous	Chitosan was used as co-excipient, and EDC was used as cross-linker. Nanoparticles were pH-responsive: uptake and drug release were increased in acidic conditions.	[13, 14]
		About 190 nm in size; spherical shape	Resveratrol	-	Dimethyl sulfoxide was used as a desolvating agent and Pluronic F-68 as an emulsifier. Sericin and Pluronic F-68 concentrations influenced particle size. The release profile was influenced by both drug and sericin concentrations.	[16]
		About 120 nm in size; spherical morphology	Non-viral DNA	-	Ethanol was used as a desolvating agent and glutaraldehyde as cross-linker. The surface of nanoparticles was coated with cationic poly-L-lysine to increase drug loading.	[17]
	Emulsification-diffusion method	About 200-300 nm in size; round shape	Niacinamide	-	A water/silicone emulsion method was proposed. CaCl ₂ was used to achieve ionic gelation of sericin nanoparticles. Nanoparticle formation was influenced by CaCl ₂ and sericin concentrations and speed of homogenizer.	[18]
Nanofibres	Electrospinning	From about 200 to 400 nm in diameter; smooth surface	-	Topical/implantation	Fibre morphology was influenced by sericin concentration and spinning parameters (acceleration voltage, spinning distance, flow rate). Sericin was in a random coil conformation.	[19]

		About 145 nm in diameter	-	Topical/implantation	Sericin concentration influenced fibres morphology. Sericin was present in a random coil conformation.	[20]
		About 180 nm in diameter	AgNO ₃	Topical/implantation	Chitosan and PVA were used as co-excipients. The addition of AgNO ₃ reduced fibre diameter (to 95 nm).	[21]
		About 400-600 nm in diameter	-	Implantation	PCL was used as co-excipient. By increasing the sericin content, the fibre diameter decreased. Sericin improved cell adhesion and proliferation and stimulated the production of the extracellular matrix (ECM) components.	[24]
		About 179–285 nm in size	-	Implantation	PVA was used as co-excipient. Both sericin concentration and process parameters influenced the fibre diameter. Sericin was in a random coil conformation.	[25]
		Between 240 nm and 380 nm in size	Sericin	Topical/implantation	Chitosan was used as co-excipient. Sericin provided ROS-scavenging, healing and antibacterial properties.	[26]
		From 130 to 160 nm in size	Sericin	Topical/implantation	<i>Bombyx mori</i> and <i>Antheraea assama</i> sericins were used. PVA was used as co-excipient. Sericin provided ROS-scavenging, healing and antibacterial properties.	[27]
		From 300 to 1500 nm in size	Sericin, copper and zinc ions	Topical/implantation	Gelatin and halloysite nanotubes (HNTs) were used as co-excipients. Sericin and copper/zinc ions provided healing and antibacterial properties.	[28]

Table 6.1: An overview of the sericin-based nano-drug systems

6.2 Silk Sericin Nanoparticles

So far, the scientific community has not completely satisfied all potential uses of sericin in its pure state for the development of nanostructured systems. Indeed, because of its hydrophilic characteristics, silk sericin has to be stabilised in aqueous solution by conjugation, cross-linking or blending with other polymers, in order to create nano-systems able to encapsulate both lipophilic and hydrophilic drugs for biomedical, pharmaceutical, and cosmetic applications. [1] In detail, several methods are used to produce silk sericin nanoparticles, including self-assembly after conjugation/functionalisation with polymers or other compounds, electro-spraying, desolvation with various cross-linking mechanisms, and emulsification techniques. Based on the chosen method of preparation, it is possible to obtain sericin nanoparticles with different particle size, size distribution, morphology and surface charge. [2] Each technique has advantages and disadvantages, so the decision of an appropriate method is fundamental according to the final drug delivery application. Additionally, the physicochemical nature of sericin often makes the nanoparticle preparation difficult; for this reason, it is still necessary to focus on the stability problems of the sericin in the different experimental conditions, intending to increase the properties of a “noble” material largely used in biomedicine, pharmaceuticals and cosmetics.

In nanomedicine, one of the most common cytocompatible and biodegradable polymers applied with sericin is the poloxamer (also known as Pluronic[®], the name coined by its inventor). It belongs to the class of nonionic triblock copolymers composed of a central hydrophobic chain of polypropylene oxide (PPO) flanked by two hydrophilic chains of polyethylene oxide/glycol (PEO or PEG). Thanks to its chemical and physical properties, poloxamers are employed both alone as nano-carrier in drug delivery, or as stabilizers of other polymers/proteins in the nanoparticle formulation. In this regard, Mandal and colleagues [3] reported a method to prepare nanoparticles using *Antheraea mylitta* sericin and pluronic surfactants. Briefly, the authors solubilised the pluronic and sericin in a 1:5 ratio (protein:surfactant) in an organic solvent which was subsequently added dropwise to deionised H₂O under stirring. Sericin nanoparticles were formed by self-assembly, which is defined as the spontaneous and reversible organisation of molecular units into ordered structures by non-covalent interactions. In aqueous solutions, and above the critical micelle concentration, the pluronic organises into micelles by exploiting its amphiphilic properties. Micelles consist in a hydrophobic core-shell structure, made of PPO, surrounded by a corona made of PPE.[4] The protein chains of sericin arrange at the interface of the core-shell

nanoparticles, ensuring protein stability in aqueous solution, without the use of a cross-linking agent (Figure 6.1).

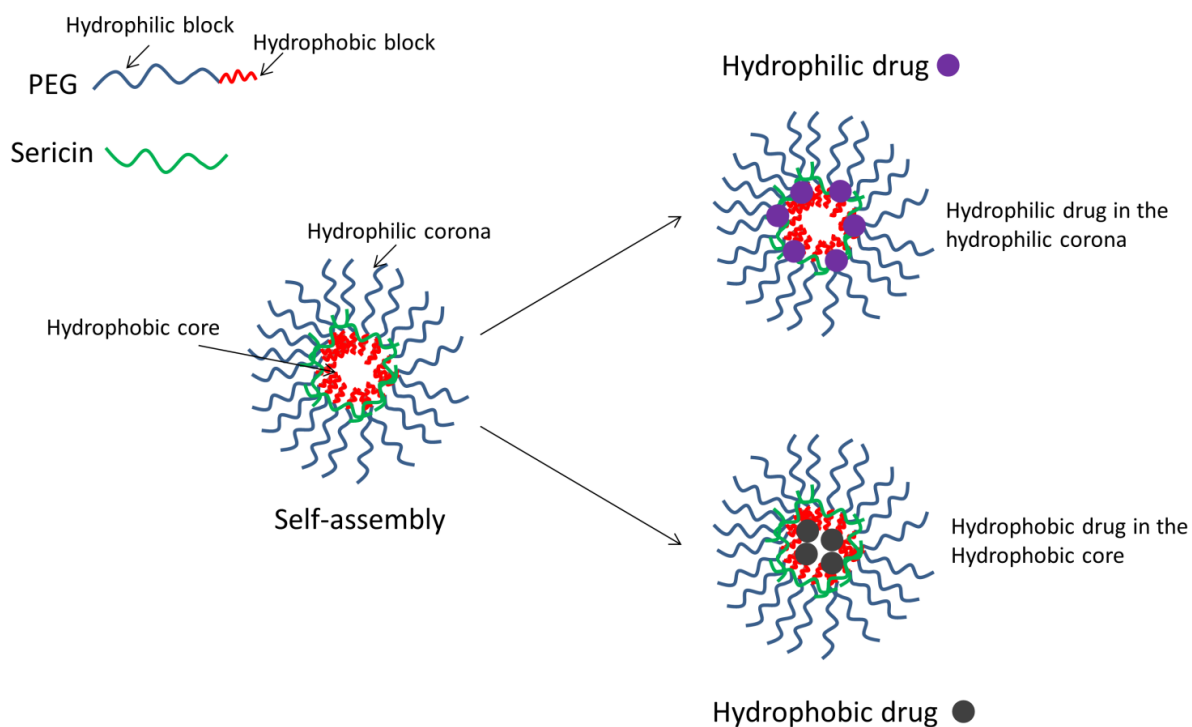


Figure 6.1: A schematic representation showing the self-assembly of sericin-poloxamer nanoparticles. In aqueous solutions, above the critical micelle concentration, the amphiphilic molecules of poloxamer self-assemble. The resulting structure is made of a hydrophobic core-shell surrounded by a hydrophilic corona. The protein chains of sericin arrange at the interface of the core-shell nanoparticles. Hydrophobic drugs are incorporated within the hydrophobic core of the nanoparticles, while hydrophilic drugs are loaded within the hydrophilic corona

Interestingly, for the preparation of nanoparticles, the author tested two different poloxamers (Pluronic F-127 and F-87) and four different solvents (dioxane, dimethylformamide, dimethyl sulfoxide, and tetrahydrofuran) without observing significant differences in the particle size, which ranges from 100 to 110 nm. Additionally, the stability of all the nanoparticles in aqueous solution was demonstrated up to 10 days. Importantly, with this method, sericin nanoparticles can load both hydrophilic and hydrophobic drugs. In essence, a hydrophobic drug may reside within the hydrophobic core of the micellar structure, while a hydrophilic drug is expected to reside within the corona, which is relatively hydrophilic (Figure 6.1).

The authors chose paclitaxel as the hydrophobic drug and FITC-inulin as the hydrophilic one; the encapsulation efficiency of FITC-inulin and paclitaxel was estimated to be around 50-60%

w/w, and it slightly increased the dimensions of nanoparticles. When tested *in vitro*, sericin nanoparticles were rapidly taken up by cells and achieved a faster and prolonged delivery of the drug. For the paclitaxel-loaded nanoparticles, cytotoxicity was assessed on breast cancer cell lines evidencing higher efficacy when compared with the free drug. Interestingly, for the next *in vivo* applications, to increase the targeting of nanoparticles, the outer shell of the polymeric micelle can be functionalised to target specific antibodies/receptors. Additionally, PEG functionalisation can be performed to improve stability in the biological fluids, to prolong the lifetime into the bloodstream, reducing the uptake by the reticuloendothelial system and thus the kidney and/or hepatic elimination. [5]

Similarly, Orlandi and colleagues recently prepared sericin nanoparticles for the loading of polyphenols. [6] According to previously procedures [3], Pluronic F-127 was used as an excipient. The nanoparticles had a diameter less than 150 nm and were able to encapsulate both hydrophilic and hydrophobic molecules, providing a slow and controlled release in phosphate buffered saline. It was demonstrated that the encapsulation into nanoparticles preserved the anti-oxidant, anti-elastase and anti-tyrosinase properties of polyphenols; all formulations promoted the metabolic activity of mesenchymal stem cells over 72 h, and protected cells against oxidative stress damage.

Cho and colleagues prepared self-associated nanoparticles based on silk sericin and PEG units. [7] At first, the authors prepared sericin-PEG conjugates. To this end, PEG was reacted with sericin, and the formation of conjugates was confirmed by the proton signal shift of the tyrosine residues evidenced by Proton Nuclear Magnetic Resonance Spectroscopy. Only the serine residues were involved in the interaction between the silk protein and PEG, while no modifications of other amino acid groups were observed. Subsequently, the sericin-PEG was precipitated in ethanol, forming polymeric micelles with a regular shape and size ranging from 200 to 400 nm. The simultaneous presence of the sericin and polymer in the nanoparticles was confirmed by Fourier Transform Infrared Spectroscopy (FTIR) and Circular Dichroism measurements (CD). In detail, the FTIR spectrum of sericin nanoparticles showed bands attributable to amides I and II of the protein (at 1647 and 1527 cm^{-1} , respectively) and $-\text{CH}_2$ and C-O-C stretching peaks of the PEG (at 2883 and 1114 cm^{-1} , respectively). The CD spectrum evidenced that the structural conformation of sericin shifted from random-coil to β -sheet domains, as a consequence of the sericin-PEG bond.

The attachment of hydrophobic moieties to hydrophilic polymers or proteins has long been proposed to construct nano-sized supramolecular self-assemblies. In this regard, a research group from China recently reported the successful preparation of folate-conjugated sericin

nanoparticles loaded with doxorubicin for anticancer therapy. [8] At first, sericin was functionalized with hydrazine hydrate (chosen as a cross-linking agent) through the condensation reaction between the carboxyl group of the glutamic and aspartic acid of the protein and hydrazine. Then, doxorubicin was covalently linked to hydrazine-functionalized sericin through pH-sensitive hydrazone bonds. The hydrophobicity of doxorubicin and the hydrophilicity of sericin promoted the formation of nanoconjugates. Finally, for actively targeting cancer cells that overexpress folate receptors, the authors covalently grafted folate to the nanoconjugates (Figure 6.2).

Doxorubicin loaded nanoparticles were spherical and with an average size of about 40 nm. After conjugation with folate, nanoparticles retained the spherical shape while a slight increase in the average size and a decrease of the zeta potential were observed. The reduction of the surface charges is probably due to the higher ratio of carboxyl groups to amino groups on the surface of nanoconjugates, which is the consequence of the consumption of the amino groups during the folate conjugation. After conjugation with hydrazine, the physico-chemical characterisation by FTIR revealed the typical sericin peaks of amide I (at 1655 cm^{-1} , due to C=O stretching), amide II (1540 cm^{-1} , deriving from N-H in-plane bend), and amide III (1243 cm^{-1} , due to C-N stretches) as well as two other peaks at 1043 cm^{-1} and 953 cm^{-1} , attributed by the authors to the existence of hydrazide bonds ($-\text{CONHNH}_2$) after the successful linking between the hydrazine and the sericin. The FTIR spectrum of doxorubicin-loaded nanoparticles showed additional peaks at 1410 , 1122 , 1020 , and 988 cm^{-1} , attributed by the authors as possible signals due to the different quinone and ketone carbonyls of the drug. When folate was grafted, new peaks appeared in the spectrum at 1610 cm^{-1} (C=O stretching) and 1566 cm^{-1} (N-H bending) indicating the amino bonds formed between the carboxyl groups of folate and the primary amines of sericin nanoconjugates.

The authors demonstrated that the drug release was dependent on the cleavage of the pH-sensitive hydrazone bonds between the doxorubicin and silk sericin. As a consequence, nanoparticles release doxorubicin only in acidic conditions. Therefore, it can be supposed that nanoparticles will remain stable during the blood circulation (pH 7.2) and release the drug only after being internalised into acidic lysosomes of cells (pH 4.0-6.0), thus reducing adverse effects. After demonstrating the *in vitro* cytocompatibility and *in vivo* hemocompatibility, the efficacy of cancer-targeting of the nanoparticles was tested on human oral epithelium carcinoma cell line, which expresses folate receptors. After 3 h of incubation, significant cellular uptake of nanoparticles was observed.

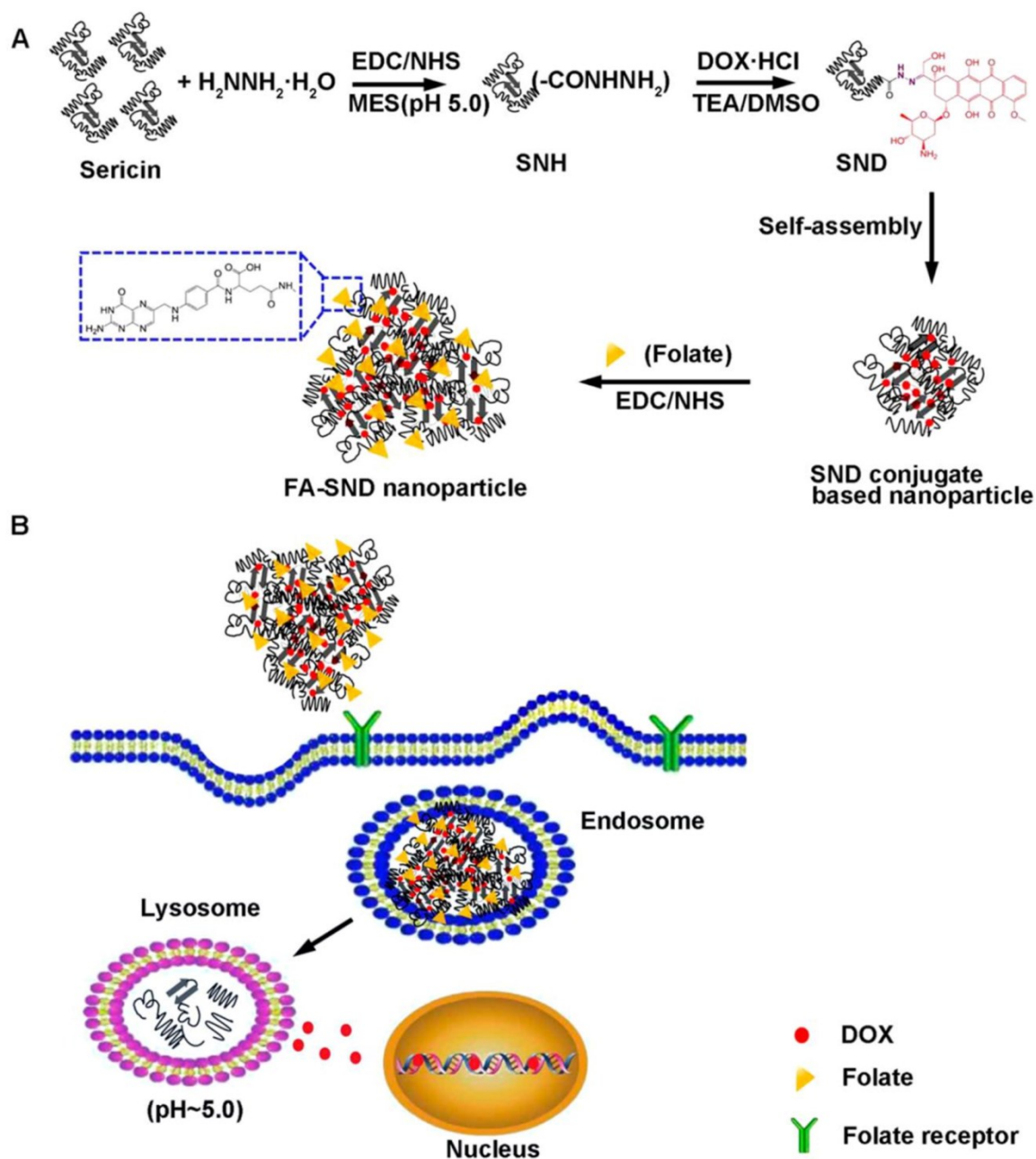


Figure 6.2: (A) Schematic representation showing the preparation of folate-conjugated sericin nanoparticles loaded with doxorubicin. At first, sericin is functionalised with hydrazine groups *via* carbodiimide reactions; then, doxorubicin (red) is grafted to hydrazine-functionalized sericin through acid-sensitive hydrazone bonds. The attachment of hydrophobic doxorubicin onto hydrophilic sericin induces amphiphilic conjugation resulting in the formation of nano aggregates in aqueous media. Finally, folate is covalently grafted to the nanoconjugates via a reaction between sericin's primary amines and the N-hydroxysuccinimide ester of folate. (B) Folate-conjugated sericin nanoparticles were uptake by cells through folate-receptors mediated endocytosis and delivered into endosomes and lysosomes, where the acidic pH triggered doxorubicin release. Reprinted from ref. [8] with permission from American Chemical Society, Copyright 2016

Conversely, the presence of free folate drastically inhibited the cellular uptake of the nanoparticles, demonstrating that it was strictly dependent on folate receptors. In contrast, the nanoparticles were barely uptaken by a mouse fibroblast cell line, which presented a low expression of folate receptors.

Finally, Parisi and colleagues combined poly-ethyl cyanoacrylate and silk sericin. They prepared nanospheres by interfacial polymerisation in acidic aqueous solutions. [9] Such nanospheres were prepared in order to improve the gastrointestinal absorbable amount of the fenofibrate, a hydrophobic drug used in hypercholesterolemia and hypertriglyceridemia as a lipid-regulating agent. To synthesise nanospheres, sericin was dissolved in an HCl solution (pH 4.0) at 50 °C under magnetic stirring and, then, ethyl 2-cyanoacrylate was added dropwise to the aqueous polymerisation medium. After the polymerisation reaction, the nanoparticles suspension was neutralised with 0.1 M NaOH until it reached pH 6.0. The resulting nanoparticles were collected from the suspension by centrifugation, washed with distilled water, and finally, dried overnight under vacuum. The average diameter of nanoparticles was 175 ± 12 nm with the poly-dispersity index (PDI) equals to 0.201, indicating the presence of a homogeneous population in the particle suspension, and with a zeta potential of about -30.0 mV. Nanospheres presented good hydrophilic and swelling properties in both gastric and intestinal simulating fluids as well as good mucoadhesive properties. The latter is mainly due to the presence of sericin (positively charged) which interacting with the mucin (negatively charged) by electrostatic interactions. As a result, *in vitro* and *in vivo* tests highlighted an improved absorption of fenofibrate in the gastrointestinal tract. Notably, the daily supplement in the diet of rats of sericin nanoparticles loaded with fenofibrate caused a significant decrease in the levels of very-low-density and the low-density lipoproteins.

The electrospraying technique has also been proposed for the fabrication of sericin-based nanoparticulate materials of different composition, morphology, texture and size. During electrospraying, a liquid flows out of a tensioned capillary tube and, thanks to electrical forces, fine droplets are formed. Both the flow rate of the liquid and the voltage at the capillary nozzle can, of course, influence the size of the electrosprayed droplets, ranging from hundreds of micrometres down to several tens of nanometer. [10]

In their work, Hazeri and colleagues proposed electro-spray to produce stable nanoparticles based on sericin with a mean size lower than 80 nm, which is smaller than the particles obtained by using other methods, such as precipitation or spray drying. [11] Sericin was at first extracted from *Bombyx mori* cocoons by degumming in distilled water at 120 °C for 1 h;

the obtained solution was then filtered, to remove fibroin residues and impurities, dialysed against water (12 kDa molecular weight cut-off) to discard ions and small protein chains, and freeze-dried. The electrospaying solution was prepared by dissolving sericin into a mixture of LiBr and dimethylsulfoxide. The electrospaying produced nanoparticles with a regular shape and spherical structure.

The authors investigated the effect of the process parameters on the nanoparticle size and morphology. While morphology was not affected, the particle size was strongly influenced by the variation of the process parameters. As an example, on increasing the sericin concentration from 0.1 to 0.9% w/w, larger average particle sizes were obtained. Of note, at concentrations higher than 2% w/w, the electrospaying fails, as the adhesion forces between the protein macromolecules increase, as well as the viscosity of the solution, making it impossible to break down the solution into droplets. Higher voltages lead, instead, to the formation of smaller sericin nanoparticles. In fact, when the voltage is increased, more powerful coulombic explosions are present, as a consequence of the higher charge on the droplets. In this case, even the distance nozzle-collector has an important role: if it is too short, droplets have higher acceleration, and they reach the collector very quickly, leaving not enough time for solvent evaporation and thus generating larger particle size. In this regard, the researchers identified as optimal the distance needle-collector from 20 to 25 cm. Finally, an increase in the particle size was observed by increasing the feed rate of the sericin solution. In fact, this provides higher amounts of sericin solution emerging from the nozzle and thus bigger initial droplets. After electrospaying, evidence of an altered sericin structure was revealed by X-ray diffraction but not from FTIR analysis, as well as a reduction in sericin crystallinity. Moreover, it was evidenced that the ordered parts are composed of tiny crystallites known as β -sheets.

Desolvation is considered a rapid and easy method to prepare silk protein-based nanoparticles, without the use of toxic reagents and surfactants. It has been primarily employed in the preparation of fibroin-based nanoparticles, where organic solvents are exploited to change the conformational structure of the protein from Silk I (soluble in water) to Silk II (insoluble in water). In the literature, few examples of sericin-based nanoparticles prepared by the desolvation technique can be found. Unfortunately, for sericin, no conformational changes can be exploited so stabilisers and cross-linking agents are required.

A research group from India exploited the desolvation method for the preparation of sericin nanoparticles.[12] By this technique, authors have been able to prepare nanoparticles with size ranging from about 150 to 200 nm and stable up to six months. Briefly, the authors used

ethanol as a desolvating solvent, in which the drug, atorvastatin, was previously dissolved. Sericin was added to ethanol (ratio 1:6), then nanoparticles were precipitated and crosslinked by using different concentrations of genipin (10, 20, 40% w/w), an excellent natural cross-linker, extracted by *Gardenia jasminoides ellis* fruits (Figure 6.3).

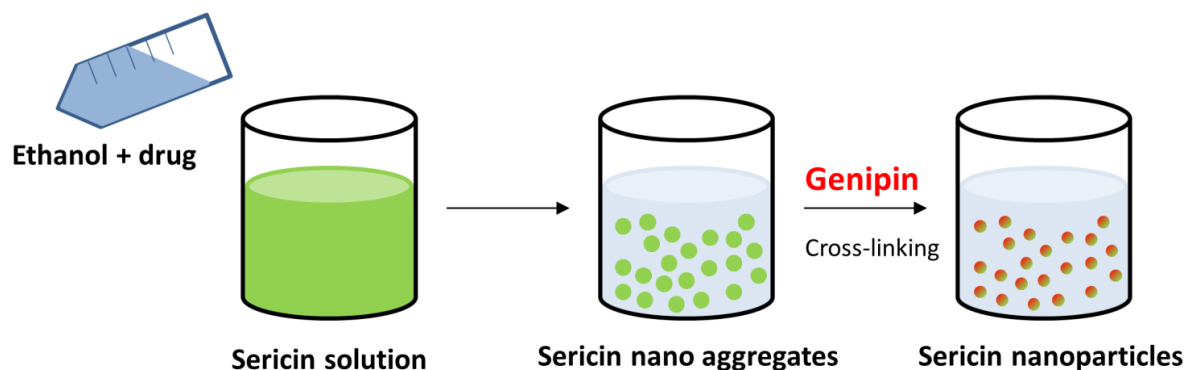


Figure 6.3: Sericin nanoparticle preparation by the desolvation method. Ethanol, the desolvating agent, is added to the sericin solution inducing the formation of aggregates. The drug, atorvastatin, is incorporated within sericin aggregates, that are then stabilised by crosslinking with genipin

Specifically, by a nucleophilic attack, genipin reacts with the amine group of sericin resulting in a dihydropyran ring-opening reaction. Additionally, upon reaction with genipin, sericin may undergo polymerisation as a consequence of the formation of both intermolecular and intramolecular covalent bonds. It is worth mentioning that compared to the commonly employed cross-linkers, such as glutaraldehyde, genipin has lower toxicity. In this regard, when tested *in vitro* on cells, nanoparticles were found to be safe and biocompatible. Interestingly, depending on both the genipin concentration and cross-linking time, the particle size was influenced. Low concentration of genipin and short cross-linking time led to smaller particles, while higher concentrations of genipin, as well as longer cross-linking time, significantly increased the particle size. This can be a consequence of particle aggregation, that occurs after inter-particle cross-linking by reaction with amine groups. The authors achieved a proper drug loading, which was strictly correlated to the particle size (an increase in the particle size leads to high drug-carrying capacity). Interestingly, the atorvastatin release from the nanoparticles changed depending on the genipin concentration and cross-linking time. As an example, on increasing the genipin concentration, the cross-linking time, or both,

a slow release of drug was observed: authors suggested that the rigidity of the more crosslinked sericin matrix hinders the penetration of water, thus slowing down degradation, diffusion and erosion of the protein matrix. The *in vivo* studies suggested that these nanoparticles could be promising for oral treatment of hyperlipidemia. In fact, the authors treated rats with hyperlipemia with 10 mg/kg of atorvastatin sericin nanoparticles, by oral administration for eight days and observed lower blood lipid levels and a significant increase in high-density lipoprotein with respect to free atorvastatin (10 mg/kg).

Other cross-linking mechanisms have been proposed. As an example, Hu and co-workers [13] developed a two-step cross-linking. At first, the negatively charged sericin was physically reacted with the positively charged chitosan in aqueous solution; then, a cross-linking with 1-ethyl-3-(3-(dimethylamino) propyl) carbodiimide hydrochloride (EDC) was provided to improve the structural integrity of nanoparticles (Figure 6.4). The preparation method is straightforward: an acetate solution (1% w/v) containing chitosan (0.05 mg/mL), with pH adjusted to 5, is added dropwise to a sericin solution (1 mg/mL); weight chitosan:sericin ratio of 1:20 is proposed. Finally, EDC is introduced, and the nanoparticles are collected by centrifugation and freeze-dried. Of note, the method proposed by the researchers is free of organic solvents or surfactants, which may lead to safety and toxicity concerns. With this method, the primary driving force for nanoparticle formation is the electrostatic interaction which occurs between the negatively charged sericin (a protein with carboxyl groups) and the positively charged chitosan (a polyelectrolyte bearing several positively charged amino groups). Therefore, during the nanoparticle formation, sericin strongly binds chitosan, leading to the formation of complexed nanoparticles which are further stabilised by the EDC cross-linking (Figure 6.4).

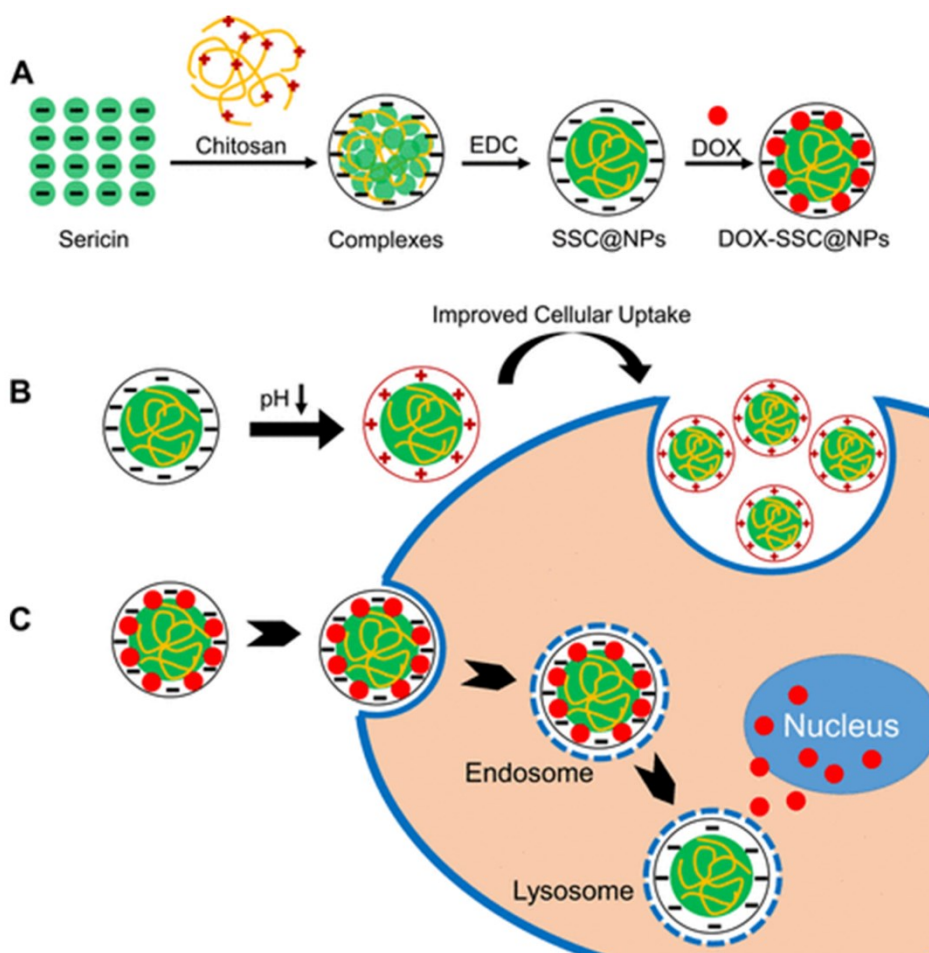


Figure 6.4: (A) Schematic representation showing the preparation of sericin nanoparticles by a two-step cross-linking method. In aqueous solutions, sericin is negatively charged and physically react with chitosan, which is positively charged, leading to the formation of complexed nanoparticles which are further stabilised by the EDC cross-linking. (B) In acidic conditions, nanoparticles show a positive charge, due to the increased amino/carboxyl ratio, which facilitates the cellular uptake and the intracellular drug release (C). Reproduced from ref. [13] with permission from American Chemical Society, Copyright 2017

Doxorubicin was loaded into nanoparticles by incubation, at the end of the preparation process, by adding the drug aqueous solution (0.5 mg/mL) to the nanoparticle suspension (weight ratio of 1:10). The average size of nanoparticles was about 200 nm, with a narrow size distribution, and their zeta potential was about -10 mV. No significant changes in particle size, size distribution, and morphology were observed between doxorubicin-loaded and unloaded sericin nanoparticles. Instead, the zeta potential of nanoparticles slightly decreased as a consequence of the shielding effect of the positively charged doxorubicin binding to the surface of nanoparticles. Notably, the nanoparticles displayed pH-responsive surface charge-reversal, from a negative charge in a neutral environment to a positive charge in a tumour

intracellular acidic microenvironment (pH 6.0), due to the increased amino/carboxyl ratio in the nanoparticles. When tested *in vitro*, in pH 6.0 conditions, the positive charge of nanoparticles resulted in increased uptake by HeLa cells with respect to the negatively charged nanoparticles at pH 7.4. In acidic conditions, the doxorubicin release from nanoparticles was increased. As a consequence, doxorubicin toxicity on tumour cells was increased with respect to the free drug, making such nanoparticles a promising functional nano-carrier for pH-responsive anticancer drug delivery.

It is worth mentioning that in a consequent paper, the same research group demonstrated the stability of sericin nanoparticles when subjected to technological processes, such as freeze-drying, or when put in contact with biological fluids.[14] It is of primary importance that nanoparticles remain highly dispersible and structurally intact during the whole manufacturing process or when interacting with body fluids, like the blood. Indeed, nanoparticle instability in the biological fluids can lead to aggregation, the onset of inflammatory responses and even acute toxicity, compromising safety and biocompatibility. The authors prepared the same nanoparticles, loaded with doxorubicin and without any stabiliser or cryoprotectant, and further explored their colloidal stability, re-dispersibility, and *in vivo* biocompatibility. The nanoparticles demonstrated decent colloidal stability due to the hydrophilic properties of sericin preventing nanoparticle aggregation in biological fluids (the so-called 'hydrophilic repulsion'[15]) (Figure 6.5). In fact, the amino acidic composition of nanoparticles showed to be very close to the one of sericin, and thus it is made for more than 70% by Ser, Thr, Asp, Glu and Lys. The water molecules of the body fluid bind with these hydrophilic amino acids forming a steric layer of water on the surface of the nanoparticles and thus avoid the absorption of serum proteins.

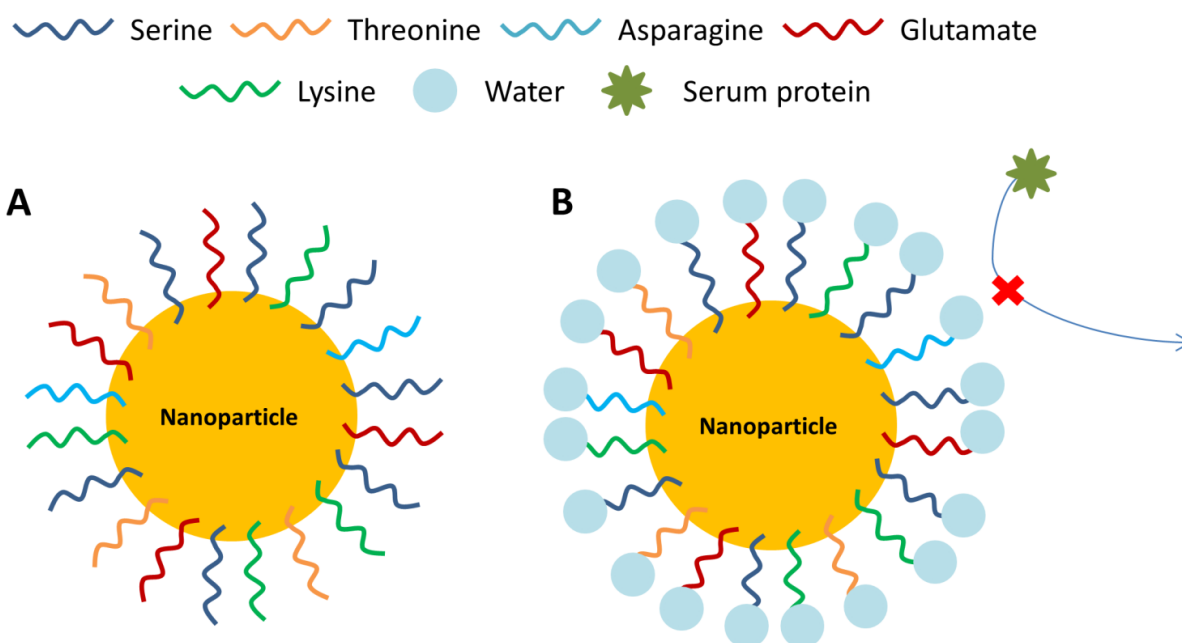


Figure 6.5: The hydrophilic repulsion effect. (A) Nanoparticles are rich in hydrophilic amino acids, which bind the water molecules (B). The steric layer of water avoids the absorption of serum proteins on the surface of the nanoparticles

Additionally, sericin also preserved the size and dispersibility of nanoparticles, even in the absence of cryoprotectants. Only for doxorubicin-loaded nanoparticles, the redispersibility was reduced; as suggested by the authors, this was probably due to the increased hydrophobicity of the nanosystem (doxorubicin is an amphiphilic molecule). Moreover, nanoparticles were shown to be *in vitro* blood compatible (no haemolysis or activation of the coagulation cascade), and *in vivo* biocompatible when administrated intravenously (400 mg/kg). Finally, pharmacokinetic studies demonstrated a reduced distribution of doxorubicin-loaded nanoparticles in the heart, thus alleviating the typical cardiotoxic adverse effects of doxorubicin.

The desolvation method was recently exploited by Suktham and colleagues to produce sericin nanoparticles loaded with resveratrol, a natural polyphenol with remarkable antioxidant and anti-inflammatory properties. [16] Briefly, sericin aqueous suspension was added to dimethylsulfoxide containing Pluronic F-68 (0.5% w/v) as a surfactant. The active, resveratrol, was firstly dissolved in ethanol and then added to the pluronic solution. Interestingly, the concentrations of both sericin and pluronic were varied in the fabrication process, and their effect on nanoparticle size was investigated. The addition of the surfactant, as well as the increase of its concentration, resulted in nanoparticles with smaller sizes. In

detail, the smallest nanoparticle size (about 190 nm) was obtained using the pluronic surfactant at a concentration of 0.5% w/v, and a sericin concentration of 0.6% w/v. The zeta potential became more negative with increased surfactant concentrations; in fact, nanoparticles prepared with pluronic at 1.5% w/v showed greatest electrostatic repulsions, thus preventing the aggregation and the increase in particle size. All the nanoparticles were stable when stored at room temperature up to 4 months. Depending on the sericin and resveratrol concentrations, different entrapment efficiency was observed, and the highest value was revealed at the lowest resveratrol (100 ppm) and sericin concentrations. The *in vitro* release studies showed a gradual release of resveratrol from nanoparticles, which was influenced by both the drug and sericin concentrations. At resveratrol concentration of 100 ppm, the release was completed after 24 h, but it was retarded at higher drug concentrations, and it was slowest for nanoparticles with the highest sericin content. The authors suggested that, probably, the resveratrol loaded into nanoparticles can interact with sericin *via* phenolic hydrogen bonding, causing an increase of the matrix density, thus slowing down the drug release. When tested *in vitro*, both native and resveratrol-loaded nanoparticles were non-toxic to human skin fibroblast cells, while the resveratrol-loaded nanoparticles showed significant toxicity to Caco-2 colorectal adenocarcinoma cells.

Finally, in the study conducted by Das and co-workers, sericin obtained from the mulberry silkworm *Bombyx mori* cocoons was used to construct a protein-based platform for non-viral DNA delivery through the protein desolvation method. [17] Briefly, sericin nanoparticles were obtained by adding dry ethanol to a sericin solution (5 mg/mL) in Tris-HCl buffer (1M, pH 7.4) and then stabilised with glutaraldehyde (2% v/v). The ratio of Tris-HCl-ethanol 1:2 (% v/v) was optimal for preparing silk sericin nanoparticles with a hydrodynamic diameter of about 120 nm and a surface zeta potential of -25.6 mV (Figure 6.6 a). The PDI was found to be 0.1 ± 0.1 (mean value \pm standard deviation), which confirmed the mono-dispersity of the solution. Although stable in aqueous storage conditions at 4 °C for five days (Figure 6.6 b), sericin nanoparticles displayed a certain degree of aggregation, which can be explained by the increasing Van der Waals forces between the nanostructures. Overall, the preparation method did not alter the secondary structure of the sericin protein, as FTIR analysis demonstrated the manifest presence of the amide I and amide II absorption peaks (Figure 6.6 c). Finally, micrographs obtained by using scanning and transmission electron microscope (SEM and TEM) showed a spherical morphology of the sericin nanoparticles and the distinct electro-negative core structure of about 70 nm (Figure 6.6 d-e).

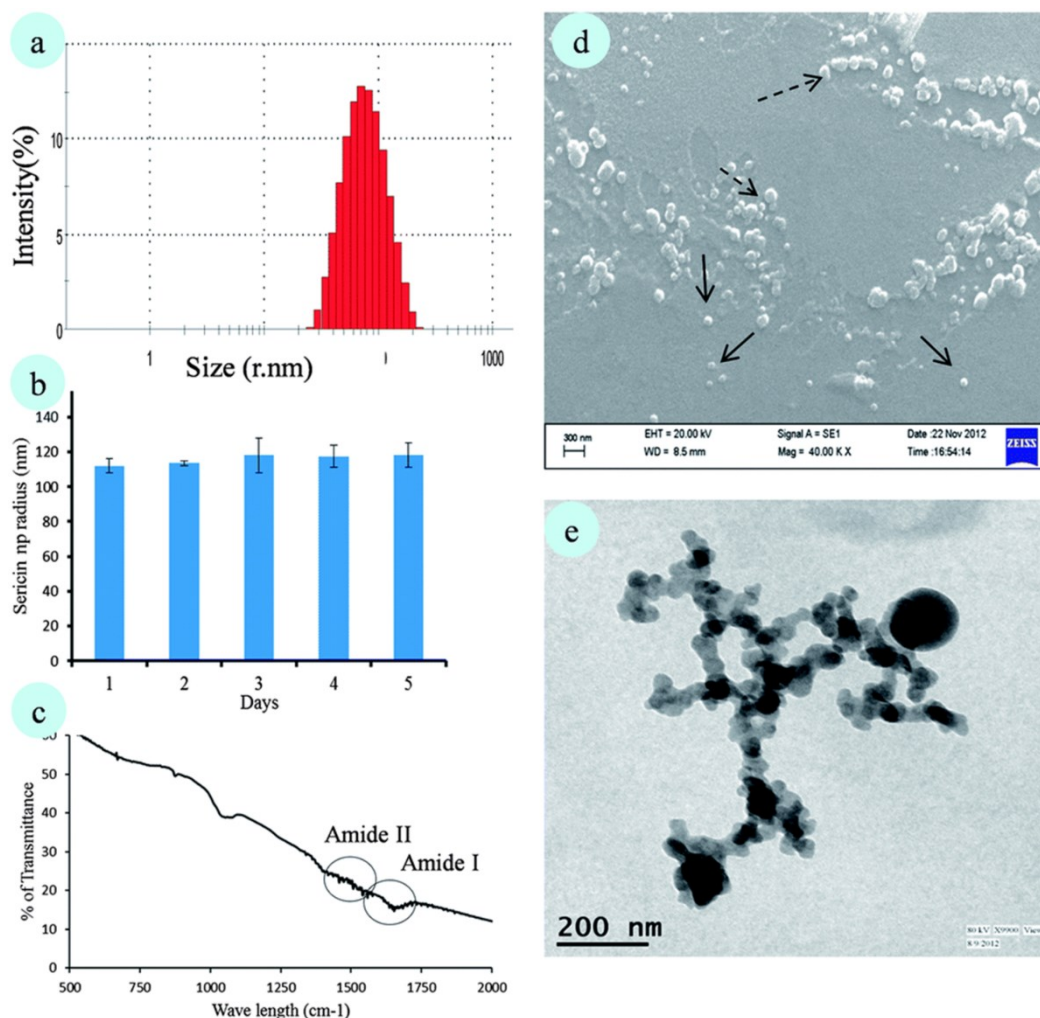


Figure 6.6: Particle size distribution (a), stability (b), FTIR spectrum (c), and morphological investigation of sericin nanoparticles (SEM and TEM images in the panel d and e, respectively) prepared by the desolvation method. Reproduced from ref [17] with permission from The Royal Society of Chemistry

Despite their good technological properties, sericin nanoparticles prepared by Das and colleagues proved to be unsuitable for gene delivery, as they displayed a negatively charged surface. Indeed, electrostatic interactions between the negatively charged genetic material and a positive charged micro/nano-drug delivery systems are generally exploited to achieve proper drug loading. To overcome this problem, the surface of nanoparticles was coated with cationic poly-L-lysine molecules. Due to this functionalisation, DNA enveloped the surface of nanoparticles and interestingly, also reduced the aggregation. *In vitro*, it was demonstrated that the DNA packaging into sericin nanoparticles increased the amount of transported DNA without compromising the cell viability.

Even the emulsion technique has been proposed in the literature to entrap different bioactive compounds into micro- and nano-drug delivery systems. To the best of our knowledge, only one attempt has been proposed in the literature to prepare sericin nanoparticles by this technique. [18] Specifically, Orachun and co-workers proposed a water/silicone emulsion method. Briefly, a sericin and niacinamide solution (2 and 20% w/v, respectively) was emulsified into silicone oil containing 5% v/v silicone emulsifier. The ionic gelation of sericin nanoparticles was achieved by adding CaCl_2 as a cross-linking reagent. Interestingly, some parameters able to influence the nanoparticle formation were studied, such as the concentrations of CaCl_2 (2, 4, 6 and 8% w/v) and sericin (0.5, 1 and 2% w/v), the time (15, 30 and 60 min) and the speed of homogeniser (6500, 9500 and 13500 rpm). The homogenisation time was the only parameter that did not influence, in a significant manner, the size of nanoparticles. Increasing the concentration of sericin and CaCl_2 led to an increase in the particle size, while an increase in the homogenisation speed led to nanoparticles with smaller size. The optimal nanoparticles, with a size of about 230 nm, were obtained for the following conditions: sericin concentration 2% w/v, CaCl_2 concentration 8% w/v, homogenising speed 1000 rpm and homogenising time 15 min.

6.3 Silk Sericin Nanofibers

Nanofibers are gaining a global interest for multiple application fields, including tissue engineering, drug delivery, preparation of functional nanotubes, catalyst supports, thin fibres for filtration application, and so on. In biology, the term nanofibre more frequently refers to a fibre with diameter below 100 nm. The terms mat or mesh define a collection of nanofibers and, depending on the orientation of fibres, they are termed as either woven (oriented in highly regular patterns) or non-woven (randomly orientated).

The electrospinning technique is particularly suitable to prepare nanofibers for many biomedical applications based on polymer and polymer composites, both synthetic and natural, including collagen, gelatin, chitosan, poly (lactic acid) (PLA), poly (D, L-lactide-co-glycolide) (PLGA), polycaprolactone (PCL), and also silk sericin.

In this regard, Zhang and colleagues proposed the electrospinning technique to achieve nanofibers from the sericin-hope silkworm species. [19] In their work, the researchers dissolved sericin in trifluoroacetic acid in a concentration range between 2 and 12% w/w. Importantly, the sericin concentration, as well as the spinning parameters (*e.g.* the

acceleration voltage, the spinning distance, the flow rate of spinning), strongly influenced the morphology of electrospun fibres. In contrast, the distribution of electrospun fibre diameters was not directly related to the concentration of the solution. In detail, concentrations of sericin solution above 10% w/w were suitable to obtain nanofibers with smooth surfaces and a circular cross-section. The mean diameter of the fibres decreased on increasing the acceleration voltage, with an excellent spinnability achieved at an acceleration voltage above 32 kV. Regarding the effect of the spinning distance, after fixing the sericin concentration and the acceleration voltage, the authors observed that average diameters faintly increased with increasing spinning distances. Indeed, the sericin fibre diameter was of about 200 nm and 345 nm at the spinning distances of 6 and 12 cm, respectively. When the spinning distance was set to above 9 cm, the nanofibers had smooth surfaces without beads; however, a distance of 15 cm was not suitable for fabricating sericin nanofibers. Finally, the thickness of the electrospun fibres was influenced by the flow rate of spinning solutions. In fact, continuous and fine sericin nanofibers can be produced at 25 kV with the optimum flow rate value about 0.06 cm/min. FTIR spectra confirmed the random coil conformation (1651 cm^{-1} and 1527 cm^{-1} , amide I and II peaks) of all the sericin electrospun fibres. That structural organisation can cause the thermal degradation of the nanofibers at a lower temperature than degummed sericin, which is instead characterised by β -sheet structure.

A similar study was conducted by Khan and co-workers to determine the best electrospinning conditions to produce sericin nanofibers, starting from a sericin solution in TFA. [20] As previously reported [19], sericin concentration influenced fibre morphology. At low concentrations, only beads were observed; beaded fibres were produced using sericin concentrations between 8.5% w/w and 14.2% w/w (Figure 6.7 a-d), while sericin nanofibers with round cross-sections and smooth surfaces were achieved using an optimum sericin/TFA solution at the concentration 20.9% w/w (Figure 6.7 e,f).

Regarding the dimensional distribution, electrospun nanofibers had an average diameter of 145 and 184 nm, starting from sericin/TFA solutions concentrated 20.9 and 22.9% w/w, respectively. Overall, the mean diameters increased with increasing concentration of the protein solution. In particular, the viscosity was the main parameter for deciding the fibre diameter. In fact, high values of viscosity resulted in the preparation of smooth fibres without beads, while lower viscosity favoured fine beaded filaments. The FTIR results demonstrated the conformational change of silk sericin nanofibers from β -sheet to random-coil, while Differential Scanning calorimetry (DSC) measurements showed two endothermic bands: a first one corresponding to the thermal decomposition of sericin, and a second one due to the

presence of TFA, which disappeared after heating the sample (due to the evaporation of the residue solvent).

In the preparation of nanofibers, sericin is combined with other polymeric materials to enhance its mechanical properties. As an example, a research group from Iran prepared a nanofibrous mat by electrospinning a solution of sericin, chitosan (Cs) and PVA (in different volume ratios) to which AgNO_3 was added as an antimicrobial agent. [21]

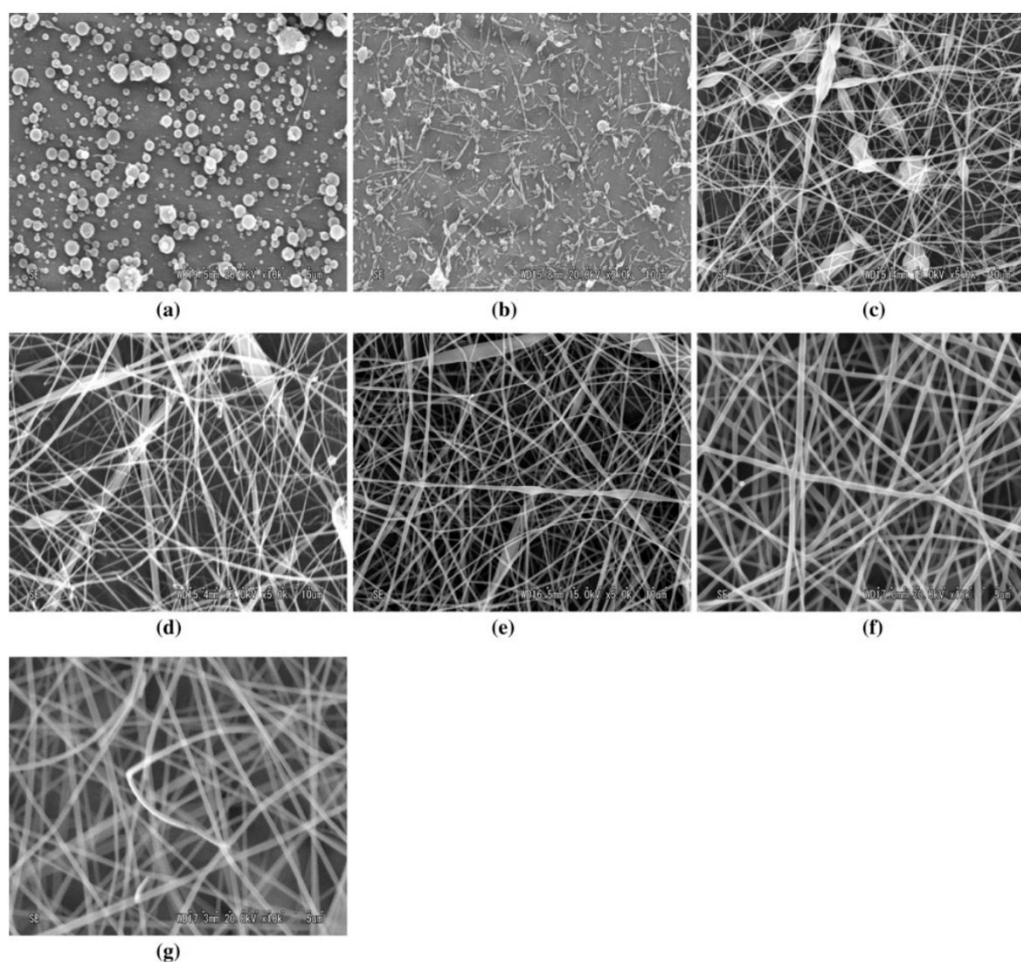


Figure 6.7: SEM images of electrospun sericin nanofibers. Fibres were electrospun at voltage (25 kV) and spinning distance (15 cm) and varying the sericin concentration in TFA solution: a 8.5% w/w, b 9.6% w/w, c 11.7% w/w, d 14.2% w/w, e 16.5% w/w, f 20.9% w/w, and g 22.9% w/w. Reproduced from [20] with permission from Springer Nature, Copyright 2013

The effects of electrospinning conditions on the morphology and diameter of nanofibers were investigated. Also, the capacity of nanofibers to inhibit *Escherichia coli* growth was demonstrated *in vitro*. Overall, the mean diameter of nanofibers decreased with increasing voltages (Figure 6.8) and, after setting 22 kV as voltage, the formulations with a volume ratio

Cs/SS/PVA of 25/25/50 and 35:15:50 were the best to produce nanofibers with smooth surfaces without beads.

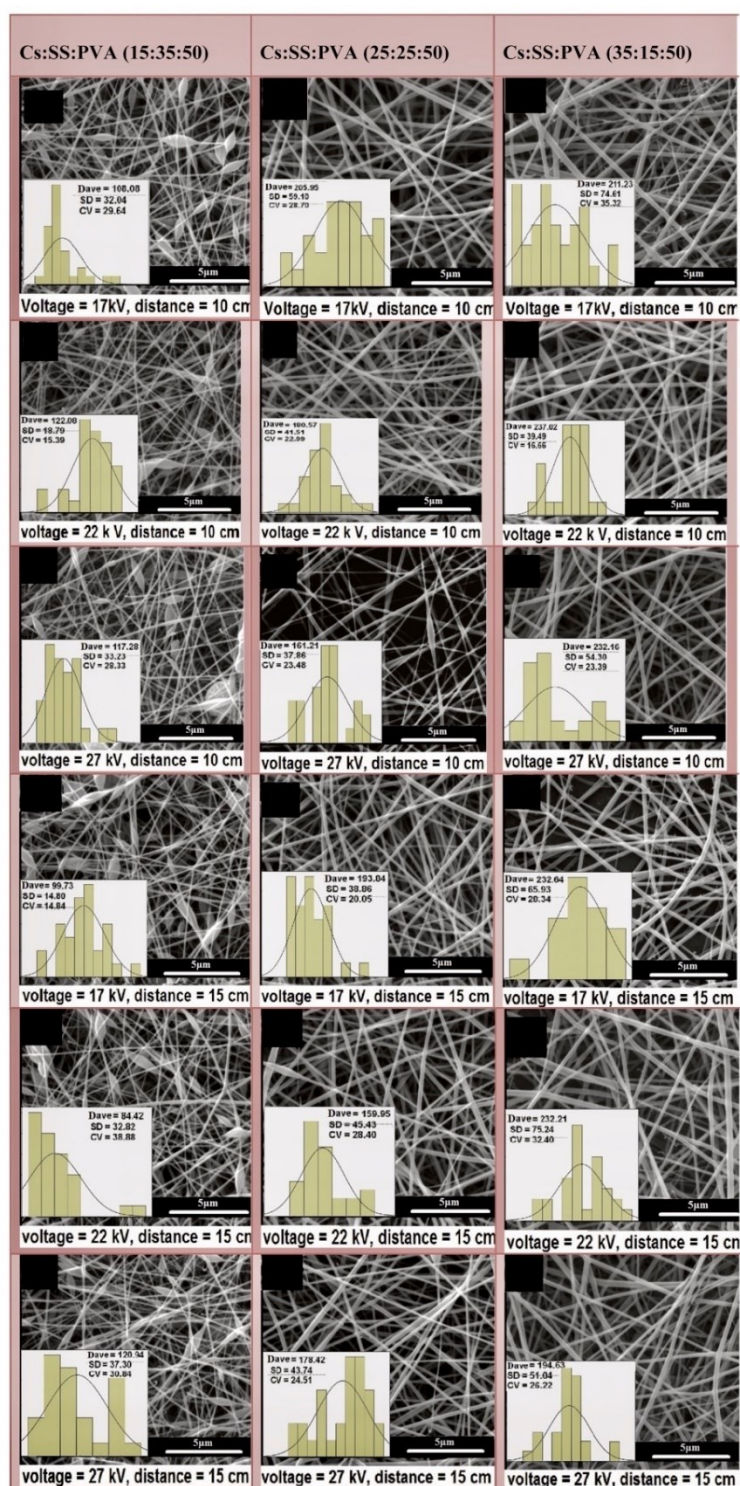


Figure 6.8: SEM images and diameter distribution of Cs/SS/PVA nanofibers. The analysis was performed considering three different volume ratios, three voltages (17, 22, 27 kV) and two spinning distances (10 and 15 cm) at the constant feed rate 0.25 ml/h. Reproduced from ref. [21] with permission from Elsevier, Copyright 2014

The effect of AgNO₃ on Cs/SS/PVA nanofiber diameter was also evaluated: introducing AgNO₃ in the electrospinning solution caused a decrease in the mean diameter of nanofibers. EDXA spectroscopy demonstrated that nano silvers were well distributed in the nanofiber mat and the FTIR spectra of nanofibers showed peaks at 3384 cm⁻¹ (O-H, N-H stretching vibrations and inter hydrogen bonding) and peaks at 2938 cm⁻¹, 1656 cm⁻¹, and 1541 cm⁻¹ assigned to C-H, amide I, and amide II bands, confirming the simultaneous presence of Cs, SS, and PVA compounds. Finally, Cs/SS/PVA nanofibers with AgNO₃ showed 100 % antibacterial activity against *Escherichia coli*.

Sericin is often combined with PVA to prepare composite nanofibers with applications different from the drug delivery-field. As an example, Zhao and colleagues prepared composite nanofibers (based on sericin, PVA and β -cyclodextrin) intended to remove organic dye from water solution [22], while Yan and collaborators prepared sericin and PVA nanofibers and investigated their effect on the epithelial-mesenchymal transition of A549 cells. [23]

Nanofibers, mainly achieved by the electrospinning technique, have a high potential also for tissue engineering applications. Tissue engineering represents a practical approach to promote tissue repair or functional tissue replacement in regenerative medicine and consists of the integrated use of cells and biomaterials/scaffolds. Specifically, the scaffold may provide a suitable microenvironment for the proper regeneration of functional tissue by mimicking critical features of the extracellular matrix (ECM) at sub-micron and nanometer scales. Moreover, scaffolds can serve as a delivery system for cells (e.g. the mesenchymal stem cells), growth factors (such as the platelet lysate) or both, intended for providing signals able to trigger the tissue regeneration process. When the scaffold is intended to deliver cells, the mechanical strength of the synthetic polymers is often combined with the cell-friendly properties of natural polymers, such as sericin. In this regard, the combination of sericin with other polymers, such as polycaprolactone (PCL), polyvinyl alcohol or chitosan has been successfully reported in the literature. As an example, Li and co-workers proposed sericin and PCL-based nanofibrous scaffold, prepared by an emulsion electrospinning procedure, for cell delivery in the tissue regeneration field. [24] PCL was proposed to improve the structure and electro-spinnability of scaffolds, due to its excellent electro-spinnability, good mechanical properties, and slow degradation. At the same time, sericin was chosen to improve cell adhesion and proliferation and to stimulate the production of the ECM components. To this end, sericin and PCL solutions (in LiBr and hexafluoroisopropanol, respectively) were mixed in different volume ratios and electrospun (the voltage was set between 15 and 20 kV and the

spinning distance applied was of 12-15 cm). PCL and sericin nanofibres appeared with a smooth surface and regular tubular shape (Figure 6.9) and with good surface wettability. Again, sericin played an essential role in the preparation process. By increasing the sericin content (and thus the conductivity of blend solutions) the fibre diameter and the elongation properties slightly decreased, the tensile strength considerably increased, and non-uniform bead structures appeared in the nano-fibrous scaffolds.

FTIR analyses were performed to investigate the chemical and conformational composition of scaffolds after electrospinning. In the spectrum of PCL and sericin nanofibers, the typical peaks of the polymer and protein were observed. However, after electrospinning, the peaks of sericin shifted from 1518 to 1527 cm^{-1} for amide II, and from 1626 to 1648 cm^{-1} for the amide I. This data confirmed the conformation change of the sericin from β -sheet to random-coil domains, probably caused by the breakdown of intermolecular hydrogen bonds during the dissolution of the protein in the hexafluoroisopropanol solution. When tested *in vitro*, sericin improved fibroblast adhesion and proliferation, as well as the expression of Transforming Growth Factor (TGF)- β 1 and collagen I (but not collagen III) by FEK4 cells. *In vivo* testing, performed on Sprague Dawley rats, demonstrated that four weeks after implantation, PCL and sericin scaffolds were fully colonised by cells (Figure 6.10). Interestingly, this event may have been facilitated by the formation of pores on the nanofibrous scaffolds due to sericin degradation. No adverse effects have been observed.

Eslah and colleagues prepared instead sericin and PVA nanofibers intending to demonstrate their potential in tissue engineering. [25] First, the researchers selected a mixture of water and dimethyl sulfoxide to solubilise PVA and sericin, which was then electrospun. Interestingly, the researchers also investigated how the diameter distribution of sericin and PVA nanofibers changed as a function of the concentration of both sericin and PVA in the solution, and the electrospinning parameters. By increasing sericin concentration, the fibre diameter increases, as a consequence of the higher viscosity of the solution that has higher resistance to the drawing forces exerted by the electrospinning zone. When higher voltages and feed rate were applied, more polymer solution was expelled from the nozzle tip, thus causing an increase of nanofiber diameter. A nozzle-collector distance from 15 to 25 cm reduced fibre diameter. On the contrary, setting the spinning distance from 25 to 30 cm increased fibre diameter. The physical-chemical characterisation revealed that the nanofiber stability increased with the increasing the amount of sericin, thanks to the formation of hydrogen bonds between the polymer and the protein macromolecules.

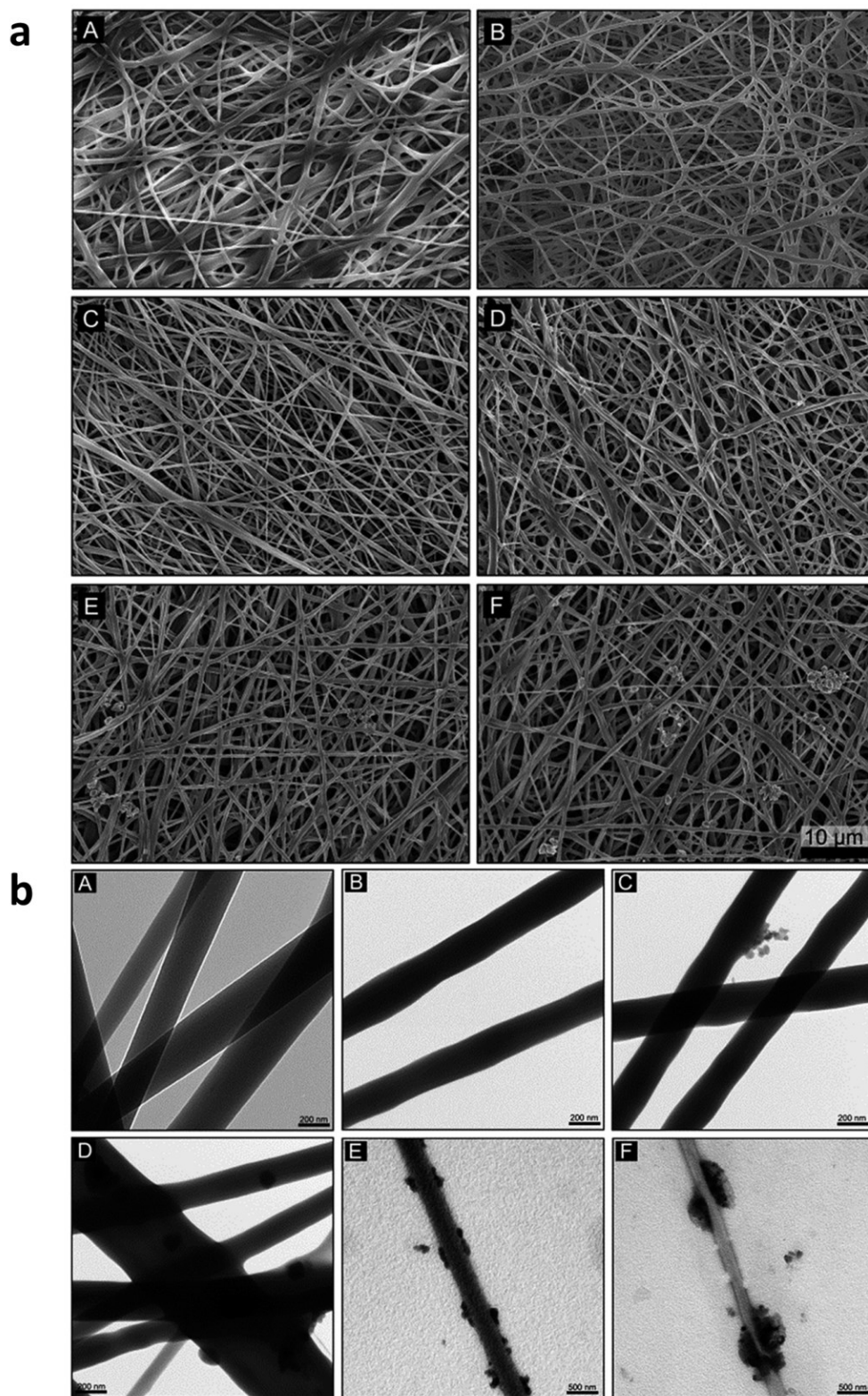


Figure 6.9: SEM (a) and TEM (b) images of electrospun PCL and sericin nanofibres. Each panel illustrates the morphology of scaffolds using different sericin concentrations: (A) PCL, (B) PCL/SS 91% w/w, (C) PCL/SS 82% w/w, (D) PCL/SS 73% w/w, (E) PCL/SS 64% w/w, (F) PCL/SS 55% w/w. Reproduced from ref [24] with permission from the Royal Society of Chemistry

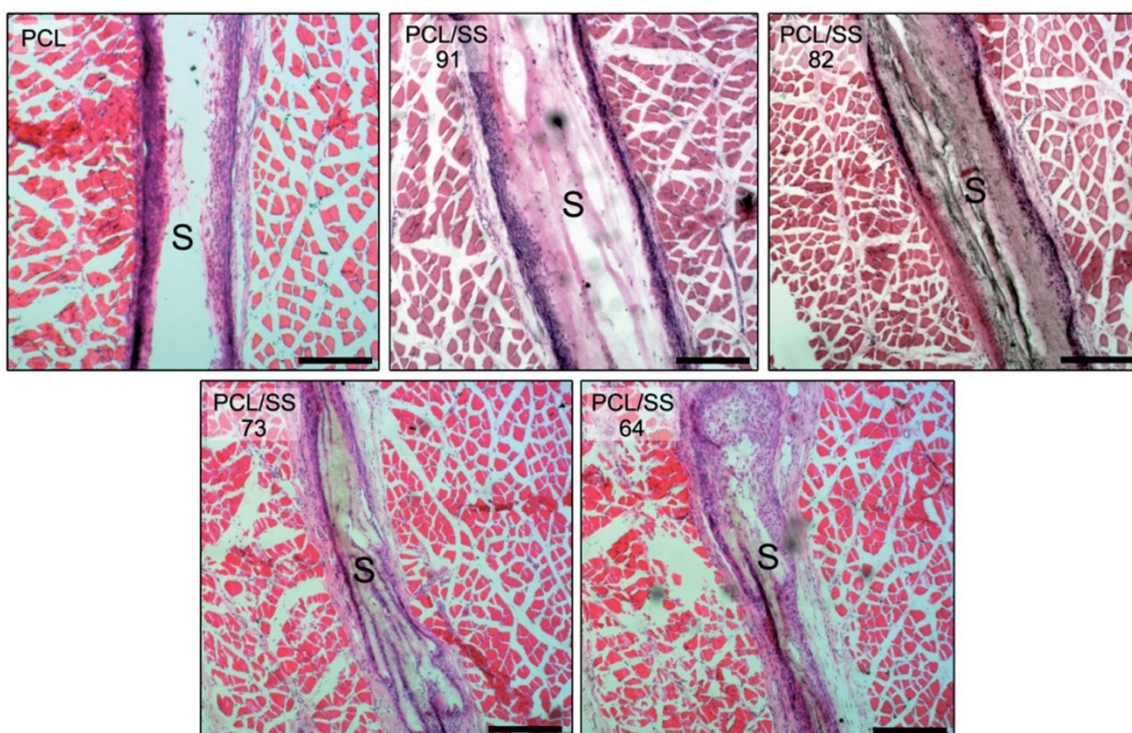


Figure 6.10: Illustration of hematoxylin/eosin staining of scaffolds prepared with PCL and different sericin concentrations (91, 82, 73 and 64 % w/w). The scaffolds are labelled with “S”. Scale bar: 500 μ m. Reproduced from ref [24] with permission from the Royal Society of Chemistry

Sericin electrospun fibres are often used also in the wound dressing field. Sericin electrospun fibres are employed to protect the wound, to facilitate the absorption of wound exudates or fluids from the wound site maintaining the desired moist microenvironment, to promote the wound healing process, and to prevent the bacterial infections. For these applications, sericin can be considered both as an excipient and the active ingredient, due to the multiple biological properties which it possesses. Zhao and colleagues prepared chitosan/sericin composite nanofibers which demonstrated *in vitro* cytocompatibility and promotion of fibroblast cell proliferation, as well as excellent intrinsic antibacterial properties against both Gram-positive and negative bacteria.[26] Gilotra and colleagues prepared instead nanofibrous wound dressings based on PVA combined with sericin extracted from *Bombyx mori* or *Antheraea assama* cocoons. [27] For both the sericin types, the wound dressing fabricated in the form of fibrous mats exhibited nanometric size, ideal physico-chemical properties, high swelling capacity, ROS-scavenging and wound healing activity. Also, the dressings had intrinsic antibacterial properties and were biocompatible, as demonstrated both *in vitro*, by examining cytokine release from immune cells, and *in vivo* by subcutaneous implantation in mice.

Interestingly, the biological activities were mainly related to the presence of sericin. Finally, Massoumi and colleagues developed an innovative wound dressing with intrinsic antibacterial properties combining sericin with gelatin and halloysite nanotubes (HNTs) as a carrier for copper and zinc ions. [28] Nanofibers were obtained by an electrospinning process, and formic acid was used as the solvent. The addition of Zn^{2+} and Cu^{2+} ions promoted the conductivity of the electrospun solution and consequently led to the formation of fine fibres. Both ions were uniformly dispersed throughout the nanofiber network in the scaffolds as proved by EDS mapping and TEM images. The addition of HNTs did not alter the morphology of the fibres but decreased the average fibre diameter. Indeed, positively charged HNTs reduced the electrical conductivity of the electrospun solutions and enhanced the surface charge density of the electrospun jet, resulting in smaller fibre formation.

References

- [1] B. Crivelli, S. Perteghella, E. Bari, M. Sorrenti, G. Tripodo, T. Chlapanidas, M.L. Torre, Silk nanoparticles: from inert supports to bioactive natural carriers for drug delivery, *Soft Matter* 14(4) (2018) 546-557.
- [2] D. Verma, N. Gulati, S. Kaul, S. Mukherjee, U. Nagaich, Protein Based Nanostructures for Drug Delivery, *Journal of Pharmaceutics* (2018).
- [3] B.B. Mandal, S.C. Kundu, Self-assembled silk sericin/poloxamer nanoparticles as nanocarriers of hydrophobic and hydrophilic drugs for targeted delivery, *Nanotechnology* 20(35) (2009).
- [4] Z.L. Tyrrell, Y. Shen, M. Radosz, Fabrication of micellar nanoparticles for drug delivery through the self-assembly of block copolymers, *Progress in Polymer Science* 35(9) (2010) 1128-1143.
- [5] H. Otsuka, Y. Nagasaki, K. Kataoka, PEGylated nanoparticles for biological and pharmaceutical applications, *Advanced Drug Delivery Reviews* 64 (2012) 246-255.
- [6] G. Orlandi, E. Bari, L. Catenacci, M. Sorrenti, L. Segale, S. Faragò, M. Sorlini, C.R. Arciola, M.L. Torre, a.S. Perteghella, Polyphenols-Loaded Sericin Self-Assembling Nanoparticles: A Slow-Release for Regeneration by Tissue-Resident Mesenchymal Stem/Stromal Cells, *Pharmaceutics* (12) (2020) 381.
- [7] K.Y. Cho, J.Y. Moon, Y.W. Lee, K.G. Lee, J.H. Yeo, H.Y. Kweon, K.H. Kim, C.S. Cho, Preparation of self-assembled silk sericin nanoparticles, *International Journal of Biological Macromolecules* 32(1-2) (2003) 36-42.

- [8] L. Huang, K. Tao, J. Liu, C. Qi, L. Xu, P. Chang, J. Gao, X. Shuai, G. Wang, Z. Wang, L. Wang, Design and Fabrication of Multifunctional Sericin Nanoparticles for Tumor Targeting and pH-Responsive Subcellular Delivery of Cancer Chemotherapy Drugs, *Acs Applied Materials & Interfaces* 8(10) (2016) 6577-6585.
- [9] O.I. Parisi, M. Fiorillo, L. Scrivano, M.S. Sinicropi, V. Dolce, D. Iacopetta, F. Puoci, A.R. Cappello, Sericin/Poly(ethylcyanoacrylate) Nanospheres by Interfacial Polymerization for Enhanced Bioefficacy of Fenofibrate: In Vitro and In Vivo Studies, *Biomacromolecules* 16(10) (2015) 3126-3133.
- [10] A. Jaworek, A.T. Sobczyk, Electrospraying route to nanotechnology: An overview, *Journal of Electrostatics* 66(3-4) (2008) 197-219.
- [11] N. Hazeri, H. Tavanai, A.R. Moradi, Production and properties of electrosprayed sericin nanopowder, *Science and Technology of Advanced Materials* 13(3) (2012).
- [12] J. Kanoujia, M. Singh, P. Singh, S.A. Saraf, Novel genipin crosslinked atorvastatin loaded sericin nanoparticles for their enhanced antihyperlipidemic activity, *Materials Science & Engineering C-Materials for Biological Applications* 69 (2016) 967-976.
- [13] D. Hu, Z. Xu, Z. Hu, B. Hu, M. Yang, L. Zhu, pH-Triggered Charge-Reversal Silk Sericin-Based Nanoparticles for Enhanced Cellular Uptake and Doxorubicin Delivery, *Acs Sustainable Chemistry & Engineering* 5(2) (2017) 1638-1647.
- [14] D. Hu, T. Li, Z. Xu, D. Liu, M. Yang, L. Zhu, Self-stabilized silk sericin-based nanoparticles: In vivo biocompatibility and reduced doxorubicin-induced toxicity, *Acta Biomaterialia* 74 (2018) 385-396.
- [15] A.E. Nel, L. Maedler, D. Velegol, T. Xia, E.M.V. Hoek, P. Somasundaran, F. Klaessig, V. Castranova, M. Thompson, Understanding biophysicochemical interactions at the nano-bio interface, *Nature Materials* 8(7) (2009) 543-557.
- [16] K. Suktham, T. Koobkokkruad, T. Wutikhun, S. Surassmo, Efficiency of resveratrol-loaded sericin nanoparticles: Promising bionanocarriers for drug delivery, *International Journal of Pharmaceutics* 537(1-2) (2018) 48-56.
- [17] S.K. Das, T. Dey, S.C. Kundu, Fabrication of sericin nanoparticles for controlled gene delivery, *Rsc Advances* 4(5) (2014) 2137-2142.
- [18] T. Orachun, W. Wisuitiprot, N. Waranuch, Development of Niacinamide Loaded-Sericin Nanoparticle Using Water in Silicone Technique, in: I. Press (Ed.) 2012 International Conference on Biological and Life Sciences, IACSIT Press, Singapore, 2012.

- [19] X. Zhang, M.M.R. Khan, T. Yamamoto, M. Tsukada, H. Morikawa, Fabrication of silk sericin nanofibers from a silk sericin-hope cocoon with electrospinning method, *International Journal of Biological Macromolecules* 50(2) (2012) 337-347.
- [20] M.M.R. Khan, M. Tsukada, X. Zhang, H. Morikawa, Preparation and characterization of electrospun nanofibers based on silk sericin powders, *Journal of Materials Science* 48(10) (2013) 3731-3736.
- [21] E. Hadipour-Goudarzi, M. Montazer, M. Latifi, A.A.G. Aghaji, Electrospinning of chitosan/sericin/PVA nanofibers incorporated with in situ synthesis of nano silver, *Carbohydrate Polymers* 113 (2014) 231-239.
- [22] R. Zhao, Y. Wang, X. Li, B. Sun, Z. Jiang, C. Wang, Water-insoluble sericin/beta-cyclodextrin/PVA composite electrospun nanofibers as effective adsorbents towards methylene blue, *Colloids and Surfaces B-Biointerfaces* 136 (2015) 375-382.
- [23] S. Yan, X. Li, J. Dai, Y. Wang, B. Wang, Y. Lu, J. Shi, P. Huang, J. Gong, Y. Yao, Electrospinning of PVA/sericin nanofiber and the effect on epithelial-mesenchymal transition of A549 cells, *Materials Science & Engineering C-Materials for Biological Applications* 79 (2017) 436-444.
- [24] L. Li, Y. Qian, C. Lin, H. Li, C. Jiang, Y. Lv, W. Liu, K. Cai, O. Germershaus, L. Yang, The effect of silk gland sericin protein incorporation into electrospun polycaprolactone nanofibers on in vitro and in vivo characteristics, *Journal of Materials Chemistry B* 3(5) (2015) 859-870.
- [25] S. Eslah, H. Tavanai, M. Morshed, Electrospinning and characterization of poly (vinyl alcohol)-sericin nanofibers as a potential for tissue engineering applications, *Journal of the Textile Institute* 107(8) (2016) 949-957.
- [26] R. Zhao, X. Lia, B. Sun, Y. Zhang, D. Zhan, Z. Tang, X. Chen, C. Wang, Electrospun chitosan/sericin composite nanofibers with anti-bacterial property as potential wound dressings., *International Journal of Biological Macromolecules* 68 (2014) 92-97.
- [27] S. Gilotra, D. Chouhan, N. Bhardwaj, S.K. Nandi, B.B. Mandal, Potential of silk sericin based nanofibrous mats for wound dressing applications, *Materials Science & Engineering C-Materials for Biological Applications* 90 (2018) 420-432.
- [28] H. Massoumi, J. Nourmohammadi, M.S. Marvi, F. Mortarzadeh, Comparative study of the properties of sericin-gelatin nanofibrous wound dressing containing halloysite nanotubes loaded with zinc and copper ions, *International Journal of Polymeric Materials and Polymeric Biomaterials* 68(18) (2019) 1142-1153.

Aim

In this PhD thesis, the potential exploitation of sericin in the pharmaceutical, cosmetic, and biomedical fields was investigated. In detail, the research activity covered three distinct aims. At first, it was compared sericins extracted by two different degumming processes to evaluate which extraction method could best preserve their quality and cytocompatibility (**Aim 1**). Indeed, it is well known that diverse extraction methods result in types of sericin remarkably different in composition, molecular weight distribution, physical-chemical properties and also biological activity. In this context, complementary chromatographic techniques were proposed to reconstruct a fingerprint representative for hydrophilic, hydrophobic and dimensional characteristics of sericins. Next, sericin was formulated in nanostructured drug delivery systems for targeting naturally-derived flavonoid to tissue-resident mesenchymal stem/stromal cells for regenerative purposes (**Aim 2**). Finally, the recovery of sericins from silk industrial wastewater by a tangential filtration was investigated (**Aim 3**). In fact, despite its high biological value, in the textile industry sericin represents a waste product, released in the wastewater with high environmental impact. The recovery of sericin by-products from the degumming stage can represent an important economic and social benefit for cleverly sustainably closing the circular economy loop.

Results

In the results section of the PhD thesis, three scientific papers are reported.

Paper 2 compared the effects of two different extraction methods on hydrophilic, hydrophobic sericin properties, and molecular weight profile. RP, HILIC, and SEC complementary chromatographic methods were used for the analytical characterization, while size distribution was determined by using the optimized SEC-MS chromatography to maximize both the dimensional selectivity and technique sensitivity. Also, sericins were evaluated in terms of *in vitro* biological activity (free radical scavenging, anti-tyrosinase, and anti-elastase) and cell metabolic activity by using MTT assay on human fibroblasts to confirm their cytocompatibility for cosmetic and biomedical purposes.

Once extracted and characterized, sericin is an optimal biomaterial for the formulation of drug delivery systems both as an excipient and active. In this regard, **Paper 3** overcome the physical-chemical instability of sericin in the aqueous solution by a self-assembly method to produce nanosized carriers. These nanosystems were employed for the slow-release of polyphenols to regenerate tissue-resident mesenchymal stem/stromal cells. Three polyphenols were loaded into nanoparticles: proanthocyanidins, epigallocatechin gallate, and quercetin with remarkable antioxidant and anti-inflammatory properties. Nanoparticles were fully characterized, their biological activity (antioxidant, anti-tyrosinase, and anti-elastase) was evaluated and the cytocompatibility and protection effect from hydrogen peroxide were performed on hMSCs.

Finally, **Paper 4** explained the possibility of recovering sericin from the wastewater of the silk textile industry. In detail, wastewater sericin was compared to standard degummed sericin after being subjected to different technological stabilization treatments: freeze-drying, spray-drying and sterilization. SDS-PAGE, SEM, DLS, FTIR, and DSC/TGA were used to determine the sericin quality; cytotoxicity and cytoprotective effect against oxidative stress were carried out on fibroblasts, while immunomodulatory capacity on stimulated human Peripheral Blood Mononuclear Cells. Finally, *in vitro* biological activity (free radical scavenging, anti-tyrosinase, and anti-elastase) was evaluated.



Chromatographic profiling of silk sericin for biomedical and cosmetic use by complementary hydrophilic, reversed phase and size exclusion chromatographic methods



Sara Tengattini, Giulia Orlandi, Sara Perteghella, Elia Bari, Marialaura Amadio, Enrica Calleri, Gabriella Massolini, Maria Luisa Torre, Caterina Temporini*

Abstract

Silk sericin (SS) is, together with silk fibroin (SF), one of the two proteins forming the silkworm cocoon. SS is ideal ingredient for cosmetic applications in the formulation of specific products for skin care and hair due to its peculiar physical-chemical composition. SS also showed a great potential in different pharmacological and biotechnological applications, as anticancer drug, anticoagulant, cell culture additive, wound healing agent and drug delivery carrier.

Reasons for SS use in biomedical applications derive from its physical-chemical composition. As a consequence, a detailed characterization of SS in terms of average molecular weight, molecular weight distribution and hydro/lipophilic character is crucial to properly address and assess its quality, cosmetic or pharmacological use.

In this study, the application of different and complementary chromatographic modes allows a detailed investigation of SS protein isolated from wastewater using two diverse extraction methods. Hydrophilic interaction liquid chromatography (HILIC using an AdvanceBio Glycan Map column) and reverse phase (RP using Symmetry300 C18 column) were applied to intact protein characterization to derive data on protein hydrophilicity and on hydrophobic components of the two SS preparations (SS#1 and SS#2). A higher hydrophilic character of SS#1 was observed by HILIC trace, coherently with the preparation method used, while no significant differences in hydrophobicity were detectable in the RPLC separations. Size distribution was also defined by using a SEC-UV-MS method (using TSKgel SuperSW2000 column) properly optimized to maximize both the size selectivity and the method sensitivity.

Taken together, the chromatographic data allowed to better characterize the SS samples obtained by different extraction methods, and the structural properties were correlated to their biological activities.

1. Introduction

Silk sericin (SS) and silk fibroin (SF) are the two major proteins present in the silk derived from *Bombyx mori*, fibroin is the core structural protein while sericin is the glue-like protein that holds fibroin fibers together. The raw silk is constituted by 75–80% w/w of FS and by 25-30% w/w of SS [1] [2]. SF is almost water-insoluble protein, consisting of layers of antiparallel β -sheets in the natural fibers [2], two non-polar amino acids, glycine and alanine, are the main components of the amino acid composition of SF (76%). The interesting mechanical properties of FS have been exploited in the fields of textiles, tissue engineering, drug delivery, imaging, and sensing for advanced applications [3-5]. Sericin is a globular water-soluble glycoprotein containing both random coil and β -sheet structures [1] and consists of 18 mainly polar amino acids (78%) with a molecular weight that ranges from 10-20 to 370-400 kDa [6]. Sericin is, therefore, a family of proteins with wide-ranging molecular weights distribution. In the production of SF for textile industry, it is necessary to remove SS using a degumming process, mainly based upon the water solubility of SS, to obtain shiny and soft handle fibres. Thus, SS represents a by-product of textile industry usually discharged in wastewater. Recently, it has been demonstrated that SS exhibits important biological activities (antioxidant, anti-bacterial, anti-cancer and anti-inflammatory) [7] as well as wound healing properties, suggesting that this protein can be successfully used for medical, biological and biotechnological applications [8, 9]. In addition, SS can be used as a vehicle for drug delivery due to its biodegradability and cell biocompatibility [2]. Thus, the recovery and recycling of SS by-products from degumming processes could be economically interesting [10].

The chemical composition of SS protein is slightly different depending on the silkworm variety (different strains of *B. mori*) and on the diverse degumming processes [11, 12], and it has been demonstrated that physical-chemical properties and molecular heterogeneity (change in amino acid composition and molecular weight) affect functional properties of SS [13-15].

The typical SS composition, reported in literature, consists of serine, glycine and aspartic acid, however other amino acids (i.e. glutamic acid, tryptophan and proline) can be present according to SS classification based on water solubility. Amino acid (AA) composition of SS has been investigated by high-performance liquid chromatography (HPLC) [16]. SS can be

also classified based on the molecular weight distribution [13]. The large range of molecular weights of sericin (10 to 400 kDa) is a consequence of the extraction conditions used (i.e. temperature, pH, processing time) which results in different denaturation/degradation degree, thus yielding diverse sized and heterogeneous products. During the extraction from cocoons, the thermal and chemical treatments seem to denature and/or to degrade the protein resulting in low molecular weight polypeptides. Low-molecular-weight SS is used in blends for cosmetics since it helps to enhance the elasticity of skin (anti-wrinkle and anti-aging effects) [7]. Sericin also enhances the light-screening effect of UV filters like triazines and cinnamic acid esters [14]. Concerning medical applications, high-molecular-weight SS has been proven to be more effective mainly as antioxidant agent, and studies of the macrophage response of silk protein concludes that sericin does not manifest inflammatory activity when present in soluble form [15].

Thus, a detailed characterization of SS in terms of average molecular weight, molecular weight distribution and hydro/lipophilic character is crucial to properly address and assess the quality of SS for biomedical applications.

The analytical characterization of SS from different degumming methods is mainly focussed on the definition of AA composition and molecular mass distribution. The reported analytical approach for AA quantification is RPLC-UV separation of amino acids released after extensive acidic treatment [1, 16] or by classic amino acid analyser [1, 17]. Sodium dodecyl sulphate-polyacrylamide gel electrophoresis (SDS-PAGE) [11, 18] and size exclusion chromatography (SEC)/gel permeation chromatography (GPC) [12, 19] are the most commonly used methods for dimensional characterization of SS extracts. To our best knowledge, only one paper reports a RPLC-UV separation of polypeptides obtained by acidic degumming using citric acid. The separation was performed on a C8 column with UV detection, and no additional characterization of eluting species was carried out. [20]. At present, no HILIC method for SS characterization has been reported.

In this study, we developed complementary chromatographic methods, namely reverse phase chromatography (RP), hydrophilic interaction chromatography (HILIC) and size exclusion chromatography (SEC), to compare SS samples obtained by two degumming processes: autoclave and sodium carbonate treatment. Moreover, the *in vitro* biological properties (antioxidant, anti-tyrosinase and anti-elastase) and cytocompatibility profile of SS samples were studied.

Given the structural complexity of SS, SEC revealed as the most informative method. A high-performance SEC column from Tosoh bioscience (TSKgel SuperSW2000) was considered to

derive average molecular weight and molecular weight distribution of SS samples obtained from different extraction strategies. For this purpose, a calibration curve with standard proteins was built and a detailed study on the relationships between mobile phase composition (i.e. pH, organic modifier, additives) and elution order of standard proteins was also carried out to demonstrate that the pH of mobile phase and the isoelectric point of the proteins must be carefully considered to guarantee a size-based separation. This is of utmost importance in case of unknown protein composition of a mixture, such as SS, in order to derive reliable information on size and size-distribution.

To gain a deeper characterization of SS samples resulting from different extraction procedures, a SEC MS-compatible method was developed for the first time. An optimization study of the method was carried out by using a design of experiment (DoE) approach to assess MS-compatible conditions and to maximize both the size selectivity and the method sensitivity. The two SS samples were also evaluated in terms of biological activity and some structure-activity relationships were observed.

2. Materials and methods

2.1 Reagents and Chemicals

Ammonium formate, ammonium acetate, trifluoroacetic acid (TFA), acetonitrile (ACN), methanol (MeOH), sodium carbonate, 2,2-diphenyl-1-picrylhydrazyl (DPPH), tyrosinase enzyme, L-tyrosine, elastase enzyme, N-Succinyl-Ala-Ala-Ala-p-Nitroanilide (AAAPVN), TRIS buffer and standard silk sericin (SS_{std}) were purchased from Sigma-Aldrich (Milan, Italy). Sodium hydroxide, potassium dihydrogen phosphate (KH₂PO₄), sodium sulphate (Na₂SO₄) were from Carlo Erba Reagenti (Milan, Italy). Natriumazide (NaN₃) Water was obtained from a Direct-Q™ system Millipore (Millipore, Milan, Italy). All the reagents were of analytical grade. Ponceau S staining solution was from Biotium (Fremont, CA).

2.2 Sericin preparation

Two SS samples extracted by two different degumming processes (autoclave and sodium carbonate treatment) were prepared starting from white *Bombyx mori* cocoons (Orgosolo strain). For autoclave water extraction a previously proposed method was used [7]; briefly, cocoons were cut in dime-sized pieces and added to deionized water solution (1 g cocoons / 40 mL water). After 1 hour of treatment at 120°C obtained solution was freeze-dried (8×10^{-1} mbar, -50 °C for 72 h; Modulyo® Edwards Freeze Dryer, Kingston, NY, USA). For the

second treatment an alkali-based degumming method was considered [17]: cut cocoons were added to sodium carbonate water solution (0.5% w/v) (1 g cocoons / 18 mL Na₂CO₃) and boiled for 30 min. After this time, obtained solution was dialysed in distilled water for 3 days (cellulose tube, 3-5 kDa MWCO); purified sericin solution was freeze-dried.

Both SS samples were preserved at -20 °C until further analysis. Lyophilized SS was dissolved in water at 2.5 mg/mL solutions before analysis.

2.3 SDS-PAGE

Proteins of SS#1 and SS#2 samples (250 µg) were separated on 10% SDS-polyacrylamide gel electrophoresis and transferred to a nitrocellulose membrane. The membrane was rinsed with distilled water and incubated in a Ponceau S staining solution [0.1% (w/v) Ponceau S dissolved in 5% (v/v) acetic acid] for 5 min at room temperature on an orbital shaker. After rinsing with distilled water to remove the background staining, the membrane image was captured by scanning.

2.4 Chromatographic systems

For chromatographic analysis, SS samples were solubilized in water to reach a final concentration of 2.5 mg/mL.

LC-UV separations were performed on an Agilent HPLC series 1100 system (Santa Clara, CA, USA), equipped with mobile phase online degasser, quaternary pump, autosampler, column thermostated compartment and diode array detector.

For LC-MS experiments, a Dionex Ultimate 3000 HPLC system (Thermo Fisher Scientific, Waltham, MA, USA) controlled by Chromeleon software (version 6.8) was connected to a linear trap quadrupole (LTQ) MS with an ESI source (Thermo Fisher Scientific, Waltham, MA, USA), controlled by Xcalibur software 1.4.

2.5 Chromatographic methods and conditions

2.5.1 RP-UV

The analytical column was a Symmetry300 C18 (2.1 x 100 mm, 3.5 µm 300 Å pore size). The mobile phase was composed of water (A) and ACN (B), both containing 0.1% TFA. Chromatographic conditions consisted of 5 min under isocratic conditions (5% B), then a linear gradient from 5% to 60% B in 20 min. The column temperature was maintained at 45

°C, the injection volume was 5 μL (SS 2.5 mg/mL in water). Elution was carried out at constant flow of 200 $\mu\text{L}/\text{min}$. UV adsorption was monitored at 280 nm.

2.5.2 HILIC-UV

The analytical column was an AdvanceBio Glycan Map (2.1 x 150 mm, 2.7 μm). The mobile phase was composed of ACN (A) and water (B), both containing 0.1% TFA. Chromatographic conditions consisted of linear gradient from 5% to 25% B in 15 min, from 25% to 80% B in the following 15 min. The column temperature was maintained at 50 °C, the injection volume was 5 μL (SS 1.25 mg/mL in 50/50 water/ACN). Elution was carried out at constant flow of 200 $\mu\text{L}/\text{min}$. UV adsorption was monitored at 280 nm.

2.5.3 SEC-UV

The analytical column was TSKgel SuperSW2000 (4.6 x 300 mm, 4 μm ID, 125 Å pore size). The standard mobile phase was Na_2SO_4 0.1 M, NaN_3 0.05% in 0.1M phosphate buffer; pH 6.7. The column temperature was maintained at 25 °C, the injection volume was 5 μL (SS 2.5 mg/mL in water). Elution was carried out at constant flow of 350 $\mu\text{L}/\text{min}$. UV adsorption was monitored at 280 nm.

2.6 Optimization of SEC-MS method

For the development of MS-compatible SEC method a full factorial (2^5) design was applied. Five experimental factors (x_1 : buffer composition, x_2 : buffer molarity, x_3 : organic solvent, x_4 : percentage of organic solvent and x_5 : percentage of TFA) were considered. The levels of factors x_1 – x_5 were selected on the basis of theoretical aspects. For each of 32 resulting mobile phases, retention time (rt) of SS_{std} , rt of SS#1, rt of SS#2, height of SS_{std} peak and area of SS_{std} peak were collected. DoE calculations were performed using R for Microsoft Windows, version 3.0.0, R Foundation for Statistical Computing. The R-based software has been developed by the Group of Chemometrics of the Italian Chemical Society [<http://gruppochemiometria.it>].

2.7 *In vitro* biological activities and cytocompatibility evaluation

2.7.1 ROS-Scavenging activity

To evaluate the antioxidant properties of SS samples we used the method proposed by [21], with some modifications. Each SS sample (concentrations 2.5, 5, 8 and 10 mg/mL) was added to DPPH methanolic solution (0.0056% w/v) in volume ratio 1:9 and incubated in the dark for 1 h; after this time, reaction mixture was centrifuge (3000 g, 5 min) and supernatant was spectrophotometrically analysed at 515 nm (Synergy HT, BioTek, Swindon, UK). Results are expressed as mean ROS-scavenging percentage activity:

$$\% \text{ activity} = [(A_{\text{ctr}} - A_{\text{samp}}) / A_{\text{ctr}}] * 100$$

Where A_{ctr} is the absorbance of negative control (reaction mixture without SS) and A_{sample} is the absorbance of considered sample subtracted of black value (reaction mixture without DPPH).

All analyses were performed in triplicate.

2.7.2 Anti-tyrosinase activity

The ability of SS to inhibit tyrosinase enzyme was evaluated using the protocol proposed by [17]. 12.5 μL of tyrosinase enzyme, solubilized in phosphate buffer solution (pH 6.8, concentration 500 IU/mL), was added to 50 μL of each SS sample (concentrations 2.5, 5, 8 and 10 mg/mL) and incubated for 10 min; after this time, 62.5 μL of L-tyrosine substrate (0.3 mg/mL) was added to the reaction mixture. The kinetic reaction between tyrosinase and L-tyrosine was monitored by spectrophotometric analysis (Synergy HT, BioTek) at 480 nm for a total time of 30 min (a measure every minute).

Results are expressed as mean anti-tyrosinase percentage activity:

$$\% \text{ activity} = [(A_{\text{ctr}} - A_{\text{samp}}) / A_{\text{ctr}}] * 100$$

Where A_{ctr} is the absorbance of negative control (reaction mixture without SS) and A_{sample} is the absorbance of considered sample subtracted of black value (reaction mixture without enzyme and substrate).

All analyses were performed in triplicate.

2.7.3 Anti-elastase activity

Anti-elastase properties of SS samples were determined using the method proposed by [22], partially modified. Porcine pancreatic elastase, solubilized in phosphate buffer (pH 6.8, concentration 500 IU/mL), was mixed and incubated for 20 min with each SS sample

(concentrations 2.5, 5, 8 and 10 mg/mL) (volume ratio 1:1); after the incubation time, the AAAPVN substrate was added. Spectrophotometric analysis (Synergy HT, BioTek) of final reaction mixture was performed at 410 nm for 35 min (measurements every minute).

Results are expressed as mean anti-elastase percentage activity:

$$\% \text{ activity} = [(A_{\text{ctr}} - A_{\text{samp}}) / A_{\text{ctr}}] * 100$$

Where A_{ctr} is the absorbance of negative control (reaction mixture without SS) and A_{sample} is the absorbance of considered sample subtracted of black value (reaction mixture without enzyme and substrate).

All analyses were performed in triplicate.

2.7.4 Cytocompatibility (MTT test)

Human fibroblasts were cultured in Dulbecco's Modified Eagle's Medium (DMEM) High Glucose with 10% fetal bovine serum, penicillin 100 U/mL, streptomycin 100 µg/mL, amphotericin 0.25 µg/mL, glutamine 4 mM and sodium pyruvate 1 mM.

Fibroblasts were seeded into 96-well plate (10 000 cells/cm²) and incubated (37 °C, 5% CO₂) with SS samples for 24 and 48 h. We solubilized SS samples in DMEM-HG and diluted to obtain 5 concentrations: 12, 120, 500, 1000 and 2500 µg/mL. At the end of incubation time, samples were removed, and cells were washed with PBS. 100 µl of 3-(4,5-dimethylthiazol-2-yl)-2,5-diphenyltetrazolium bromide (MTT) solution (0.5 mg/ml, Euroclone, Milan, Italy) were added to each well and incubated for three hours; after this time, MTT solution was removed and 100 µl of DMSO was added. The optical density of obtained solution was measured (Synergy HT) at 570 nm and 670 nm (reference wavelength). Untreated cells were considered as control (100 % metabolic activity). Cell metabolic activity (%) was calculated as follow: $100 \times (OD_{\text{sample}} / OD_{\text{ctr}})$. Each condition was tested in triplicate.

2.8 Statistical Analysis

Antioxidant, anti-tyrosinase and anti-elastase results were statistically analysed using a linear generalized Analysis of Variance model (ANOVA) while the Fisher's least significant difference (LSD) procedure was applied to evaluate the differences between means (STATGRAPHICS XVII; Statpoint Technologies, Inc., Warrenton, VA, USA). Degumming process and sample concentration were considered as fixed factors. ANOVA model was also used to analyse the cytocompatibility data.

The enzymatic kinetics of tyrosinase and elastase enzymes were elaborated using the Michaelis-Menten model $y = (V_{\max} \times x) / (K_m + x)$, where y is the absorbance at time x , K_m is the moment in which the activity is equal to half the maximum and V_{\max} is the maximum speed of the enzyme (Graph-Pad Prism software). For all the analyses, the statistical significance was set up at $p < 0.05$.

3. Results and Discussion

Data reported in literature support the view that SS has an inner, middle and outer layered structure with specific amino acid composition. The outer layer is reported as the most water soluble and is solubilized in 100°C boiling water for 2 h. The middle layer is soluble in water at 120 °C for 2 h; the inner layer can be solubilized in a 0.2% aqueous sodium carbonate solution after boiling for 0.5 h [1]. Based on these evidences it is now assumed that diverse preparation methods result in types of SS remarkably different in composition, heterogeneity, physical-chemical properties and, lately, bioactivities. SS characterization is commonly performed either by PAGE or by GPC/SEC, and a wide variety of molecular weight polypeptides have been estimated [16, 23].

In this study, two samples of SS were used, namely SS#1 and SS#2, produced by autoclave and sodium carbonate treatment, respectively. After a preliminary PAGE separation, for a more robust and reliable characterization of SS samples, different chromatographic methods and selectivity were explored to properly define the characteristics of each SS sample and correlate them to their biological activities.

3.1 RP and HILIC chromatographic profile

Silk protein samples obtained by two extraction methods were first analysed by SDS-PAGE (Figure 1_S). A unique, continuous band was observed for both the samples, revealing an extraordinary wide molecular mass distribution in both the SS, from about 30 to over 130 kDa, being a unique band eluting between those MW markers. No distinction of dominant bands was observed; thus, this analytical approach was considered not suitable for the discrimination of the considered samples based on their protein content and size distribution.

In order to obtain a representative fingerprint of the protein mixture contained in the two SS preparations, different and orthogonal chromatographic methods have been exploited. Given the AA composition of SS reported in literature, both polar and hydrophobic residues were expected to be present in all the proteoforms at a different extent based on the type of

preparation method used. For this reason, both HILIC and RPLC were considered. In addition, modern SEC was applied to derive size-distribution information.

Reverse phase separation resulted in a series of unresolved peaks eluting between 12 and 19 min in both samples (Figure 1 A). The slope of the gradient was assessed at 2.75% as no further chromatographic improvements came from its reduction. SS#1, prepared in autoclave, is expected to contain larger molecules coming from the most superficial layers of SS. These layers are more rich in hydrophilic residues: Ser is present at 28% in the outer, 25.57% in the middle, 13.32% in the inner layer, while lipophilic residues become more abundant in the inner layer rather than the surface (i.e. Leu and Ile increase from 1.21 to 4.06% and from 0.79 to 3.76%, respectively) [1]. On the contrary, smaller peptide units can be expected from the more drastic SS#2 preparation method (bicarbonate treatment), coming from all the layers of SS. Looking at the RP traces of the two preparations, however, it might be deduced that the sum of these two structural changes (hydrophobicity and size) results in a highly heterogeneous protein mixture with similar chromatographic elution in RP.

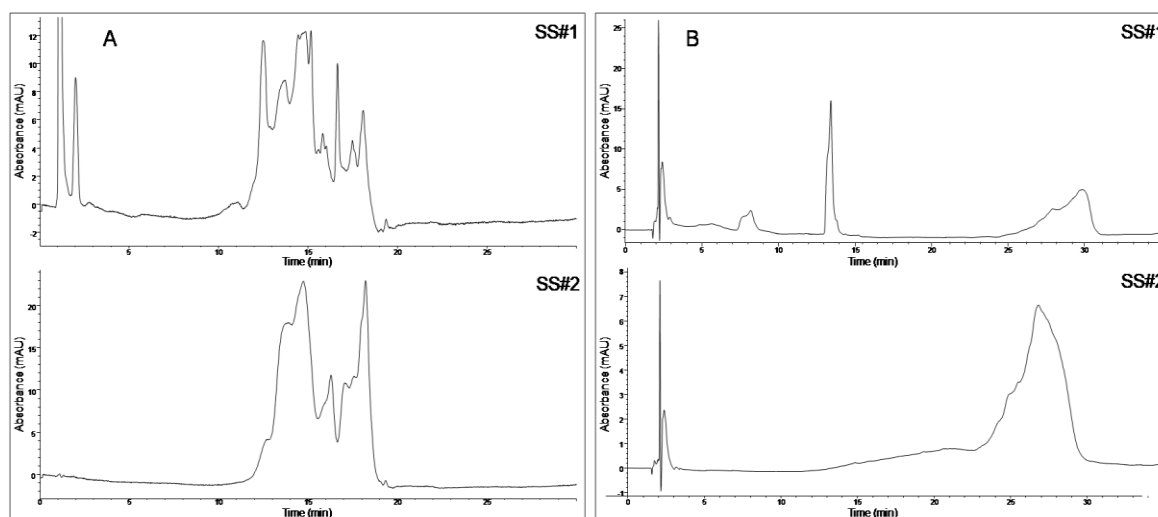


Figure 1: Chromatographic profile obtained with A) RP-UV separation and B) HILIC-UV separation of SS#1 and SS#2 samples

The same samples were then eluted on an HILIC stationary phase using an AdvanceBio Glycan Map column with high water percentages (up to 80%). In this condition a multiple and complex retention mechanism instead of pure hydrophilic partitioning can take place [24]. The chromatographic traces obtained with two-step gradient (from 5% to 25% B in 15 min, from 25% to 80% B in the following 15 min), revealed the presence of a dominant broad peak

eluting between 20 and 32 min, corresponding to SS (Figure 1 B). In SS#1, the apex of such broad peak elutes at 29.9 min, while in SS#2 a less retained peak (26.7 min) was observed. This evidence might suggest a higher hydrophilic character of SS#1 coherently with the preparation method. Interestingly, this latter sample presents an intense additional peak at 13.4 min, possibly corresponding to LMW compounds. These peaks were detected in the SS#1 sample only, thus might be characteristics of the preparation method.

3.2 SEC Separation

A conventional SEC-UV method was also applied and a TSKgel SuperSW2000 column was selected considering the type of sample to be analyzed and its expected MW range, as reported in the literature. A typical mobile phase (Na_2SO_4 0.1 M, NaN_3 0.05% in 0.1M phosphate buffer; pH 6.7) was used. The calibration curve was built using five standard proteins from 11 to 600 kDa, and a good linearity (R^2 0.9958) was obtained between LogMW and elution volume (Table 1_S, Figure 2_S). Retention time (rt) and peak width (W) are informative for sample average mass and MW distribution, respectively. The chromatograms obtained for both the preparations (Figure 2) are characterized by very large peaks as a confirmation of the huge heterogeneity of the samples. SS#1 is characterized by a mean MW_{calc} of 61 kDa, with a W of 8.1 min. One additional peak is evident at the VHMW, suggesting the presence of aggregates with an area % of 2.3, and one on the solvent front (rt 12.2 min) corresponding to the LMW components already detected in the HILIC trace. SS#2 is composed of lower molecular weight proteins, with a mean MW_{calc} of 11 kDa, and a less heterogeneous composition, being the W of 5.7 min. This sample denotes also a lower tendency to aggregate, as no additional peaks were observed corresponding to VHMW species. This result support the hypothesis that autoclave treatment is less drastic and produces SS with higher MW than sodium carbonate, characterized by a more heterogeneous size distribution and more prone to aggregate.

Since MS detection could allow to reach a deeper characterization of SS samples, a MS-compatible method was developed. The main issue in interfacing SEC with MS is due to the inherent incompatibility of the mobile phases containing high concentrations of non-volatile salts. The substitution of the traditional mobile phases with volatile ones at reduced ionic strength might, in turn, result in altered elution order of the proteins.

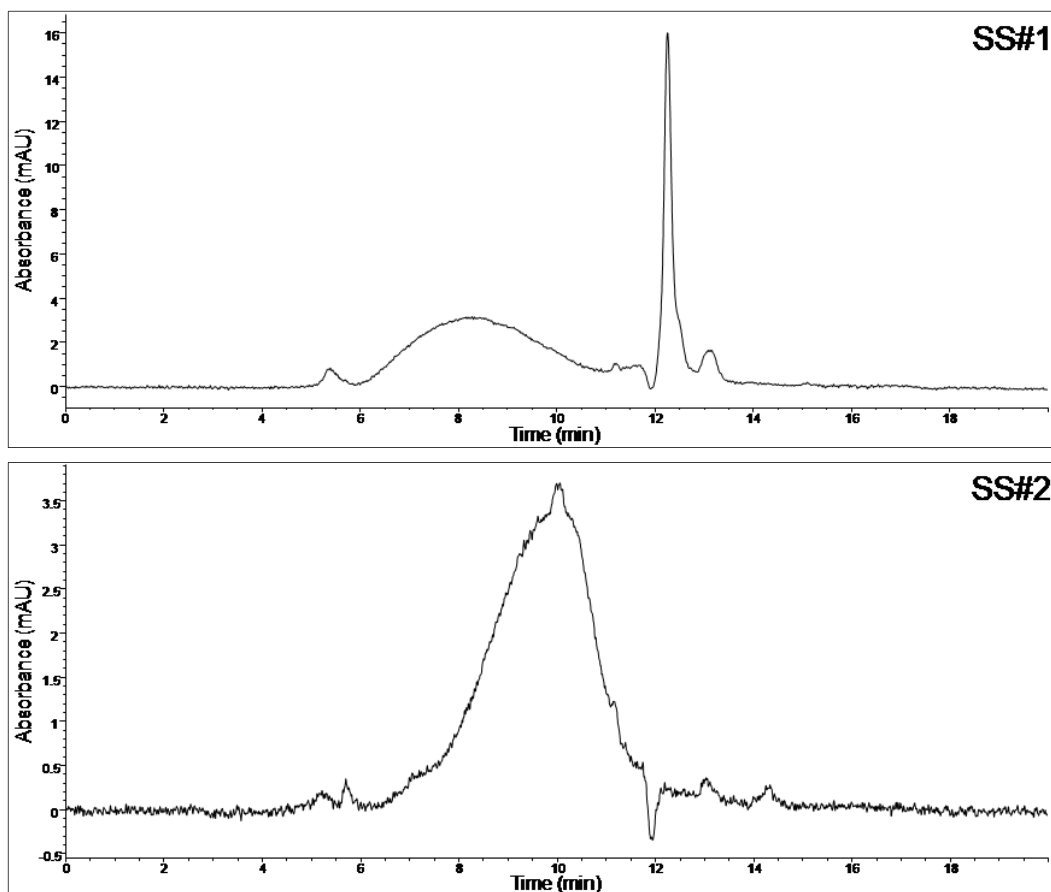


Figure 2: Chromatographic profiles obtained with SEC-UV methods for SS#1 and SS#2 samples

A SEC-MS method reported in literature, consisting of 100 mM ammonium acetate, pH 6.7, was considered as starting point [25]. To properly verify the correctness of size-based separation in these conditions, seven standard proteins were analysed (Table 1). Four out of the seven standards did not elute in accordance to their MW. This suggested us to more deeply check the protein behaviour also in the reference elution conditions (Na_2SO_4 0.1 M, NaN_3 0.05% in 0.1M phosphate buffer; pH 6.7). Ag85B and Tb10.4 proteins were analysed, and it turned out that also under standard conditions the correctness of elution order was not maintained for one of them.

These evidences can be ascribed to secondary ionic/hydrophobic interactions that might occur between proteins and stationary phase possibly affecting the size-based separation. Two principal type of ionic or electrostatic interactions can affect SEC: (i) ionic adsorption, when protein and chromatographic media have opposite charges, resulting in low sample recovery

and peak tailing; (ii) ion-exclusion, when stationary phase and analytes have the same charge, causing a repulsive exclusion of analytes from the pores, which results in an elution volume lower than expected based on the hydrodynamic radius of the analyte. Changes in ionic strength and pH of the mobile phase can reduce such electrostatic interactions while contemporarily enhancing hydrophobic ones. In this case, the addition of an organic modifier can be evaluated [26].

For a successful application of SEC to complex biomolecules mixtures aimed at guaranteeing a size-based elution order of unknown components, these parameters were considered. The effect of the buffer concentration was primarily studied by decreasing its value from 100 to 75 and 25 mM. No differences in the elution order of the seven standard proteins were observed (Table 1), only a slight reduction of the separation window (1.02; 1.09; 1.21 mL respectively). The effect of pH on elution order was also explored in detail and at pH 2.5 the correct elution order of the seven proteins was observed despite to the narrower separation window (0.93 mL, Table 1). This phenomenon can be ascribed to the role of protein isoelectric point in the formation of additional interactions with the stationary phase.

Similarly, also the effect of ACN on the elution order was studied (Table 1). The presence of ACN does not affect the elution order, while improving the peak shape of some critical proteins (i.e. Tb10.4). The separation window is slightly reduced (from 0.97 mL to 0.77 mL).

Protein	Characteristics			Phosphate buffer 0.1M, Na ₂ SO ₄ 0.1 M, pH 6.7	CH ₃ COONH ₄ pH 6.7			CH ₃ COONH ₄ 25 mM pH 6.7		CH ₃ COONH ₄ 25 mM pH 4.0		CH ₃ COONH ₄ 25 mM pH 2.5	
	PM (kDa)	pI	Gravy index		100	75	25	0% ACN	20% ACN	0% ACN	20% ACN	0% ACN	20% ACN
Thyreoglobulin	660	5.5	-0.257	Y	Y	Y	Y	Y	Y	N	Y	Y	
Rituximab	144	9.1	-0.048	Y	N	N	N	N	N	N	Y	Y	
BSA	67	5.6	-0.475	Y	Y	Y	Y	Y	Y	N	Y	Y	
Ag85B	30	4.9	-0.179	N	Y	Y	Y	Y	Y	Y	Y	Y	
β-lactoglobulin	18.4	5.2	-0.162	Y	Y	Y	Y	Y	Y	N	Y	Y	
Ribonuclease A	13.7	9.6	-0.663	Y	N	N	N	N	N	N	Y	Y	
TB10.4	11	4.6	-0.266	Y	N	N	N	N	Y	Y	Y	Y	

Table 1: Effect of mobile phase composition on the elution order of standard proteins (Y= in accordance with its MW; N= not in accordance with its MW)

Once assessed the conditions allowing the proper elution order of standard proteins, a two-level, five-factor full factorial design was used, focussed to maximize the selectivity and sensitivity of the MS-compatible method in the analysis of SS samples. A commercial SS was also used as a reference.

Five experimental factors were selected as influencing the chromatographic output, namely the buffer composition (x_1), the buffer molarity (x_2), the organic solvent (x_3), the percentage of organic solvent (x_4) and the percentage of the ion pairing reagent (x_5). The levels of factors x_1 – x_5 were selected on the basis of theoretical considerations. Variables and levels are reported in Table 2.

Variable		(-)	(+)	Validation
x_1	Buffer	Ammonium acetate	Ammonium formate	Ammonium formate
x_2	Buffer molarity (mM)	5	25	12.5
x_3	Organic solvent	ACN	MeOH	ACN
x_4	Organic solvent (%)	0	20	10
x_5	TFA (%)	0	0.1	0.05

Table 2: Variables and level selected for DoE experiments

The first considered responses were the retention times of SS_{std} (y_1), SS#2 (y_2) and SS#1 (y_3). Coefficients and significance obtained showed a very similar behaviour for SS_{std} and SS#2 (Figure 3A and 3C_S). In both cases a significant influence of x_1 and x_2 was observed, resulting in a shift to higher times by increasing the buffer molarity and by using formate buffer compared to acetate. This behaviour might be ascribed to the different buffering range of the two buffers. The other variables did not significantly affect their retention times. The analyses of SS#1 (Figure 3B_S) showed a lower influence of buffer molarity, while the effect of the type of buffer was comparable. Moreover, for this sample the presence of TFA as ion pairing reagent resulted in a decrease of retention times.

Based on this behaviour, the ability of the system to discriminate among the different samples was rationalized. For SS_{std} and SS#2 the Δ rts was not significantly improved by any condition. On the contrary, the different behaviour between SS_{std} and SS#1 allowed to derive

mobile phase conditions able to maximize the Δ rts (considered as response y_4 , Figure 3D_S). In particular, the higher buffer molarity and the presence of TFA resulted favourable. However, the coefficient of interaction x_2x_5 suggests that it is not convenient to keep both variables at high level.

The peak height (y_5) and peak area (y_6) of SS_{std} were also considered as responses, since they can be representative of method sensitivity and recovery, respectively.

In the case of SS_{std} peak height, all the parameters except for the type of buffer, showed to have an influence (Figure 3E_S). The presence of TFA and the buffer molarity are the most significant ones. Again, the interaction suggests selecting between high buffer molarity and TFA presence. Concerning SS_{std} peak area, all the five factors resulted highly significant (Figure 3F_S).

The computed rts and standard peak area values, obtained when x_2 , x_4 and x_5 were set at the centre value of the experimental domain, in presence of ammonium acetate and ACN (Table 2), agreed with the measured parameters. Differently, the predicted SS_{std} peak height was significantly lower compared to the experimental value, probably due to the non-linear effect of TFA concentration on peak efficiency inside the experimental domain.

According to the predicted interaction x_2x_5 , TFA percentage and buffer molarity should be set at opposite level. Considering the tendency of ammonium salts to induce the formation of adducts increasing the heterogeneity of the resulting MS spectra, buffer molarity was set at 5 mM and, consequently TFA was adjusted at 0.1%. Ammonium acetate and ACN were selected as they demonstrated to improve peak area, and ACN percentage was set at 20% as it can positively influence MS signal.

Marker standards were analysed with the optimized mobile phase allowing to confirm the correct elution order and deduce the linear correlation between elution volume and LogMW ($y = 0.6588x + 9.616$, $R^2 = 0.9116$).

The method was applied to SEC-UV-MS analysis of SS#1 and SS#2. The resulting UV chromatograms are reported in Figure 3.

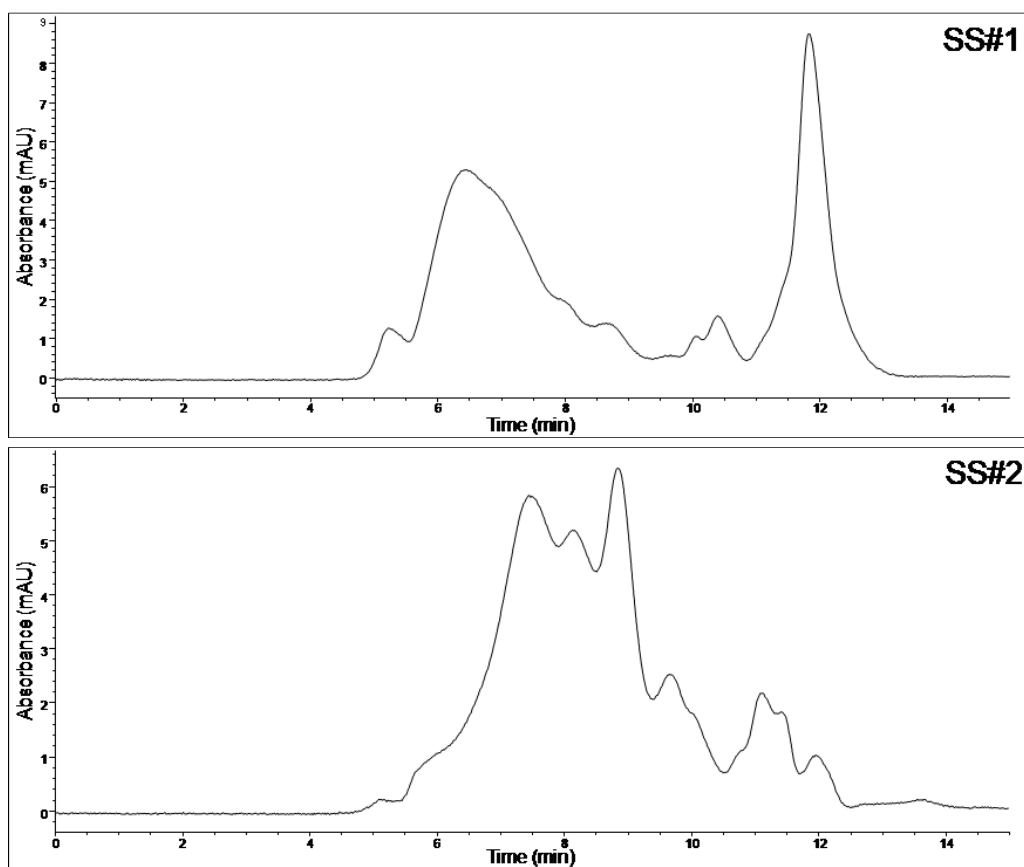


Figure 3: Chromatographic profiles obtained with MS-compatible SEC-UV methods for SS#1 and SS#2 samples

A mean MW_{calc} of 63 kDa for SS#1 and 14 kDa for SS#2 was found. These data are closely in agreement with the results obtained by applying the standard reference mobile phase, and might find correlation with the SDS-PAGE results reported in Figure 1_S. The huge heterogeneity of the proteoforms present in both the samples resulted in too much overlap for ions observed in the lower m/z portion of the ESI spectra where multiply charged ions appear, hence, average masses were difficult to extract. Instead, representative MS spectra were acquired for low molecular weight species, that are known to significantly contribute to the biological activity of SS, allowing to highlight differences in the composition of the two samples.

In the elution range between 8.2 and 12.8 min, a total of 18 ions were detected with a MW ranging from 670 to 2766 Da (Table 2_S), four of which were in common between the two samples. The lower molecular weight species were observed predominantly in SS#1 and might correspond to polyphenols and flavonoids typically preserved with the water-based extraction method. Conversely, SS#2 sample is mainly characterized by species with masses

over 1000 Da, which might correspond to peptides deriving from the more extensive hydrolytic treatment.

3.3 Biological activity of SS

ROS-scavenging ability of SS samples was studied by DPPH method. ANOVA analysis of obtained results demonstrated that both degumming process and sample concentration were significant ($p < 0.001$). Using the water-based autoclave degumming process (SS#1) at the highest tested concentration (10 mg/mL) a significant antioxidant activity of $40.5 \pm 5.13\%$ was obtained (Figure 4A). Also, SS#2 showed a moderate activity, corresponding to 20%. For both samples a dose dependent increase of antioxidant properties was observed, leading to expect a further increase of this activity in more concentrated preparations (i.e. by adding stabilizing agents).

Regarding the SS ability to inhibit tyrosinase enzyme, the sodium carbonate treatment allowed to obtain a SS sample almost ineffective (Figure 4B, red line) with a mean activity lower to 2% at all considered concentrations, while the water-based extraction method preserved the anti-tyrosinase properties of SS. Overall, a mean inhibitory activity in the range of 10-32% with a dose-dependent trend (Figure 4B, blue line) was observed for SS#1. The Michaelis-Menten model allowed us to elaborate the tyrosinase kinetic by the evaluation of K_m and V_{max} data.

In Table 3 the kinetic parameters of both SS samples at the highest tested concentration (10 mg/mL) are reported. Both SS samples showed no differences in terms of K_m values with respect to the free enzyme (negative control mixture). On the other side, the autoclave-extracted sample presented a significant decrease of V_{max} value, as demonstrated by the absence of overlap between the confidence intervals of treatment group and negative control (Table 3). According to the theory [27] this behaviour allows to hypothesize that SS obtained by water-based degumming process acts as a competitive inhibitor.

The SS composition is the key point of its anti-oxidant and anti-tyrosinase activities; in particular, it has been demonstrated that both biological properties are related to the amino acid composition (in particular to the presence of hydroxyl groups) and to the polyphenols and flavonoids content [7, 28, 29]. The autoclave treatment allows to solubilize mainly the external layer of SS, the one with the highest polar amino acids content, supporting its activity.

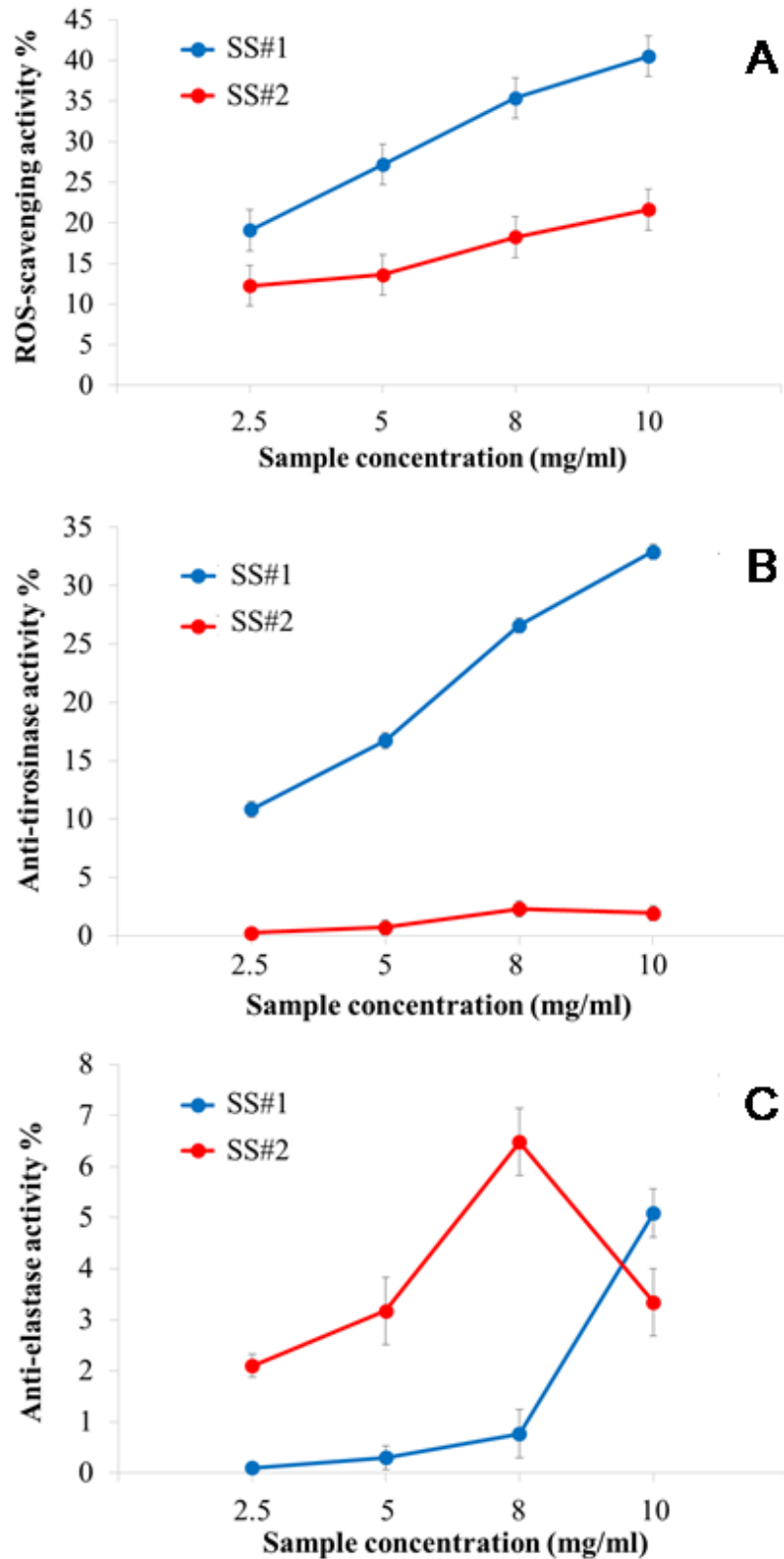


Figure 4: ROS-scavenging activity (A), anti-tyrosinase (B) and anti-elastase (C) activity percentage of SS obtained by two different degumming methods: water (blue line) and Na_2CO_3 (red line) treatment. Results are reported as mean values and least significant difference (LSD) intervals, ANOVA. The overlap of two LSD intervals graphically indicate the absence of significant differences ($p > 0.05$)

	CTR-	Arbutin	Water	Na₂CO₃
V_{max} ± St.Err	1.659 ± 0.0292	2.819 ± 0.5164	1.139 ± 0.0481	1.682 ± 0.0413
K_m ± St.Err	29.140 ± 0.9118	168.4 ± 35.57	33.73 ± 2.396	30.83 ± 1.315
95% CI V_{max}	1.604 to 1.718	2.057 to 4.536	1.048 to 1.250	1.604 to 1.770
95% CI K_m	27.44 to 30.98	116.0 to 286.9	29.21 to 39.27	28.32 to 33.64

Table 3: Michaelis-Menten model results reported in terms of V_{max} and K_m (mean values ± standard error, and 95% confidence intervals) for negative control (enzyme + substrate), positive control (enzyme + substrate + arbutin) and treatment group (enzyme + substrate + SS samples at the concentration 10 mg/mL)

The alkali treatment, being more drastic, induces the hydrolysis of more internal layers resulting in a mix of polar and hydrophobic polypeptide chains, coherently expressing less intense antioxidant and anti-tyrosinase activities.

The anti-elastase properties of both tested SSs resulted as lower than 8% at all considered concentration (Figure 4C). Despite the poor inhibitory activity, a different trend with respect to the ROS- scavenging and anti-tyrosinase properties was observed; in fact, SS isolated by the sodium carbonate treatment presented a higher mean inhibitory activity if compared to the autoclave-extracted protein. Literature data support the evidence that to enhance elastase inhibition hydrophobic interactions with enzymatic catalytic site are necessary which induce the elastase conformational change [30]. The obtained results (Figure 4C) are in accordance with the structural features of the SS samples: the lower content of non-polar amino acids, such as proline, phenylalanine, and valine, could explain the low inhibitory activity of SS#1, while in SS#2 the presence of smaller peptides with and overall increased hydrophobicity confers to this preparation a slightly improved anti-elastase activity.

Also the cytocompatibility of SS samples was investigated. Human fibroblasts cell metabolic activity was higher than 90% at all considered concentrations (0.012-2.5 mg/mL) in both the samples. Despite that, the ANOVA analysis showed a significant effect of degumming process ($p < 0.001$) and, in particular, water-extracted sericin resulted as higher cytocompatible sample with a metabolic activity % higher than 100% (with respect to the negative control, untreated cells). SS extracted by sodium carbonate treatment showed no cytotoxic effect, but significantly reduced the cell metabolic activity (88.635 ± 6.4300 and 90.324 ± 5.5408 for 24 and 48 h of treatment, respectively; mean values ± standard deviation) (Figure 4_S).

4. Conclusions

Sericin is a family of proteins highly heterogeneous in molecular weight distribution and amino acid composition obtained by the hydrolysis of the silk cocoons. Depending on the degumming process used, different hydrolysis degree can be obtained resulting in larger/external or smaller/internal polypeptide mixtures also diverse in amino acid composition.

In this paper SS obtained by different degumming methods has been analyzed using three analytical approaches, RP, HILIC and SEC, to obtain a chromatographic fingerprint representative for its hydrophilic, hydrophobic and size characteristics.

A detailed study was also carried out to optimize size exclusion chromatography for MS-coupling and to assess the appropriate size-based discrimination mechanism. The optimized SEC-MS method allowed to properly define the size distribution of SS obtained by different degumming methods and to profile the low molecular weight components.

Taken together, the chromatographic results suggested a close relationship between SS average molecular weight and molecular weight distribution, and the hydrophilic/hydrophobic character. The extraction with water in autoclave results in large proteoforms with a mean MW of around 60 kDa, with a very wide size distribution, coherent with a less exhaustive hydrolysis. The most superficial layers of sericin are released using this preparation method, which can be confirmed by their enhanced hydrophilic character in the HILIC trace. Conversely, the treatment with bicarbonate that is known to be more drastic, results in lower MW protein mixture (mean MW around 10 kDa), less heterogeneous in size and composed of both polar and hydrophobic components coming from all the layers of sericin as observed in the RP and HILIC traces.

The samples tested for their antioxidant, anti-tyrosinase and anti-elastase properties showed a different behaviour which was in accordance with the structural features derived by the chromatographic characterization. Hydrophilicity enhances the antioxidant and anti-tyrosinase (with a competitive mechanism) activities, which are maximized in the water-soluble SS sample (SS#1). These properties are still present, even if at a lower extent, in the SS prepared by bicarbonate treatment, where also an anti-elastase activity was observed, probably favoured by the presence of hydrophobic residues from the inner layers.

The proposed analytical method to define the quality characteristics of SS might support the preparation of SS samples with higher size homogeneity and optimized biological activities.

5. Author Statement

Sara Tengattini: Investigation (Analytical); Writing Giulia Orlandi: Investigation (Technological, SS preparation); Sara Perteghella: Investigation (Technological, SS preparation and activity evaluation); Writing Elia Bari: Investigation (SS activity evaluation); Marialaura Amadio: Investigation (SDS-PAGE); Enrica Calleri: Conceptualization, Writing (Original and Review); Gabriella Massolini: Supervision (Analytical); Maria Luisa Torre: Supervision (Technological), Project administration; Caterina Temporini: Conceptualization, Supervision, Project administration

6. Declaration of Competing Interest

The authors declare no conflict of interest.

References

- [1] T.T. Cao, Y.Q. Zhang, Processing and characterization of silk sericin from *Bombyx mori* and its application in biomaterials and biomedicines, *Materials Science & Engineering C-Materials for Biological Applications* 61 (2016) 940-952.
- [2] L.D. Koh, Y. Cheng, C.P. Teng, Y.W. Khin, X.J. Loh, S.Y. Tee, M. Low, E.Y. Ye, H.D. Yu, Y.W. Zhang, M.Y. Han, Structures, mechanical properties and applications of silk fibroin materials, *Progress in Polymer Science* 46 (2015) 86-110.
- [3] T. Chlapanidas, M.C. Tosca, S. Faragò, S. Perteghella, M. Galuzzi, G. Luccioni, B. Antonioli, F. Ciancio, V. Rapisarda, D. Vigo, M. Marazzi, M. Faustini, M.L. Torre, Formulation and characterization of silk fibroin films as a scaffold for adipose-derived stem cells in skin tissue engineering, *International Journal of Immunopathology and Pharmacology* 26 (2013) 43-49.
- [4] S. Farago, G. Luccioni, S. Perteghella, B. Vigani, G. Tripodo, M. Sorrenti, L. Catenacci, A. Boschi, M. Faustini, D. Vigo, T. Chlapanidas, M. Marazzi, M.L. Torre, A dry powder formulation from silk fibroin microspheres as a topical auto-gelling device, *Pharmaceutical Development and Technology* 21(4) (2016) 453-462.
- [5] S. Perteghella, B. Crivelli, L. Catenacci, M. Sorrenti, G. Bruni, V. Necchi, B. Vigani, M. Sorlini, M.L. Torre, T. Chlapanidas, Stem cell-extracellular vesicles as drug delivery systems: New frontiers for silk/curcumin nanoparticles, *International Journal of Pharmaceutics* 520(1-2) (2017) 86-97.

- [6] L.K.H. Rocha, L.I.L. Favaro, A.C. Rios, E.C. Silva, W.F. Silva, T.P. Stigliani, M. Gunger, R. Lima, J.M. Oliveira, N. Aranha, M. Tubino, M. Vila, V.M. Balcao, Sericin from *Bombyx mori* cocoons, Part I: Extraction and physicochemical-biological characterization for biopharmaceutical applications, *Process Biochemistry* 61 (2017) 163-177.
- [7] T. Chlapanidas, S. Farago, G. Lucconi, S. Perteghella, M. Galuzzi, M. Mantelli, M.A. Avanzini, M.C. Tosca, M. Marazzi, D. Vigo, M.L. Torre, M. Faustini, Sericins exhibit ROS-scavenging, anti-tyrosinase, anti-elastase, and in vitro immunomodulatory activities, *International Journal of Biological Macromolecules* 58 (2013) 47-56.
- [8] E. Bari, S. Perteghella, S. Farago, M.L. Torre, Association of silk sericin and platelet lysate: Premises for the formulation of wound healing active medications, *International Journal of Biological Macromolecules* 119 (2018) 37-47.
- [9] E. Bari, S. Perteghella, G. Marrubini, M. Sorrenti, L. Catenacci, G. Tripodo, M. Mastrogiacomo, D. Mandracchia, A. Trapani, S. Farago, P. Gaetani, M.L. Torre, In vitro efficacy of silk sericin microparticles and platelet lysate for intervertebral disk regeneration, *International Journal of Biological Macromolecules* 118 (2018) 792-799.
- [10] P. Aramwit, T. Siritientong, T. Srichana, Potential applications of silk sericin, a natural protein from textile industry by-products, *Waste Management & Research* 30(3) (2012) 217-224.
- [11] T.V. Chirila, S. Suzuki, N.C. McKirdy, Further development of silk sericin as a biomaterial: comparative investigation of the procedures for its isolation from *Bombyx mori* silk cocoons, *Progress in Biomaterials* 5(2) (2016) 135-145.
- [12] T. Siritientong, W. Bonani, A. Motta, C. Migliaresi, P. Aramwit, The effects of *Bombyx mori* silk strain and extraction time on the molecular and biological characteristics of sericin, *Bioscience Biotechnology and Biochemistry* 80(2) (2016) 241-249.
- [13] Y. Takasu, H. Yamada, K. Tsubouchi, Isolation of three main sericin components from the cocoon of the silkworm, *Bombyx mori*, *Bioscience Biotechnology and Biochemistry* 66(12) (2002) 2715-2718.
- [14] R. Dash, M. Mandal, S.K. Ghosh, S.C. Kundu, Silk sericin protein of tropical tasar silkworm inhibits UVB-induced apoptosis in human skin keratinocytes, *Molecular and Cellular Biochemistry* 311(1-2) (2008) 111-119.
- [15] M. Giovanni, J.Q. Yue, L.F. Zhang, J.P. Xie, C.N. Ong, D.T. Leong, Pro-inflammatory responses of RAW264.7 macrophages when treated with ultralow concentrations of silver, titanium dioxide, and zinc oxide nanoparticles, *Journal of Hazardous Materials* 297 (2015) 146-152.

- [16] J.H. Wu, Z. Wang, S.Y. Xu, Preparation and characterization of sericin powder extracted from silk industry wastewater, *Food Chemistry* 103(4) (2007) 1255-1262.
- [17] P. Aramwit, S. Damrongsakkul, S. Kanokpanont, T. Srichana, Properties and antityrosinase activity of sericin from various extraction methods, *Biotechnology and Applied Biochemistry* 55 (2010) 91-98.
- [18] P. Aramwit, S. Kanokpanont, T. Nakpheng, T. Srichana, The Effect of Sericin from Various Extraction Methods on Cell Viability and Collagen Production, *International Journal of Molecular Sciences* 11(5) (2010) 2200-2211.
- [19] T.L. da Silva, A.C. da Silva, M. Ribani, M.G.A. Vieira, M.L. Gimenes, M.G.C. da Silva, Evaluation of Molecular Weight Distribution of Sericin in Solutions Concentrated via Precipitation by Ethanol and Precipitation by Freezing/Thawing, *Ibic2014: 4th International Conference on Industrial Biotechnology* 38 (2014) 103-108.
- [20] A. Kurioka, F. Kurioka, M. Yamazaki, Characterization of sericin powder prepared from citric acid-degraded sericin polypeptides of the silkworm, *Bombyx mori*, *Bioscience Biotechnology and Biochemistry* 68(4) (2004) 774-780.
- [21] J. Fan, L. Wu, L. Chen, X. Mao, F. Ren, Antioxidant activities of silk sericin from silkworm *Bombyx mori*, *Journal of Food Biochemistry* 33 (2009) 74-88.
- [22] K.A. Nam, S.G. You, S.M. Kim, Molecular and physical characteristics of squid (*Todarodes pacificus*) skin collagens and biological properties of their enzymatic hydrolysates, *Journal of Food Science* 73(4) (2008) C249-C255.
- [23] D. Gupta, A. Agrawal, A. Rangi, Extraction and characterization of silk sericin, *Indian Journal of Fibre & Textile Research* 39(4) (2014) 364-372.
- [24] M. Dembek, S. Bocian, Pure water as a mobile phase in liquid chromatography techniques, *Trac-Trends in Analytical Chemistry* 123 (2020).
- [25] A. Goyon, V. D'Atri, O. Colas, S. Fekete, A. Beck, D. Guillarme, Characterization of 30 therapeutic antibodies and related products by size exclusion chromatography: Feasibility assessment for future mass spectrometry hyphenation, *Journal of Chromatography B-Analytical Technologies in the Biomedical and Life Sciences* 1065 (2017) 35-43.
- [26] E.S.P. Bouvier, S.M. Koza, Advances in size-exclusion separations of proteins and polymers by UHPLC, *Trac-Trends in Analytical Chemistry* 63 (2014) 85-94.
- [27] S. Zolghadri, A. Bahrami, M.T.H. Khan, J. Munoz-Munoz, F. Garcia-Molina, F. Garcia-Canovas, A.A. Saboury, A comprehensive review on tyrosinase inhibitors, *Journal of Enzyme Inhibition and Medicinal Chemistry* 34(1) (2019) 279-309.

- [28] J.P. Kumar, B.B. Mandal, The inhibitory effect of silk sericin against ultraviolet-induced melanogenesis and its potential use in cosmeceutics as an anti-hyperpigmentation compound, *Photochemical & Photobiological Sciences* 18(10) (2019) 2497-2508.
- [29] I. Chiochio, M. Mandrone, C. Sanna, A. Maxia, M. Tacchini, F. Poli, Screening of a hundred plant extracts as tyrosinase and elastase inhibitors, two enzymatic targets of cosmetic interest, *Industrial Crops and Products* 122 (2018) 498-505.
- [30] Y.H. Hong, E.Y. Jung, D.O. Noh, H.J. Suh, Physiological effects of formulation containing tannase-converted green tea extract on skin care: physical stability, collagenase, elastase, and tyrosinase activities, *Integrative Medicine Research* 3(1) (2014).

SUPPLEMENTARY MATERIAL

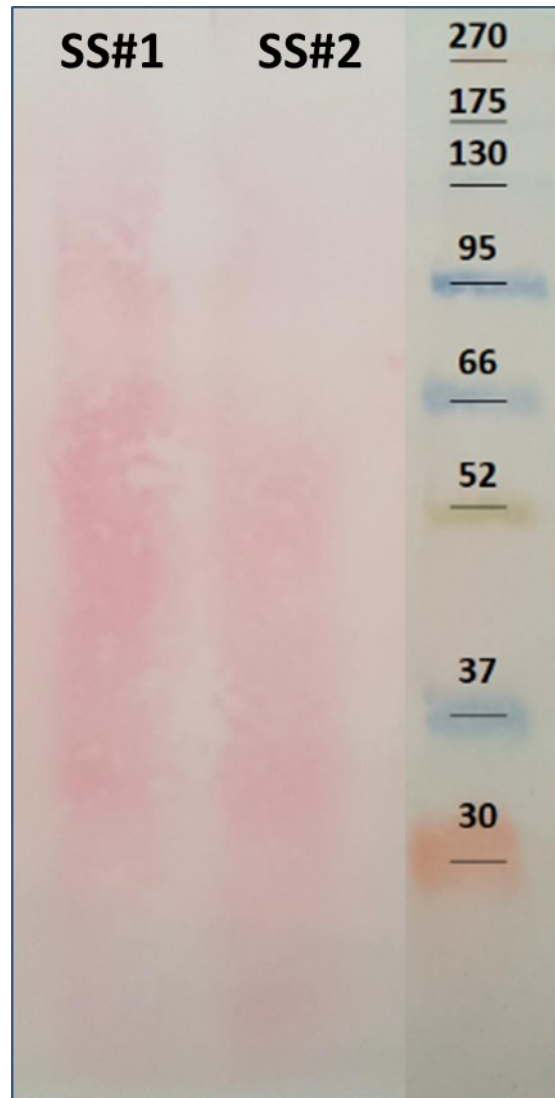


Figure 1_S: Photograph of the transfer membrane containing SS#1, SS#2 and coloured molecular weight marker (in lane 1, 2, and 3, respectively)

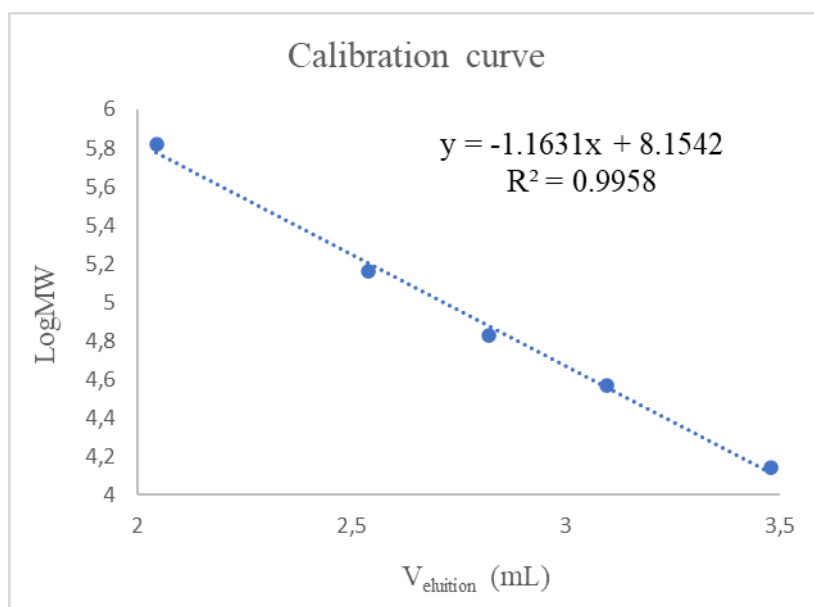


Figure 2_S: Calibration curve derived from the analysis of five protein standards. Column: TSKgel SuperSW2000; mobile phase: Na₂SO₄ 0.1 M, NaN₃ 0.05% in 0.1 M phosphate buffer; pH 6.7. For further details see experimental section

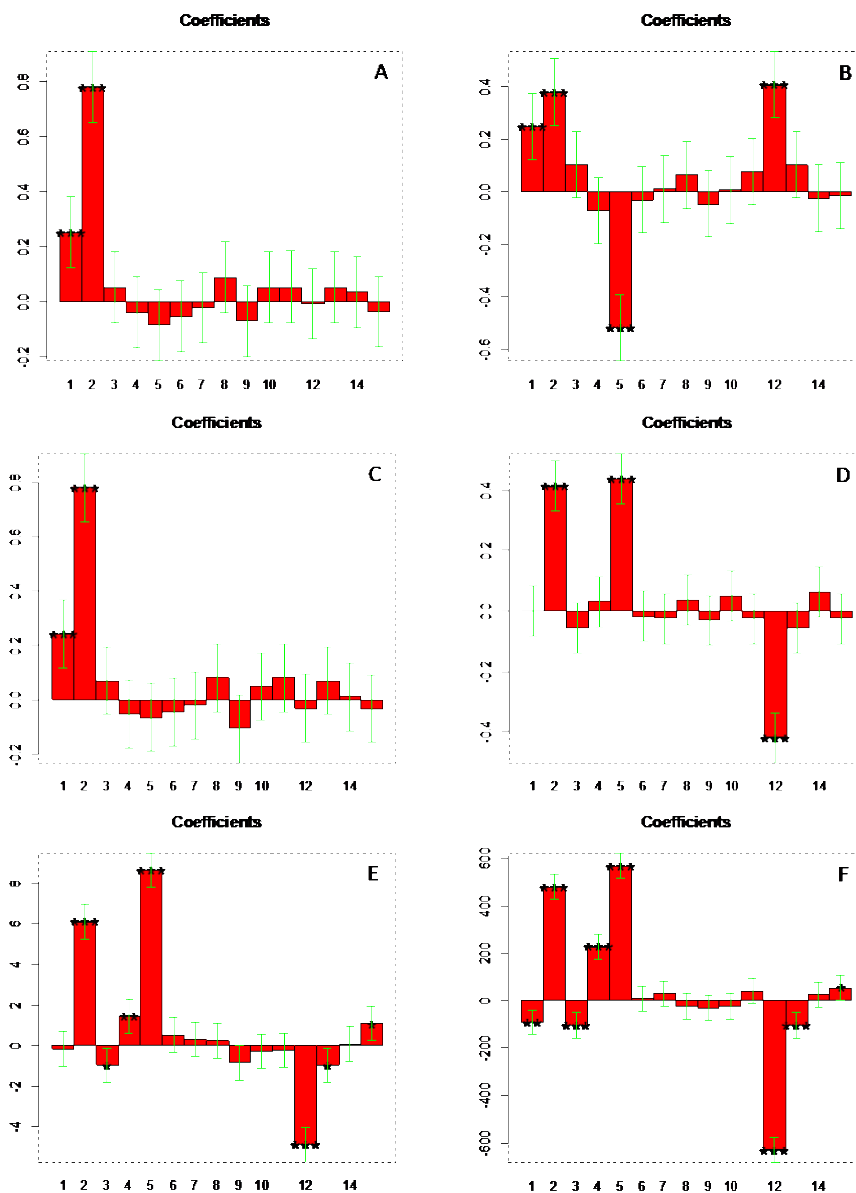


Figure 3_S: Coefficients and significance obtained for (A) y_1 , (B) y_2 , (C) y_3 , (D) y_4 , (E) y_5 , (F) y_6 . The numbers on the x-axis refer to the coefficients of the terms of the model ($Y = b_0 + b_1 \cdot X_1 + b_2 \cdot X_2 + b_3 \cdot X_3 + b_4 \cdot X_4 + b_5 \cdot X_5 + b_6 \cdot X_1X_2 + b_7 \cdot X_1X_3 + b_8 \cdot X_1X_4 + b_9 \cdot X_1X_5 + b_{10} \cdot X_2X_3 + b_{11} \cdot X_2X_4 + b_{12} \cdot X_2X_5 + b_{13} \cdot X_3X_4 + b_{14} \cdot X_3X_5 + b_{15} \cdot X_4X_5$). The height of the boxes (y-axis) represents the value of each coefficient. The whiskers represent the confidence interval computed for each coefficient, and the stars on the boxes refer to the p-value for each coefficient following the notation of * for $p \leq 0.05$, ** $p \leq 0.01$, *** $p \leq 0.001$

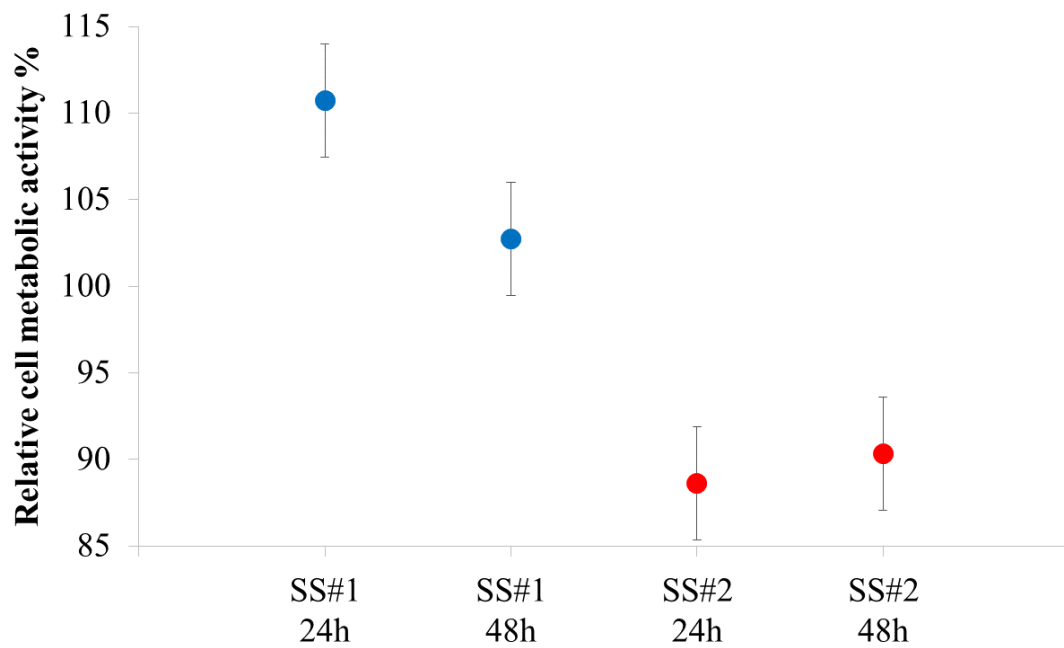


Figure 4_S: Relative cell metabolic activity % of human fibroblasts after the treatment with SS for 24 and 48 hours. Results are reported as mean values (considering all tested concentrations) and least significant difference (LSD) intervals, ANOVA. The overlap of two LSD intervals graphically indicate the absence of significant differences ($p > 0.05$)

Protein	t_R ± DS (min)	V_{eluit} ± DS (mL)	MW (kDa)	LogMW
Thyroglobulin	5.843 ± 0.001	2.045 ± 0.000	660.0	5.820
Rituximab	7.259 ± 0.001	2.541 ± 0.000	144.0	5.158
Bovine serum albumin	8.063 ± 0.007	2.822 ± 0.002	67.0	4.826
β-lactoglobulin	8.849 ± 0.001	3.097 ± 0.000	36.8*	4.566
Ribonuclease A	9.941 ± 0.003	3.479 ± 0.001	13.7	4.137

DS= standard deviation.

*molecular weight is 18400 Da but at the pH of the mobile phase it exists in dimeric form in solution.

Table 1_S: Data obtained from the analysis of five protein standards. Column: TSKgel SuperSW2000; mobile phase: Na₂SO₄ 0.1 M, NaN₃ 0.05% in 0.1M phosphate buffer; pH 6.7. For further details see experimental section







#	m/z	Charge	MW (Da)	SS#1	SS#2
1	671.17	1	670.17	X	
2	679.67	1	678.67	X	
3	696.25	1	695.25	X	
4	696.50	1	695.50	X	
5	697.67	1	696.67	X	
6	740.50	1	739.50	X	
7	791.08	1	790.08		X
8	807.08	1	806.08	X	X
9	826.17	1	825.17	X	X
10	869.50	1	868.50		X
11	1083.58	1	1082.58		X
12	1157.42	1	1156.42		X
13	713.00	2	1424.00		X
14	735.50	2	1469.00	X	X
15	1878.33	1	1877.33		X
16	1187.17	2	2372.34	X	
17	1187.17	2	2372.34		X
18	1384.33	2	2766.66	X	X

Table 2_S: List of ions detected by the SEC-MS analysis of SS#1 and SS#2, in the elution window 8.2-12.8 min



Article

Polyphenols-Loaded Sericin Self-Assembling Nanoparticles: A Slow-Release for Regeneration by Tissue-Resident Mesenchymal Stem/Stromal Cells

Giulia Orlandi ^{1,†}, Elia Bari ^{1,†}, Laura Catenacci ¹, Milena Sorrenti ¹, Lorena Segale ², Silvio Faragò ³, Marzio Sorlini ^{4,5}, Carla Renata Arciola ^{6,7}, Maria Luisa Torre ^{1,5,*} and Sara Perteghella ^{1,5}

Abstract: Mesenchymal stem/stromal cells (MSCs) are a therapeutic target to promote tissue regeneration, mainly when oxidative stress-mediated damage is involved in disease pathogenesis. Here, slow-release silk sericin nanoparticles (SNPs) loaded with natural antioxidant polyphenols were developed to sustain regeneration by tissue-resident MSCs. SNPs were prepared by exploiting a self-assembly method with poloxamer and were loaded with proanthocyanidins (P), quercetin (Q) or epigallocatechin gallate (E). SNPs, with a diameter less than 150 nm, were able to encapsulate both hydrophilic (P and E) and hydrophobic (Q) drugs. A slow and controlled release was obtained from SNPs for all the actives in PBS, while in EtOH, Q and E showed a burst release but P did not. Kinetic models revealed lower diffusion of P than other biomolecules, probably due to the higher steric hindrance of P. The *in vitro* anti-oxidant, anti-elastase and anti-tyrosinase properties of SNPs were assessed: loading the P and E into SNPs preserved the *in vitro* biological activities whereas for Q, the anti-elastase activity was strongly improved. Moreover, all formulations promoted MSC metabolic activity over 72 h. Finally, SNPs exhibited a strong ability to protect MSCs from oxidative stress, which supports their potential use for regenerative purposes mediated by tissue-resident MSCs.

Keywords: silk-sericin nanoparticles; proanthocyanidins; quercetin; epigallocatechin gallate; tissue regeneration; mesenchymal stem/stromal cells

1. Introduction

The potential use of mesenchymal stem/stromal cells (MSCs) in tissue regeneration is based on their ability to produce a large variety of bioactive trophic factors that stimulate neighboring parenchymal cells to repair damaged tissues [1] [2] [3]. Therefore, MSCs are now considered as a therapeutic target to promote healing in many chronic and acute degenerative diseases, particularly when oxidative stress damage is involved in the pathogenic mechanisms. In fact, oxidative stress has detrimental effects on the longevity and metabolic functions of MSCs. It inhibits proliferation, increases senescence and ageing by down-regulating autophagy [4], and it inhibits MSC immunomodulation [2, 5]. Flavonoids, which have strong antioxidant activity, could effectively protect MSCs from oxidative damage and, consequently, from senescence and ageing.

In this work, silk sericin nanoparticles (SNPs) were developed to target the delivery of proanthocyanidins (P), quercetin (Q) and epigallocatechin gallate (E) to MSCs. P, Q and E are flavonoids that belong to different subclasses. P are condensed tannins, which are abundantly present in flowers, fruits and seeds of various plants, where they act as a defense mechanism against pathogens and predators. Q is a flavanol, and it is primarily found in fruits and vegetables, while E is categorized as catechin and it is abundantly present in tea. Multiple biological effects have been attributed to P, Q and E, including antioxidant, anti-tyrosinase, anti-elastase, anti-inflammatory, antimicrobial and anti-cancer properties [6-8]. Notably, the anti-elastase activity of flavonoids may be helpful in slowing down the degradation of the elastin in tissue, which is generally caused by the excess of protease activity that follows tissue damage [9].

Silk sericin (SS) is a globular water-soluble protein synthesized in the labial gland of the silkworm *Bombyx mori*. SS has a molecular weight higher than 200 kDa and consists mainly of polar amino acids (78%), in particular serine and aspartic acid, while non-polar amino acids make up 22% of the protein. However, there are still significant differences in the amino acid composition according to the cocoon variety [10]. Notably, SS also contains flavonoids and carotenoids as impurities, which are responsible for its intrinsic antioxidant, anti-tyrosinase and anti-elastase activity [11]. In recent years, SS has been considered and managed as a waste product from the textile industry. Recently, however, SS biological properties have been exploited for biomedical and pharmaceutical purposes [12-17].

In the drug delivery field, SS has been employed, among other proteins, in the formulation of drug delivery systems in the form of both micro [18, 19] and nanoparticles [14, 20]. Protein-

based nano-systems are being used to improve the cellular uptake and the body's distribution of the drug, as well as to replace materials that are not biocompatible or have a negative impact on the environment. In this context, its excellent biocompatibility, controllable biodegradability, and non-immunogenicity make SS an ideal candidate for the formulation of drug delivery systems. Also, a recent review pointed out that thanks to their intrinsic biological activity, silk proteins, including SS, may be able to improve and support some of the effects of the active principle ingredient [14]. Unfortunately, nanoparticles based on SS "alone" cannot be obtained, due to its physicochemical instability, which is a result of its high water-solubility. To overcome this problem, several formulation strategies have been proposed, including conjugation, cross-linking or blending with other polymers [21-23], protein functionalization [24] or by employing particular techniques, such as the desolvation method [25] and electrospraying [26]. It has been previously shown that silk-based nanoparticles are effectively taken in by MSCs [27, 28], however, efforts need to be made to guarantee the slow release of actives after MSC internalization. Indeed, one of the limitations to date for the use of nanoparticles in therapy is that in many cases there is a burst release of the drug after administration, which corresponds to the release of the drug fraction adsorbed on the external surface of the nanoparticle. Therefore, the drug is released before reaching its pharmacological target, namely, MSCs, which leads to lower activity [29]. In this context, we first developed slow-release SNP formulations that did not have this detrimental burst release effect; moreover, we investigated the kinetics of drug release to clarify the drug delivery mechanisms. Then, SNP biological activities were investigated *in vitro* in terms of its antioxidant, anti-elastase and anti-tyrosinase activity. Finally, *in vitro* studies were performed on tissue-resident MSCs that mediate regeneration. In particular, the potency of SNPs was assessed with respect to metabolic activity improvement and protection against oxidative stress damage.

2. Materials and Methods

2.1. Materials

Dimethyl sulfoxide (DMSO), ethanol (EtOH), hydrochloric acid (HCl) and hydrogen peroxide (H₂O₂) were purchased from Carlo Erba, Milan, Italy. Pluronic F-127 (Lutrol[®] F127) was purchased from BASF, Ludwigshafen, Germany. 3-(4,5-dimethylthiazol-2-yl)-2,5-diphenyltetrazolium bromide (MTT), arbutin, 2,2-diphenyl-1-picrylhydrazyl (DPPH), E, *N*-Succinyl-Ala-Ala-Ala-*p*-Nitroanilide, pancreatic porcine elastase (PPE), polysorbate 20,

Tris(hydroxymethyl)aminomethane (TRIS), tyrosinase, and Q were purchased from Sigma Aldrich, Milan, Italy. P was purchased from Indena, Milan, Italy.

2.2. Nanoparticle Preparation and Characterization

2.2.1. Silk Sericin Extraction

Bombyx mori poly-hybrid cocoons were cut into pieces and degummed in an autoclave (Systec V-65, Wurttemberg, Germany) at 120 °C for 1 h (40 mL water/g of cocoons) [11]. The obtained SS solution was filtered using 70 µm cell strainers (Thermo Fisher Scientific, Milan, Italy) to eliminate larger impurities, frozen at –80 °C and freeze-dried (Modulyo® Edwards Freeze dryer, Kingston, New York, NY, USA) at 8×10^{-1} mbar and –50 °C for 72 h. Finally, SS powder was stored at –20 °C until use.

2.2.2. Nanoparticle Preparation

SNPs were prepared according to previously reported procedures with modifications [21]. Briefly, freeze-dried SS powder and Pluronic® F-127 were dissolved in DMSO at a final concentrations of 0.5 and 2.5% (w/v), respectively. The active ingredient was added to the solution at a final concentration of 0.1% (w/v) and maintained under magnetic stirring at 37 °C until complete dissolution. Subsequently, the resultant solution mixture was added dropwise to deionized water under stirring, allowing the formation of SNPs by self-assembly. The obtained nanoparticle suspension was then dialyzed against deionized water using cellulose dialysis tubes (12-14 kDa, Thermo Fisher Scientific, Milan, Italy) for 72 h, sonicated for 1 h and centrifuged at $3000 \times g$ for 5 min (Thermo Scientific SL8 Centrifuge, Milan, Italy) to precipitate aggregates. The supernatant fraction was collected, frozen at –80 °C, and freeze-dried (Modulyo® Edwards Freeze dryer, Kingston, New York, NY, USA) at 8×10^{-1} mbar and –50 °C for 72 h, and stored at room temperature until use. Overall, four formulations were considered, as reported in Table 1.

Formulation	Active Ingredient	Theoretical Drug Loading (% w/w)
SNP	/	/
SNP-P	Proanthocyanidins (P)	3.2
SNP-Q	Quercetin (Q)	3.2
SNP-E	Epigallocatechin gallate (E)	3.2

Table 1: Formulations considered for the study

2.2.3. Drug Loading, Production Yield and Encapsulation Efficiency Evaluation

SNP drug loading was evaluated by a spectrophotometer method (UV/VIS Spectrometer Lambda20, PerkinElmer, Wellesley, MA, USA) at 279, 275 and 373 nm for P, E and Q, respectively. Briefly, SNP-P and SNP-E were dissolved in deionized water plus HCl (0.1%, v/v) (1 and 2 mg/mL, respectively) while SNP-Q was dissolved in ethanol 96% (v/v) at the final concentration of 1 mg/mL, and maintained at mild magnetic stirring in the dark. The drug content was measured from standard calibration curves obtained by analyzing a concentration range of 10-80 µg/mL, $R^2 = 0.99$ for P; 0.5-20 µg/mL for Q, $R^2 = 0.98$; 5-50 µg/mL for E, $R^2 = 0.99$. EtOH or water was considered as blank. The drug loading (% w/w) of each formulation was calculated from the ratio between the total drug content (extrapolated from the calibration curve) and the concentration of analyzed SNPs. Each measurement was performed in triplicate.

SNP production yield was calculated according to Equation (1) as follows:

$$Y(\%) = \frac{\text{(total weight of nanoparticles)}}{\text{(weight of sericin + weight of drug + weight of poloxamer)}} \times 100 \quad (1)$$

Encapsulation efficiency (EE%) was determined as the percentage ratio between the actual entrapped drug and the drug dissolved in the DMSO solution during SNP preparation.

2.2.4. Nanoparticle Size Distribution

SNP size distribution was analyzed by nanoparticle tracking analysis (NTA) using NanoSight NS300 equipment (Malvern Panalytical, Grovewood Rd, WR14 1XZ, Great Malvern,

Worcestershire, UK). SNPs were dispersed in water, vortexed, and sonicated for 5 min before carrying out NTA analyses. For each batch, five measurements of 90 s each were performed.

2.2.5. Morphological Evaluation by Scanning Electron Microscopy (SEM)

SNP morphology was evaluated by SEM (MIRA3, Tescan, Brno, Czech Republic). Freeze-dried SNPs were carbon-sputter coated under argon before performing the morphological evaluation.

2.2.6. Physical-Chemical Characterization

Thermal analysis, supported by Fourier-transform infrared spectroscopy (FTIR), was used to characterize polymer, SS and drug bulks, as well as unloaded and drug-loaded SNPs. Temperature and enthalpy values were measured by differential scanning calorimetry (DSC) by a Mettler STAR^e system (Mettler Toledo, Novate Milanese, Milan, Italy) equipped with a DSC821^e module and an intracooler device for sub-ambient temperature analysis (Julabo FT 900). Samples in the range 1–3 mg were weighed (Mettler M3 Microbalance) and placed in sealed aluminum pans with pierced lids ($\beta = 10$ K/min, nitrogen atmosphere (flow rate 50 mL/min), -10/400 °C temperature range). The instrument was preventively calibrated with indium as a standard reference. Measurements were carried out at least in triplicate.

A Mettler STAR^e thermogravimetric analysis (TGA) system (Mettler Toledo, Novate Milanese, Milan, Italy) with simultaneous DSC (TGA/DSC1) was used to measure mass losses upon heating 2–3 mg samples in alumina crucibles with lids ($\beta = 10$ K/min, nitrogen atmosphere (flow rate 50 mL/min, 30/400 °C temperature range). Calibration procedure and triplicate measurements were applied, as for DSC above.

Mid-IR (650-4000 cm^{-1}) spectra were recorded on powder samples using a Spectrum One FTIR spectrophotometer (Perkin-Elmer, Wellesley, Minneapolis, MN, USA) equipped with a MIRacle™ ATR device (Pike Technologies, Madison, WI, USA) (resolution 4 cm^{-1}).

2.2.7. In Vitro Drug Release Test

The drug release from SNPs was evaluated by the dialysis technique according to the previously reported procedure in [30], with slight modifications. Experiments were repeated considering two different dissolution media: (i) EtOH/water in a 50/50 ratio for all the actives

(P, Q and E) or (ii) PBS for P and E, and PBS + polysorbate 20 (6% w/w) for Q. Briefly, for each batch 200 mg of SNPs were suspended in 5 mL of dissolution media and put into a dialysis membrane (3.5 kDa MWCO, Thermo Fisher Scientific, Milan, Italy). Each dialysis tube was incubated in 50 mL of dissolution media and maintained under mild magnetic stirring at 37 °C. At each considered time point, an aliquot of release medium was collected and replaced with fresh medium to maintain sink conditions. The amount of released drug was determined by a spectrophotometric method (UV/VIS Spectrometer Lambda20, PerkinElmer, Wellesley, MA, USA) analyzing the release media at 279, 275 and 373 nm for P, E and Q, respectively. The drug concentration was extrapolated from a calibration curve previously prepared (P 5-80 µg/mL, R² = 0.99; Q 0.5-15 µg/mL, R² = 0.99; E 5-30 µg/mL, R² = 0.98). Each experiment was performed in triplicate. The cumulative amount of released drug was calculated as a percentage using the following Equation (2):

$$\text{Cumulative amount of drug released (\%)} = C_i / C_0 \times 100 \quad (2)$$

where C_i is the amount of the drug released at a definite time interval and C₀ is the loaded drug amount.

2.2.8. Drug Release Kinetic Study

The *in vitro* drug release data was interpolated using different kinetic models, as reported below.

Higuchi

$$F(t) = k \times t^{0.5} \quad (3)$$

$$F(t) = 100 \times (1 - C \times \exp^{-k \times t}) \quad (4)$$

where $F(t)$ is the amount of drug dissolved at time t and k is the release constant. Equation (4) was reproduced from (Equation (2.12) from [31])

Peppas–Sahlin

$$F(t) = k_1 \times t^m + k_2 \times t^{(2 \times m)} \quad (5)$$

where $F(t)$ is the amount of drug dissolved at time t , k_1 is the diffusion constant, k_2 is the erosion constant and m is the diffusional exponent, indicative of the drug release mechanism.

Ritger–Peppas

$$F(t) = k \times t^n \quad (6)$$

where $F(t)$ is the amount of drug dissolved at time t , k is the release constant, and n is the release exponent, indicative of the drug release mechanism.

Zero-order

$$F(t) = k \times t \quad (7)$$

where $F(t)$ is the amount of drug released in time t , and k is the release constant.

Korsmeyer–Peppas

$$F(t) = k_{KP} \times t^n \times Q_0 \quad (8)$$

where $F(t)$ is the amount of drug released at time t , k_{KP} is the release constant, n is the release exponent, indicative of the drug release mechanism, and Q_0 is the initial amount of drug.

2.3. *In Vitro* Biological Activity

2.3.1. ROS-Scavenging Activity

The ROS-scavenging activity of SNPs was evaluated by the DPPH colorimetric assay as previously reported [13, 18, 32, 33] with slight modifications. Briefly, each SNP formulation was tested considering different final concentrations in the final reaction mix (15, 10, 5 and 2.5 mg/mL) and their free drug equivalent concentration calculated from the loading data. SNPs were left 24 h under magnetic stirring at room temperature to allow the release of actives. Either 120 μ L of SNP or free drug samples were added to 1080 μ L of a DPPH solution (0.0056% w/v in methanol 70% v/v). The reaction mix was incubated in the dark at room temperature, centrifuged at $3000 \times g$ for 5 min and subjected to spectrophotometric analysis (Synergy HT, BioTek, Swindon, United Kingdom) at 515 nm. A reaction mix without sample was used as a negative control. ROS-scavenging activity percentage was calculated according to the following formula:

$$\text{ROS-scavenging activity (\%)} = [(A_{\text{ctr}} - A_{\text{samp}})/A_{\text{ctr}}] \times 100 \quad (9)$$

where A_{ctr} is the absorbance of the negative control and A_{samp} is the absorbance of the sample. Each experiment was performed in triplicate.

2.3.2. Anti-Elastase Activity

The anti-elastase activity was investigated for each SNP formulation considering different final concentrations in the final reaction mix (15, 10, 5 and 2.5 mg/mL) and their free drug equivalent concentration calculated from the loading data. SNPs were left for 24 h under magnetic stirring at room temperature to allow the release of actives. Then, the procedure reported by Bari and colleagues was employed [34]. Briefly, PPE was solubilized in phosphate buffer pH 6.8 (0.5 IU/mL). The substrate *N*-Succinyl-Ala-Ala-Ala-*p*-Nitroanilide was diluted in TRIS buffer to obtain a final concentration of 0.41 mM. Each sample was incubated for 20 min with the enzyme, and subsequently, the substrate was added. The kinetic reaction was monitored by spectrophotometric analysis (Synergy HT, BioTek, Swindon, United Kingdom) at 410 nm for 35 min (one measurement each minute). The reaction mix in the absence of sample was used as a negative control, while E was considered as a positive control (concentration tested: 7.2 mg/mL). All analyses were performed in triplicate, and the results are reported as the anti-elastase activity percentage, calculated using the following equation:

$$\text{Anti-elastase activity (\%)} = [(A_{\text{ctr}} - A_{\text{samp}})/A_{\text{ctr}}] \times 100 \quad (10)$$

where A_{ctr} is the absorbance of the negative control and A_{samp} is the absorbance of the sample.

2.3.3. Anti-Tyrosinase Activity

The anti-tyrosinase activity of SNPs was evaluated by spectrophotometric analysis of the kinetic reaction between the enzyme tyrosinase and L-tyrosine substrate. For each SNP formulation, the anti-tyrosinase activity was tested considering different final concentrations in the final reaction mix (15, 10, 5 and 2.5 mg/mL) and their free drug equivalent concentration calculated from the loading data. SNPs were left for 24 h under magnetic stirring at room temperature to allow the release of actives. The enzyme tyrosinase was solubilized in phosphate buffer pH 6.8 to obtain a final concentration of 500 IU/mL. The tyrosinase solution was pre-incubated for 10 min with each sample and, consequently, the L-tyrosine substrate was added to the reaction mix. The enzymatic reaction was spectrophotometrically analyzed (Synergy HT, BioTek, Swindon, United Kingdom) at 480 nm for 35 min (one measurement each minute). The reaction mix without sample was used as a negative control, while arbutin was considered as a positive control (concentration tested:

2.5 mg/mL). All analyses were conducted in triplicate, and the results are reported as anti-tyrosinase activity percentage, calculated using the formula:

$$\text{Anti-tyrosinase activity (\%)} = [(A_{\text{ctr}} - A_{\text{samp}})/A_{\text{ctr}}] \times 100 \quad (11)$$

where A_{ctr} is the absorbance of the negative control and A_{samp} is the absorbance of the sample.

2.3.4. Cell Metabolic Activity Evaluation

The cytocompatibility and proliferation ability of SNP formulations were evaluated on human adipose mesenchymal stem cells (MSCs). MSCs were isolated from adipose tissue samples, as reported in the Supplementary Materials. MSCs fulfilled adherence to the International Society for Cellular Therapy criteria [35]. MSCs were seeded in a 96-well plate (5 000 cells/cm²) and cultured with DMEM/F12 supplemented with 10% (v/v) fetal bovine serum (FBS), 100 U/mL penicillin, 100 µg/mL streptomycin, 0.25 µg/mL amphotericin, 4 mM glutamine, 1 mM sodium pyruvate. After 24 h, the supernatants were replaced with 100 µL of culture medium (not supplemented with FBS) containing SNPs at the final concentrations of 0.8, 0.4, and 0.2 mg/mL, or their free drug equivalent concentrations calculated from the loading data. SNPs were left for 24 h under magnetic stirring at room temperature to allow the release of actives. After 24, 48 and 72 h of incubation, supernatants were discarded, cells were then washed with PBS, and 100 µL of MTT solution (0.5 mg/mL) was added to each well. After three hours of incubation, the MTT solution was removed, and 100 µL of DMSO was added. Untreated cells were considered as control (100% of metabolic activity). The absorbance was measured by a microplate reader (Synergy HT, BioTek, Swindon, United Kingdom) at 570 nm and 670 nm (reference wavelength). Each condition was tested in triplicate, and the percentage of cell metabolic activity was calculated as follows:

$$\text{Cell metabolic activity (\%)} = 100 \times (\text{Abs}_{\text{sample}}/\text{Abs}_{\text{ctr}}) \quad (12)$$

where $\text{Abs}_{\text{sample}}$ is the mean value of the measured absorbance of the tested samples, and Abs_{ctr} is the mean value of the measured absorbance of cells not incubated with SNPs or free drug. All experiments were performed in triplicate.

2.3.5. Oxidative Stress Protection Test

SNPs have been tested in terms of cell protection from the oxidative stress damage. MSCs were seeded in 96-well plate (5 000 cells/cm²) and treated with 100 µL of culture medium containing SNPs at the final concentrations of 0.8, 0.4 and 0.2 mg/mL or their free drug equivalent concentration calculated from the loading data. SNPs were left 24 h under magnetic stirring at room temperature to allow the release of actives. After 24 h, the media was discarded, and 100 µL of hydrogen peroxide (1.5 mM) solution were added to each well. Cells not incubated with H₂O₂ were considered as control. After 24 h, for the cells incubated with or without H₂O₂, an MTT test was performed to evaluate the cellular metabolic activity, calculated as previously reported in Section 2.3.4. All experiments were performed in triplicate.

2.4. Statistical Analysis

Raw data were processed by STATGRAPHICS XVII (Statpoint Technologies, Inc., Warrenton, VA, USA). For data with a normal distribution, a linear generalized analysis of variance model (ANOVA) was used and combined with Fisher's least significant difference (LSD) procedure to evaluate the differences between the groups. In detail, drug loading results were analyzed considering the batch as a fixed factor and the drug loading as the response variable. NTA analysis results were analyzed considering the formulation as a fixed factor and mean diameter, mode, d₁₀, d₅₀ and d₉₀ as the response variables. Release data were processed considering the amount of active released as the response variable and the formulation and times as the fixed factors. Cumulative drug release data was interpolated and curve kinetic parameters for each model were determined using Graph-Pad Prism software version 8.0.1 (GraphPad Software 2365 Northside Dr. Suite 560 San Diego, CA 92108, USA). The ROS-scavenging data were elaborated considering the sample as a fixed factor, the concentration as a covariate and the ROS-scavenging activity (%) as the response variable. Anti-elastase and anti-tyrosinase raw data were elaborated considering the sample and time as fixed factors, the concentration as a covariate and the activity % as response variables. The enzymatic kinetics of anti-tyrosinase and anti-elastase activity were elaborated with Michaelis-Menten model kinetics $y = (V_{max} \times x) / (K_m + x)$, where y is the absorbance at time x , K_m is the moment in which the activity is equal to half the maximum and V_{max} is the maximum speed of the enzyme [11]. Graph-Pad Prism software version 8.0.1 (GraphPad Software 2365 Northside Dr. Suite 560 San Diego, CA 92108, USA) was used to calculate the

curve parameters. For each curve, V_{\max} and K_m were analyzed with an ANCOVA model, considering the sample as a fixed factor and the sample concentration as a covariate. The differences between the groups were analyzed with the LSD test for multiple comparisons. Proliferation data were analyzed considering the sample concentration and time as fixed factors, the concentration as a covariate and the cell metabolic activity (%) as the response variable. Oxidative stress data were elaborated considering H_2O_2 concentrations (0 or 1.5 mM) and the sample as fixed factors, the sample concentrations as a covariate and the cell metabolic activity (%) as the response variable. For all the analyses, the statistical significance was set up at $p < 0.05$. Unless otherwise specified, data are expressed as mean \pm standard deviation.

3. Results and Discussion

SS is a promising biocompatible and bioactive material and it was selected here for the preparation of nanoparticles, and to obtain the slow release of naturally-derived biologically active substances. Specifically, SNPs were prepared by exploiting a self-assembly method with poloxamer; three different active ingredients were loaded into SNPs: P, Q and E. For each formulation, three different batches were prepared.

The process yield (%) in the SNP preparations ranged from $60.9 \pm 0.46\%$ for SNP-Q to $63.8 \pm 4.25\%$ for SNP-P. These values are compatible with the small batch sizes (about 1.5 g) obtained in our lab-scale process. The SNPs were able to encapsulate both hydrophilic (P and E) and hydrophobic (Q) drugs (Table 2). Considering the proposed structure of SNPs (Figure 1A), hydrophobic drugs should reside in the inner core of the micellar structure, while a hydrophilic drug is expected to reside within the corona, which is relatively hydrophilic. It can be supposed that the interaction between hydrophilic actives and the hydrophilic corona is due to the formation of ionic interactions or hydrogen bonds, while hydrophobic actives are entrapped in the hydrophobic core by hydrophobic effects and Van der Waals forces [36]. The statistical analysis revealed no significant differences in terms of drug loading and encapsulation efficiency among different batches of the same active ingredient ($p > 0.05$), indicating proper standardization of the final product (see Figure S1 reported in the Supplementary Materials). However, significant differences were found between the different actives considered ($p < 0.001$). In detail, encapsulation efficiency (EE) values were higher for the hydrophilic drugs P and E than for the hydrophobic Q (Table 2).

Nanoparticle Formulation	Process Yield (%)	Drug Loading (%) w/w	Encapsulation Efficiency (%)
SNP	62.6 ± 5.68 ^a	-	-
SNP-P	63.8 ± 4.25 ^a	2.6 ± 0.37 ^a	82.2 ± 11.58 ^a
SNP-Q	60.9 ± 0.46 ^a	0.7 ± 0.21 ^b	20.5 ± 6.59 ^b
SNP-E	63.7 ± 1.79 ^a	1.3 ± 0.17 ^c	41.5 ± 5.25 ^c

Table 2: SNP formulations and composition details. The process yield (%), drug loading (%) and encapsulation efficiency (%) are reported as mean values ± standard deviation, n = 3, of at least three independent experiments for each batch. Different letters (a, b, c) among the same column correspond to significant differences between groups ($p < 0.05$), while the same letter indicates no significant differences ($p > 0.05$)

As previously reported [37, 38], drug-core compatibility is one of the most critical factors that may influence the loading efficiency of SNPs. Sunoqrot and colleagues [39] reported that, according to the Flory–Huggins interaction parameter, ideally, the highest drug-core compatibility is achieved when the water solubility values of the drug and hydrophobic core are equal. In our case, the different solubility of poloxamer and Q (50 mg/mL vs. 2 mg/mL in water at 25 °C) may have affected the drug loading and explain the low encapsulation efficiency.

All nanoparticles were nanometric in size. SNP-E showed a higher average diameter (201.4 ± 15.15 nm) compared to SNP-P (141.2 ± 15.15 nm) and SNP-Q (137.4 ± 12.37 nm) (mean value ± SE, n = 5). Statistical analysis revealed that the encapsulation of active substances did not significantly influence the particle size and size distribution ($p > 0.05$). These results were confirmed by SEM morphological investigation: all SNP formulations showed a nanometric size and spherical shape with a smooth surface (Figure 1 B–E).

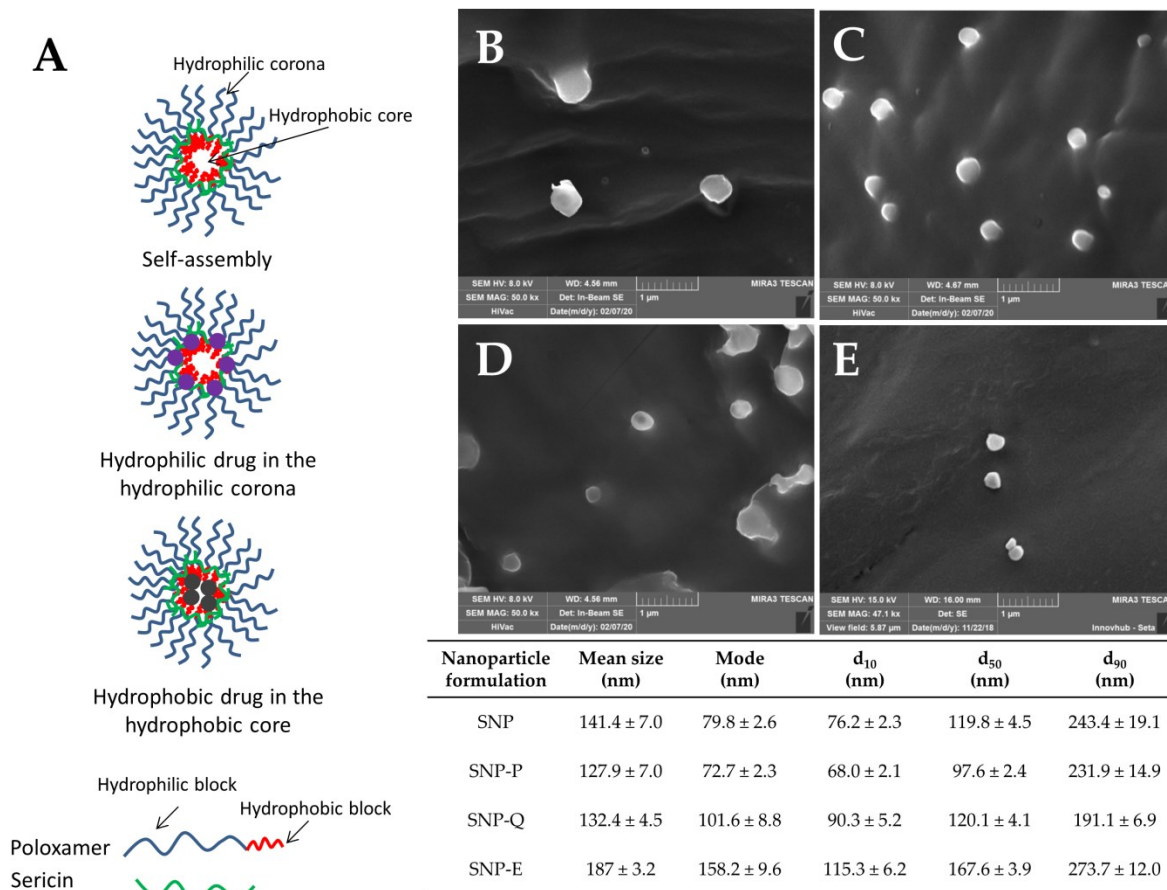


Figure 1: (A) Proposed structure for silk sericin nanoparticles (SNPs). SEM images and particle size distribution of SNP-P (B), SNP-Q (C), SNP-E (D) and SNP (E). Scale bar 1 μm . Nanoparticle tracking analysis (NTA) results are reported as mean, mode, d_{10} , d_{50} and d_{90} values, all of them \pm standard error, $n = 5$. Statistical analysis revealed no significant differences in particle size and particle size distribution among the different formulations ($p > 0.05$)

Thermal analysis, supported by FTIR spectroscopy, was used to characterize polymer, SS and free drugs, as well as unloaded and drug-loaded SNPs. In Figure 2, for example, the thermal profiles of SNP-Q are reported. The DSC profile of Lutrol[®] F127 (curve a) shows an endothermic effect at $T_{\text{peak}} = 58.1 \pm 0.8 \text{ }^\circ\text{C}$ ($T_{\text{onset}} = 55.2 \pm 0.4 \text{ }^\circ\text{C}$, $\Delta H_{\text{m}} = 110 \pm 1 \text{ J g}^{-1}$) due to melting, followed by an exothermic effect peaking at about $155 \text{ }^\circ\text{C}$ due to the melt decomposition [40]. Q is a crystalline compound showing a DSC thermal profile with an initial broad effect at about $118 \text{ }^\circ\text{C}$ due to dehydration (as confirmed by TGA mass loss of $0.8 \pm 0.5\%$, curve not reported), and a second endothermic effect at $T_{\text{peak}} = 321.9 \pm 0.2 \text{ }^\circ\text{C}$ ($T_{\text{onset}} = 319.1 \pm 0.5 \text{ }^\circ\text{C}$, $\Delta H_{\text{m}} = 168 \pm 3 \text{ J g}^{-1}$) corresponding to melting, followed by exothermic

decomposition at about 350 °C (curve b). In the trace of loaded SNPs (curve c), the thermal effect due to the polymer melting is still present with thermal and enthalpic parameters slightly lower at $T_{\text{peak}} = 55.8 \pm 0.6 \text{ °C}$ ($T_{\text{onset}} = 53.5 \pm 0.5 \text{ °C}$, $\Delta H_{\text{m}} = 99 \pm 2 \text{ J g}^{-1}$) due to the presence of the other ingredients in the system as impurities. At about 150 °C, an effect due to the glassy-rubbery transition ($T_{\text{midpoint}} = 146 \pm 2 \text{ °C}$, red circle) attributable to the random coil domains present in the amorphous region of the SS protein structure and also, the exothermic peak at $200 \pm 2 \text{ °C}$, which can be attributed to the transition from the random coil to β -structure of SS, are visible. These effects in the DSC curve of loaded SNPs confirm the presence of the protein in nanoparticles. No effect due to the presence of the active is evident, suggesting that probably Q is molecularly dispersed in the polymer. Also, it is probably not possible to detect the presence of Q in the final system due to the superimposition of drug melting with the polymer decomposition. The DSC profile of SNP-P is not reported because of its flat profile due to the prevalent amorphous nature of the active. In the system with E, despite its crystalline nature, in the SNP-E it was not possible to detect any endothermic effect due to drug melting because of the low drug content and its molecular dispersion.

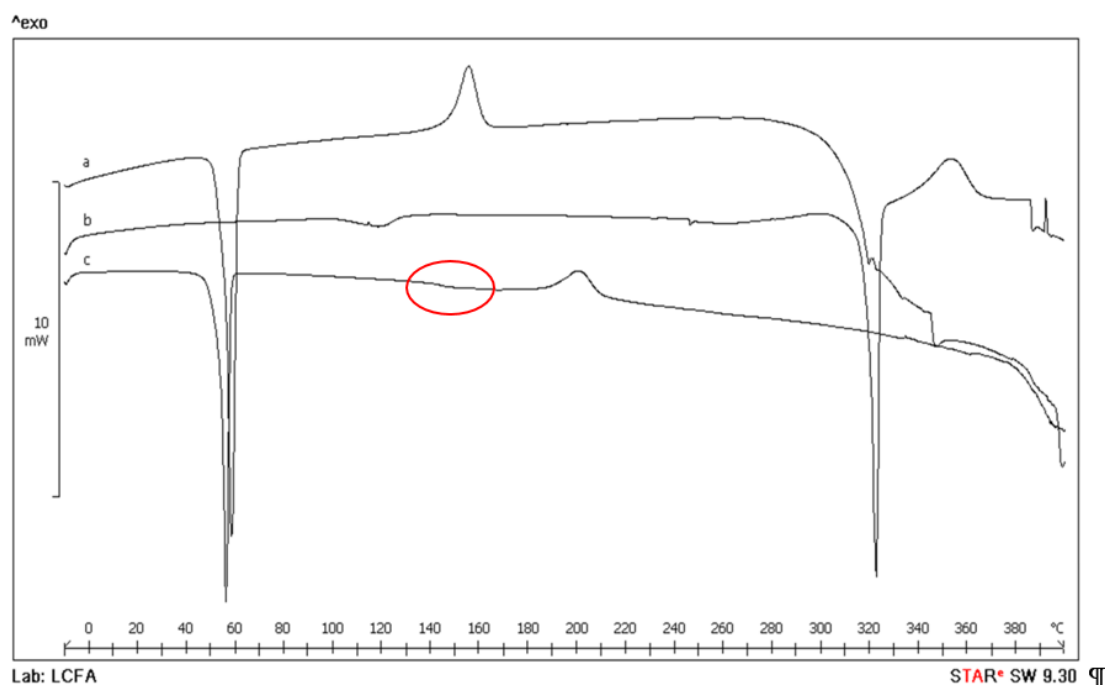


Figure 2: Differential scanning calorimetry (DSC) thermal profile of Lutrol[®] F127 (curve a), Q (curve b) and SNP-Q (curve c)

In Figure 3, FTIR spectra of Lutrol[®] F127, SS as well as unloaded and loaded SNPs are reported. The spectrum of Lutrol[®] F127 shows a band at 2882 cm⁻¹ due to C–H stretching vibration and a band at 1466 cm⁻¹ due to C–H bending vibration. SS exhibited broadband peaked at 3262 cm⁻¹ due to the stretching of the N–H bond of amides in concomitance with the absorption of the O–H groups, and the typical bands of C–O stretching at 1643 and N–H bending at 1513 cm⁻¹ of amide I and II, respectively. In the FTIR spectrum of unloaded SNPs, these bands are still visible, confirming the presence of the protein in the polymer system, but shifted to higher wavenumbers, 1648 and 1530 cm⁻¹, respectively, as a consequence of silk-sericin poloxamer nanoparticles formulation causing SS transition into the β -sheet structure, as also highlighted by the thermal data. This spectrum is superimposable to that of the loaded SNPs. The characteristic signals of Q (not reported in the figure) in the region between 1700–1100 cm⁻¹ were masked in the recorded spectrum of SNP-Q by the intense signals of SS. The same results are recorded also for the SNP-E. Instead, for the SNP-P system, the FTIR spectrum is not reported because the amorphous character of the drug causes a broadening of the bands with a final bad resolution.

Drug release from SNPs was investigated considering two dissolution media, and the data are reported in Figure 4 as a function of time. For both of the dissolution media, statistical analysis showed that formulation and time were statistically significant in influencing SNP performance ($p < 0.05$). In EtOH, SNP-E and SNP-Q showed a burst release; after 8 h, up to 36% and 25% of the whole loaded drug was released, respectively. At the same time, SNP-P released only 5% of the whole drug (Figure 4A). A plateau, corresponding to about 60%, 50% and 25% of the whole drug released, was observed after 48 h for SNP-E, SNP-Q and SNP-P, respectively. In PBS (or PBS + polysorbate 20 for Q), all the actives were released in a controlled manner. The hydrophilic actives were more easily released; after 48 h, the time at which a plateau was reached, SNP-P and SNP-E released 50% of the whole loaded drug, while SNP-Q released only 20% (Figure 4B). At the end of the drug release tests, the amount of actives not released from SNPs (or that remained in the membranes) was determined. The results confirmed the mass balance (Supplementary Materials).

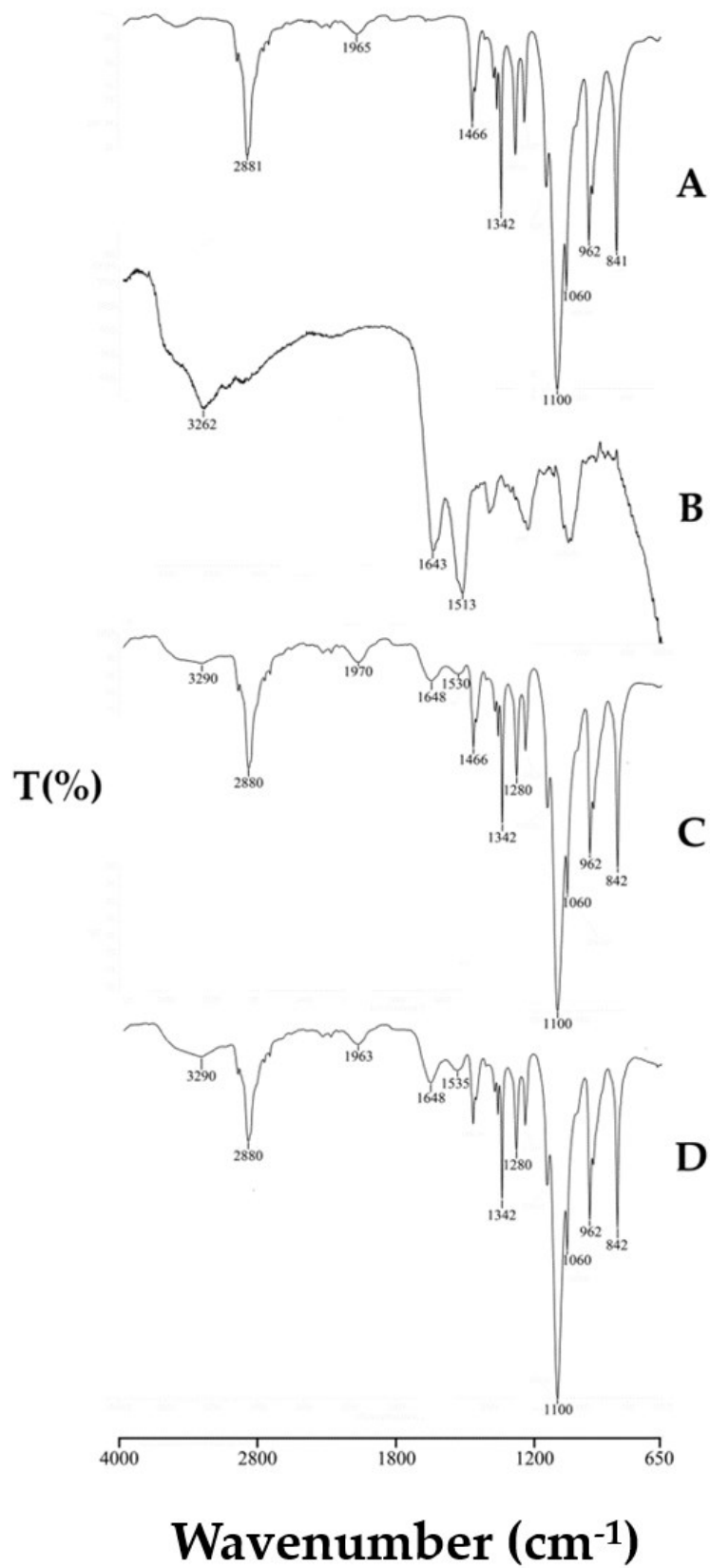


Figure 3: FTIR spectra of Lutrol® F127 (A), sericin (B), unloaded SNP (C) and loaded SNP-Q (D)

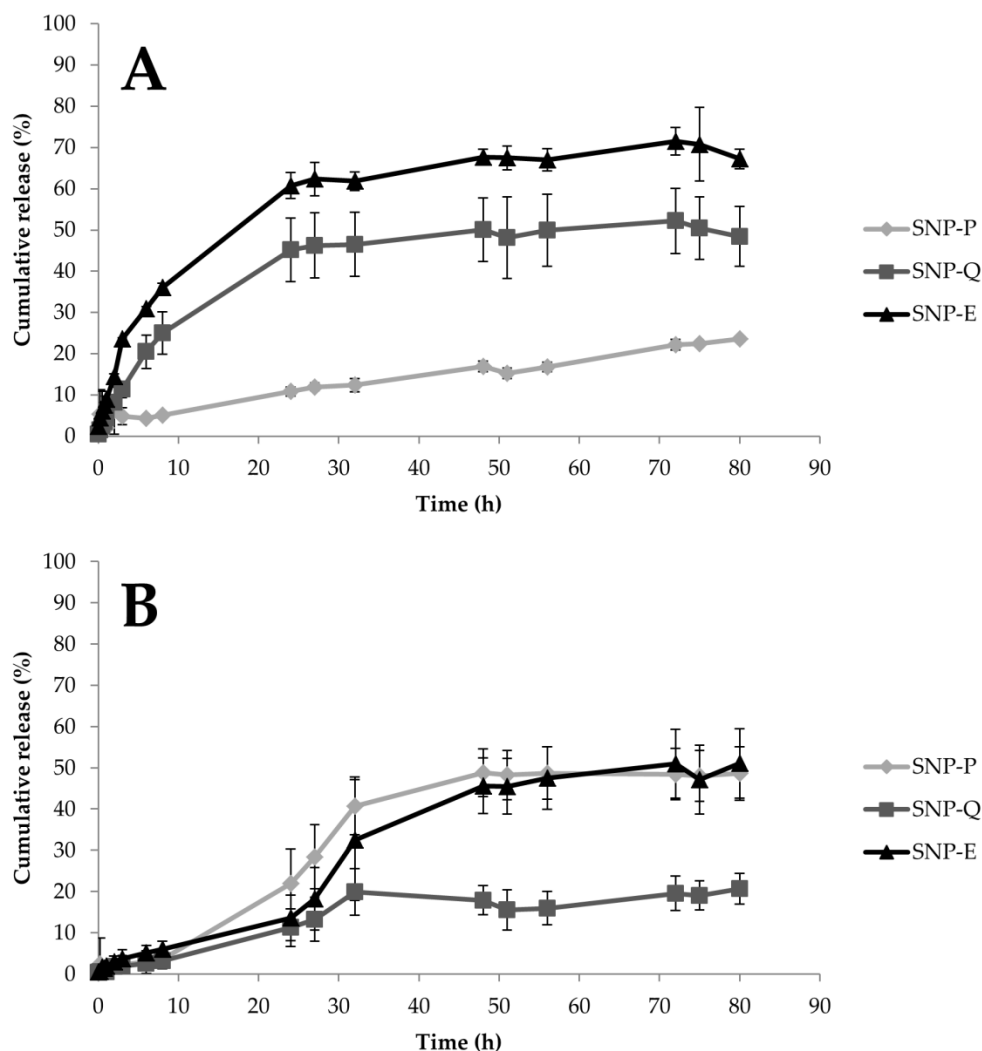


Figure 4: *In vitro* drug release profiles for SNPs in EtOH/water 50/50 v/v (A) or PBS (for SNP-P and SNP-E) and PBS + polysorbate 20 (for Q) (B). Data are reported as the cumulative drug release percentage (mean values \pm standard deviation, n = 9) of at least three independent experiments for each batch

Release profiles suggest a destructure of the micellar structure of SNPs in EtOH, leading to an increased liberation rate of E and Q compared to what happens in PBS. On the other hand, the release of P is slower in EtOH compared to PBS. The chemical structures of actives, as well as the different solubility of SS in the release media, explain these different release profiles. Firstly, SS is less soluble in EtOH 50% v/v than in water, due to the lower polarity of the solvent. Also, P has complex chemical structure, in which catechins or flavanols are linked together by C–C bridges forming oligomers (from dimers to pentamers) or polymers (up to 60 units). P is bulkier than E and Q and it spreads slowly through SS (which in EtOH is less soluble). E and Q which have a lower molecular weight and steric hindrance than P, are

released much faster. Moreover, it has to be considered that hydrophilic actives E and P reside in the hydrophilic external structure of SNPs (Figure 1 A), and because they have a shorter path to follow, they are released more quickly. Q instead, being lipophilic, resides in the internal lipophilic core (Figure 1 A) and has to spread through the hydrophilic layer made of SS and poloxamer. This latter aspect also explains the lower release of Q in PBS medium. Finally, the slow second-phase or lag-phase (observed for P and E in PBS) suggests a densely packed system with low porosity, and this effect could also be the result of pore closure, sericin–pluronic interactions, or drug sericin–pluronic drug interactions.

Drug release data were further processed by elaborating the kinetic model of the release systems. The goal of modeling the release process is to gain a deeper understanding of the release mechanisms of a specific material. Release models describe the release of the encapsulated molecules as a function of time and provide information about the exact mass transport mechanisms involved in the drug release. Higuchi, Peppas–Sahlin, Ritger–Peppas and zero-order are among the most employed models. Table 3 lists the results of *in vitro* release model fitting for SNP-P, SNP-Q and SNP-E. Different release behaviors were observed in the different dissolution media. Drug release from SNPs in PBS followed the Peppas–Shalin model, where both the Fickian contribution (first term of the equation) and the case-II relaxation contribution (second term of the equation) are considered [41]. Specifically, k_1 is the constant related to the Fickian kinetics (diffusion constant); k_2 is the constant related to case-II relaxation kinetics (erosion constant) and m is the diffusional exponent. As $k_2 > k_1$, and the k_1 value is negative, it is indicative that case-II relaxation is predominant in the diffusion phenomenon in the release of the active substances from SNPs. This was also confirmed by the Ritger–Peppas model, for which proper fittings were calculated ($R^2 = 0.89$ for P, 0.88 for E and 0.84 for Q): the n exponent was between 0.43 and 0.85, thus confirming the non-Fickian behavior. In EtOH, E and Q were released from SNPs in an almost-Fickian mode, while P was released by a Fickian diffusion. Indeed, according to Ritger–Peppas and Korsmeyer–Peppas models, n values for E and Q were 0.3654 and 0.417, respectively, while for P, the n value was 0.522. According to both equation models, n values lower than 0.5 are indicative of almost-Fickian diffusion, while an n value equal to 0.5 is indicative of pure Fickian diffusion. This behavior was also confirmed by the good fitting revealed for the Higuchi models, which describe the drug release as a diffusion process based on the Fick's law, which is square root time dependent. Of note, k values were higher for E and Q with respect to P, thus confirming what was previously supposed regarding the lower diffusibility of P due to the higher steric hindrance of the molecule.

Model	Equation	Sample	Dissolution Medium	Coefficients (95% Confidence Bounds)	Sum of Squares	R ²	Degrees of Freedom	SE
Higuchi	$F(t) = k \times t^{0.5}$	SNP-E	PBS	$k = 5.516$ (5.261, 5.771)	11,734	0.8421	161	0.1290
			EtOH	$k = 9.265$ (8.821, 9.709)	3787	0.9051	53	0.2213
		SNP-Q	PBS	$k = 2.319$ (2.137, 2.501)	635.8	0.8396	53	0.09066
			EtOH	$k = 6.895$ (6.620, 7.170)	13,653	0.8378	161	0.1392
		SNP-P	PBS	$k = 5.801$ (5.564, 6.039)	10,214	0.8694	161	0.1204
			EtOH	$k = 2.432$ (2.285, 2.579)	416.5	0.868	53	0.07338
Higuchi (eq 2.12 from [31])	$F(t) = 100 \times (1 - C \times \exp(-k \times t))$	SNP-E	PBS	$C = 0.9979$ (0.9819, 1.014) $k = 0.009999$ (0.009381, 0.01063)	7962	0.8928	160	C 0.008122 k 0.0003151
			EtOH	$C = 0.8826$ (0.8430, 0.9226) $k = 0.02064$ (0.01780, 0.02389)	4440	0.8888	52	C 0.01936 k 0.00136
		SNP-Q	PBS	$C = 0.9837$ (0.9687, 0.9987) $k = 0.003084$ (0.002645, 0.003528)	786.6	0.8016	52	C 0.007455 k 0.0002181
			EtOH	$C = 0.9222$ (0.8972, 0.9472) $k = 0.0118$ (0.01064, 0.01300)	18,407	0.7813	160	C 0.01246 k 0.0005668
		SNP-P	PBS	$C = 0.9947$ (0.9785, 1.011) $k = 0.01071$ (0.01005, 0.01138)	8025	0.8974	160	C 0.008183 k 0.0003287
			EtOH	$C = 0.9658$	327.5	0.8962	52	C

				(0.9562, 0.9755)				0.004806
				$k = 0.002922$				k
				(0.002637, 0.003208)				0.0001423
				$k_1 = -3.034$				
				(-8.640, 1.090)				k_1 2.849
			PBS	$k_2 = 3.714$	8357	0.8875	159	k_2 2.02
		SNP-E		(1.074, 7.992)				m
				$m = 0.3323$				0.04814
				(0.2638, 0.4380)				
			EtOH	$k_1 \sim$	1090	0.9727	51	$k_1 \sim$
				$k_2 \sim$				$k_2 \sim$
				$m \sim$				$m \sim$
				$k_1 = -7.5$				
				(-27.08 to 0.4361)				k_1 6.388
			PBS	$k_2 = 8.15$	577.1	0.8544	51	k_2 5.974
		SNP-Q		(-0.06646 to 27.32)				m
				$m = 0.1724$				0.05588
				(0.08940, 0.3108)				
			EtOH	$k_1 \sim$	10,742	0.8724	159	$k_1 \sim$
				$k_2 \sim$				$k_2 \sim$
				$m \sim$				$m \sim$
				$k_1 = -11.42$				
				(-20.48, -4.672)				k_1 4.707
			PBS	$k_2 = 11.6$	7805	0.9002	159	k_2 4.058
		SNP-P		(6.151, 19.67)				m 0.02951
				$m = 0.2289$				
				(0.1850, 0.2822)				
			EtOH	$k_1 \sim$	388.6	0.8768	51	$k_1 \sim$
				$k_2 \sim$				$k_2 \sim$
				$m \sim$				$m \sim$
				$k = 1.783$				
			PBS	(1.226, 2.496)	8458	0.8861	160	k 0.3431
				$n = 0.7854$				n 0.04708
				(0.7028, 0.8766)				
				$k = 15.63$				
			EtOH	(13.45, 17.91)	2137	0.9465	52	k 1.207
				$n = 0.3654$				n 0.02005
				(0.3300, 0.4039)				

Zero order	$F(t) = k \times t$	SNP-Q	PBS	$k = 1.744$ (1.011, 2.692) $n = 0.5727$ (0.4632, 0.7069)	616.2	0.8446	52	k 0.4702 n 0.06732		
			EtOH	$k = 9.531$ (7.955, 11.21) $n = 0.4169$ (0.3751, 0.4626)	12,705	0.849	160	k 0.9111 n 0.0245		
		SNP-P	PBS	$k = 2.983$ (2.248, 3.852) $n = 0.6691$ (0.6057, 0.7385)	8480	0.8916	160	k 0.4643 n 0.03845		
			EtOH	$k = 2.232$ (1.346, 3.297) $n = 0.522$ (0.4223, 0.6480)	415.2	0.8684	52	k 0.4251 n 0.04789		
		SNP-E	PBS	$k = 0.7373$ (0.7070, 0.7676)	9473	0.8725	161	0.01536		
			EtOH	$k = 1.156$ (1.027, 1.284)	18,129	0.5458	53	0.06416		
		SNP-Q	PBS	$k = 0.3012$ (0.2718, 0.3306)	948.1	0.7608	53	0.01467		
			EtOH	$k = 0.8692$ (0.8122, 0.9263)	33,494	0.602	161	0.02889		
		SNP-P	PBS	$k = 0.7643$ (0.7302, 0.7984)	11,981	0.8468	161	0.01728		
			EtOH	$k = 0.3172$ (0.2920, 0.3423)	694.3	0.7799	53	0.01256		
		Korsmeyer–Peppas	$F(t) = k_{KP} \times t^n \times Q_0$	SNP-E	PBS	$k_{KP} = 1.783$ (1.226, 2.496) $n = 0.7854$ (0.7028, 0.8766)	8458	0.8861	160	k_{KP} 0.3431 n 0.04708
					EtOH	$k_{KP} = 15.63$ (13.45, 17.91) $n = 0.3654$ (0.3300, 0.4039)	2137	0.9465	52	k_{KP} 1.207 n 0.02005
SNP-Q	PBS			$k_{KP} = 1.744$ (1.011, 2.692)	616.2	0.8446	52	k_{KP} 0.4702		

		$n = 0.5727$ (0.4632, 0.7069)				n 0.06732
	EtOH	$k_{KP} = 9.531$ (7.955, 11.21) $n = 0.4169$ (0.3751, 0.4626)	12,705	0.849	160	k_{KP} 0.9111 n 0.0245
	PBS	$k_{KP} = 2.983$ (2.248, 3.852) $n = 0.6691$ (0.6057, 0.7385)	8480	0.8916	160	k_{KP} 0.4643 n 0.03845
SNP-P	EtOH	$k_{KP} = 2.232$ (1.346, 3.297) $n = 0.522$ (0.4223, 0.6480)	415.2	0.8684	52	k_{KP} 0.4251 n 0.04789

Table 3: Results of *in vitro* release model fitting for SNP-P, SNP-Q and SNP-E. Kinetic elaborations were performed on release data obtained from at least three independent experiments for each batch. ~ indicates that the analysis performed was “ambiguous”; therefore, the fit does not nail down the values of all the parameters, and 95% confidence bounds cannot be reported. These latter data were not considered in the interpretation of results

The ROS-scavenging activity results are reported in Figure 5. The statistical analysis revealed that ROS-scavenging activity was significantly influenced by the sample ($p < 0.001$) but not by concentration ($p > 0.05$). All the active ingredients (P, Q and E) showed excellent antioxidant properties, with ROS-scavenging activity % values above 90%, even at the lowest concentration tested. For the unloaded SNPs, the average ROS-scavenging activity % was 15.60 ± 0.893 . The encapsulation of Q and E into SNPs preserved their antioxidant activity as no significant differences were found between Q and SNP-Q or between E and SNP-E ($p > 0.05$). Conversely, for P the encapsulation into SNPs significantly reduced the ROS-scavenging activity % ($p < 0.05$). Overall, our data are in accordance with the literature, where antioxidant properties have been reported for P [42], Q [43], E [44] and sericin [11, 18].

In vitro biological activity of unloaded and loaded SNPs was subsequently assessed in terms of anti-elastase and anti-tyrosinase activity (Figure 6). Unloaded SNPs showed good intrinsic anti-elastase activity, which was higher than 70% starting from the 5 mg/mL concentration (Figure 6 A–C).

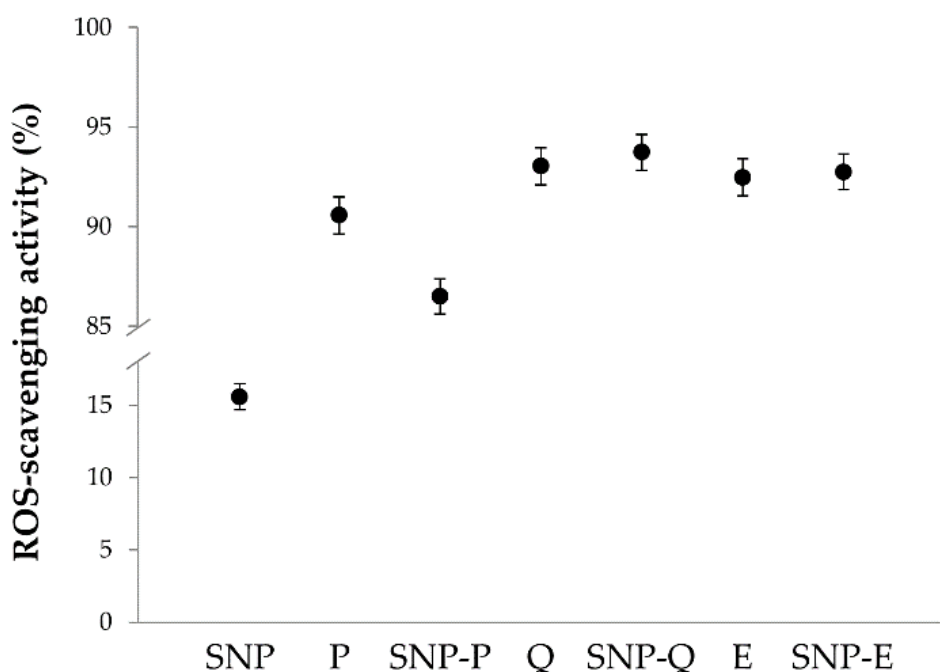


Figure 5: Results of average ROS-scavenging activity (%) as a function of SNP formulations (SNP, SNP-P, SNP-Q and SNP-E) and the equivalent amount of free actives (P, Q and E). Only data related to the highest concentration tested are reported (0.8 mg/mL for SNPs and the equivalent amount of free actives). Multifactor ANOVA, mean values \pm LSD, $n = 3$

Therefore, the ability of SS to inhibit the elastase enzyme was also preserved when assembling the protein as a nanoparticle. Conversely, unloaded SNP showed low anti-tyrosinase activity at all of the concentrations tested (Figure 6 D–F), despite the literature reports on the ability of SS to inhibit tyrosinase [11]. In this case, we supposed that the conformational changes in SS proteins, when assembled as a nanoparticle, hinder the interaction with the enzyme. Good anti-elastase activity was observed at all the concentrations tested, for both P and E (Figure 6 A, C), thus confirming previous reports in the literature [45–47]. For SNP-P and SNP-E, the anti-elastase activity was lower compared to the equivalent amount of free drug (Figure 6 A,C). A synergic anti-elastase effect was observed only for SNP-Q; after the encapsulation, the anti-elastase activity % of Q increased from $1.28 \pm 0.168\%$ to $87.7 \pm 5.67\%$ (at the highest concentration tested) (Figure 6 B). In accordance with the literature, P and E showed a dose-dependent anti-tyrosinase activity. The anti-tyrosinase activity of both P and Q decreased after encapsulation into SNPs; only E, when encapsulated into SNPs, retained good inhibitory properties. The lower activity of loaded SNPs, with respect to the equivalent amount of free drugs, may be a result of (i) a lower amount of active (P, Q and E) that can interact and inhibit the enzyme, as it is not entirely released by SNPs after 24 h (see the release profiles reported in Figure 4); or (ii) the steric hindrance created by SNPs, which could hinder the link or interaction of the free compound/SS with the enzyme.

The enzymatic kinetics of anti-elastase and anti-tyrosinase activity were further elaborated with a model of Michaelis-Menten kinetics to extrapolate the V_{\max} and K_m values, as reported in Table 4.

For the V_{\max} of anti-elastase activity, no differences were observed among the samples and the negative control ($p > 0.05$), while the K_m of unloaded SNPs was significantly higher than the negative control ($p = 0.0107$). Regarding the anti-tyrosinase activity, the statistical analysis revealed no differences in the K_m and V_{\max} of all samples with respect to the negative control ($p > 0.05$). The calculation of V_{\max} and K_m values provides more information about the inhibition mechanism. In particular, a distinction between enzyme inactivators and inhibitors can be made. Enzyme inactivators generally induce conformational changes, also mediated by the solvent molecules, in the tertiary and quaternary structure of the enzyme [48]. True inhibitors, instead, act according to a competitive, non-competitive, and mixed type (competitive/non-competitive) mechanism, modifying the kinetics of the enzyme, and thus K_m and V_{\max} . According to the literature, flavonoids, such as P and Q, and catechins, such as E, act as elastase and tyrosinase inactivators by forming hydrophobic interactions with the enzymes, thus inducing a conformational change, or by chelating metals [45].

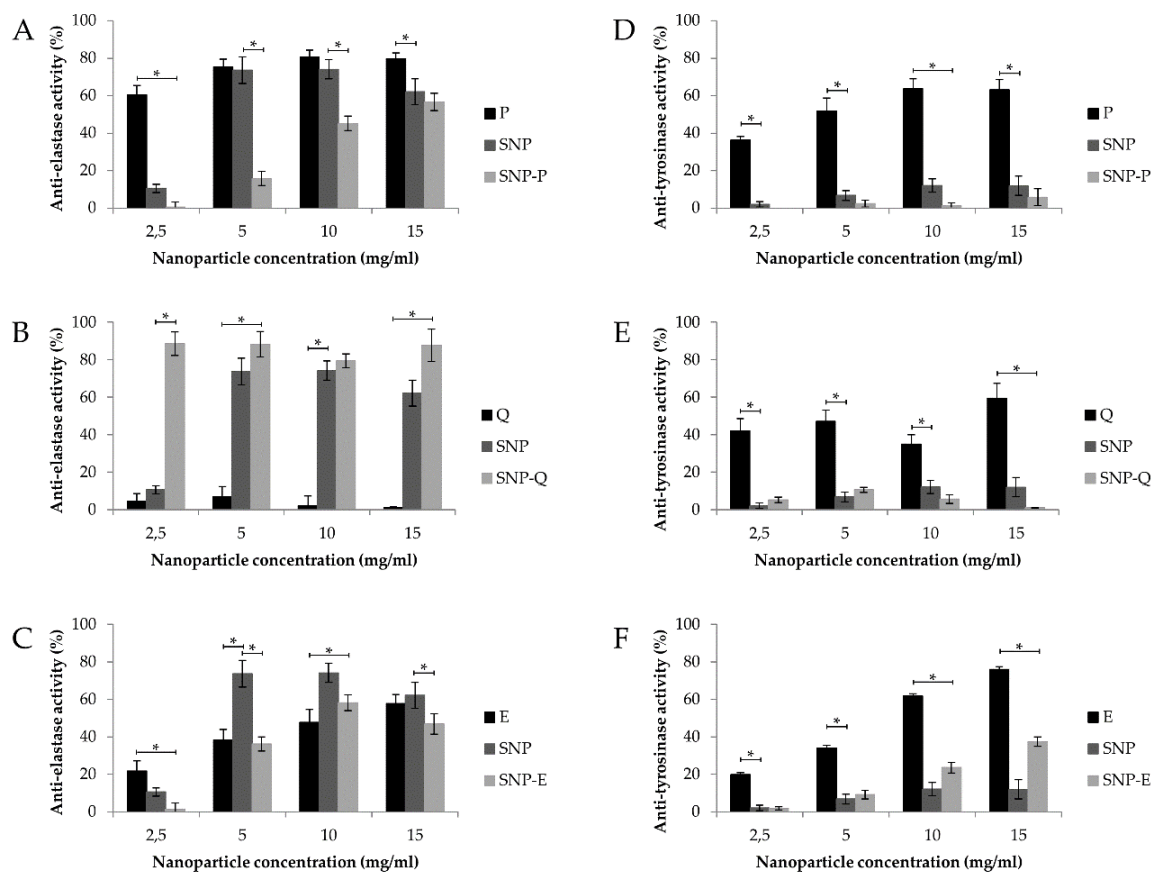


Figure 6: *In vitro* anti-elastase (A–C) and anti-tyrosinase (D–F) activity of SNP, SNP-P, SNP-Q and SNP-E, and an equivalent amount of free drug (P, Q and E). Data are reported as mean values \pm standard deviation, $n = 3$. * denotes a statistically significant difference ($p < 0.05$).

Sample	Anti-Elastase Activity				Anti-Tyrosinase Activity			
	K_m		V_{max}		K_m		V_{max}	
	Mean	SE	Mean	SE	Mean	SE	Mean	SE
SNP	233.65 ^a	51.147 ^a	2.94 ^a	0.982	66.91 ^{a,b}	39.928	2.71 ^{a,b,c}	0.940
SNP-P	37.30 ^{b,c}	36.166 ^{a,b}	1.09 ^{a,b}	0.694	78.37 ^{a,b}	46.105	4.11 ^{b,c}	1.086
SNP-Q	9.74 ^{b,c}	36.166 ^{a,b}	0.80 ^{a,b}	0.694	91.48 ^{a,b}	39.928	4.67 ^c	0.940
SNP-E	109.145 ^{a,b}	36.166 ^{a,b}	2.00 ^{a,b}	0.694	183.37 ^b	46.105	4.68 ^{b,c}	1.086
P	47.16 ^{b,c}	36.166 ^b	0.46 ^b	0.694	14.47 ^a	39.928	0.43 ^a	0.941
Q	10.02 ^{b,c}	36.166 ^{a,b}	0.78 ^{a,b}	0.694	81.79 ^{a,b}	46.105	1.55 ^{a,b}	1.085
E	41.37 ^{b,c}	21.809 ^b	0.51 ^b	0.419	226.5 ^b	79.857	6.69 ^c	1.881
CTR -	10.50 ^c	27.339 ^{a,b}	1.83 ^{a,b}	0.525	42.09 ^a	3.018	2.12 ^{a,b}	0.711

Table 4: V_{max} and K_m values for each sample analyzed. Multifactor ANOVA, mean values \pm standard error, $n = 9$. Different letters (a, b, c) indicate significant differences between the means ($p < 0.05$), whereas the same letter indicates no significant difference ($p > 0.05$).

The SS mechanism of action in inhibiting elastase and tyrosinase enzymes has not yet been deeply investigated. It can be supposed that SS anti-elastase and anti-tyrosinase properties are the result of different mechanisms, which include the chelation of metals (such as copper and iron), the reducing ability of amino acids (e.g., serine, threonine, and aromatic amino acids) and the presence of secondary metabolites, such as flavonoids [49, 50]. In this work, for both elastase and tyrosinase, all the samples were shown to be enzyme inactivators, with the exception of unloaded SNPs which increased K_m and left V_{max} unchanged, thus demonstrating they act as competitive inhibitors of elastase, directly binding to the active site of the enzyme. Figure 7 reports the percentage of MSC cell metabolic activity values after treatment, at the highest concentration (0.8 mg/mL), with unloaded and loaded SNPs and the equivalent amount of free actives.

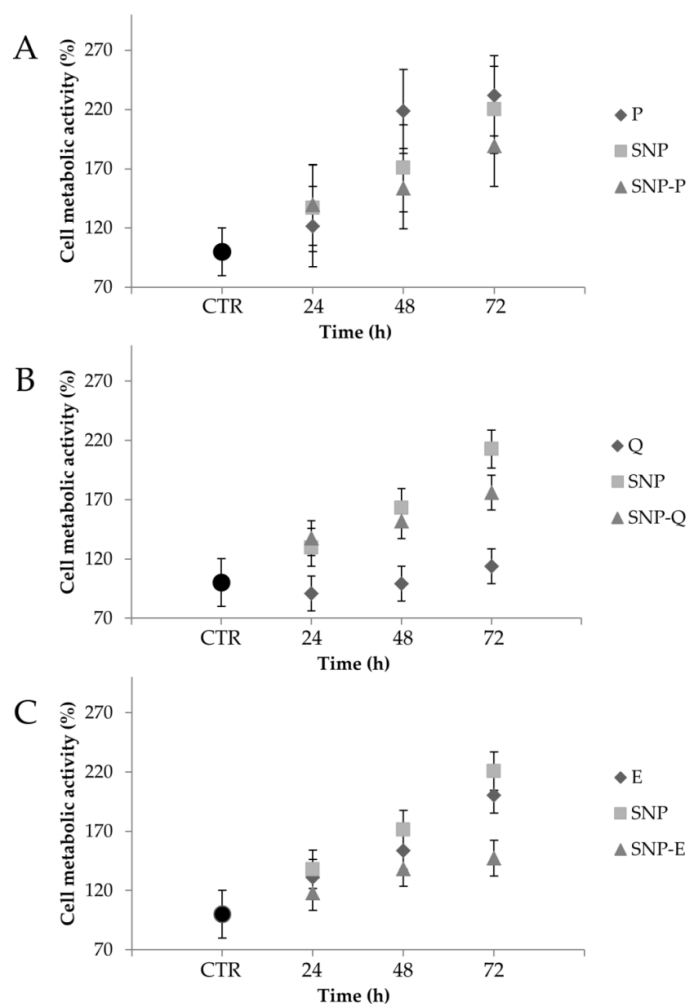


Figure 7: Cell metabolic activity % of mesenchymal stem/stromal cells (MSCs) treated with the highest dosage (0.8 mg/mL) of SNP, SNP-P (A), SNP-Q (B) and SNP-E (C), and the equivalent amount of free drug (P, Q and E). Untreated cells were considered as CTR (100% of metabolic activity). Multifactor ANOVA, mean values \pm least significant difference (LSD), $n = 3$

No cytotoxic effects were revealed. Statistical analysis revealed that sample concentration was not significant ($p = 0.634$); therefore, only the highest concentration tested (0.8 mg/mL) is reported in the figure. The metabolic activity of the untreated cells (CTR) was not modified over time ($p > 0.05$). Instead, after addition of all the samples, a time-dependent increase ($p < 0.05$) in the cell metabolic activity % was observed with respect to FBS-free medium (CTR). Statistical analysis revealed no differences among SNP, SNP-P and P ($p > 0.05$) at all considered times (Figure 7A). After 72 h, the cell metabolic activity of MSCs treated with E and unloaded SNPs was higher than SNP-E ($p < 0.05$). A significant increase in the cell metabolic activity was observed only for Q, at all the considered times, when encapsulated into SNPs ($p < 0.05$). The increased cell metabolic activity after treatment with SNPs can be related to the well-known mitogen effect of SS [18, 51, 52]. To the best of our knowledge, the proliferation ability of P has not been reported on MSCs, however, it has shown good regenerative properties on other cell lines [53]. Similar to the findings of Kim and colleagues, an inhibition in cell metabolic activity was observed when treating MSCs with Q [54]. This effect was avoided after encapsulation into SNPs. Finally, other authors have reported the ability of E in enhancing the cell proliferation and differentiation of adipose-derived MSCs [55]. Interestingly, the same authors reported that E enhanced MSC differentiation into endothelial progenitor cells, thus supporting the employment of such an active for tissue regeneration purposes.

Figure 8 compares the results of *in vitro* evaluation of SNP protective effect against oxidative damage of MSCs. Exposure to H_2O_2 1.5 mM lowered the cell metabolic activity % significantly ($p < 0.05$), thus proving the suitability of the experimental conditions (both H_2O_2 concentration and contact time) in inducing oxidative damage. All the samples were shown to protect MSCs from oxidative stress as the cell metabolic activity % was significantly higher than CTR in their presence ($p < 0.05$). SNP-P highly protected MSCs against H_2O_2 damage ($p < 0.05$) in a dose-dependent manner, while no differences were found between P and SNP ($p > 0.05$). The same trend was observed for SNP-E, which protected cells much more significantly than E and SNP ($p < 0.05$). Instead, for Q, the encapsulation into SNPs did not increase the oxidative stress protection. Overall, the cytoprotective properties can be attributed to both SS and the active ingredients, for which the antioxidant properties are well-reported in the literature, as reported in the previous sections. Overall, the inclusion of the active in SNPs increased the cytoprotective properties, probably as a consequence of increased cell uptake, as previously demonstrated [28].

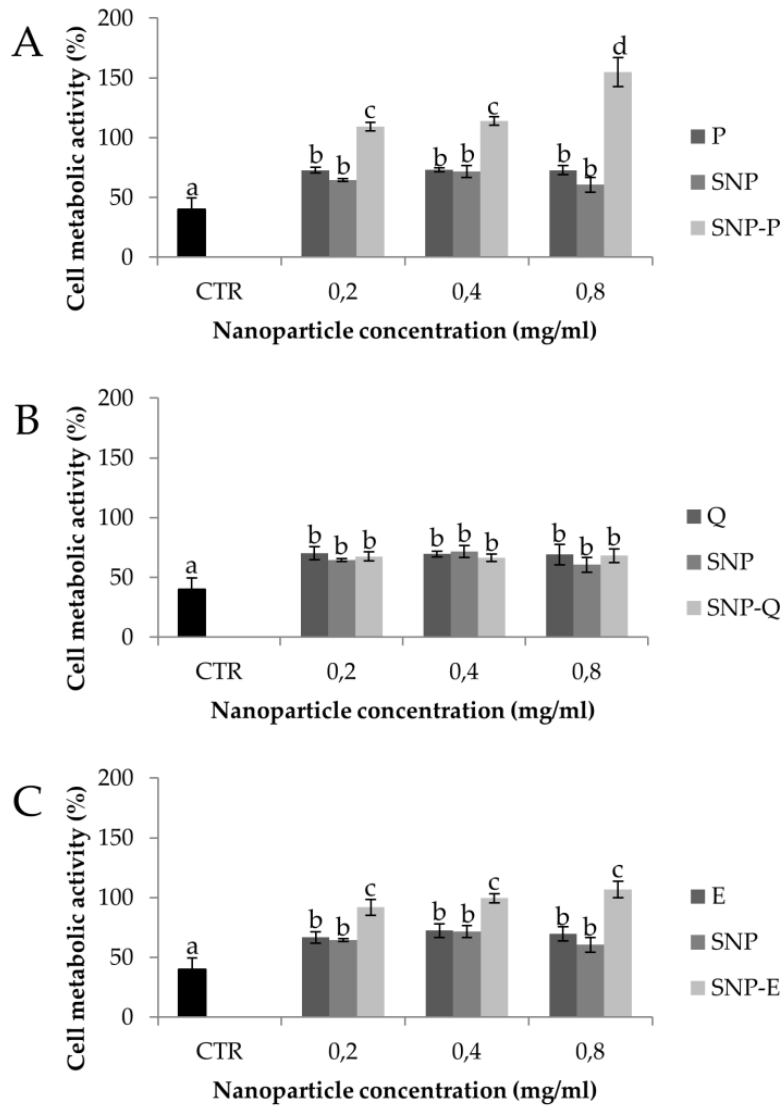


Figure 8: Cytoprotective properties of SNP-P (A), SNP-Q (B), SNP-E (C) compared to unloaded nanoparticles (SSNP) and the equivalent amount of free drugs on MSCs treated with H_2O_2 1.5 mM for 24 h (CTR). Multifactor ANOVA, mean values \pm least significant difference (LSD), $n = 3$. Different letters (a, b, c) indicate significant differences between the means ($p < 0.05$), whereas the same letter indicates no significant difference ($p > 0.05$)

4. Conclusions

In this paper, SNPs were prepared by exploiting a self-assembly method with poloxamer for targeting naturally-derived flavonoids (P, Q and E) to MSCs. SNPs had a diameter less than 150 nm, rounded morphology, and were able to encapsulate both hydrophilic (P and E) and hydrophobic (Q) drugs, without significantly influencing particle size distribution or morphology. Physical-chemical characterization revealed that SNP integrity was preserved after drug encapsulation. A slow and controlled release profile was obtained from SNPs for all the actives in PBS, while in EtOH, a burst release was revealed for Q and E but not for P. Elaboration of drug release data by kinetic models revealed that P presents a lower diffusion index with respect to the other biomolecules, which is reasonable given their higher steric hindrance. For all the actives, in PBS drug release was mainly controlled by case-II relaxation, while in EtOH it was controlled by diffusion. All SNPs showed *in vitro* anti-oxidant, anti-elastase and anti-tyrosinase properties. The loading of P and E into SNPs preserved the *in vitro* biological activity, whereas for Q, the anti-elastase activity was strongly improved. All formulations promoted the metabolic activity of MSCs over 72 h, and protected cells against oxidative stress damage. Both findings can be related to the mitogen and antioxidant properties of both sericin and actives. Overall, the results reported in this paper support the employment of SNPs for targeting naturally-derived flavonoid to tissue resident MSCs for regenerative purposes.

Author Contributions: Conceptualization, E.B., S.F., M.L.T. and S.P.; methodology, G.O. and E.B.; validation, G.O., E.B. and M.L.T.; formal analysis, M.L.T.; investigation, G.O., E.B., L.C., M.S. (Milena Sorrenti) and L.S.; resources, S.F.; writing—original draft preparation, G.O. and E.B.; writing—review and editing, E.B., M.S. (Marzio Sorlini), L.S., C.R.A. and M.L.T.; supervision, E.B., M.L.T. and S.P.; project administration, M.L.T. and S.P.; funding acquisition, M.S. (Marzio Sorlini), M.L.T., L.S. and S.P. All authors have read and agreed to the published version of the manuscript.

Funding: This work was partially supported by Interreg V-A Italy-Switzerland 2014-2020, ATEx-Advanced Therapies Experiences. Project ID 637541.

Acknowledgments: The authors thank Artefil S.r.l. for the doctoral fellowship to O.G., Nembri Industrie Tessili S.r.l., Capriolo, BG, Italy for providing *Bombyx mori* cocoons, and Ilaria Giuseppina Tredici from the Arvedi Laboratory, CISRiC (Centro Interdipartimentale di Studi e Ricerche per la Conservazione del Patrimonio Culturale, Pavia, Italy for the SEM analyses. Also, the contributions by the “5 per mille” research grants to the Rizzoli Orthopaedic Institute of Bologna and by the RFO and Pallotti Legacy research grants to DIMES of the University of Bologna are gratefully acknowledged.

Conflicts of Interest: M.S. (Marzio Sorlini), M.L.T. and S.P. are co-founders and members of the advisory board of the company Pharmaexceed S.r.l. This company had no role in the design of the study, in the collection, analyses, or interpretation of data, in the writing of the manuscript, or in the decision to publish the results.

References

- [1] Y. Fu, L. Karbaat, L. Wu, J. Leijten, S.K. Both, M. Karperien, Trophic Effects of Mesenchymal Stem Cells in Tissue Regeneration, *Tissue Engineering Part B-Reviews* 23(6) (2017) 515-528.
- [2] Y. Li, Q. Wu, Y. Wang, L. Li, H. Bu, J. Bao, Senescence of mesenchymal stem cells, *Int. J. Mol. Med.* 39 (2017) 775-782.
- [3] E. Bari, I. Ferrarotti, M.L. Torre, A.G. Corsico, S. Perteghella, Mesenchymal stem/stromal cell secretome for lung regeneration: The long way through "pharmaceuticalization" for the best formulation, *Journal of Controlled Release* 309 (2019) 11-24.
- [4] D.Y. Zhang, Y.F. Chen, X.B. Xu, H.Y. Xiang, Y.Z. Shi, Y. Gao, X.W. Wang, X.F. Jiang, N. Li, J.P. Pan, Autophagy inhibits the mesenchymal stem cell aging induced by D-galactose through ROS/JNK/p38 signalling, *Clinical and Experimental Pharmacology and Physiology* 47(3) (2020) 466-477.
- [5] R.A. Denu, P. Hematti, Effects of Oxidative Stress on Mesenchymal Stem Cell Biology, *Oxidative Medicine and Cellular Longevity* 2016 (2016).
- [6] V.A.D. Alexander, A. Radhakrishnan, P. Subramani, Overviews of Biological Importance of Quercetin: A Bioactive Flavonoid, *Pharmacogn. Rev* 10 (2016) 84-89.
- [7] A. Rauf, M. Imran, T. Abu-Izneid, H. Iahfisham Ul, S. Patel, X.D. Pan, S. Naz, A.S. Silva, F. Saeed, H.A.R. Suleria, Proanthocyanidins: A comprehensive review, *Biomedicine & Pharmacotherapy* 116 (2019).

- [8] L. Bartosikova, J. Necas, Epigallocatechin gallate: a review, *Veterinari Medicina* 63(10) (2018) 443-467.
- [9] S.M. McCarty, S.L. Percival, Proteases and Delayed Wound Healing, *Adv. Wound Care* 2 (2013) 438-447.
- [10] Y.J. Wang, Y.Q. Zhang, Three-layered sericins around the silk fibroin fiber from *Bombyx mori* cocoon and their amino acid composition, *Silk: Inheritance and Innovation - Modern Silk Road* 175-176 (2011) 158-+.
- [11] T. Chlapanidas, S. Farago, G. Lucconi, S. Perteghella, M. Galuzzi, M. Mantelli, M.A. Avanzini, M.C. Tosca, M. Marazzi, D. Vigo, M.L. Torre, M. Faustini, Sericins exhibit ROS-scavenging, anti-tyrosinase, anti-elastase, and in vitro immunomodulatory activities, *International Journal of Biological Macromolecules* 58 (2013) 47-56.
- [12] L. Lamboni, M. Gauthier, G. Yang, Q. Wang, Silk sericin: A versatile material for tissue engineering and drug delivery, *Biotechnology Advances* 33(8) (2015) 1855-1867.
- [13] E. Bari, C.R. Arciola, B. Vigani, B. Crivelli, P. Moro, G. Marrubini, M. Sorrenti, L. Catenacci, G. Bruni, T. Chlapanidas, E. Lucarelli, S. Perteghella, M.L. Torre, In Vitro Effectiveness of Microspheres Based on Silk Sericin and *Chlorella vulgaris* or *Arthrospira platensis* for Wound Healing Applications, *Materials* 10(9) (2017).
- [14] B. Crivelli, S. Perteghella, E. Bari, M. Sorrenti, G. Tripodo, T. Chlapanidas, M.L. Torre, Silk nanoparticles: from inert supports to bioactive natural carriers for drug delivery, *Soft Matter* 14(4) (2018) 546-557.
- [15] E. Bari, S. Perteghella, S. Farago, M.L. Torre, Association of silk sericin and platelet lysate: Premises for the formulation of wound healing active medications, *International Journal of Biological Macromolecules* 119 (2018) 37-47.
- [16] P. Aramwit, T. Siritientong, T. Srichana, Potential applications of silk sericin, a natural protein from textile industry by-products, *Waste Management & Research* 30(3) (2012) 217-224.
- [17] M. Nardini, S. Perteghella, L. Mastracci, F. Grillo, G. Marrubini, E. Bari, M. Formica, C. Gentili, R. Cancedda, M.L. Torre, M. Mastrogiacomo, Growth Factors Delivery System for Skin Regeneration: An Advanced Wound Dressing, *Pharmaceutics* 12(2) (2020).
- [18] E. Bari, S. Perteghella, G. Marrubini, M. Sorrenti, L. Catenacci, G. Tripodo, M. Mastrogiacomo, D. Mandracchia, A. Trapani, S. Farago, P. Gaetani, M.L. Torre, In vitro efficacy of silk sericin microparticles and platelet lysate for intervertebral disk regeneration, *International Journal of Biological Macromolecules* 118 (2018) 792-799.

- [19] P. Aramwit, R. Yamdech, S. Ampawong, Controlled Release of Chitosan and Sericin from the Microspheres-Embedded Wound Dressing for the Prolonged Anti-microbial and Wound Healing Efficacy, *Aaps Journal* 18(3) (2016) 647-658.
- [20] K. Suktham, T. Koobkokuad, T. Wutikhun, S. Surassmo, Efficiency of resveratrol-loaded sericin nanoparticles: Promising bionanocarriers for drug delivery, *International Journal of Pharmaceutics* 537(1-2) (2018) 48-56.
- [21] B.B. Mandal, S.C. Kundu, Self-assembled silk sericin/poloxamer nanoparticles as nanocarriers of hydrophobic and hydrophilic drugs for targeted delivery, *Nanotechnology* 20(35) (2009).
- [22] K.Y. Cho, J.Y. Moon, Y.W. Lee, K.G. Lee, J.H. Yeo, H.Y. Kweon, K.H. Kim, C.S. Cho, Preparation of self-assembled silk sericin nanoparticles, *International Journal of Biological Macromolecules* 32(1-2) (2003) 36-42.
- [23] O.I. Parisi, M. Fiorillo, L. Scrivano, M.S. Sinicropi, V. Dolce, D. Iacopetta, F. Puoci, A.R. Cappello, Sericin/Poly(ethylcyanoacrylate) Nanospheres by Interfacial Polymerization for Enhanced Bioefficacy of Fenofibrate: In Vitro and In Vivo Studies, *Biomacromolecules* 16(10) (2015) 3126-3133.
- [24] L. Huang, K.X. Tao, J. Liu, C. Qi, L.M. Xu, P.P. Chang, J.B. Gao, X.M. Shuai, G.B. Wang, Z. Wang, L. Wang, Design and Fabrication of Multifunctional Sericin Nanoparticles for Tumor Targeting and pH-Responsive Subcellular Delivery of Cancer Chemotherapy Drugs, *Acs Applied Materials & Interfaces* 8(10) (2016) 6577-6585.
- [25] J. Kanoujia, M. Singh, P. Singh, S.A. Saraf, Novel genipin crosslinked atorvastatin loaded sericin nanoparticles for their enhanced antihyperlipidemic activity, *Materials Science & Engineering C-Materials for Biological Applications* 69 (2016) 967-976.
- [26] N. Hazeri, H. Tavanai, A.R. Moradi, Production and properties of electrosprayed sericin nanopowder, *Science and Technology of Advanced Materials* 13(3) (2012).
- [27] S. Perteghella, B. Crivelli, L. Catenacci, M. Sorrenti, G. Bruni, V. Necchi, B. Vigani, M. Sorlini, M.L. Torre, T. Chlapanidas, Stem cell-extracellular vesicles as drug delivery systems: New frontiers for silk/curcumin nanoparticles, *International Journal of Pharmaceutics* 520(1-2) (2017) 86-97.
- [28] W. Guo, L. Deng, J. Yu, Z. Chen, Y. Woo, H. Liu, T. Li, T. Lin, H. Chen, M. Zhao, L. Zhang, G. Li, Y. Hu, Sericin nanomicelles with enhanced cellular uptake and pH-triggered release of doxorubicin reverse cancer drug resistance, *Drug Delivery* 25(1) (2018) 1103-1116.
- [29] P. Couvreur, Nanoparticles in drug delivery: Past, present and future, *Advanced Drug Delivery Reviews* 65(1) (2013) 21-23.

- [30] B. Crivelli, E. Bari, S. Perteghella, L. Catenacci, M. Sorrenti, M. Mocchi, S. Farago, G. Tripodo, A. Prina-Mello, M.L. Torre, Silk fibroin nanoparticles for celecoxib and curcumin delivery: ROS-scavenging and anti-inflammatory activities in an in vitro model of osteoarthritis, *European Journal of Pharmaceutics and Biopharmaceutics* 137 (2019) 37-45.
- [31] D. Caccavo, An overview on the mathematical modeling of hydrogels' behavior for drug delivery systems, *International Journal of Pharmaceutics* 560 (2019) 175-190.
- [32] E. Bari, S. Perteghella, D. Di Silvestre, M. Sorlini, L. Catenacci, M. Sorrenti, G. Marrubini, R. Rossi, G. Tripodo, P. Mauri, M. Marazzi, M.L. Torre, Pilot Production of Mesenchymal Stem/Stromal Freeze-Dried Secretome for Cell-Free Regenerative Nanomedicine: A Validated GMP-Compliant Process, *Cells* 7(11) (2018).
- [33] F.S.R. della Cuna, J. Calevo, E. Bari, A. Giovannini, C. Boselli, A. Tava, Characterization and Antioxidant Activity of Essential Oil of Four Sympatric Orchid Species, *Molecules* 24(21) (2019).
- [34] E. Bari, I. Ferrarotti, D. Di Silvestre, P. Grisoli, V. Barzon, A. Balderacchi, M.L. Torre, R. Rossi, P. Mauri, A.G. Corsico, S. Perteghella, Adipose Mesenchymal Extracellular Vesicles as Alpha-1-Antitrypsin Physiological Delivery Systems for Lung Regeneration, *Cells* 8(9) (2019).
- [35] M. Dominici, K. Le Blanc, I. Mueller, I. Slaper-Cortenbach, F.C. Marini, D.S. Krause, R.J. Deans, A. Keating, D.J. Prockop, E.M. Horwitz, Minimal criteria for defining multipotent mesenchymal stromal cells. The International Society for Cellular Therapy position statement, *Cytotherapy* 8(4) (2006) 315-317.
- [36] N.A.N. Hanafy, M. El-Kemary, S. Leporatti, Micelles Structure Development as a Strategy to Improve Smart Cancer Therapy, *Cancers* 10(7) (2018).
- [37] R. Khonkarn, S. Mankhetkorn, W.E. Hennink, S. Okonogi, PEG-OCL micelles for quercetin solubilization and inhibition of cancer cell growth, *Eur. J. Pharm. Biopharm.* 79 (2011) 268-275.
- [38] Y. Li, L. Yang, Driving forces for drug loading in drug carriers, *Journal of Microencapsulation* 32(3) (2015) 255-272.
- [39] S. Sunoqrot, A. Alsadi, O. Tarawneh, R. Hamed, Polymer type and molecular weight dictate the encapsulation efficiency and release of Quercetin from polymeric micelles, *Colloid and Polymer Science* 295(10) (2017) 2051-2059.
- [40] L. Catenacci, M. Sorrenti, G. Bruni, C.M. Bonferoni, G. Sandri, G. Bettinetti, Characterization of silver sulfadiazine-loaded solid lipid nanoparticles by thermal analysis, *Journal of Thermal Analysis and Calorimetry* 111(3) (2013) 2149-2155.

- [41] N.A. Peppas, J.J. Sahlin, A SIMPLE EQUATION FOR THE DESCRIPTION OF SOLUTE RELEASE .3. COUPLING OF DIFFUSION AND RELAXATION, *International Journal of Pharmaceutics* 57(2) (1989) 169-172.
- [42] Y.S. Park, M.H. Jeon, H.J. Hwang, M.R. Park, S.H. Lee, S.G. Kim, M. Kim, Antioxidant activity and analysis of proanthocyanidins from pine (*Pinus densiflora*) needles, *Nutrition Research and Practice* 5(4) (2011) 281-287.
- [43] T. Hatahet, M. Morille, A. Shamseddin, A. Aubert-Pouessel, J.M. Devoisselle, S. Begu, Dermal quercetin lipid nanocapsules: Influence of the formulation on antioxidant activity and cellular protection against hydrogen peroxide, *International Journal of Pharmaceutics* 518(1-2) (2017) 167-176.
- [44] S. Legeay, M. Rodier, L. Fillon, S. Faure, N. Clere, Epigallocatechin Gallate: A Review of Its Beneficial Properties to Prevent Metabolic Syndrome, *Nutrients* 7(7) (2015) 5443-5468.
- [45] Y.H. Hong, E.Y. Jung, D.O. Noh, H.J. Suh, Physiological effects of formulation containing tannase-converted green tea extract on skin care: physical stability, collagenase, elastase, and tyrosinase activities.
- [46] S. Pientaweeratch, V. Panapisal, A. Tansirikongkol, Antioxidant, anti-collagenase and anti-elastase activities of *Phyllanthus emblica*, *Manilkara zapota* and silymarin: an in vitro comparative study for anti-aging applications, *Pharmaceutical Biology* 54(9) (2016) 1865-1872.
- [47] M.A. Bos, B. Vennat, M.T. Meunier, M.P. Pouget, A. Pourrat, J. Fialip, Procyanidins from tormentil: Antioxidant properties towards lipoperoxidation and anti-elastase activity, *Biological & Pharmaceutical Bulletin* 19(1) (1996) 146-148.
- [48] S. Zolghadri, A. Bahrami, M.T.H. Khan, J. Munoz-Munoz, F. Garcia-Molina, F. Garcia-Canovas, A.A. Saboury, A comprehensive review on tyrosinase inhibitors, *Journal of Enzyme Inhibition and Medicinal Chemistry* 34(1) (2019) 279-309.
- [49] N. Kato, S. Sato, A. Yamanaka, H. Yamada, N. Fuwa, M. Nomura, Silk protein, sericin, inhibits lipid peroxidation and tyrosinase activity, *Bioscience Biotechnology and Biochemistry* 62(1) (1998) 145-147.
- [50] I. Kubo, I. Kinst-Hori, Flavonols from saffron flower: Tyrosinase inhibitory activity and inhibition mechanism, *J. Agric. Food Chem.* 47 (1999) 4121-4125.
- [51] T.T. Cao, Y.Q. Zhang, Processing and characterization of silk sericin from *Bombyx mori* and its application in biomaterials and biomedicines, *Materials Science & Engineering C-Materials for Biological Applications* 61 (2016) 940-952.

- [52] S. Sapru, S. Das, M. Mandal, A.K. Ghosh, S.C. Kundu, Nonmulberry silk protein sericin blend hydrogels for skin tissue regeneration - in vitro and in vivo, *International Journal of Biological Macromolecules* 137 (2019) 545-553.
- [53] D. Kulakowski, A.A. Leme-Kraus, J.W. Nama, J. McAlpine, S.N. Chen, G.F. Pauli, S. Ravindran, A.K. Bedran-Russo, Oligomeric proanthocyanidins released from dentin induce regenerative dental pulp cell response, *Acta Biomaterialia* 55 (2017) 262-270.
- [54] Y.J. Kim, Y.C. Bae, K.T. Suh, J.S. Jung, Quercetin, a flavonoid, inhibits proliferation and increases osteogenic differentiation in human adipose stromal cells, *Biochemical Pharmacology* 72(10) (2006) 1268-1278.
- [55] W. Widowati, C. Tan Sardjono, C. Wijaya, D.R. Laksmiawati, F. Sandra, Extract of *Curcuma longa* L. and (-)-Epigallo Catechin-3-Gallate Enhanced Proliferation of Adipose Tissue-derived Mesenchymal Stem Cells (AD-MSCs) and Differentiation of AD-MSCs into Endothelial Progenitor Cells, *J. US China Med. Sci.* 9 (2012) 22-29.

SUPPLEMENTARY MATERIAL

Isolation and Expansion of Human Adipose-Derived Mesenchymal Stromal Cells

Adipose tissues were obtained from three patients (mean age was 47 ± 4) undergoing abdominoplasty surgery after informed consent (ASST Grande Ospedale Metropolitano Niguarda, Milan). Clinical sheets of donors (identity, gender, age, tissue processing, sampling site, the day of collection and anamnesis) were filed by the surgery-responsible structure. Donors with septicemia or extensive infections, syphilis, type B and C hepatitis, HIV, Creutzfeld-Jacobs disease, viral or unknown neurological diseases, human GH treatment, and malignant tumours were excluded from the trial. Tissue samples were repeatedly washed with Phosphate Buffer Saline (PBS, pH= 7.14) without Ca^{2+} and Mg^{2+} and mechanically minced by surgical scissors. Tissue digestion was performed with 0.075% (w/v) type II collagenase solubilized in PBS with Ca^{2+} and Mg^{2+} plus 1% penicillin/streptomycin and 1% (w/v) amphotericin B at 37 °C. After 1 hour, Dulbecco's modified Eagle's Medium (DMEM) and Ham's medium F12 (DMEM/F12, ratio 1:1) supplemented by 10% (v/v) fetal bovine serum (FBS) was added to cell suspension; the digested tissue was filtered on 70 μm cell strainer (Greiner Bio-One, Milan, Italy) and centrifuged at 600 g for 5 min [1,2]. Recovered stromal vascular fraction was cultured in monolayer conditions (100,000 cells/cm²) in DMEM F12, 10% (v/v) FBS, 1% (v/v) penicillin/streptomycin and 1% (v/v) amphotericin B. Once MSCs reached sub-confluence, they were treated with 0.05% (v/v) trypsin-EDTA and seeded onto flasks (10,000 cells/cm²) at 37°C and 5% CO₂ and cultured until P6 in DMEM F12, 10% (v/v) FBS, 1% (v/v) penicillin/streptomycin and 1% (v/v) amphotericin B. All MSCs were tested to assure all the requirements needed for clinical use in terms of identity (according to the International Society for Cellular Therapy), sterility (according to Eu. Ph. 9.0, 2.6.27), tumorigenesis and karyotype.

Supplementary Figure

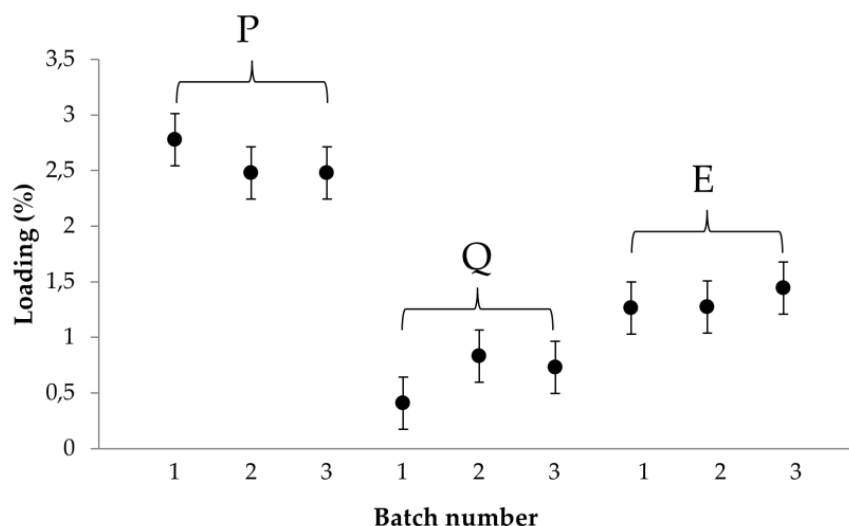


Figure S1. Drug loading (% w/w) of different batches (1, 2 and 3) for SNPs loaded with P, Q and E. Multifactor ANOVA, mean values \pm least significant difference (LSD), $n = 3$

Experiment to Confirm Drug Loading and Drug Release

An additional experiment was performed to confirm the drug loading and drug release data. Drug release experiments were repeated for each formulation in duplicate following the procedures reported in section 2.2.7. Briefly, for each batch 200 mg of SNPs were suspended in 5 ml of dissolution media and put into a dialysis membrane (3.5 kDa MWCO, Thermo Fisher Scientific, Milan, Italy). Each dialysis tube was incubated in 50 mL of dissolution media and maintained under mild magnetic stirring at 37 °C. After 80 h, the amount of released drug was determined by a spectrophotometric method (UV/VIS Spectrometer Lambda20, PerkinElmer, Wellesley, MA, USA) analyzing the release media at 279, 275 and 373 nm for P, E and Q, respectively. The drug concentration was extrapolated from a calibration curve previously prepared (P 5-80 $\mu\text{g/mL}$, $R^2 = 0.99$; Q 0.5-15 $\mu\text{g/mL}$, $R^2 = 0.99$; E 5-30 $\mu\text{g/mL}$, $R^2 = 0.98$). The cumulative amount of released drug was calculated in percentage using the following equation:

$$\text{Cumulative amount of drug released (\%)} = C_i/C_0 \times 100 \quad (\text{S1} \\ 3)$$

where C_i was the amount of the drug released at 80 hours and C_0 was the loaded drug amount. Then, SNPs inside the dialysis bag were recovered and bring to a final volume of 50 mL by using the dissolving media reported in the section 2.2.3. In detail, SNP-P and SNP-E were dissolved in deionized water plus HCl (0.1%, v/v), while SNP-Q were dissolved in ethanol 96% (v/v) maintaining mild magnetic stirring in the dark. The dialysis membranes were repeatedly washed with the abovementioned dissolution media to recover all SNPs. The drug content was measured from standard calibration curves obtained analyzing a concentration range of 10-80 $\mu\text{g/mL}$, $R^2 = 0.99$ for P; 0.5-20 $\mu\text{g/mL}$ for Q, $R^2 = 0.98$; 5-50 $\mu\text{g/mL}$ for E, $R^2 = 0.99$. Data are reported as mean value \pm standard deviation ($n = 2$).

In vitro drug release data confirmed what reported in the text of the manuscript. In EtOH, the percentage of drug released was 21.34 ± 5.639 for SNP-P, 50.69 ± 12.387 for SNP-Q and 63.35 ± 6.581 for SNP-E. In PBS, SNP-P and SNP-E released the 44.72 ± 8.593 and 48.27 ± 7.542 percentage of the whole drug, respectively, while SNP-Q released the 18.47 ± 6.522 . After EtOH release, the amount of drug recovered after dissolution of SNPs was 73.22 ± 2.68 for SNP-P, 44.85 ± 5.986 for SNP-Q and 33.23 ± 4.896 for SNP-E. After PBS release, the amount of drug recovered after dissolving SNPs was 48.87 ± 2.569 for SNP-P, 75.58 ± 9.635 for SNP-Q and 47.58 ± 5.841 for SNP-E. Overall, the results confirmed that the drug not released was retained into SNPs.

References

1. Gaetani, P.; Torre, M.L.; Klinger, M.; Faustini, M.; Crovato, F.; Bucco, M.; Marazzi, M.; Chlapanidas, T.; Levi, D.; Tancioni, F., et al. Adipose-derived stem cell therapy for intervertebral disc regeneration: An in vitro reconstructed tissue in alginate capsules. *Tissue Engineering Part A* **2008**, *14*, 1415–1423, doi:10.1089/ten.tea.2007.0330.
2. Faustini, M.; Bucco, M.; Chlapanidas, T.; Lucconi, G.; Marazzi, M.; Tosca, M.C.; Gaetani, P.; Klinger, M.; Villani, S.; Ferretti, V.V., et al. Nonexpanded Mesenchymal Stem Cells for Regenerative Medicine: Yield in Stromal Vascular Fraction from Adipose Tissues. *Tissue Engineering Part C-Methods* **2010**, *16*, 1515–1521, doi:10.1089/ten.tec.2010.0214.

Eco-sustainable silk sericin from by-product of textile industry can be employed for cosmetic, dermatology and drug delivery

Giulia Orlandi, Silvio Faragò, Silvia Menato, Marzio Sorlini, Fabrizio Butti, Michela Mocchi, Ilaria Donelli, Laura Catenacci, Milena L Sorrenti, Stefania Croce, Lorena Segale, Maria L Torre ✉, Sara Perteghella

Abstract

BACKGROUND: in the last decade, many researchers demonstrated the biological activities of native *Bombyx mori* silk sericin (SS), and its use is widespread in the cosmetic and biomedical field. However, SS is a polluting material from the silk fibroin textile industry. This paper aims to demonstrate that the industrial wastewater-derived SS has many biological properties, and can be used as an eco-friendly product for cosmetic/pharmaceutical purposes with an important impact on the circular economy.

RESULTS: we focused on the SS derived from an ad hoc extraction process or industrial degumming wastewater. Both products were preserved with three different methods: lyophilization, spray-drying and sterilization. All SS were characterized in terms of amino acid content, molecular weight, physical-chemical properties, morphology and size distribution; then we evaluated the biological properties, the cytocompatibility/cytoprotective profile, and the immunomodulatory abilities of SS. Free radical scavenging, anti-tyrosinase, and anti-elastase activities of waste SS were confirmed. Waste and standard SS were cytocompatible on human fibroblasts; all SS samples inhibited the proliferation of stimulated Peripheral Blood Mononuclear Cells in a dose-dependent manner. Waste SS showed a significant effect on tumor necrosis factor α and interleukin 10 release.

CONCLUSIONS: these results pave the way for using textile wastewater-derived SS to obtain high-value-added products for cosmetic and/or pharmaceutical purposes.

Keywords: Silk sericin; textile wastewater; immunomodulatory activity; anti-elastase activity; textile/biomedical circular economy; sericin cytocompatibility.

1. Introduction

Silk produced by *Bombyx mori* silkworms is composed of two main proteins, namely fibroin and sericin. Silk fibroin (SF) is a fibrous protein widely used in textiles, industrial and medical fields whereas silk sericin (SS) is a hydrophilic globular protein proposed as bioactive compound and/or as an excipient for cosmetic and pharmaceutical purposes. [1-4] The numerous research studies carried out on SS have demonstrated that this protein possesses many intrinsic biological properties, such as photo-protective, antioxidant, moisturizing, anti-bacterial, proliferative and immunomodulant. [5-9] According to a 2015 Voluntary Cosmetic Registration Program – FDA survey, it was demonstrated that about 5 000 tons of sericin were used only in the USA, and only for cosmetics, every year. [10]

Before using SF and SS, it is necessary to separate the proteins by degumming processes (extraction in boiling water, alkaline extraction, and extraction in an autoclave). [11] SS tested until now, is derived by an ad hoc degumming process performed on *Bombyx mori* cocoons in research laboratories or industries producing sericin. [9, 12] Despite the interesting biological properties of SS, this protein still represents a by-product of the textile industry; the discarded degumming wastewater leads to environmental contamination and requires high oxygen demand for microbe-mediated degradation. According to circular economy fundamentals, it could be advantageous to recover and reuse this product in cosmetics and/or pharmaceutical fields.

In the last decade, the circular economy had much resonance as a way to use resources more sustainably, reducing produced wastes and environmental pollution. [13] In the textile industry, the possibility to reuse SS as a bioactive excipient in pharmaceutical and cosmetic fields can be a concrete example of the adoption of the circular economy measures. The industrial degumming process exploits the addition of soap, alkalis, acids or organic amines to the water to remove SS more effectively, producing large amounts of SS into wastewater as pure waste. Properly treating SS-rich wastewater allows SS extraction, recovery and reuse, resulting in significant environmental, economic and social benefits. The textile company can experience reduced economic and environmental impacts: on one side, revenue can be generated by selling recovered SS; on the other, it reduces the processing costs of wastewater treatment. The filtration method can be used to extract SS, processing 50 L/h of SS-rich wastewater with half the energy consumption and an 80% reduction in production cost compared with the traditional lyophilization equipment adopted in the pharma industry. [14] To date, there are two reasons why those volumes are not recovered for cosmetics and

pharmaceutical use: first, the quality of the SS fraction could be related to the degumming method, which leads to high sericin degradation, limiting its effectiveness in cosmetics applications; [15] second, the discharged SS-rich wastewater has to be treated in order to remove water from the solution. Several technologies can be used for this activity, including lyophilization, spray-drying and ultrafiltration. All of these require additional consumption of energy and the provision of equipment.

Despite the advantages related to the recycling of wastewater product, the use of SS obtained from textile industry presents some limitations. In particular, the SS was in aqueous solution, and this physical form promotes microbial growth, reducing protein stability over time. To overcome this problem, it is possible to dry or sterilize the product.

This work aims to examine and demonstrate, for the first time, the feasibility of the pharmaceutical and cosmetic use of SS recovered from textile industry wastewater. This aim can be achieved with the physical-chemical characterization and determination of the *in vitro* biological properties, hence demonstrating, that the employment of waste sericin in a plethora of cosmetic, cosmeceutical and pharmaceutical products will be possible as an easily recoverable ingredient for cleverly sustainably closing the circular loop.

2. Materials and methods

2.1 SS sample preparation

In this study, we combined two different sources of SS (an ad hoc degumming process developed in the laboratory or industrial wastewater containing SS and other compounds), and three different technological processes as preservation methods (lyophilization, spray-drying and sterilization) (Table 1). For all experiments, we used *Bombyx mori* poly-hybrid cocoons (white monovoltine).

Concerning the ad hoc degumming process, we used a simple method, previously reported in the literature, [5, 9, 12, 16] which allowed us to obtain a water-based SS solution and that was different from the degumming technique adopted in the textile industry (aimed at optimizing the characteristic of silk fibroin). Briefly, cocoons (supplied by Nembri Industrie Tessili S.r.l., Capriolo, BG, Italy) were cut and boiled in an autoclave (Systec V-65, Wurttemberg, Germany) at 120 °C for 30 min (20 mL water per gram of cocoons).

Regarding the industrial degumming, the textile industry started from silk yarns (20/22 Den-22.444 Tex) purchased by a silk factory in Sichuan (China). Yarns are obtained by the immersion of *Bombyx mori* cocoons in hot water (40-50 °C), and by subsequent brushing and

reeling procedures; all these steps are needed to stitch the seven single cocoon filaments need to obtain a silk yarn of 20/22 Den. For the wastewater-derived SS extraction, each silk yarn was subjected to an autoclave (100 °C, 30 min) degumming process using a commercial carbonate-based alkaline soap (GP SOLV PHT, GP TEXTRON S.r.l., CO, Italy; the chemical composition is not available because is patented). At the end of the extraction, obtained SS solution (containing alkaline soap) was concentrated and purified by the ultrafiltration technique (ceramic membranes, molecular cut off 15 kDa, a pump of 7.5 kW, pressure 2.5 Bar).

All obtained aqueous SS solutions (from both lab-scale and industrial process) were divided into three aliquots subjected to three different technological processes: lyophilization, spray-drying and sterilization. For the lyophilization, the samples were frozen at -80 °C and freeze-dried (Modulyo® Edwards Freeze dryer, Kingston, New York, USA) at 8×10^{-1} mbar and -50 °C for a week. The freeze-dried products were then stored at room temperature until the use.

Spray-dried samples were obtained using a Büchi Mini Spray-Dryer (Flawil, Switzerland), equipped with a nozzle. In particular, both SS solutions (obtained by the ad hoc lab-scale process and by the industrial wastewater) were processed considering the same concentration range (0.8-1.4% w/w) and with the same process parameters: pump 6 mL/min; inlet temperature 120 °C; outlet temperature 80 °C; air pressure 3 bar; fluid flow 500-600 mL/h.

The sterilization process was performed using a cycle of the SS solutions in an autoclave (Systec V-65, Wurttemberg, Germany) at 121 °C for 15 min, as reported in Pharmacopoeia.

For each treatment group (Table 1), three batches were prepared and analyzed.

ID sample	Source	Treatment
Deg-Lyo	Degumming	Lyophilization
Deg-Spray	Degumming	Spray-drying
Deg-Ster	Degumming	Sterilization
Waste-Lyo	Wastewater	Lyophilization
Waste-Spray	Wastewater	Spray-drying
Waste-Ster	Wastewater	Sterilization

Table 1: Sericin samples considered for the study

2.2 SS Characterization

The effect of SS source (lab-scale degumming water or wastewater) on amino acid composition was evaluated analyzing the freeze-dried samples (Deg-Lyo and Waste-Lyo).

All SS samples (Table 1) were characterized in terms of molecular weight distribution by sodium dodecyl sulfate-polyacrylamide gel electrophoresis (SDS-PAGE), physical-chemical properties by Fourier transform infrared spectroscopy (FTIR) and differential scanning calorimetry (DSC). Moreover, morphology and particle size distribution were evaluated by scanning electron microscopy (SEM) and dynamic light scattering (DLS), respectively.

2.2.1 Determination of the amino acid composition

The amino acid sequence of freeze-dried SS was evaluated through ion-exchange chromatography using an automatic amino analyzer (Biochrom 30+, Cambridge, UK), after acid hydrolysis of the protein. Freeze-dried samples were treated with HCl (6 mol/L) and phenol as a stabilizer, for 24 h at 110 °C. The samples were injected into a pre-column and then into a cation-exchange resin column at a checked temperature; as eluents, six buffer solutions, with different pH and ionic strength, were considered to separate the amino acids according to their affinity for the mobile and stationary phases. At the end of the chromatographic run, the eluent-sample mixtures were treated with ninhydrin, a highly selective indicator for the amino acids, which reacts with amino groups, leading to a purple-coloured complex. This so-called complex was analyzed with a spectrophotometer at 570 and 440 nm.

2.2.2 Electrophoresis

The molecular weight of the SS samples was evaluated using a vertical Mini-PROTEAN Tetra cell system (Bio-Rad, Milan, Italy). Two different running polyacrylamide gel concentrations were considered to evaluate low and high molecular weights (12% and 6%, respectively); stacking gels were used at 4%. SS samples were solubilized in bidistilled water at 70 °C to obtain solutions at the concentration of 10 mg/mL. The solutions were then dissolved in the reduced sample buffer (0.5 mol/L Tris-HCl, pH 6.8), containing bidistilled water, glycerol, SDS 10% w/v and Coomassie Brilliant Blue, in the presence of β -mercaptoethanol (ratio of sample to reduced sample buffer was 1:1) at 70 °C for 1 h. Two

standards were used to identify high and low molecular weights. The high molecular weight markers were myosin, α_2 -macroglobulin, β -galactosidase, transferrin, and glutamic dehydrogenase (Amersham HMW calibration kit 17-0615-01); the low molecular weight markers were phosphorylase B, albumin, ovalbumin, carbonic anhydrase, trypsin inhibitor and α -lactalbumin (Amersham LMW calibration kit 17-0446-01). When the electrophoretic run had finished, the gels were coloured with Coomassie Brilliant Blue 0.1%, ethanol 40% and acetic acid 10% overnight, followed by two bleaching steps: the first (40% methanol, 7% acetic acid) for 1 h and the second (5% methanol, 7% acetic acid) for 1 h, until the markers bands appeared.

2.2.3. FTIR spectroscopy

FTIR spectra of the dried samples (Deg-Lyo, Waste-Lyo, Deg-Spray and Waste-Spray) were obtained using a spectrophotometer (Spectrum One, Perkin-Elmer, Wellesley, MA, USA) equipped with a MIRacle™ ATR device (Pike Technologies, Madison, WI, USA). The IR spectra in transmittance mode were obtained in the spectral region of 650-4000 cm^{-1} by the accumulation of 64 scans with a resolution of 4 cm^{-1} .

2.2.4 Differential scanning calorimetry

Temperature and enthalpy values were measured with a Mettler STARE system (Mettler Toledo, Italy) equipped with DSC81^e Module and an Intracooler device for sub-ambient temperature analysis (Jukabo FT 900) on 2-3 mg samples (Deg-Lyo, Waste-Lyo, Deg-Spray and Waste-Spray) in 40 μL sealed aluminium pans with pierced lid (method: 10-400 $^{\circ}\text{C}$ temperature range; heating rate $\beta = 10 \text{ K/min}$; nitrogen air atmosphere flux 50 mL/min). The instrument was previously calibrated with indium, as a standard reference, and measurement was carried out at least in triplicate.

2.2.5 Simultaneous thermogravimetric analysis (TGA/DSC 1)

Mass losses were recorded with a Mettler STARE system TGA on 3-4 mg samples in 70 μL alumina crucibles with lid (method: 30-400 $^{\circ}\text{C}$ temperature range; heating rate $\beta = 10 \text{ K/min}$;

nitrogen air atmosphere flux 50 mL/min). The instrument was previously calibrated with indium, as a standard reference, and measurement was carried out at least in triplicate.

2.2.6 Morphological investigation

SS sample morphology was investigated using a scanning electron microscope with field emission gun (Mira 3, Tescan, Brno, Czech Republic), high vacuum mode, 15 kV and secondary electrons (SEs) detector. Samples were placed on aluminium stubs and coated with gold-palladium.

2.2.7 Dynamic light scattering

The particle size distribution of SS microparticles (Deg-Spray and Waste-Spray samples) was analyzed with a laser light scattering granulometer equipped with a small cell volume (120 mL, 5% obscuration) (Beckman Coulter LS230, Miami, Fl, USA), setting the refractive index at 1.359 for ethanol. SS powders were dispersed in ethanol (99% v/v) and sonicated for 10 min. The instrument performed five replicates of 90 s each.

2.3 SS *in vitro* biological properties

The biological properties of all SS samples were investigated in terms of free radical scavenging, anti-tyrosinase, and anti-elastase activity; cytotoxicity and cytoprotective effect against oxidative stress were determined on fibroblasts and immunomodulatory ability on peripheral blood mononuclear cells (PBMCs).

2.3.1 Free radical scavenging activity

The antioxidant activity of the SS samples was evaluated by 2,2-diphenyl-1-picrylhydrazyl (DPPH) colorimetric assay as reported by Fan et al. [17] Briefly, DPPH solution (Sigma Aldrich; 0.0056% w/v in methanol) was added to aqueous SS solutions (2.5, 5, 8 and 10 mg/mL). The reaction mixture, composed of 120 µl of sample and 1080 µl of DPPH, was incubated in the dark at room temperature, and subsequently centrifuged at 3000 x g for 5 min

in order to eliminate sericin-insoluble residues. The supernatant was subjected to spectrophotometric analysis (Synergy HT, BioTek, Swindon, UK) at 515 nm. For each sample, the absorbance data obtained were subtracted from the blank value (reaction mixture in the absence of DPPH). The reaction mixture in the absence of SS was considered as a negative control. The analyses were performed in triplicate. The free radical scavenging percentage activity was calculated using the following formula:

$$\% \text{ activity} = [(A_{\text{ctr}} - A_{\text{samp}}) / A_{\text{ctr}}] * 100$$

where A_{ctr} = negative control absorbance and A_{samp} = SS sample absorbance

2.3.2 Anti-tyrosinase activity

The anti-tyrosinase activity of SS was evaluated by spectrophotometric analysis of the kinetic reaction between the enzyme tyrosinase and L-tyrosine substrate (Sigma Aldrich, Milan, Italy) in accordance with Aramwit. [18] SS samples were tested at concentrations of 2.5, 5, 8 and 10 mg/mL. A stock solution of silk sericin was prepared at a concentration of 10 mg/mL, corresponding to the maximum solubility of the protein in aqueous solution. Then, we diluted the stock solution appropriately to obtain the other selected dilutions. The same principle was adopted to prepare silk sericin samples to evaluate the antioxidant and anti-elastase activity. The enzyme tyrosinase was solubilized in phosphate buffer pH 6.8 to obtain a final concentration of 500 IU/mL. The tyrosinase solution was pre-incubated for 10 min with each SS sample and, consequently, the L-tyrosine substrate was added to the reaction mixture. The enzymatic reaction was spectrophotometrically analyzed (Synergy HT) at 480 nm for 30 min (measurements every minute). The reaction mixture in the absence of sample was used as a negative control, while arbutin (Sigma Aldrich) was considered as a positive control. Each absorbance value obtained during reaction kinetics was subtracted from the absorbance of the white mixture, composed of each SS sample in the absence of enzyme and substrate. All analyses were conducted in triplicate. The results were reported as a percentage anti-tyrosinase activity using the following formula:

$$\% \text{ activity} = [(A_{\text{ctr}} - A_{\text{samp}}) / A_{\text{ctr}}] * 100$$

where A_{ctr} = negative control absorbance and A_{samp} =SS sample absorbance

2.3.3 Anti-elastase activity

The inhibitory effect of each SS sample on the elastase enzyme was evaluated using the method previously described by Nam et al., [19] with some modifications. Pancreatic porcine elastase (Sigma Aldrich) was solubilized in phosphate buffer pH 6.8 (0.5 IU/mL). The substrate N-succinyl-Ala-Ala-Ala-p-nitroanilide (Sigma Aldrich) was diluted in TRIS buffer to obtain a final concentration of 0.41 mmol/L. Each SS sample (2.5, 5, 8, 10 mg/mL) was incubated for 20 min with the enzyme, and subsequently, the substrate was added. The kinetic reaction was monitored by spectrophotometric analysis (Synergy HT) at 410 nm for 35 min (measurements every minute). The reaction mixture in the absence of sample was used as a negative control, while the epigallocatechin gallate (Sigma Aldrich) was considered as a positive control. Each absorbance value of the sample was subtracted from the absorbance of the white mixture (SS sample without enzyme and substrate). All analyses were performed in triplicate. The results were reported as a percentage anti-elastase activity using the following formula:

$$\% \text{ activity} = [(A_{\text{ctr}} - A_{\text{samp}}) / A_{\text{ctr}}] * 100$$

where A_{ctr} = negative control absorbance and A_{samp} = SS sample absorbance

2.3.4 Cytotoxicity evaluation by cell metabolic activity determination (MTT assay)

Human fibroblasts were cultured *in vitro* in Dulbecco's Modified Eagle's Medium (DMEM) High Glucose supplemented with 10% fetal bovine serum, penicillin 100 U/mL, streptomycin 100 µg/mL, amphotericin 0.25 µg/mL, glutamine 4 mmol/L and sodium pyruvate 1 mmol/L. For MTT assay, cells were seeded into 96-well plate (10 000 cells/cm²) and treated for 24 and 48 h (37 °C, 5% CO₂) with SS samples (concentrations: 12, 120, 500, 1000 and 2500 µg/mL). [7, 20] Cells were then washed with phosphate-buffered saline (PBS) and 100 µL 3-(4,5-dimethylthiazol-2-yl)-2,5-diphenyltetrazolium bromide (MTT) solution (0.5 mg/mL) were added to each well. After 3 h of incubation, the MTT solution was removed and 100 µL dimethyl sulfoxide (DMSO) was added. Untreated cells were considered as control (100% metabolic activity). Optical density was measured on Synergy HT at 570 and 670 nm (reference wavelength). Each condition was tested in triplicate.

Cell metabolic activity (%) was calculated as $100 \times (OD_{\text{sample}}/OD_{\text{ctr}})$.

2.3.5 Cytoprotective effect against oxidative stress

Human fibroblasts were seeded in a 96-well plate (10 000 cells/cm²) and treated with each SS sample (120, 500 and 1000 µg/mL). After 24 h of incubation, cells were washed with PBS and treated with hydrogen peroxide (H₂O₂, 0.75 mmol/L) for 24 h. An MTT assay was then performed to evaluate the cell metabolic activity of cells using Synergy HT, as previously described. Untreated cells were considered as control (100% cell metabolic activity). Each condition was tested in triplicate. [8]

2.3.6 Antiproliferative assay and release of tumor necrosis factor α (TNF- α), interferon γ (IFN- γ) and interleukin 10 (IL-10)

Each SS sample was investigated for *in vitro* antiproliferative activity on activated PBMCs. *In vitro* TNF- α , IFN- γ and IL-10 secretion was also evaluated by enzyme-linked immunosorbent assay (ELISA; Tema Ricerca, Bologna, Italy). PBMCs were isolated from the heparinized venous blood of two healthy volunteers by gradient centrifugation (Lym-phoprep, Axis-Shield) [21] and seeded (10 000 cells per well) into the 96-well plate using RPMI 1640 medium added with 10% fetal calf serum (FCS). To evaluate SS immunogenicity, PBMCs were treated with or without SS solutions at the concentrations 12, 120 and 500 µg/mL. After 72 h of treatment, ³H-thymidine (³HTdR, 0.5 µCi per well, Amersham Pharmacia Biotech, Chalfont St Giles, UK) was added to each well, and the radioactivity was measured (TopCount, Packard Instrument, Waltham, MA, USA). Results were expressed as the stimulation index (SI = cpm of treated cultures / cpm of untreated cultures), where cpm of treated cultures were counted for a minute of cells treated with SS. To evaluate SS immunomodulatory activity, PBMCs were treated with or without SS at the above concentrations in the presence of phytohemagglutinin (PHA, 4 µg/mL), maintaining the same culture conditions. Results were expressed as residual proliferation (RP = SI treated / SI untreated*100), where SI treated was calculated from PBMCs cultured in the presence of both SS and PHA, while SI untreated was obtained from PBMCs cultured in the presence of only PHA, without SS samples. The supernatants of PHA-activated PBMCs, cultured with or without SS samples, were also collected to quantify the cytokine release by ELISA according to manufacturer's instructions. IL-10 was chosen as an example of the anti-inflammatory cytokine, with TNF- α and IFN- γ as models of pro-inflammatory cytokines. Absorbance was

measured at 450 nm (Titertek Plus MS 212-ICN, Milan, Italy), and the cytokine concentration (expressed in pg/mL) was calculated with respect to the standard curve.

2.4 Statistical Analysis

STATGRAPHICS XVII (Statpoint Technologies, Inc., Warrenton, VA, USA) was used to analyze the data by a linear generalized analysis of variance model (ANOVA). Fisher's least significant difference (LSD) procedure was applied to evaluate the differences between means.

The free radical scavenging data were elaborated considering the type of sample (source and treatment) and its concentration as fixed factors. To determine the IC₅₀ value of the antioxidant activity that is, the concentration of the silk sericin that provokes a response equal to 50%, the data were elaborated by Graph-Pad Prism software, normalizing the response to run between 0% and 100%. The used model was $Y = 100 / (1 + 10^{(X - \text{Log IC}_{50})})$.

For anti-tyrosinase and anti-elastase results, we considered the time and type of sample and the sample concentration as fixed factors. The enzymatic kinetics of anti-tyrosinase and anti-elastase activity were elaborated with Michaelis-Menten model kinetics, $y = (V_{\text{max}} \times x) / (K_m + x)$, where y is the absorbance at time x , K_m is the moment at which the activity is equal to half the maximum and V_{max} is the maximum speed of the enzyme. [5] Graph-Pad Prism software was used to calculate the curve parameters. For each curve, V_{max} and K_m were analyzed with an analysis of covariance (ANCOVA) model, considering the sample as a fixed factor and the sample concentration as a covariate. The differences between the groups were analysed with the LSD test for multiple comparisons. Cell metabolic activity data, obtained from MTT assay, was analyzed considering the SS concentration, type of sample, incubation time and hydrogen peroxide treatment as fixed factors.

For all the analyses, the statistical significance was set up at $p < 0.05$.

3. Results and discussion

Many research studies have demonstrated that SS extracted from native silk cocoons is a bioactive compound. In our work, we aimed to prove that SS from textile wastewater, maintains its biological properties, and can be employed in an environmentally-sustainable way, reducing produced wastes and environmental pollution. Three different conservation

methods (freeze-drying, spray-drying and sterilization) has been employed to optimize SS shelf-life.

First, the effect of the SS source on the amino acid composition was evaluated by chromatographic analysis, after acid hydrolysis, on Waste-Lyo and Deg-Lyo samples (Table 2).

Amino acid	Retention time	Waste-Lyo	Deg-Lyo
Aspartic acid	14.7	16.07	17.22
Threonine	20	7.97	8.12
Serine	21.8	26.26	28.05
Glutamic acid	27.2	4.47	4.95
Glycine	37.4	8.85	9.52
Alanine	38.6	3.13	3.36
Valine	44.5	2.52	2.72
Isoleucine	55.1	0.59	0.41
Leucine	56.5	1.85	1.29
Tyrosine	59.4	5.17	4.93
Phenylalanine	62.5	0.65	0.8
Lysine	80.6	2.68	2.94
Histidine	83.5	1.49	1.47
Arginine	94	4.18	4.28
Proline	35.2	0.78	<0.01
Total content		86.62	90.03

Table 2: The amino acid content of the freeze-dried SS samples (Waste-Lyo and Deg-Lyo). For each amino acid are reported the retention time (min) and the weight percentage in two treatment groups

The obtained results did not evidence any substantial differences between the two SS sources; overall, our results confirmed that sericin is a hydrophilic protein with a high content of charged and polar amino acids. According to the findings reported by Siritientong and colleagues, [22] we observed that the acids present in the highest percentage are serine,

aspartic acid, glycine, threonine, tyrosine and glutamic acid for both Waste-Lyo and Deg-Lyo samples.

SDS-PAGE was performed to qualitatively evaluate the molecular mass distribution of the freeze-dried, spray-dried and sterilized SS (Figure 1 and Table 3).

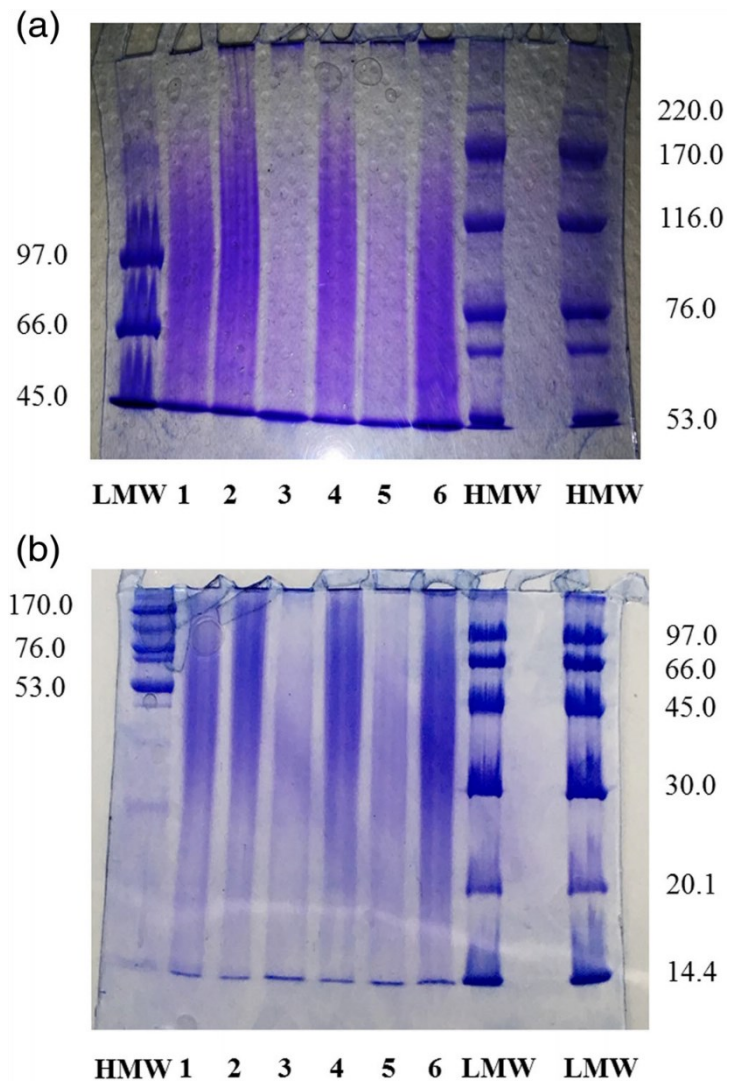


Figure 1: SDS-PAGE of sericin samples using stacking gel to 4% and running gel to 6% (a) and stacking gel to 4% and running gel to 12% (b)

Sample	Code
Deg-Lyo	1
Waste-Lyo	2
Deg-Spray	3
Waste-Spray	4
Deg-Ster	5
Waste-Ster	6
SDS-standard 1	LMW
SDS-standard 2	HMW

Table 3: Sericin samples used for electrophoresis (SDS-page). For each treatment group, a code is reported according to the loading of the sample into the well. SDS-markers were used for molecular weight determination: standard 1 for low molecular weights (LMW) and standard 2 for high molecular weights (HMW)

A unique and continuous band was observed for all samples, revealing a wide molecular mass distribution in the SS as a function of the source and the technological treatment considered. In particular, the SS discarded in the industrial wastewater showed a profile more populated by high molecular weights (from 20 to 220 kDa) than the SS degummed in the laboratory (from 20 to 170 kDa). [11] Studies conducted at the industrial level have shown that using columns with different cut-off lead to solutions of sericin with several ranges of molecular weights. [23] In fact, the process of tangential ultrafiltration conducted in the industry allows us to adopt a higher cut-off compatible with the required level of industrial productivity than laboratory processing. [24]

Despite SDS-PAGE being a commonly used experimental method to analyze the molecular masses of protein or polypeptide subunits, for many researchers involved in electrophoresis experiments with silk sericin it seems that it is not easy to obtain a good SDS-PAGE profile with clear bands. [25] The main difficulty is not related to the SDS-PAGE method itself but it often due to the main experimental parameters such as processing, degumming, drying, dissolution steps, which cause physicochemical stress in the silk sericin, with a significant impact on polymerization grade and molecular weight distribution.

The samples were therefore characterized by FTIR spectroscopy, and the spectra of Deg-Lyo (a), Waste-Lyo (b), Deg-Spray (c) and Waste-Spray (d) samples are shown and compared in Figure 2.

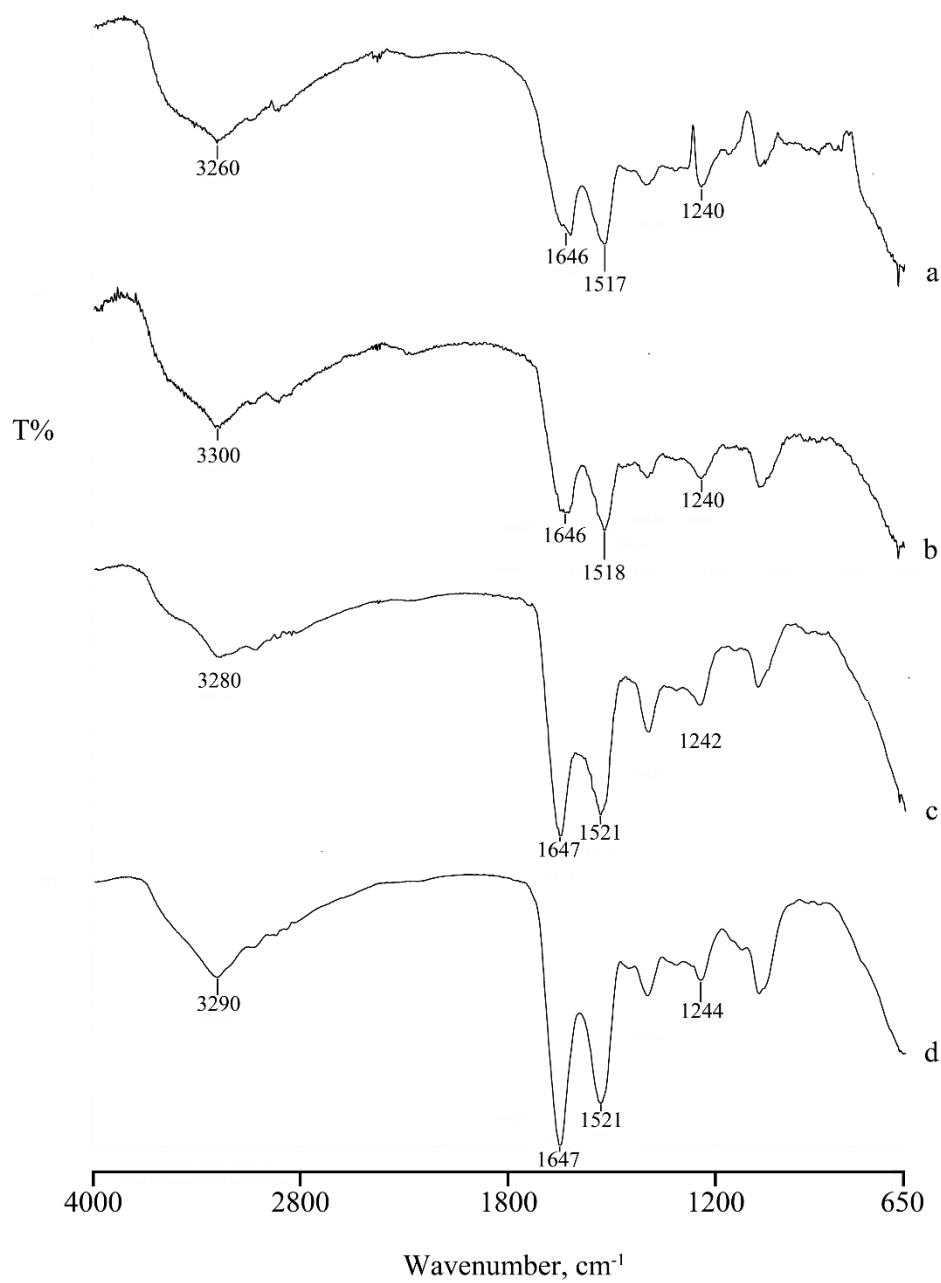


Figure 2: FTIR spectra of Deg-Lyo (a), Waste-Lyo (b), Deg-Spray (c) and Waste-Spray (d) samples

All samples presented the sericin characteristic bands, principally correlated with the random coil conformation of SS. In particular, we observed three bands at about 1640, 1520 and 1250 cm^{-1} due to the presence of Amide I, Amide II and Amide III, respectively. The absorption of the C=O stretching was registered at about 1640 cm^{-1} , and therefore at a lower wavenumber than the traditional carbonyl, as a result of the resonance effect, and typical of the random coil conformation. Finally, all samples presented a band at 3330 cm^{-1} due to the N-H stretching. This band is superimposed on -OH groups absorption of serine and threonine, amino acids which are abundant in the silk protein, causing a broadening of the signal.

The absence of shifts in the characteristic bands of both Deg and Waste samples confirmed that there are not differences between the four dried samples. In Figure 3 are reported the DSC profiles of Deg-Lyo (curve a) and Waste-Lyo (curve b) samples and the TGA profiles of Deg-Spray (curve c) and Waste-Spray (curve d) samples as an example of thermal data.

In all DSC traces a first large endothermic peak at about 90 °C due to water evaporation was evident. This peak was followed by a glass transition effect ($T_{\text{midpoint}} = 200 \pm 2$ °C) related to the higher presence of random coil domains in the amorphous region in SS and other endo/exothermic effects attributable to the SS thermal decomposition.

The TGA profile of all samples confirmed the water evaporation of about 8% in the temperature range 35-150 °C and the following thermal decomposition from about 220 °C indicating no differences in thermal stability between the four products.

Solid-state characterization allowed us to conclude that both SS sources and dried treatments did not influence the physicochemical properties of obtained products.

SEM investigation of all SS samples demonstrated that the preservation method influenced the protein morphology (Figure 4).

In particular, the spray-drying technique allowed to obtain collapsed microparticles, as reported by other authors. [7, 26] Granulometric analysis showed a monomodal trend for both samples (data not presented); microparticles presented a volume-weighted mean diameter of 2.71 ± 1.310 μm and 1.86 ± 0.884 μm (mean \pm standard deviation) for Deg-Spray and Waste-Spray, respectively. Minimal differences in the starting sample concentration could explain the differences in terms of mean diameter between the two treatment groups: however, we observed the same granulometric distribution profile and the same morphology and, for this reason, we demonstrated that the extraction technique does not influence the spray-drying process. Spray-drying is a drying method useful to obtain sericin collapsed microspheres with controlled dimensions [6]; one of the principal advantages is the high drying speed to reduce

thermal damage of the material. In fact, as long as the particles do not become completely dried, evaporation takes place without the product being subjected to overheating. Moreover, large amounts of product can be produced by spray-dryer; obtained powders are easily rehydrated and dispersed at the time of use.

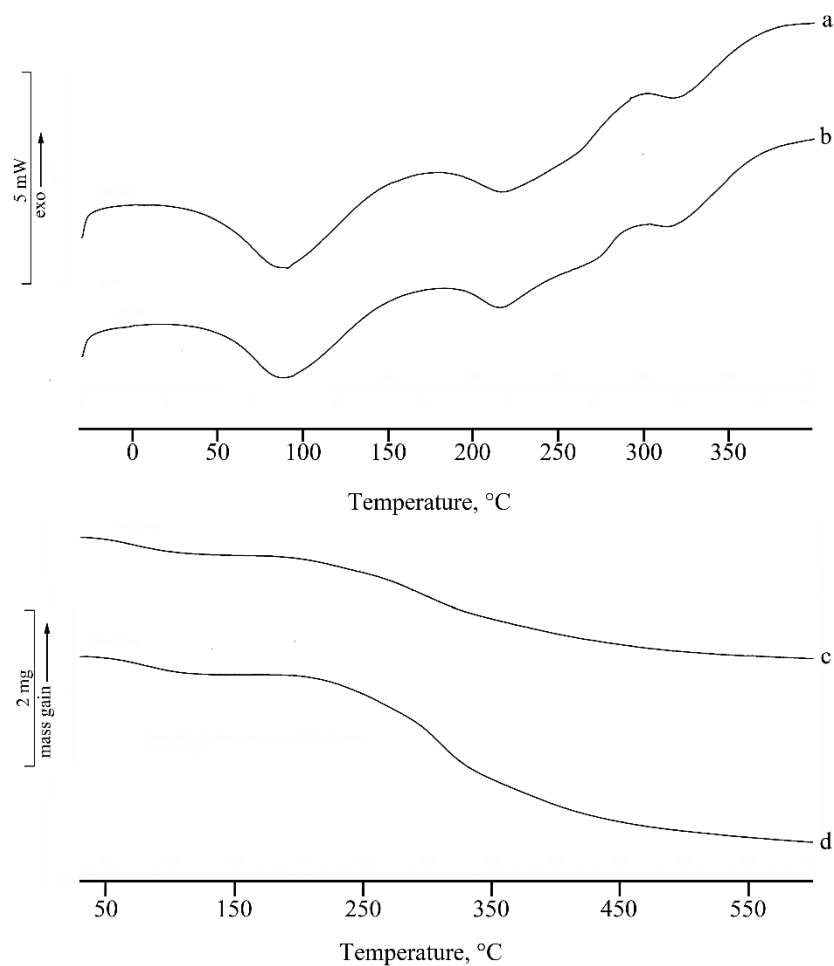


Figure 3: DSC curves of Deg-Lyo (a) and Waste-Lyo (b) products and TGA curves of Deg-Spray (c) and Waste-Spray (d) samples

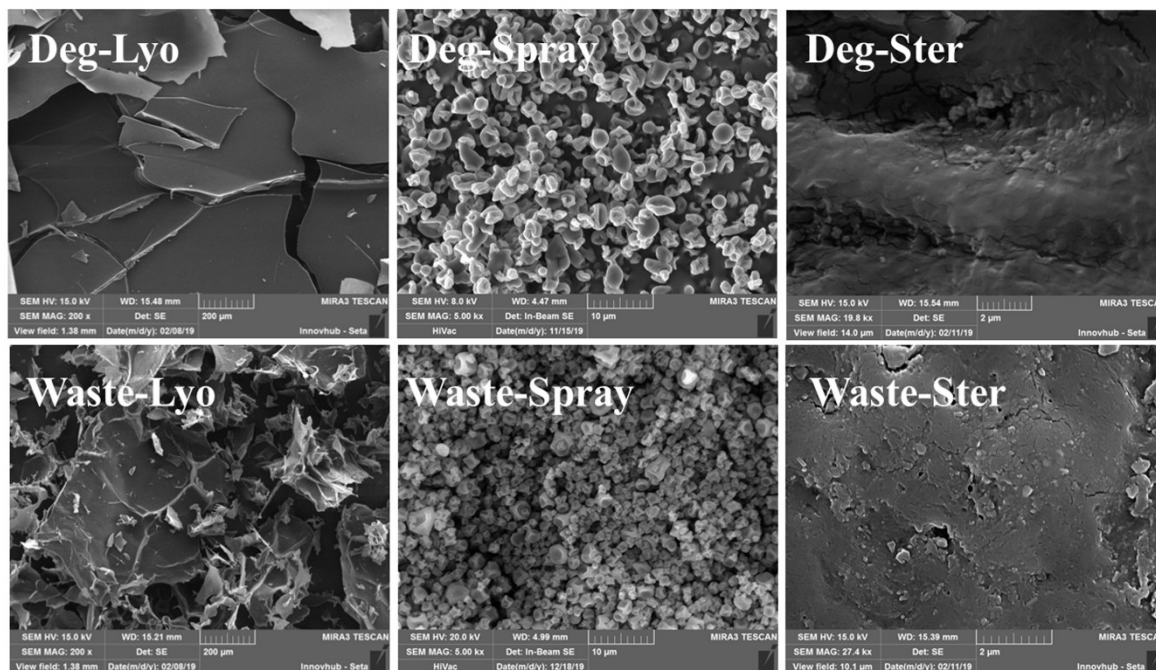


Figure 4: SEM images of the degummed (Deg) and wastewater (Waste) sericin, considering three treatments: lyophilization (Lyo, scale bar 200 μm), spray-drying (Spray, scale bar 10 μm) and sterilization (Ster, scale bar 2 μm). Different scale bars were considered in order to better observe each sample; the same scale bar was used for samples obtained by the same treatment (e.g. Waste-Spray and Deg-Spray)

Freeze-dried samples (Deg-Lyo and Waste-Lyo) did not show any structural or morphological peculiarities; overall, both samples appeared as a rough and irregular surface. Freeze-drying is a valid drying method proposed in the literature to decrease the denaturation degree of a protein and to obtain a porous material with interconnecting pores. [27] Lyophilization ensures the permanent dispersion of a biomaterial, which can be dried, forming a porous solid, [27] dissolving with great rapidity and effectiveness when necessary. Moreover, bacterial growth cannot take place in the frozen material, and a protein product is very resistant to such undesirable phenomena after being freeze-dried.

High energy consumption, long process time and high costs represent the principal disadvantages of the lyophilization and spray-drying techniques. In this contest, autoclave treatment could represent an alternative preservation approach of the SS, in order to obtain sterilized biomaterial in a fast, cheap and eco-friendly way, routinely used in a laboratory to sterilize different reagents and equipment. [17] The morphological evaluation of two liquid sterilized samples (Deg-Ster and Waste-Ster) required solvent evaporation before SEM

analysis; for this reason, sterilized SS were added to the stubs and dried to room temperature. SEM images showed that Deg-Ster and Waste-Ster samples presented an amorphous morphology.

The *in vitro* biological properties of all SS samples were evaluated. Antioxidant, anti-tyrosinase and anti-elastase activities of SS were tested to define the anti-ageing and photoprotective profile of the protein after different treatments.

Regarding the free-radical scavenging potential, the data obtained from statistical analysis showed a significant effect of protein source and treatment ($p < 0.05$). Overall, degummed SSs showed better antioxidant ability with respect to wastewater-derived protein. Degummed SS presented a concentration-dependent trend for all treatment groups (Figure 5); freeze-dried SS (Deg-Lyo) allowed us to obtain the most promising results, reaching a free radical scavenging ability of $83.4 \pm 13.51\%$ (mean value \pm standard deviation) at a concentration of 10 mg/mL. These data were in agreement with those reported by Fan et colleagues. [17]

SS derived from the industrial process (Waste samples) had a lower antioxidant capacity than the native protein, at all tested concentrations. In detail, Waste-Lyo, Waste-Spray and Waste-Ster samples presented a mean antioxidant activity lower than 10%, without any differences between treatment groups and sample concentrations ($p > 0.05$, Figure 5).

Data obtained by DPPH assay were also statistically analyzed to determine the IC_{50} values. These results confirmed that SS derived from textile wastewater had lower antioxidant properties (Table 4). On the other hand, Deg-Lyo SS resulted as the most promising sample, with an IC_{50} value of 4.43 mg/mL. No differences ($p < 0.05$) were revealed between Deg-Spray and Deg-Ster samples, which presented IC_{50} values of about 20 mg/mL (Table 4).

These data confirmed that the DPPH radical scavenging activity of the SS is strongly influenced by the technological procedure chosen to preserve silk protein, but also by the degumming process and other parameters, e.g. silkworm strains [5, 28] and diet [29].

All these parameters influenced the chemical compositions of SS, and consequently the biological properties of silk protein. In addition, Manosroi et al. [30] demonstrated that freeze-dried SS, degummed by autoclave treatment, showed a higher free radical scavenging activity with respect to SS obtained by the soap-alkaline degumming process. Although the latter method is more effective for removing sericin from silk fibroin during industrial silk production, the recovered SS is often not of high quality, owing to its degradation and to purification steps needed to remove the chemical impurities into the SS aqueous solution. [9]

In the work published by Wu et al., [31] the ethanol precipitation method was proposed to recover SS from silk industrial wastewater. This recovery method was effective in obtaining

an SS-based dried product with a high degree of purity and an IC_{50} value of 31 mg/mL. SS can be used as a skin whitening agent, thanks to its tyrosinase inhibition activity. The statistical analysis demonstrated a significant effect of all considered variables (treatment group, time and sample concentration; $p < 0.0001$) on SS anti-tyrosinase activity. As observed from the DPPH assay, the degummed samples presented a higher anti-tyrosinase ability. In particular, SS subjected to spray-drying technique (Deg-Spray) presented the highest inhibitory effect on tyrosinase enzyme already at a concentration 5 mg/mL, as shown in Figure 5 ($60.45 \pm 1.04\%$). Overall, Waste SSs had lower anti-tyrosinase capacity than the native protein extracted in our research laboratory.

All waste-derived samples presented a mean activity lower than 20%, at all considered concentrations (Figure 5). As additional reference material, see also Supporting Information Figure S1.

Tyrosinase is the main regulator of melanin production during the melanogenesis process, as a defence against UV rays. [5, 32] Overexpression of the tyrosinase is often responsible for hyperpigmentation disorders and ageing. In 2018, Aramwit et al. determined the anti-tyrosinase effect of urea-extracted SS on human *Staphylococcus aureus* peptidoglycan (PEG)-stimulated melanocytes and artificial model of skin, using an *in vitro* model of hyperpigmentation. SS at all tested concentrations significantly caused a decrease in tyrosinase production on melanin pigments compared with non-treated melanocytes. Moreover, similar results were obtained after 10 days of SS treatment on the tyrosinase expression in artificial skin. [33] Aramwith et al.'s results were in agreement with the data reported in this work.

SS amino acid composition influenced, in the same manner, both free radical scavenging and anti-tyrosinase activities of SS; in particular, high content of hydroxyl groups, polyphenols and flavonoids positively improve the antioxidant and anti-tyrosinase profile of SS. [5, 34-36] Raw data obtained from the spectrophotometric analyses of tyrosinase reaction kinetics were also processed to calculate K_m and V_{max} (Table 5). No differences ($p > 0.05$), in terms of K_m and V_{max} , were observed for Waste-Spray, Deg-Ster and Waste-Ster samples in comparison with negative control (substrate + enzyme, without sericin). On the other hand, Deg-Lyo, Waste-Lyo and Deg-Spray samples induced a significant modification of K_m and/or V_{max} values.

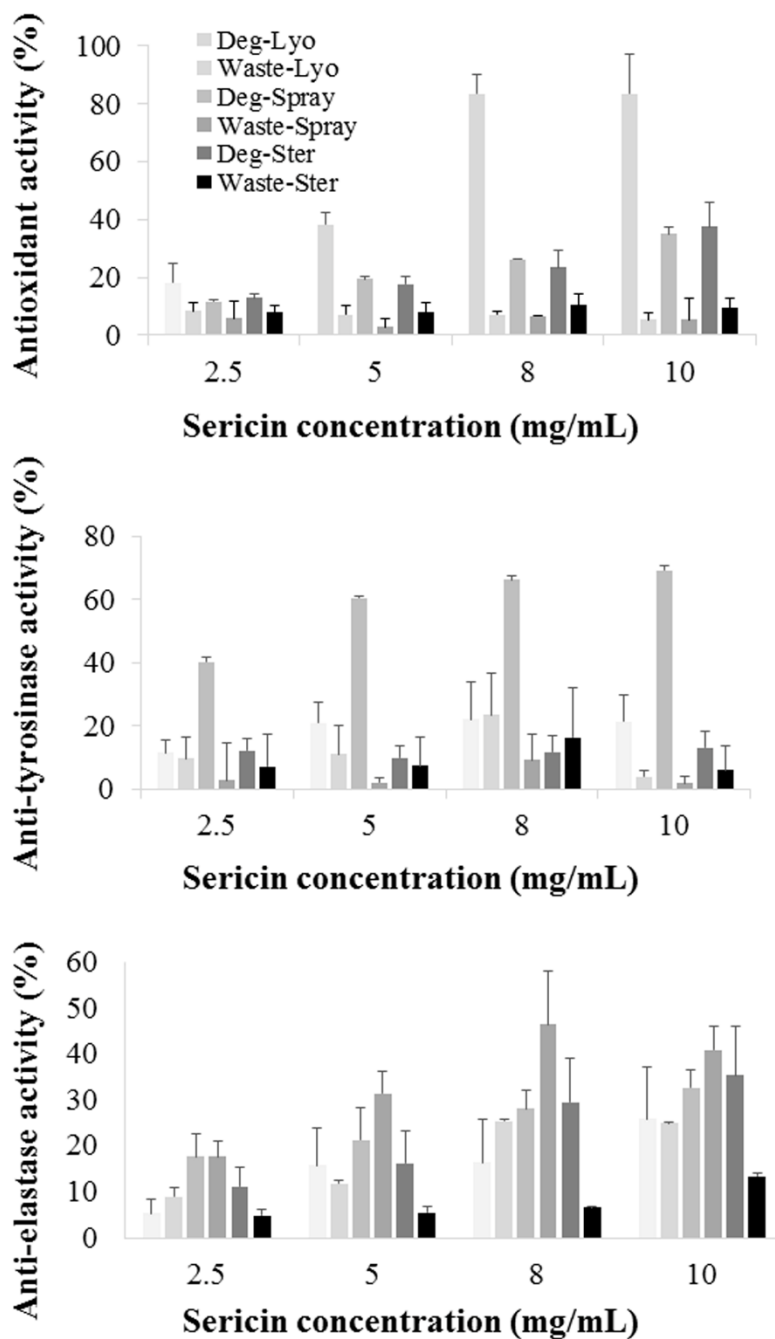


Figure 5: Free radical scavenging, anti-tyrosinase, and anti-elastase activity percentage of SS samples. Data are reported as mean values and standard deviations (n = 3)

ID sample	IC ₅₀	95% CI
Deg-Lyo	4.43 ^d	3.40 - 5.72
Deg-Spray	20.28 ^c	18.99 - 21.69
Deg-Ster	20.49 ^c	18.87 - 22.32
Waste-Lyo	109.80 ^a	85.19 - 152.00
Waste-Spray	135.10 ^a	76.14 - 469.40
Waste-Ster	73.47 ^b	59.29 - 95.19

Table 4: Antioxidant activity of the silk sericin samples expressed in terms of IC₅₀ values (mg/mL). Data are reported as mean values and 95% confidence intervals (n = 3). Different letters indicate significant differences ($p < 0.05$) between treatment groups

According to the Michaelis-Menten kinetics, Deg-Spray acted as a mixed inhibitor of tyrosinase enzyme; in fact, we observed that K_m value was not significantly different with respect to negative control while V_{max} value was incremented ($p < 0.05$) (Table 5).

ID sample	K _m		V _{max}	
	Mean	Standard Error	Mean	Standard Error
CTR	47.66 ^d	11.677	2.389 ^c	0.257
Deg-Lyo	115.343 ^a	12.037	4.161 ^a	0.264
Waste-Lyo	77.754 ^{bc}	8.533	3.099 ^b	0.187
Deg-Spray	100.734 ^{ab}	10.431	1.158 ^d	0.229
Waste-Spray	36.407 ^d	8.533	1.961 ^c	0.187
Deg-Ster	52.708 ^d	8.698	2.362 ^c	0.191
Waste-Ster	63.285 ^{cd}	6.306	2.815 ^{bc}	0.138

Table 5: K_m and V_{max} of the anti-tyrosinase activity. Data are reported as mean values and standard error (n = 3). Different letters indicate significant differences ($p < 0.05$) between treatment groups

Deg-Spray SS can bind both free enzyme and enzyme/substrate complex, causing a simultaneous change of K_m and V_{max} , compared to the negative control curve. [37, 38]

All SS samples were tested to evaluate their ability to inhibit the elastase, a key enzyme in the elastin fibres degradation. All considered variables (treatment group, time and sample concentration) showed a significant effect on elastase inhibition ($p < 0.0001$). The anti-elastase activity had a dose-dependent trend for all samples (Figure 5). The Deg-Ster and Waste-Spray samples showed the highest anti-elastase properties. Deg-Ster activity was $53.07 \pm 6.42\%$ and $56.95 \pm 7.16\%$ (mean value \pm standard deviation) at 8 mg/mL and 10 mg/mL, respectively, while Waste-Spray activity was $46.60 \pm 11.74\%$ (mean value \pm standard deviation) at 8 mg/mL and $41.07 \pm 5.15\%$ (mean value \pm standard deviation) at 10 mg/mL. Overall, other samples did not exceed 35% of anti-elastase activity. As additional reference material, see also Supporting Information Figure S1.

The K_m and V_{max} mean values of all SS samples and the negative control are reported in Table 6. According to the Michaelis-Menten kinetics, sterilized SS, coming from industrial extraction (Waste-Ster), acted as a mixed inhibitor, causing a simultaneous change of K_m and V_{max} with respect to the negative control (CTR) (Table 6). Contrarily, Waste-Lyo, Deg-spray, and Waste-spray are examples of the non-competitive inhibitors of the elastase. They bind the free enzyme or the enzyme/substrate complex in an allosteric site, causing a decrease of V_{max} without K_m value alterations. [37]

The *in vitro* cytotoxicity of SS samples was evaluated on human fibroblasts. All SS samples resulted in cytocompatible at all considered concentrations (Figure 6).

Statistical analysis evidenced a significant effect of SS source (ad hoc degumming process-derived and industrial wastewater-derived SS) and sample concentration on cell viability ($p < 0.0001$). In particular, fibroblast metabolic activity was $97.08 \pm 1.798\%$ and $84.29 \pm 1.798\%$ (mean value \pm LSD interval) for sericins derived from wastewater and degumming process, respectively.

On the other hand, the treatment of SS samples (freeze-drying, spray-drying or sterilization) and time of incubation did not affect cell metabolic activity ($p = 0.2261$). A second statistical analysis was performed considering the type of SS source and the technological treatment as a unique fixed factor. As shown in Figure 6, there were significant differences between the analyzed groups.

ID sample	K_m		V_{max}	
	Mean	Standard Error	Mean	Standard Error
CTR	11.694 ^{ab}	2.131	1.013 ^b	0.036
Deg-Lyo	13.108 ^{bc}	2.349	1.263 ^a	0.039
Waste-Lyo	20.818 ^a	1.681	0.788 ^c	0.028
Deg-Spray	14.345 ^{bc}	2.349	0.856 ^c	0.039
Waste-Spray	18.517 ^{ab}	2.349	0.775 ^c	0.039
Deg-Ster	15.685 ^{ab}	1.859	1.252 ^a	0.031
Waste-Ster	9.012 ^c	1.681	0.863 ^c	0.028

Table 6: K_m and V_{max} of the anti-elastase activity. Data are reported as mean values and standard error ($n = 3$). Different letters indicate significant differences ($p < 0.05$) between treatment groups

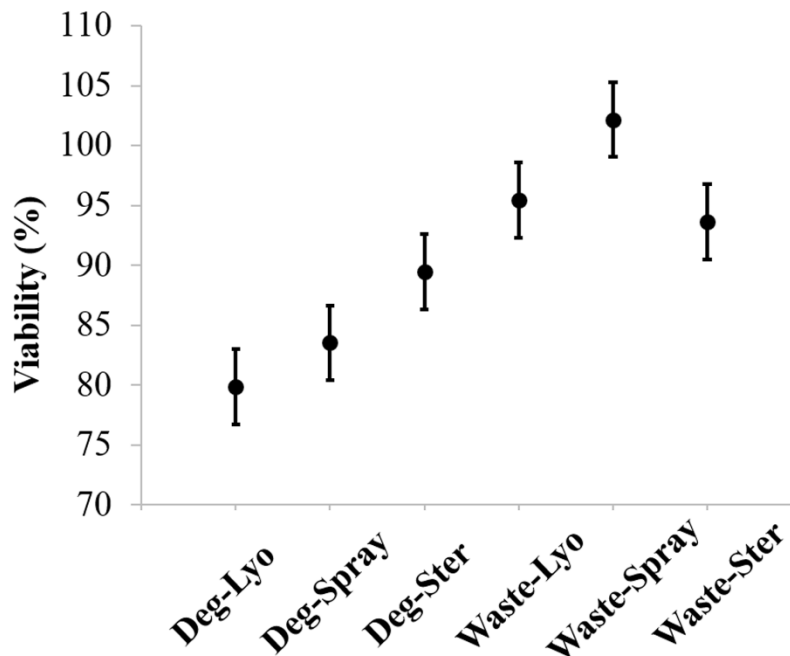


Figure 6: Cytocompatibility of SS samples on human fibroblasts. Data are expressed as mean values, of all tested concentrations, and LSD intervals of viability ($n = 243$). The overlap of two LSD intervals graphically indicates the absence of significant differences ($p > 0.05$)

In detail, Waste-Spray showed the best cytocompatibility on human fibroblasts ($102.18 \pm 3.125\%$, mean value \pm LSD interval). Overall, our results confirmed the literature data, which demonstrated the cytocompatibility of SS on different cell lines. [7, 8, 39, 40]

We also tested the ability of SS to protect human fibroblasts from damage induced by the hydrogen peroxide treatment ($0.75 \text{ mmol/L H}_2\text{O}_2$); statistical analysis demonstrated that treatment group, sample and hydrogen peroxide concentrations significantly influenced the fibroblast viability ($p < 0.005$, $n = 144$, data not presented). In particular, Deg-Ster and Waste-Spray SS showed a higher protective effect against oxidative damages, at all considered concentrations. Treatment with these SS protects the cells and prevents the cell viability decrease, which was observed in the control group (no sericin treatment).

The *in vitro* antiproliferative activity of SS samples was evaluated on stimulated human PBMCs; moreover, we tested the effect of SS sample on the release of pro and anti-inflammatory cytokines by PBMCs. PBMCs isolated from two healthy donors responded to the stimulation with PHA; all SS samples were able to inhibit the proliferation of stimulated cells in a dose-dependent manner and, in particular, the higher considered dose (0.5 mg/mL) allowed a greater reduction in the RP of PBMCs than did lower doses (0.12 and 0.012 mg/mL). Significant differences were observed between the considered treatment groups ($p < 0.0001$; Figure 7); the most promising results were obtained with SS subjected to standardized degumming and then to autoclave sterilization (Deg-Ster sample).

Considering the cytokine release assay, the data showed statistical differences between treatment groups ($p < 0.0001$). PHA-stimulated cells treated with different SS samples released lower TNF- α amount with respect to control cells (Figure 8). All samples had TNF- α levels lower than 4000 pg/mL .

Moreover, the treatment group showed no significative effect on IFN- γ release ($p > 0.05$). All samples responded similarly to the untreated PBMCs (Figure 8).

Finally, IL-10 release was evaluated on PHA-stimulated PBMCs (Figure 8). Cells treated with SS showed lower IL-10 levels than the control (CTR).

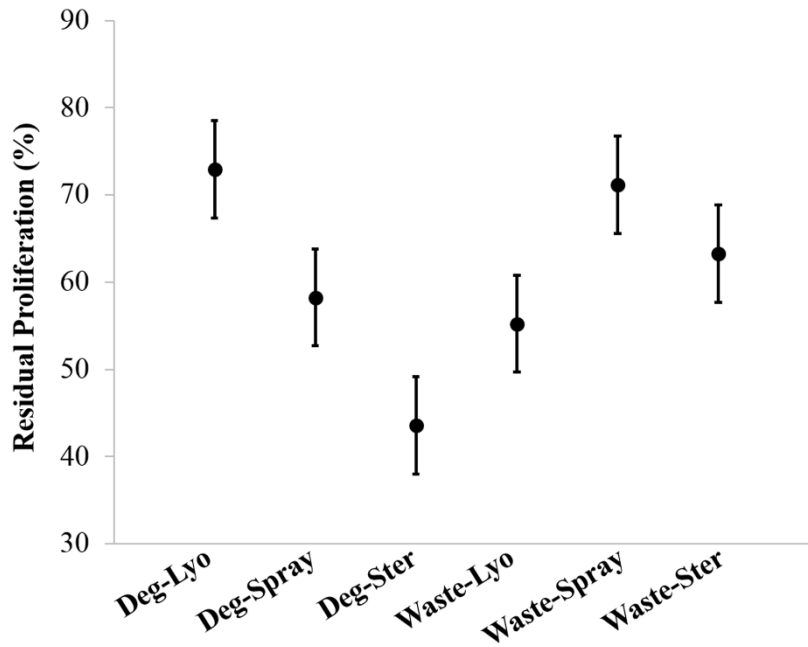


Figure 7: Antiproliferative effect of sericin samples on PHA-stimulated PBMCs. Data are expressed as mean values, of all tested concentrations, and LSD intervals of residual proliferation ($n = 108$). The overlap of two LSD intervals graphically indicates the absence of significant differences ($p > 0.05$)

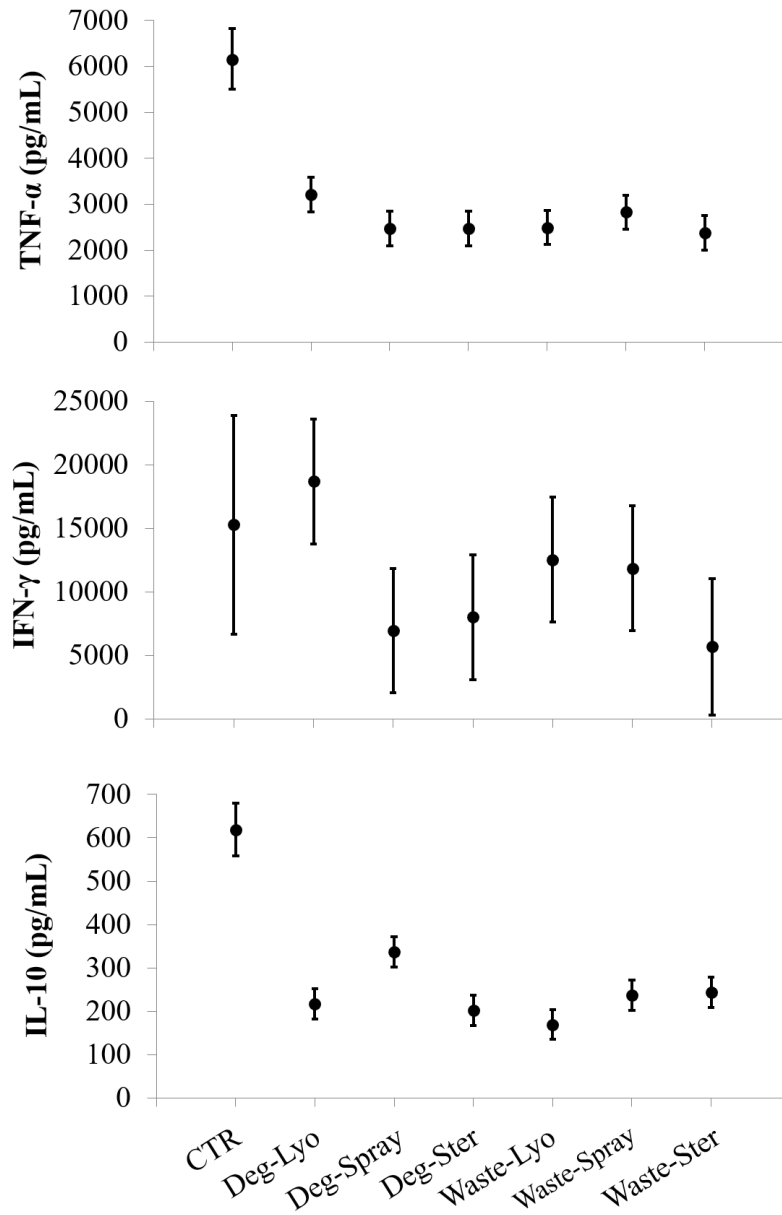


Figure 8: TNF- α , IFN- γ and IL-10 release (pg/mL) by PHA-stimulated PBMCs in the presence of sericin samples. Data are expressed as mean values and LSD intervals (n = 152). The overlap of two LSD intervals graphically indicates the absence of significant differences ($p > 0.05$)

5. Conclusions

Obtained results demonstrated that wastewater-derived SS is a biocompatible and non-immunogenic material. Moreover, we demonstrated many biological activities of the industrial SS, closely related to structural complexity, molecular weight distribution, and stability, depending on the extraction and preservation methods.

Overall, wastewater-derived SS presented better anti-elastase properties and cytocompatibility with respect to the SS obtained in our research laboratory, while no differences were evidenced in terms of cytokine release. Regarding the stabilization technique, our results demonstrated that lyophilization and spray-drying are the most promising approaches, which allowed us to maintain both the protein stability and the biological properties of the final product.

Our research aims to be a starting point for the use of textile wastewater for the production of silk sericin usable in many biomedical and biotechnological fields. For this purpose, future research will be necessary to refine the industrial degumming process in order to optimize the extraction yield and to improve the stability and half-life of the protein.

Acknowledgements

The authors thank Nembri Industrie Tessili s.r.l. (Capriolo, BG, Italy) for certified *Bombyx mori* cocoons and Prof. Sergio Schinelli and Dott. Mayra Paolillo (Drug Sciences Department, Pavia University, Italy) for allowing us to use to Synergy HT (BioTek, Swindon, UK).

This work was partially supported by Interreg V-A Italy-Switzerland 2014-2020—ATEX—Advanced Therapies Experiences, Project ID 637541.

Conflict of interest

M.S., S.P. and M.L.T. are co-founders and members of the advisory board of the company PharmaExceed s.r.l.

Author Contributions

Conceptualization and supervision: S.F., M.S., F.B., M.L.T.; investigation, G.O., M.M., I.D., L.C., M.L.S., S.C., L.S., S.P.; writing-original draft preparation: G.O., S.P., S.M.; writing-review and editing: G.O., M.S., S.M., M.L.T., S.P.

References

- [1] B. Crivelli, S. Perteghella, E. Bari, M. Sorrenti, G. Tripodo, T. Chlapanidas, M.L. Torre, Silk nanoparticles: from inert supports to bioactive natural carriers for drug delivery, *Soft Matter* 14 (2018) 546-557.
- [2] B.B. Mandal, S.C. Kundu, Selk-assembled silk sericin/poloxamer nanoparticles as nanocarriers of hydrophobic and hydrophilic drugs for targeted delivery, *Nanotechnology* 20(355101) (2009).
- [3] J. Kanoujia, M. Singh, P. Singh, S.A. Saraf, Novel genipin crosslinked atorvastatin loaded sericin nanoparticles for their enhanced antihyperlipidemic activity, *Materials Science & Engineering C-Materials for Biological Applications* 69 (2016) 967-976.
- [4] E. Bari, S. Perteghella, S. Farago, M.L. Torre, Association of silk sericin and platelet lysate: Premises for the formulation of wound healing active medications, *International Journal of Biological Macromolecules* 119 (2018) 37-47.
- [5] T. Chlapanidas, S. Farago, G. Lucconi, S. Perteghella, M. Galuzzi, M. Mantelli, M.A. Avanzini, M.C. Tosca, M. Marazzi, D. Vigo, M.L. Torre, M. Faustini, Sericins exhibit ROS-scavenging, anti-tyrosinase, anti-elastase, and in vitro immunomodulatory activities, *International Journal of Biological Macromolecules* 58 (2013) 47-56.
- [6] T. Chlapanidas, S. Perteghella, F. Leoni, S. Farago, M. Marazzi, D. Rossi, E. Martino, R. Gaggeri, S. Collina, TNF-alpha Blocker Effect of Naringenin-Loaded Sericin Microparticles that Are Potentially Useful in the Treatment of Psoriasis, *International Journal of Molecular Sciences* 15(8) (2014) 13624-13636.
- [7] E. Bari, C.R. Arciola, B. Vigani, B. Crivelli, P. Moro, G. Marrubini, M. Sorrenti, L. Catenacci, G. Bruni, T. Chlapanidas, E. Lucarelli, S. Perteghella, M.L. Torre, In Vitro Effectiveness of Microspheres Based on Silk Sericin and *Chlorella vulgaris* or *Arthrospira platensis* for Wound Healing Applications, *Materials* 10(9) (2017).
- [8] E. Bari, S. Perteghella, G. Marrubini, M. Sorrenti, L. Catenacci, G. Tripodo, M. Mastrogiacomo, D. Mandracchia, A. Trapani, S. Farago, P. Gaetani, M.L. Torre, In vitro efficacy of silk sericin microparticles and platelet lysate for intervertebral disk regeneration, *International Journal of Biological Macromolecules* 118 (2018) 792-799.
- [9] L. Lamboni, M. Gauthier, G. Yang, Q. Wang, Silk sericin: A versatile material for tissue engineering and drug delivery, *Biotechnology Advances* 33(8) (2015) 1855-1867.
- [10] <http://www.cir-safety.org/sites/default/files/slkprt062015rep.pdf>.

- [11] T.V. Chirila, S. Suzuki, N.C. McKirdy, Further development of silk sericin as a biomaterial: comparative investigation of the procedures for its isolation from *Bombyx mori* silk cocoons, *Progress in Biomaterials* 5(2) (2016) 135-145.
- [12] P. Aramwit, T. Siritientong, T. Srichana, Potential applications of silk sericin, a natural protein from textile industry by-products, *Waste Management & Research* 30(3) (2012) 217-224.
- [13] E.M. Foundation, *Intelligent Assets:Unlocking the Circular Economy Potential*, 2016.
- [14] W. Amaro, D. Andreani, S. Faragò, E. Oberrauch, M. Sorlini, Procedimento e apparecchiatura per la preparazione di materiali proteici derivanti da fibroina, in particolare per uso medicale e cosmetico, in: I.-S.S.p. l'Industria, S.U.P.d. svizzera (Eds.) Italy, 2013.
- [15] G. Yang, L. Xiao, L. Lamboni, *Bioinspired Materials Science and Engineering*, 2018.
- [16] H. Oh, J.Y. Lee, M.K. Kim, I.C. Um, K.H. Lee, Refining hot-water extracted silk sericin by ethanol-induced precipitation, *International Journal of Biological Macromolecules* 48(1) (2011) 32-37.
- [17] J. Fan, L. Wu, L. Chen, X. Mao, F. Ren, Antioxidant activities of silk sericin from silkworm *Bombyx mori*, *Journal of Food Biochemistry* 33 (2009) 74-88.
- [18] P. Aramwit, S. Damrongsakkul, S. Kanokpanont, T. Srichana, Properties and antityrosinase activity of sericin from various extraction methods, *Biotechnology and Applied Biochemistry* 55 (2010) 91-98.
- [19] K.A. Nam, S.G. You, S.M. Kim, Molecular and physical characteristics of squid (*Todarodes pacificus*) skin collagens and biological properties of their enzymatic hydrolysates, *Journal of Food Science* 73(4) (2008) C249-C255.
- [20] P. Aramwit, S. Kanokpanont, T. Nakpheng, T. Srichana, The Effect of Sericin from Various Extraction Methods on Cell Viability and Collagen Production, *International Journal of Molecular Sciences* 11(5) (2010) 2200-2211.
- [21] D. Vijayalakshmi, R. Dhandapani, S. Jayaveni, P.S. Jithendra, C. Rose, A.B. Mandal, In vitro anti inflammatory activity of Aloe vera by down regulation of MMP-9 in peripheral blood mononuclear cells, *Journal of Ethnopharmacology* 141(1) (2012) 542-546.
- [22] T. Siritientong, W. Bonani, A. Motta, C. Migliaresi, P. Aramwit, The effects of *Bombyx mori* silk strain and extraction time on the molecular and biological characteristics of sericin, *Bioscience Biotechnology and Biochemistry* 80(2) (2016) 241-249.
- [23] M.H. Wu, J.X. Yue, Y.Q. Zhang, Ultrafiltration recovery of sericin from the alkaline waste of silk floss processing and controlled enzymatic hydrolysis, *Journal of Cleaner Production* 76 (2014) 154-160.

- [24] M.L. Gimenes, V.R. Silva, M.G.A. Vieira, S.G.C. Meuris, A.P. Scheer, High molecular sericin from *Bombyx mori* cocoons: extraction and recovering by ultrafiltration, *International Journal of Chemical Engineering and Applications*, 2014, pp. 266-271.
- [25] Q. Zi, SDS-PAGE for Silk Fibroin Protein, Bio-101 Camberwell, VIC, Australia (2018).
- [26] N.H. Salunkhe, N.R. Jadhav, H.N. More, A.D. Jadhav, Screening of drug-sericin solid dispersions for improved solubility and dissolution, *International Journal of Biological Macromolecules* 107 (2018) 1683-1691.
- [27] W. Tao, M.Z. Li, R.J. Xie, Preparation and structure of porous silk sericin materials, *Macromolecular Materials and Engineering* 290(3) (2005) 188-194.
- [28] L. Butkhup, M. Jeenphakdee, S. Jorjong, S. Samappito, W. Samappito, J. Butimal, Phenolic composition and antioxidant activity of Thai and Eri silk sericins, *Food Science and Biotechnology* 21(2) (2012) 389-398.
- [29] T. Takechi, R. Wada, T. Fukuda, K. Harada, H., Takamura, Antioxidant activities of two sericin proteins extracted from cocoon of silkworm (*Bombyx mori*) measured by DPPH, chemiluminescence, ORAC and ESR methods, *Biomedical Reports* 2(3) (2014) 364-369.
- [30] A. Manosroi, K. Boonpisuttinant, S. Winitchai, W. Manosroi, J. Manosroi, Free radical scavenging and tyrosinase inhibition activity of oils and sericin extracted from Thai native silkworms (*Bombyx mori*), *Pharmaceutical Biology* 48(8) (2010) 855-860.
- [31] J.-H. Wu, Z. Wang, S.-Y. Xu, Preparation and characterization of sericin powder extracted from silk industry wastewater, *Food Chemistry* 103(4) (2007) 1255-1262.
- [32] K.U. Schallreuter, S. Kothari, B. Chavan, J.D. Spencer, Regulation of melanogenesis - controversies and new concepts, *Experimental Dermatology* 17(5) (2008) 395-404.
- [33] P. Aramwit, N. Luplertlop, T. Kanjanapruthipong, S. Ampawong, Effect of urea-extracted sericin on melanogenesis: potential applications in post-inflammatory hyperpigmentation, *Biological Research* 51 (2018).
- [34] I. Chiocchio, M. Mandrone, C. Sanna, A. Maxia, M. Tacchini, F. Poli, Screening of a hundred plant extracts as tyrosinase and elastase inhibitors, two enzymatic targets of cosmetic interest, *Industrial Crops and Products* 122 (2018) 498-505.
- [35] J.P. Kumar, B.B. Mandal, The inhibitory effect of silk sericin against ultraviolet-induced melanogenesis and its potential use in cosmeceutics as an anti-hyperpigmentation compound, *Photochemical & Photobiological Sciences* 18(10) (2019) 2497-2508.
- [36] K. Jena, J.P. Pandey, R. Kumari, A.K. Sinha, V.P. Gupta, G.P. Singh, Free radical scavenging potential of sericin obtained from various ecoraces of tasar cocoons and its

cosmeceuticals implication, *International Journal of Biological Macromolecules* 120 (2018) 255-262.

[37] D.L. Nelson, M.M. Cox, in: B. Zanichelli, Italy (Ed.), *Principi di Biochimica*, Lehninger2010, p. 203.

[38] S. Zolghadri, A. Bahrami, M.T.H. Khan, J. Munoz-Munoz, F. Garcia-Molina, F. Garcia-Canovas, A.A. Saboury, A comprehensive review on tyrosinase inhibitors, *Journal of Enzyme Inhibition and Medicinal Chemistry* 34(1) (2019) 279-309.

[39] H. Khatun, J. Egashira, M. Sakatani, N. Takenouchi, H. Tatemoto, Y. Wada, K. Yamanaka, Sericin enhances the developmental competence of heat-stressed bovine embryos, *Molecular Reproduction and Development* 85(8-9) (2018) 696-708.

[40] Y. Huang, Q. Peng, H.Y. Li, Z.D. Jia, Y. Li, Y. Gao, Novel sericin-based hepatocyte serum-free medium and sericin's effect on hepatocyte transcriptome, *World Journal of Gastroenterology* 24(30) (2018) 3398-3413.

SUPPLEMENTARY MATERIAL

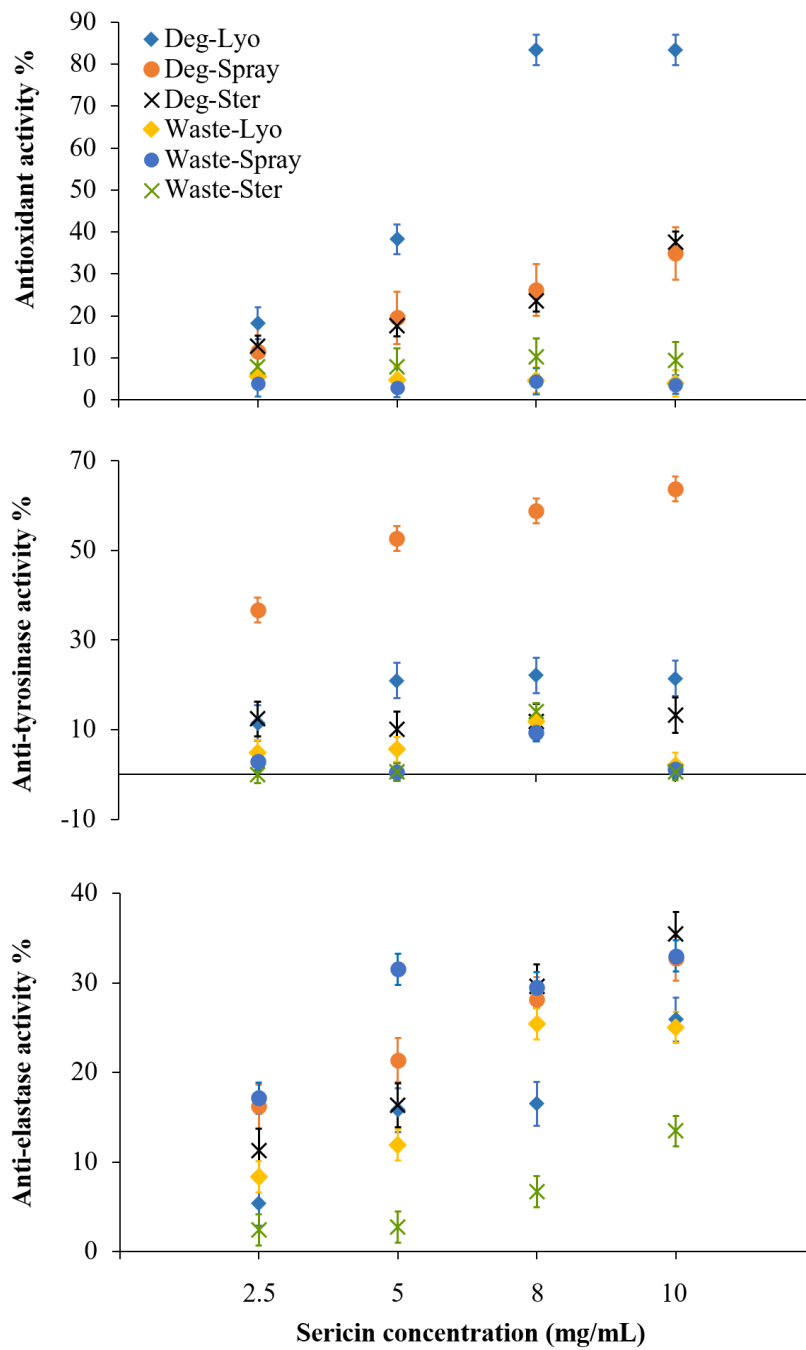


Figure S1: Antioxidant, anti-tyrosinase, and anti-elastase activity percentage of SS samples. Data are expressed as mean values and LSD intervals of viability. The overlap of two LSD intervals graphically indicates the absence of significant differences ($p > 0.05$)

Conclusions

Fibroin and sericin, as components of raw silk, differ considerably in their chemical composition and accessibility into silkworm cocoons. While the former is water-insoluble owing to its crystalline fibrous structure, the latter, as a polymer present on the surface, is more easily accessible to degumming processes. Numerous research studies have demonstrated that sericin exhibits many intrinsic biological properties, suggesting that it can be successfully used as a bioactive compound or excipient for medical, biological, and biotechnological applications.

In this regard, the PhD thesis focused on the application of sericin for pharmaceutical, cosmetic, and biomedical purposes.

By chromatographic analysis, it was demonstrated a strong relationship between the molecular weight distribution of sericin and the type of extraction method. Sericin extracted by autoclave showed a higher average molecular weight (60 kDa) and a marked content of hydrophilic amino acids than the sericin treated with sodium carbonate (10 kDa). Instead, a reduced heterogeneity in size distribution was evidenced for the sample subjected to the chemical treatment. Moreover, the conventional soap-alkaline treatment allows us to obtain the hydrolysis of more internal sericin layers resulting in a mixture of hydrophilic and hydrophobic polypeptide chains. Autoclave degumming process preserved better the antioxidant and anti-tyrosinase activity of sericin, due to the presence of hydroxyl functional groups rich in polar amino acids. Conversely, the high content of lipophilic amino acids enhanced the anti-elastase activity, at the expense of antioxidant and anti-tyrosinase properties.

The water degumming method was performed to obtain sericin then used to prepare protein-based nano-structured systems. The development of nanoparticles has allowed the improvement of the technological and biological properties of proanthocyanidins, epigallocatechin gallate, and quercetin and thereby their kinetic release. In detail, self-assembled sericin nanoparticles showed a slow and controlled release profile for both hydrophilic (proanthocyanidins, epigallocatechin gallate) and hydrophobic (quercetin) drugs in the presence of phosphate-buffered saline dissolution medium. Overall, the encapsulation into nanosystems supported the antioxidant, anti-tyrosinase, and anti-elastase activity of proanthocyanidins and epigallocatechin gallate, whereas, for quercetin, the anti-elastase

activity was strongly improved. Moreover, sericin promoted the metabolic activity of MSCs and protected cells from damage induced by oxidative stress.

Finally, following the circular economy principles, the comparison between two different sources of sericin (an ad hoc degumming process performed in the laboratory or industrial wastewater) did not reveal significant differences in terms of physical-chemical properties and biocompatibility; moreover, the tangential filtration process-induced an improvement of the anti-elastase activity. Therefore, the possibility to reuse sericin as a bioactive excipient in pharmaceutical and cosmetic fields can result in significant environmental, economic and social benefits. However, future investigations will be necessary to optimize the extraction methods and storage conditions to improve the stability and half-life of sericin.

Acknowledgements

This Ph.D. thesis has been partially supported by Innhovub (Silk division, Milan, Italy), Artefil S.R.L (Luisago, Como, Italy) and Interreg V-A Italy-Switzerland 2014-2020 (ATEX – Advanced Therapies Experiences, Project ID 637541).

I want to thank Prof. Maria Luisa Torre, Prof. Giuseppe Tripodo, Prof. Gabriella Massolini, Prof. Marialaura Amadio, Prof. Enrica Calleri, Prof. Caterina Temporini, Prof. Sergio Schinelli, Dr. Milena Sorrenti, Dr. Laura Catenacci, Dr. Mayra Paolillo, Dr. Sara Perteghella, Dr. Elia Bari, Dr. Michela Mocchi, and Dr. Sara Tengattini of the Department of Drug Sciences, University of Pavia, Pavia, Italy. Dr. Silvio Faragò and Dr. Ilaria Donelli of Innhovub-Silk division, Milan, Italy. Dr. Fabrizio Butti of Artefil S.R.L, Luisago, Como, Italy. Dr. Maria Antonietta Avanzini and Dr. Stefania Croce of Fondazione IRCCS Policlinico San Matteo, Immunology & Transplantation Laboratory/Pediatric Surgery Cell Factory & Regenerative Medicine Research Center, Pavia, Italy. Dr. Marzio Sorlini and Dr. Silvia Menato of Department of Innovative Technologies, University of Applied Sciences and Arts of Southern Switzerland, Manno, Switzerland. Dr. Lorena Segale of Department of Pharmaceutical Sciences, University of Piemonte Orientale, Novara, Italy. Prof. Carla Renata Arciola of Department of Experimental, Diagnostic, and Specialty Medicine (DIMES), University of Bologna, Bologna, Italy.